Growth Differentiation Factor 11 and Myostatin: Mechanism and Therapeutic Role in Cardiovascular Diseases

Thesis

Growth differentiation factor 11 and myostatin: mechanism and therapeutic role in cardiovascular diseases

---

Luca Camparini

A Thesis submitted in fulfilment of the requirements
of the Faculty of Life, Health and Chemical Sciences
of the Open University (UK) for the degree of Doctor of Philosophy

International Centre for Genetic Engineering and Biotechnology (ICGEB)
Trieste, Italy

Director of Studies: Prof. Francesco Loffredo

External Supervisors: Prof. Vincent Segers and Prof. Mauro Giacca

Submitted December, 2019

Ai miei genitori

che mi hanno permesso di inseguire la mia passione.

Ad Elisa
che mi accompagna in questo viaggio.

“An expert is a man who has made all the mistakes which can be made, in a narrow field.”

Niels Bohr

ABSTRACT

During life, cardiac muscle is capable of remodeling in response to an increased hemodynamic demand through cardiac hypertrophy. However, in most cases, if the stress stimuli become chronic the initially compensatory hypertrophic response evolves towards a pathological condition and heart failure. In this scenario, a therapeutic approach capable of reducing pathological cardiac hypertrophy could be beneficial.

Growth differentiation factor 11 (GDF11) is circulating factor able to reduce cardiac hypertrophy in mice. It is a member of TGF-β family, and it shares a high level of homology with myostatin (MSTN) a well-studied protein that regulates skeletal muscle mass and apparently minimal activity on cardiac mass.

Our data showed different protein levels between cardiac and skeletal muscle tissues revealed a higher abundancy of type I TGF-β receptors (ALK4/5/7) in the heart samples. Moreover, ALK7 receptor knockout induced a significant reduction in SMAD3/4 signaling only after GDF11 treatment. These results showed a differential quantity and use of ALKs receptors, possibly explaining the higher GDF11 sensitivity of cardiomyocytes compared to skeletal myocytes.

Using a model of pressure overload-induced cardiac hypertrophy it was possible to further confirm the anti-hypertrophic activity of GDF11. Interestingly, even if with lower potency, this effect was recapitulated also by MSTN, demonstrating that both peptides have overlapping effects on cardiac tissue. Furthermore, aiming to reduce controversies regarding GDF11 and MSTN serum quantifications, we contributed to develop a novel assay based on mass spectrometry that can discriminate and quantify reliably both proteins. Using this method, it was also possible to identify an age-dependent reduction of both GDF11 and MSTN ligand in mice.

In conclusion, GDF11 and MSTN share a common cardiac anti-hypertrophic activity that was not previously expected. Modulation of GDF11/MSTN signaling pathway can be considered for development of novel therapeutic strategies and new biotherapeutics.

ACKNOWLEDGMENTS

I'm really grateful to Prof. Francesco Loffredo, for the great opportunity to work in the Molecular Cardiology group and for the excellent scientific support over these years. Furthermore, I would like to thank him for taking care of all surgical procedures, for performing the systemic AAV injections and for assessing the hemodynamic data. All these techniques were fundamental to produce the *in vivo* data presented in this work.

I thank Prof. Vincent Segers and Prof. Mauro Giacca, my external supervisors, for all the useful scientific discussions that we had.

I thank Dr. Alessandro Marcello and Dr. Roberto Buccafusca for accepting to evaluate my PhD research work enclosed in this thesis.

I would like to thank Dr. Olga Shevchuk, for helping me to setup the IP protocol and for developing an LC/MS-MS-based method to discriminate GDF11 and MSTN in mice serum.

My gratitude goes also to Giulio Ciucci and Lorenzo Ciacci for their support and their help during several research activities. Without them, *in vivo* experiments would not have reached such elevated number of subjects.

I am grateful to Hashim Ali for helping me during the early years of my PhD and for sharing its knowledge about "quick protocols".

I would like to thank Ambra Cappelletto for the support, especially in finding lost aliquots of Mol Car reagents.

I am grateful to Dr. Simone Vodret and Dr. Matteo Castrichini, respectively, for the acquisition of echocardiographic images and their analysis.

I would like to thank Dr. Antonio Cannata for its help in the intramyocardial AAV9 injection and for its scientific research work.

My gratitude goes also to Dr. Natasa Skoko, Dr. Corrado Guarnaccia and to all members of the Biotechnology Development group for following and helping me during the protein purification steps.

I am grateful to Dr. Lorena Zentilin and Dr. Marina Dapas for their help in obtaining and purifying the AAV preparations.

I would like to thank all the staff of ICGEB Bio-experimentation Facility for their help and availability to house and handle our mice colonies.

I would like to thank Dr. Barbara Argenti for her help to fulfill PhD bureaucracy requests.

A special thanks goes to all the past and present colleagues at ICGEB that helped me in remarkable high number of different ways. In particular, Giulia Bortolussi, Elena Chiavacci, Riccardo Sola, Ilaria Secco, Luca Braga, Edoardo Schneider, Consuelo Torrini, Silvia Moimas, Giulia De Sabbata, Erick Mora Cardenas, Simonetta Sorrentino, Gabriele Massaria and Sara Boer.

Finally, I would like to thank ICGEB for the stimulating research environment and the financial support.

LIST OF CONTENTS

LIST OF FIGURES

LIST OF TABLES

LIST OF ABBREVIATIONS

α-SMA	α-Smooth Muscle Actin
AAV	Adeno-Associated Virus
ACE	Angiotensin Converting Enzyme
ACN	Acetonitrile
ACVR2	Activin Receptor kinase II
AHA	American Heart Association
AKT	AKT Serine/Threonine Kinase
ALK	Activin Like receptor-Kinase
Ang-II	Angiotensin II
ANP	Atrial Natriuretic Peptide
AR	Adrenergic Receptor
AT	Ang-II receptor
β-MHC	β Myosin Heavy Chain
BAP	Biotin Acceptor Peptide sequence
BM40	Basement Membrane protein 40
BMP1	Bone Morphogenic Protein 1
BMP11	Bone Morphogenic Protein 11 also known as GDF11
BNP	Brain Natriuretic Peptide
bp	base pair
BSA	Bovin Serum Albumin
CaMKII	Calmodulin-dependent protein Kinase II
Cas9	CRISPR-associated protein-9 nuclease
CBFHH	Calcium- and Bicarbonate-Free Hanks´ solution with HEPES
CHO	Chinese Hamster Ovary
CHO-F6	CHO-Furin stable clone number 6
CIP	Calf Intestinal Phosphatase
CMV	Cytomegalovirus
CRISPR	Clustered Regularly Interspaced Short Palindromic Repeats
CVD	Cardiovascular Disease
DMEM-HG	Dulbecco‟s modified Eagle‟s medium high glucose
DTT	Dithiothreitol
EC50	Half maximal effective concentration
ECM	Extracellular Matrix
EGF	Epidermal Growth Factor
ERK	Extracellular signal-Regulated Kinase
ET-1	Endotelin-1
ETA	Endotelin-A receptor
FACS	Fluorescence Activated Cell Sorting
FBS	Fetal Bovine Serum
FST	Follistatin
FSTL3	FST-like 3
FT	Flow-Through
GASP	GDF-associated serum protein-1

GC	Genome Copies
GDF11	Growth Differentiation Factor 11
GDF8	Growth Differentiation Factor 8 also known as MSTN
GPCR	G Protein-Coupled Receptor
GSK3	Glycogen Synthase Kinase 3
GW/TL	Gastrocnemius weight/tibia length ratio
h	Hours
hAAT	human α-1-antitrypsin
HBS	Hepes Buffered Saline
HDAC	Histone Deacetylase
HF	Heart Failure
HFpEF	Heart Failure with preserved Ejection Fraction
HFrEF	Heart Failure with reduced Ejection Fraction
His6	Hexa Histidine Tag
HPLC	High Performance Liquid Chromatography
HW/BW	Heart weight/body weight ratio
HW/TL	Heart weight/tibia length ratio
IAA	Iodoacetamide
IC50	Half maximal inhibitory concentration
IGF-1	Insulin like Growth Factor 1
IGF1R	IGF-1 Receptor
IMAC	Immobilized Metal Affinity Chromatography
IP	Immunoprecipitation
JNK	c-Jun N-terminal Kinase
KO	Knock-Out
LB	Luria Bertani
LC-MS/MS	Liquid chromatography tandem mass spectrometry
LV	Left Ventricular
MAB	Monoclonal AntiBody
MAPK	Mitogen Activated Protein Kinase
MCIP1	Myocyte-enriched Calcineurin Interacting Protein 1
MEF2	Myocyte Enhancer Factor 2
MEK	MAPK/ERK Kinase
min	Minutes
MMP	Matrix Metalloproteinase
MSTN	Myostatin
mtDNA	mitochondrial DNA
mTOR	mammalian Target Of Rapamycin
NaB	Sodium Butyrate
NADPH	Nicotinamide Adenine Dinucleotide Phosphate
NCX	Na+/Ca2+ exchanger
NEB	New England Biolabs
NFAT	Nuclear Factor of Activated T cells
NFDM	Non-Fat Dry Milk
NHEJ	Non-Homologous End Joining
Nox4	NADPH oxidase 4
nt	nucleotides

OD_{λ}	Optical Density
ON	Overnight
ORF	Open Reading Frame
PAI-1	Plasminogen Activator Inhibitor-1
PBS	Phosphate Buffer Saline
PCR	Polymerase Chain Reaction
PDPK1	Phosphoinositide-Dependent Protein Kinase-1
PFA	Paraformaldehyde
PGC-1α	Proliferator-activated receptor Gamma Coactivator 1α
PI3K	Phosphoinositide 3-Kinase
PKA	Protein Kinase A
PKC	Protein Kinase C
PKG	cGMP-dependent Protein Kinase
PLN	Phospholamban
PMSF	Phenylmethylsulfonyl fluoride
PRM	Parallel Reaction Monitoring
qPCR	Quantitative PCR
QW/TL	Quadriceps weight/tibia length ratio
RAAS	Renin-Angiotensin-Aldosterone-System
Rb	Rabbit
ROS	Reactive Oxygen Species
RT	Room Temperature
RyR2	Ryanodine Receptor 2
sec	Seconds
SERCA	Sarcoplasmic/Endoplasmic Reticulum Ca2+ ATPase
sgRNA	single guide RNA
SMAD	Mothers Against DPP Homolog
SNP	Single Nucleotide Polimorphism
ss	single stranded
SV40	Polyomavirus simian virus 40
TAC	Transverse Aortic Constriction
TAK1	TGF-β Activated Kinase 1
TCEP	Tris(2-carboxyethyl)phosphine
TFA	Trifluoroacetic Acid
TGFβRI	TGF-β receptor type I
TGFβRII	TGF-β receptor type II
TIMP	Tissue Inhibitor of Metalloproteinase
TLD	Tolloid like
Tm	Melting Temperature
TW/BW	Tibialis weight/body weight ratio
TW/TL	Tibialis weight/tibia length ratio
WAT	White Adipose Tissue
WB	Western Blot
WFIKKN	WAP Follistatin/Kazal Immunoglobulin Kunitz and Netrin Domain Containing
WT	Wild-Type

1. INTRODUCTION

1.1. Aging pressure on world population

For thousands of years, people have struggled to go beyond childhood, reach adult age and, if they survived wars, famine or diseases, die into their 50s or 60s. A progressive, constant improvement in life conditions accompanied by major achievements in the medical field, has drastically changed this perspective in the last decades with people in developed country able to commonly reach their 80s and 90s. This phenomenon is deeply changing the demographics of the world. At the beginning of this century there were already more people aged 60 years or older than 5 years or younger (UaH, 2012) and by 2050 there will be more than 2 billion people older than 60 (United Nations, 2015). In the European Union, according to Eurostat projection, by 2060 almost one third of the population will be over 65 years (European Commission, 2015). A similar trend can be observed in the United States where, in 2014, one person out of seven was older than 65 and, furthermore, the total number of elderly people is estimated to be more than double by 2060 (Administration of Aging, 2015). These projections indicate a strong demographic shift that countries have to take into consideration to reduce their impact on population and economy. Indeed, a 2015 United Nation report, stated “public policies are needed to mitigate the upward pressure on national health care budgets exerted by the rising costs of health care services, and the longer lifespans and increasing numbers of older persons.” (United Nations, 2015). It is important to notice that medical progresses have been able to extend the lifespan of individuals. However, such extension could generate patients with poor quality of life and with extensive health care needs. Thus, a simple reduction of health expenses will not be enough to balance the economic burden of chronic diseases (Harper, 2014). To sensibly reduce healthcare costs, it is crucial to extend the “healthspan” by promoting the healthy aging of the population. Thus, it will be possible to confine the insurgence of severe illness or disabilities in the natural last part of life, improving patients’ quality of life and reducing health care system expenses (Seals and Melov, 2014).

1.2. Impact of aging on tissue function

Aging is a time-dependent progressive decline of cell and tissue functions that decrease the organism fitness, increase its susceptibility to chronic disease and death (Oh et al., 2014)

and represents a major risk factor in the developed world (Harman, 1991). Humans, once they reach the adult age, experience slow but progressive physiological changes and functional impairments (Mitnitski et al., 2001), that during a lifetime result in an exponentially increased incidence of major chronic disease like cardiovascular diseases, neurodegenerative disease, cancer and influenza-associated hospitalization (Fig. 1) (Thompson et al., 2009).

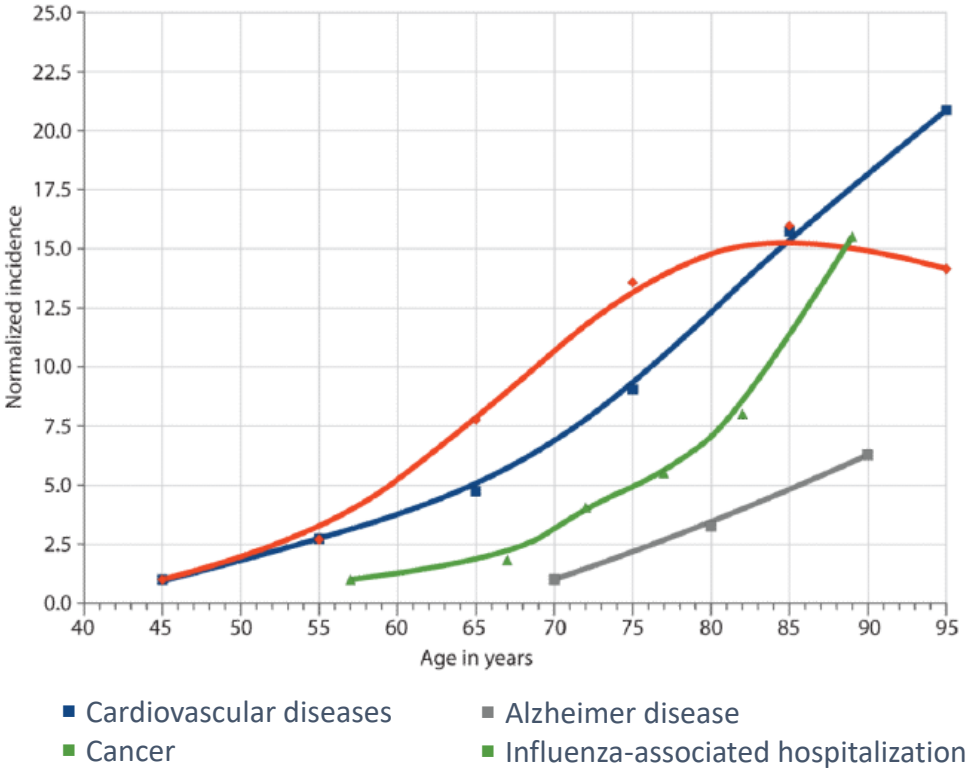

Figure 1: Age-dependent incidence increase of major chronic disease.
Cardiovascular diseases are represented by blue squares, cancer by red diamonds, Alzheimer disease by grey squares and influenza-associated hospitalization by green triangles. Image from (Rae et al., 2010).

The demographic shift described in paragraph 1.1 combined with the increased susceptibly of aged people to chronic and debilitating diseases represent the perfect recipe for a worrying future scenario where chronic disease could reach pandemic proportion. It has been predicted that by 2030, 40% of the population in United States will suffer of at least one form of cardiovascular disease (CVD) (Heidenreich et al., 2011). In parallel, by 2050, neurodegenerative diseases like Alzheimer and Parkinson disease will afflict a significant portion of United States' population with an estimated patient number of 13.8 and 1.3 million respectively (Hebert et al., 2013; Kowal et al., 2013). According to these predictions,

health care expenses for chronic disease will double or triple. Furthermore, the indirect cost of chronic diseases, due to productivity loss of the affected population, is estimated in an extra-cost spanning from 20% to 30% of the previous value. (Hebert et al., 2013; Heidenreich et al., 2011; Kowal et al., 2013).

Effective preventive strategies and treatments able to delay or reduce the deleterious effects of aging are strongly needed to avoid a global aging crisis and to improve quality of life of single individuals.

1.3. Aging and cardiovascular diseases

CVDs are the leading cause of death around the world, responsible of almost 50% of total deaths from non-communicable diseases (World Health Organization, 2014). Aging increases the risk by prolonging the exposure time to deleterious events, but also acting as one of the most important risk factors for developing CVD (North and Sinclair, 2012) (Fig.2).

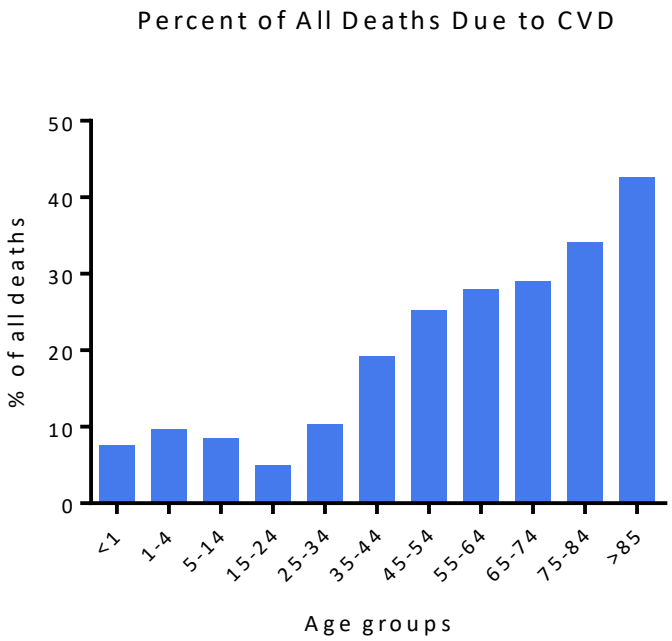

Figure 2: Percent of all deaths due to CVD by age groups (United States, 2008).
Data from (National Heart Lung and Blood Institute, 2012).

In order to understand why CVD and aging are so intertwined, it is important to identify which are the main actors involved, and how those players can exert their deleterious effects in the pathophysiology of the aging heart. It is also important to mention that those players are not working alone; the cardiovascular system is a complex machine with several

compensatory mechanisms that usually prevent its critical failure. While these compensatory events may provide a beneficial effect in the short term, a prolonged exposure to pathological stimuli may produce a vicious circle that ultimately determines heart failure. An overview of changes induced by aging on cardiovascular system is important to understand the magnitude of the problem and to develop strategies to prevent or reduce the burden of age-related CVD.

1.4. Cardiac aging

Normal cardiac aging is characterized by a number of changes at structural and functional levels. A significant increase in cardiomyocyte size accompanied by a decrease in myocyte number secondary to apoptosis together with deposition of extracellular matrix and functional changes at the cellular level can be observed with normal aging (Lakatta and Levy, 2003), contributing to the increased prevalence of cardiovascular diseases in the aging population.

1.4.1. Structural changes with aging

A number of studies on healthy subjects have shown that, even in the absence of classic cardiovascular risk factors, aging is associated with a marked increase in left ventricular (LV) hypertrophy (Gerstenblith et al., 1977; Lakatta and Levy, 2003) (Fig. 3), as shown in both the Baltimore Longitudinal Study on Aging and the Framingham Heart Study (Dai and Rabinovitch, 2009). Aging seems to redistribute asymmetrically muscle tissue within the heart with a more pronounced wall thickness on the interventricular septum compared to the free wall; these structural modification influence its own shape, changing from elliptical to sphere-like shape (Hees et al., 2002).

Aging is also associated to a progressive reduction of cardiomyocyte replication rate (Bergmann et al., 2009; Olivetti et al., 1995). Interestingly, cardiomyocyte apoptosis rate is not affected by aging, but men have a basal apoptosis rate approximately 3-folds higher than women (Mallat et al., 2001). Age-dependent changes in extracellular matrix deposition are another hallmark of the aging heart: interstitial fibrosis, collagen deposition, fibers crosslinking and fibers diameter increase in an age-dependent manner and eventually determine an increase in cardiac stiffness (Gazoti Debessa et al., 2001; Lakatta and Levy, 2003).

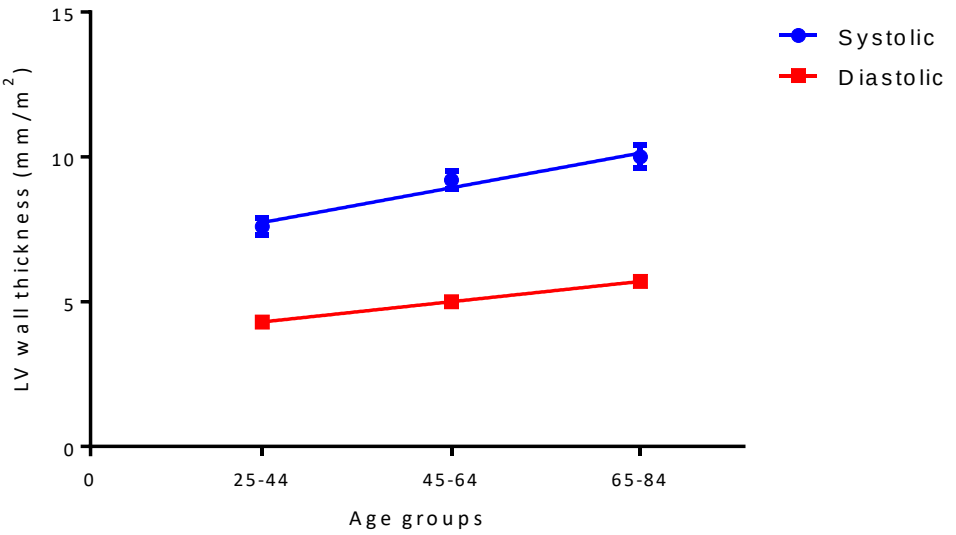

Figure 3: Left ventricular wall thickness increases with age.
Data obtained using M-mode echocardiography in healthy men and women. Data shown as mean ±SEM. Figure data were obtained from (Gerstenblith et al., 1977).

1.4.2. Age-dependent decrease of LV diastolic function

While systolic function is generally maintained with aging, after twenty years old, a slow and progressive reduction of the LV diastolic filling rate can be observed already as early as age 20 years in humans; this decline continues until it reaches, in the last part of life, the 50% of the initial filling rate (Fig. 4A) (Schulman et al., 1992; Swinne et al., 1992). The mechanisms that determine this decrease in function are mainly the maladaptive remodeling of the left ventricle and the prolonged contraction of cardiomyocyte induced by the inefficient re-uptake of Ca^{2+} ions. The net effect is a delay of the early filling of the left ventricle that is compensated by an increased atrial contraction that produces a late diastolic filling and atrial hypertrophy (Swinne et al., 1992).

Impaired ventricular filling is reflected by a shift in the E/A ratio measured by doppler. In healthy condition, the peak E correspond to the early filling of the ventricle and it is responsible for 70/75% of total ventricle filling whereas the peak A, is produced by atrial contraction and it is responsible for the remaining 20/25% of ventricle filling. Aging process impair early ventricle filling and increase active atrial filling of the ventricle shifting the E/A ratio as shown in fig. 4A-C (Lakatta and Levy, 2003).

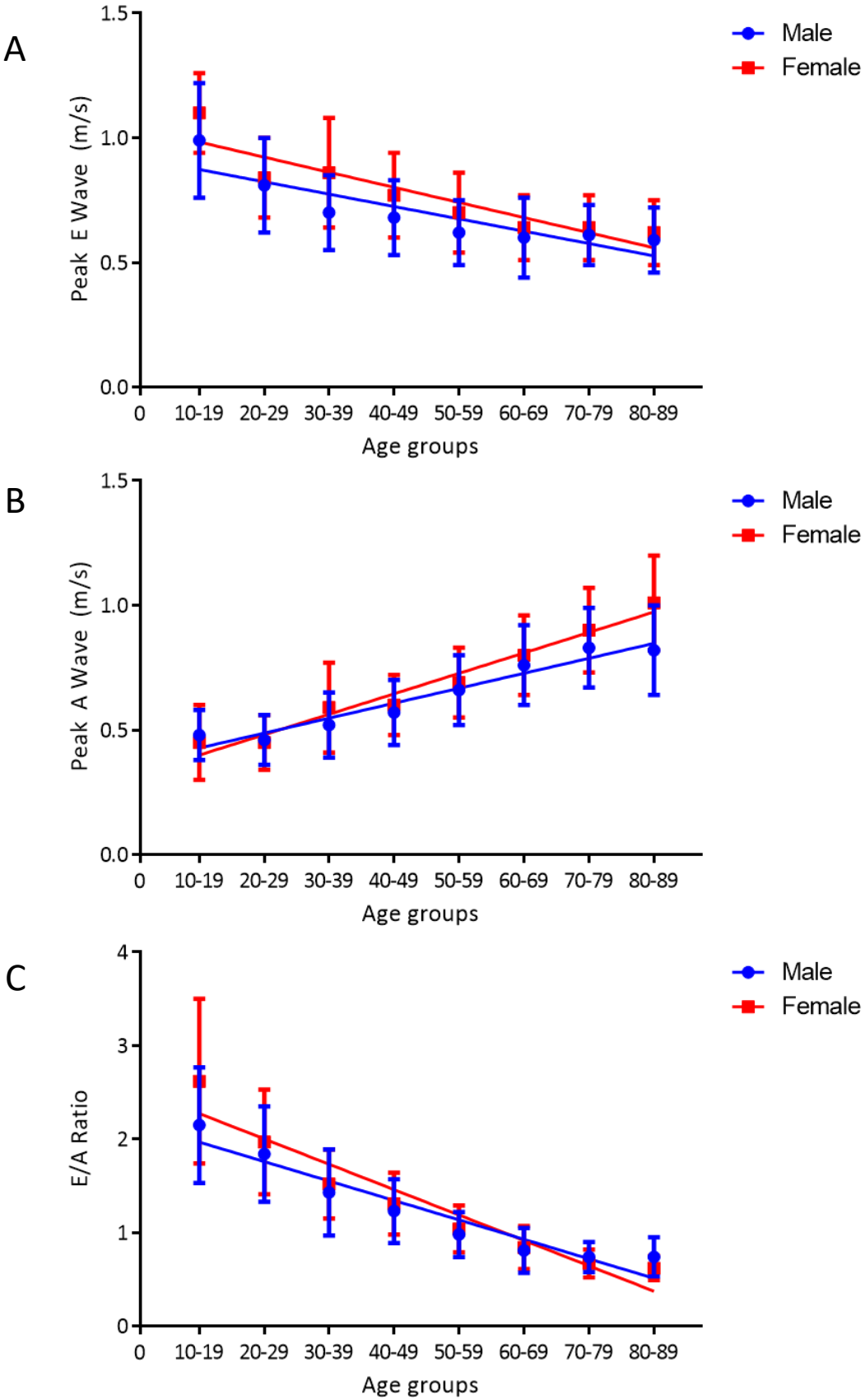

Figure 4: Changes in diastolic filling with age.
(A) Early diastolic left ventricular filling decreases with age.
(B) Late diastolic left ventricular filling induced by atrial contraction increases with age.
(C) E/A ratio declines with age and is associated to decrease of cardiac function.
Figures data were obtained from (Okura et al., 2009).

1.4.3. Heart failure (HF)

Aging is defined as the progressive loss of functionality of cells and organs to maintain proper homeostasis. As described above, age-associated structural and functional changes in the cardiovascular system challenge the cardiac reserve capacity and stress the system until it is not able to provide an adequate blood supply to the body. With time, even mild pathologic stimuli may compromise cardiac function and produce signs and symptoms of HF. HF is ”a complex clinical syndrome that results from any structural or functional impairment of ventricular filling or ejection of blood” as defined by the American Heart Association (AHA) (Yancy et al., 2013). In western world, around 1% of the population with more than 50 years is affected by HF and its incidence increase progressively with age (Redfield et al., 2003). HF diagnosis is often associated to a poor prognosis as it has been defined "More malignant than cancer”, showing a 25% of survival rate after 5 years from first hospitalization (Stewart et al., 2001). Even if mortality remains high, especially in newly diagnosed patients, new approach and drugs have improved HF prognosis, both in men and women (Levy et al., 2002; McMurray et al., 2019; Mehta et al., 2009). Traditionally, HF has been associated to an exhausted heart that is unable to pump enough blood during systole to satisfy organism needs. This type of HF with systolic dysfunction is called HF with reduced ejection fraction (HFrEF), defined by a LV ejection fraction lower than 40% (McDonagh et al., 1997; Yancy et al., 2013). More recently, a growing epidemic of HF with apparently normal systolic function has been observed. This form of HF is characterized by diastolic dysfunction and has been defined as HF with preserved ejection fraction (HFpEF) (Aurigemma et al., 1995; Lam et al., 2007). This condition has a normal sized left ventricle, often but not always with hypertrophy. Approximately 50% of patients hospitalized for heart failure have HFpEF, and similar mortality risk of patients diagnosed with HFrEF. Aging produce a number of changes that challenge the diastolic filling properties of the LV thus contributing to the epidemic of HFpEF (Borlaug and Paulus, 2011; Gottdiener et al., 2012).

1.4.4. HFpEF

HFpEF is a clinical condition characterized by signs and symptoms secondary to the impairment of diastolic properties of the left ventricle accompanied by an ejection fraction higher than 50% (Yancy et al., 2013). Diastolic dysfunction may occur as a consequence of changes that are associated with normal aging like cardiomyocyte hypertrophy, impaired

intracellular calcium handling and cardiac fibrosis. Furthermore, patients with HFpEF are more likely women, obese, affected by hypertension, diabetes, and renal disease, suggesting that multiple pathophysiological mechanisms may be responsible for the onset of HFpEF (Boonman-de Winter et al., 2012; Gottdiener et al., 2012; Shioi and Inuzuka, 2012).

1.4.4.1. Molecular mechanism of HFpEF: LV hypertrophy

Cardiomyocytes hypertrophic response:

Cardiomyocytes occupy approximately 75% of ventricular myocardial volume even if they represent about one-third of the total heart cell number (Nag, 1980; Popescu et al., 2006). Cardiomyocytes are terminally differentiated cells that lose the capacity to proliferate soon after birth, thus postnatal increased heart size is mainly accounted by cardiomyocyte enlargement (Bernardo et al., 2010; Soonpaa et al., 1996). In LV, cardiomyocytes are organized with a spiral orientation to maximize cardiac pump efficiency. Mechanical resistance and coordinated contraction are allowed by intercalated discs presents at both ends of cardiomyocytes providing electrically coupling and strong cell-cell adhesion (Vermij et al., 2017). Cardiomyocyte hypertrophy can be seen as an adaptive process in response to an increased workload; in order to match the needed pumping force, cardiomyocytes have to increase their contraction machinery. Sarcomere is the basic contractile unit of the cardiac muscle and is formed by repeated and extremely organized cluster of actin and myosin proteins (thin and thick filaments, respectively) (LeWinter et al., 2007). Depending on the initiating stimulus, sarcomeres could be added in series, increasing the cardiomyocyte length, or in parallel, increasing cardiomyocyte width. The former process is associated to an eccentric hypertrophy, characterized by increased cardiac mass and chambers volume and the latter is associated to an increased wall thickness and small reduction or no change in chambers volume (Bernardo et al., 2010). Interestingly, both eccentric and concentric hypertrophy are associated to both physiological and pathological cardiac hypertrophy (Bernardo et al., 2010).

Physiological and pathological hypertrophy

Laplace's law (Fig. 5) provides a mathematical formula to explain why thickening of LV wall is beneficial in case of mechanical load increment.

$$\text{LV wall stress} = \frac{\text{LV pressure} \times \text{LV radius}}{2 \times \text{LV wall thickness}}$$

Figure 5: Mathematical representation of Laplace's equation.
Figure generated using http://www.hostmath.com/.

Depending on a great variety of extrinsic and intrinsic stimuli, cardiomyocytes can develop two different types of LV hypertrophy, described as physiological and pathological LV hypertrophy (Frey and Olson, 2003).

Physiological hypertrophy is an adaptive remodeling of the heart as a consequence of increased demand in endurance training athletes and in pregnant women (Eghbali et al., 2006; Maron and Pelliccia, 2006). Physiologic remodeling is characterized by harmonic increase of cardiac walls and internal chambers volume, absence of fibrosis or increased cardiomyocytes deaths and improved cardiac function (Heineke and Molkentin, 2006). Pathological hypertrophy is a maladaptive cardiac remodeling secondary to a series of pathological stimuli and is present in patients affected by HFpEF (Melenovsky et al., 2007). While sharing some central hypertrophic pathways with physiological remodeling, pathological hypertrophy is accompanied by the presence of fibrosis, increased cardiomyocytes deaths and cardiac dysfunction (Heineke and Molkentin, 2006). In addition, in pathological remodeling a transcriptional shift that induces expression of the fetal gene program can be observed; that includes among others atrial natriuretic peptide (ANP), brain natriuretic peptide (BNP), α-skeletal actin and β-myosin heavy chain (β-MHC) (Frey and Olson, 2003).

While one of the differences between pathological and physiological hypertrophy could be found respectively in chronic or intermittent increased workload exposure (Bernardo et al., 2010), the intrinsic nature of the mechanical stress could represent the driving force that determine the insurgence of different forms of cardiac hypertrophy (McMullen et al., 2004; Perrino et al., 2006).

Pathways involved in cardiac hypertrophy:

Heart growth is the final event of an extremely complicated mechanism where deeply intertwined and regulated pathways interact to regulate cardiac size. Generation and characterization of transgenic and knock-out (KO) animals have helped to understand the responsible pathways and regulators involved. In the following sections the main biological pathways involved in development cardiac hypertrophy will be described. However, is important to mention that differences in hypertrophic stimuli, presence of compensatory responses from redundant proteins isoforms, different localization of overexpressed proteins or dissimilar response among KO and dominant negative mutants, have hindered a complete understanding of the mechanisms involved and some findings need further studies to be clarified (Bernardo et al., 2010).

- *IGF-1/PI3K/AKT/GSK3 pathway*

  The insulin like growth factor 1 (IGF-1) pathway, summarized in table 1A-B, aside its central role in the aging process, is one of the main regulator of physiological hypertrophy response (Kim et al., 2008; Noh et al., 2015; Shioi et al., 2000). However, exaggerate activation of this pathway can rapidly exhaust the heart and lead to HF (Delaughter et al., 1999).

  Proper pathway regulation is crucial to modulate myocardial adaptation in response to mechanical stress, balancing physiological and pathological remodeling. Several protein isoforms, activated by the same upstream protein, could lead to complete different type of cardiac hypertrophy. For example phosphoinositide 3-kinase PI3K *(p110α)* is involved in physiological hypertrophy, instead PI3K *(p110γ)* plays a role into pathological hypertrophy (Bernardo et al., 2010; McMullen et al., 2003; Oudit and Kassiri, 2007). Furthermore, glycogen synthase kinase 3 (GSK3)-α and GSK3-β are both phosphorylated by AKT, but the former phosphorylated protein is protective against pressure overload induced hypertrophy, instead the latter phosphorylated protein has the opposite effect in response to the same stimuli (Matsuda et al., 2008). Understand the exact mechanism of these interactions and how they are modulated by other signaling cascade is an area of intense research.

- *Calcium-related pathways: Calcineurin/NFAT and CaMKII signaling*

  Calcium-related pathways are summarized in table 2A-B. Their activation is strongly associated to a rapid development of cardiac hypertrophy and fibrosis and progress towards HF (Molkentin et al., 1998; Wilkins et al., 2004). Indeed, impaired calcium handling not only affects heart contractility and relaxation but also induces calmodulin activation that, in turn, stimulate both calcineurin and Ca^{2+}/calmodulin-dependent protein kinase II (CaMKII).

  The former seems to play a central role in hypertrophic pathways, leading to nuclear factor of activated T cells (NFAT) activation that can modulate other transcription factors as GATA4, myocyte enhancer factor 2 (MEF2) (Molkentin et al., 1998). Changes in the activity of the above-mentioned transcription factors can affect expression of numerous cardiac genes, inducing epigenetic modification via histone deacetylase (HDAC) and promoting the reactivation of the fetal gene program (Dirkx et al., 2013). Interestingly, calcineurin/NFAT signaling seems to be involved only in pathological hypertrophy, but further studies are required to clarify the role of myocyte-enriched calcineurin interacting protein 1 (MCIP1). MCIP1 inhibit calcineurin activity, but seems to modulate cardiac hypertrophy differently according to nature of hypertrophic stimulus (Rothermel et al., 2001; Vega et al., 2003).

  The latter is another important mediator of cardiac hypertrophy in presence of overload stimuli (Backs et al., 2009). Cardiac specific overexpression of both CaMKIIδ B and C isoforms showed profound cardiac hypertrophy in mice, fetal gene program expression and calcium handling impairment, although each one shows a different mechanisms (Zhang et al., 2002; Zhang et al., 2003). Interestingly, hyperphosphorylation of phospholamban (PLN) induced by CaMKIIδ C seems to be insufficient to compensate the decreased expression of sarcoplasmic/endoplasmic reticulum Ca^{2+} ATPase (SERCA) and aberrant function of hyperphosphorylated ryanodine receptor 2 (RyR2) (Zhang et al., 2003).

- *G protein-coupled receptors (GPCRs) in hypertrophic signaling*

  GPCRs are receptors with seven transmembrane α-helices that are extremely important in signal transduction of external stimuli. When an agonist binds a GPCR, the G protein heterotrimeric complex dissociate in two subunits, Gα and Gβγ, and both can initiate

the signaling cascade. In particular, $G\alpha_q/G\alpha_{11}$, $G\alpha_s$ and $G\alpha_i$ are the most important subunits for cardiac hypertrophic response (Frey and Olson, 2003). Angiotensin II (Ang-II) receptor, endotelin-1 (ET-1) receptor, α-adrenergic receptors (α-ARs) and β_1-ARs transduce their activation through $G\alpha_q/G\alpha_{11}$, whereas β_2-ARs coupled to $G\alpha_s$ and $G\alpha_i$ (Bernardo et al., 2010). Effects of activation of these receptors are summarized in table 3.

The activation of the adrenergic cascade seems to activate an adaptive cardiac hypertrophy response to counteract the increased mechanical overload mainly through β_1-AR. However, prolonged β_1-AR stimulation is detrimental for the heart (Engelhardt et al., 1999). Of note, reduction of β-AR desensitization seems to restore a more physiological state and improve cardiac function in presence of severe cardiomyopathies (Rockman et al., 2002).

The role of Ang-II receptors in cardiac hypertrophic seems to be of secondary importance when compared to their role in fibrosis development (Billet et al., 2008). Finally, although ET-1 receptors blockade *in vitro* and *in vivo* has showed protecting results against cardiac hypertrophy, clinical trials revealed that this approach is associated to frequent side effects (Bernardo et al., 2010).

- *Mitogen activated protein kinase (MAPK) pathways*

  MAPKs are an evolutionary family of serine/threonine kinase that are involved in numerous steps of organism development and cell homeostasis. Indeed, MAPKs are functional nodes that collect and transduce signals from a great variety of stimuli as growth factors, GPCR, cytokine and cellular stress (Rose et al., 2010). MAPK family could be divided into three subfamilies called: extracellular signal-regulated kinase (ERK), c-Jun N-terminal kinase (JNK) and p38 MAPK (Rose et al., 2010). How these subfamilies are able to affect cardiac hypertrophy is summarized in table 4 A-B.

  Briefly, despite some contrasting results, ERK pathway seems not to be critical for cardiac hypertrophy progression, however ERK2 inhibition seems to be stimulate in eccentric hypertrophy usually associated to endurance exercise (Kehat et al., 2011; Ulm et al., 2014). Interestingly also another ERK protein, ERK5, is involved in eccentric cardiac hypertrophy development (Nicol et al., 2001). On the other hand, ERK5 null mice show

reduction of pressure overload-induced cardiac hypertrophy probably due to MEF2 downregulation. (Kimura et al., 2010).

JNK role in cardiac hypertrophy is less clear, probably different nature of hypertrophic stimuli and redundancy of JNK isoforms are the main reason for this lack of consistence among studies (Rose et al., 2010). Indeed, a single deletion of JNK 1/2/3 show no change in cardiac hypertrophy progression (Tachibana et al., 2006). However, JNK activity is able to antagonize calcineurin/NFAT pathway increasing NFAT phosphorylation and blocking its transcriptional activity (Liang et al., 2003).

Similarly to JNK, p38 MAPK has numerous contrasting results that reflect mechanism complexity. Cardiac-specific expression of dominant negative p38 MAPK, MAPK/ERK kinase 3 (MEK3) and MEK6 showed increased cardiac hypertrophy in response to hypertrophic stimuli, suggesting a protecting role of p38 MAPK (Braz et al., 2003). On the other hand, in a second study, increased activity of MEK3 and MEK6 strongly activated p38 MAPK resulting in cardiac hypertrophy but associated to marked remodeling and fibrosis (Liao et al., 2001). Furthermore, p38 MAPK inhibition seems to be have a part into cardioprotective effects induced by estrogen in patients with HF (Satoh et al., 2007). Taken together, these results do not show a pivotal role of p38 MAPK activation in cardiac hypertrophy, but they are more involved in cardiac remodeling, fibrosis and HF progression.

IGF-1/PI3K/AKT/GSK3 pathway				
Protein	Role in pathway regulation	Experimental setup	Effects on cardiac hypertrophy	Reference
IGF-1	Ligand of IGF-1 receptor (IGF1R) and main pathway activator	Overexpression with α-skeletal actin promoter	At 10 weeks of age, mice show physiologic cardiac hypertrophy and increased systolic function. However, at 12 months of age, mice show pathologic cardiac hypertrophy and impaired cardiac function.	(Delaughter et al., 1999)
IGF1R	Main pathway receptor	Overexpression with α-MHC promoter	At 3 months of age, mice show physiologic cardiac hypertrophy and increased systolic function. At 12/16 months of age, mice continue to show features of physiological hypertrophy.	(McMullen et al., 2004)
IGF1R	Main pathway receptor	Cardiomyocyte specific KO	Exercise-induced hypertrophy is prevented.	(Kim et al., 2008)
PI3K (p110α)	Lipid kinase activated by IGF1R and GPCR.	Constitutively active protein overexpressed with an α-MHC promoter	Mice show cardiac hypertrophy with physiologic features.	(Shioi et al., 2000)
PI3K (p110α)	Lipid kinase activated by IGF1R and GPCR.	Dominant negative protein overexpressed with an α-MHC promoter	Mice that undergoes through pressure overload show increased cardiac hypertrophy. Mice that undergoes to physical exercise show reduced cardiac hypertrophy.	(McMullen et al., 2003)

Table 1A: Regulation of IGF-1 pathway in hypertrophy response.

IGF-1/PI3K/AKT/GSK3 pathway				
Protein	Role in pathway regulation	Experimental setup	Effects on cardiac hypertrophy	Reference
PI3K (p110γ)	Lipid kinase coupled to GPCR	KO mice	Mice show enhanced contractile function and cardiac hypertrophic protection from chronic adrenergic activation (due to a secondary mechanism on β-AR). In parallel, mice show accelerated pathological progression against pressure overload stimulus.	(Bernardo et al., 2010)
Phosphoinositide -dependent protein kinase-1 (PDPK1)	Mediator kinase activated by PI3K	Cardiomyocyte specific heterozygous KO	Exercise-induced hypertrophy is prevented but not exercise-induced mitochondrial adaptations.	(Noh et al., 2015)
AKT1	AKT1 is activated by PDPK1 downstream of PI3K but also GPCR	KO mice	Mice show blunt cardiac hypertrophy in response to exercise but in case of pressure overload mice develop an exacerbated cardiac hypertrophy.	(DeBosch et al., 2006b)
AKT2	AKT2 is activated by PDPK1 downstream of PI3K but also GPCR	KO mice	Mice show no change in cardiac hypertrophy after pressure overload but show increased apoptosis sensitivity.	(DeBosch et al., 2006a)
GSK3-α	GSK3 activity is reduced by AKT phosphorylation	Situ-specific mutation that disrupt AKT phosphorylation site	Transgenic mice show increased cardiac hypertrophy after pressure overload.	(Matsuda et al., 2008)
GSK3-β	GSK3 activity is reduced by AKT phosphorylation	Situ-specific mutation that disrupt AKT phosphorylation site	Transgenic mice show protection from cardiac hypertrophy after pressure overload.	(Matsuda et al., 2008)

Table 1B: Regulation of IGF-1 pathway in hypertrophy response.

Calcium-related pathways: Calcineurin/NFAT and CaMKII signaling				
Protein	Role in pathway regulation	Experimental setup	Effects on cardiac hypertrophy	Reference
Calcineurin	Serine-threonine phosphatase activated by calmodulin. NFAT is one of its targets	Constitutively active protein overexpressed under control of α-MHC promoter	Rapid progression of a severe pathological cardiac hypertrophy that evolve in HF.	(Molkentin et al., 1998)
Calcineurin	Serine-threonine phosphatase activated by calmodulin. NFAT is one of its targets	NFAT-luciferase reporter transgenic mouse	NFAT-luciferase activity was present in pathological remodeling but not physiological remodeling.	(Wilkins et al., 2004)
NFAT3	Transcription factor, dephosphorylated can translocate into nucleus	Overexpression under control of α-MHC promoter	No effects on cardiac hypertrophy.	(Molkentin et al., 1998)
NFAT3	Transcription factor, dephosphorylated can translocate into nucleus	Constitutively active protein overexpressed under control of α-MHC promoter	Progression of severe pathological cardiac hypertrophy.	(Molkentin et al., 1998)

Table 2A: Regulation of calcium-related pathways in hypertrophy response.

Calcium-related pathways: Calcineurin/NFAT and CaMKII signaling				
Protein	Role in pathway regulation	Experimental setup	Effects on cardiac hypertrophy	Reference
MCIP1	Inhibitor of calcineurin activity	Overexpression under control of α-MHC promoter	Inhibited cardiac hypertrophy induced by calcineurin activation, adrenergic stimulation and exercise.	(Rothermel et al., 2001)
MCIP1	Inhibitor of calcineurin activity	KO mouse	Exacerbate hypertrophic response in response to constitutive calcineurin activation, but blunted hypertrophy in response to pressure overload or chronic adrenergic stimulation.	(Vega et al., 2003)
CaMKII δ-isoform	Kinase regulated by calmodulin	CaMKIIδ null mice (Cre-loxP)	Inhibition of pathological cardiac hypertrophy induced by pressure overload.	(Backs et al., 2009)
CaMKIIδ B and C isoforms (respectively, nuclear and cytoplasmic isoforms)	Kinase regulated by calmodulin	CaMKIIδ isoforms overexpressed under control of α-MHC promoter	Transgenic mice show pathological cardiac hypertrophy, fetal program expression, reduced contractility and altered Ca^{2+} handling.	(Zhang et al., 2002; Zhang et al., 2003)

Table 2B: Regulation of calcium-related pathways in hypertrophy response.

G protein-coupled receptors (GPCR) in hypertrophic signaling				
Protein	Role in pathway regulation	Experimental setup	Effects on cardiac hypertrophy	Reference
Ang-II receptor (AT)1_a, $AT1_b$, AT2	Ang-II receptors	Single, double, triple KO mice	Lack of both AT1 receptor is associate to cardiac atrophic response. Ang-II-induced decrease in coronary flow and left ventricular systolic pressure is abolished in all genotypes deficient for $AT1_a$.	(van Esch et al., 2010)
$AT1_a$	Ang-II receptor	Constitutively active protein knock-in mice	Absence of cardiac hypertrophy, strong induction of cardiac fibrosis and diastolic dysfunction.	(Billet et al., 2007)
Endothelin-A receptor (ETA)	ET-1 receptor	Endothelin-A receptor antagonist	ETA blockage inhibits cardiac hypertrophy and β-MHC isoform increase in presence of pressure overload.	(Ichikawa et al., 1996)
β_1-AR	Predominant cardiac AR, stimulated by adrenaline and noradrenaline.	Overexpression under control of α-MHC promoter	Marked cardiac hypertrophy associated to increased short-term cardiac contractility. Long-term β_1-AR activation leads to impaired cardiac contractility and HF.	(Engelhardt et al., 1999)
β_1-AR and β_2-AR	AR stimulated by adrenaline and noradrenaline	Double KO mice	Cardiac hypertrophy and fibrosis are reduced after pressure overload.	(Kiriazis et al., 2008)
β_2-AR	AR stimulated by adrenaline and noradrenaline. Coupled to $G\alpha_s$ and $G\alpha_i$	Overexpression under control of α-MHC promoter	Following pressure overload, cardiac hypertrophy was comparable to control animals, however transgenic mice show increased fibrosis and accelerated HF progression.	(Du et al., 2000)

Table 3: Regulation of GPCR signaling in hypertrophy response.

Mitogen activated protein kinase (MAPK) pathways				
Protein	Role in pathway regulation	Experimental setup	Effects on cardiac hypertrophy	Reference
MEK1	Induce activation of ERK1/2	$ERK1^{-/-}$ $ERK2^{fl/fl}$ compared with $ERK1^{-/-}$ $ERK2^{fl/fl—NKx\text{-}Cre}$ mutant mice in MEK1 constitutively activated mice	Both single and double KO animals develop cardiac hypertrophy in response to different stimuli. However, the former mutant develops concentric hypertrophy and the latter eccentric hypertrophy.	(Kehat et al., 2011)
ERK1/2	Effectors or ERK pathway	$ERK1^{-/-}$ $ERK2^{+/-}$ double mutant mice	Double mutant mice show no impairment of physiological or pathological cardiac hypertrophy progression.	(Purcell et al., 2007)
ERK2	Main effector of ERK pathway. ERK2 is the 70% of total cardiac ERK1/2	$ERK2^{fl/fl}$ with Cre expression under control of myosin light chain 2v promoter	Mice shows impairment of pathological cardiac hypertrophy due to different stimuli, but no impairment of exercise-induced cardiac hypertrophy.	(Ulm et al., 2014)
ERK5	Effectors or ERK pathway	Constitutively active protein overexpressed under control of α-MHC promoter	Transgenic mice develop an eccentric cardiac hypertrophy that evolved in dilated cardiomyopathy and HF.	(Nicol et al., 2001)
ERK5	Effectors or ERK pathway	$ERK5^{fl/fl}$ with Cre expression under control of α-MHC promoter	Absence of ERK5 is protective against pressure overload-induced cardiac hypertrophy.	(Kimura et al., 2010)

Table 4A: Regulation of MAPK pathways in hypertrophy response.

Mitogen activated protein kinase (MAPK) pathways				
Protein	Role in pathway regulation	Experimental setup	Effects on cardiac hypertrophy	Reference
JNK 1/2/3	Main effectors of JNK pathway	Single KO mice	All mice KO show no impairment of pathological cardiac hypertrophy progression following pressure overload.	(Tachibana et al., 2006)
JNK 1/2	Main effectors of JNK pathway	Double dominant negative JNK1/2 overexpression under control of α-MHC	JNK1/2 dominant negative induced an increase of cardiac hypertrophy in response to pressure overload.	(Liang et al., 2003)
MEK3 and MEK6	Main cellular activator of p38 MAPK	Dominant negative overexpression of MKK3 or MKK6 under control of α-MHC promoter	Increased cardiac hypertrophy following pressure overload, chronic adrenergic stimulation and Ang-II.	(Braz et al., 2003)
MEK3 and MEK6	Main cellular activator of p38 MAPK	Constitutively active protein overexpressed under control of α-MHC promoter	Unchanged cardiac hypertrophy but marked fibrosis and expression of the fetal gene program.	(Liao et al., 2001)
P38 MAPK	Main effectors of p38 MAPK pathway	Dominant negative protein overexpression with α-MHC promoter	Increased cardiac hypertrophy following pressure overload, adrenergic and Ang-II stimulation.	(Braz et al., 2003)

Table 4B: Regulation of MAPK pathways in hypertrophy response.

1.4.4.2. Molecular mechanism of HFpEF: increased myocyte stiffness

Role of titin in myocyte stiffness

Titin is an enormous protein, with a canonical isoform of almost 4MDa, and it is a major determinant of myocyte stiffness (LeWinter and Granzier, 2010). This protein mechanically links Z disk to the M band of sarcomere and, thanks to its spring-like function, creating passive tension in the cardiomyocytes. Within the I region of the sarcomere, there is a titin N-terminal region that contains several tandem repeats of immunoglobulin-like domains working as the functional structure of this molecular spring (Helmes et al., 1999). Titin stiffness is modulated by protein phosphorylation, for example activity of protein kinase A (PKA) and cGMP-dependent protein kinase (PKG) decrease stiffening (residue S469 of N2B sequence), while phosphorylation by protein kinase C (PKC) increase passive stiffness (S1178 of PEVK sequence) (LeWinter and Granzier, 2010). Of note, increase of S1178 phosphorylation and decrease of S469 phosphorylation have been found in patients affected by HFpEF but not in hypertensive patients suggesting that titin alterations are involved in HFpEF development (Zile et al., 2015).

1.4.4.3. Molecular mechanism of HFpEF: changes in myocardial interstitium

Healthy myocardial interstitium

In a normal state, cardiac interstitium organizes cardiac muscle fibers providing mechanical support and allowing cardiomyocytes to develop electrical coupling and maintains contact with microvasculature (Berk et al., 2007). Interstitial collagen-based cardiac matrix network is not a simple cell scaffold but it is important for efficient cardiac function. Tensile strength is conferred by thick fibers of type I collagen whereas type III collagen has thin fibers that maintains network elasticity. Type I and type III collagen are, respectively, the 85% and the 11% of the total heart collagen (Weber, 1989). It is important to remember that in addition to collagens, the extracellular matrix (ECM) contains numerous glycosaminoglycans and glycoproteins that could interact and stores a significant amount of latent growth factors and proteases (Ignotz and Massague, 1986; Rifkin et al., 1999).

Cardiac fibroblasts are most abundant interstitial cell type in the adult mammalian heart and are the main responsible for ECM production and maintenance (Eghbali et al., 1989). After birth, the total number of fibroblasts increase markedly probably due to the increase

mechanical stress by elevated LV pressure (Banerjee et al., 2007), but after this period, during the young adult phase of life, fibroblast enter in a quiescent state showing no proliferation or inflammation activation. Less important in number but crucial for cardiac health are another group of cells present in the cardiac interstitium as vasculature cells (endothelial cells, smooth muscle cells, pericytes) and immune system cells (mast cells and macrophages) (Banerjee et al., 2007; Gersch et al., 2002).

Myocardial interstitial fibrosis

As already described in paragraph 1.4.1, aging increases myocardial interstitial fibrosis and this process is a major contributor to cardiac stiffness and diastolic dysfunction. Systolic and diastolic function are impaired by fibrosis at several levels:

- Mechanical: increased heart stiffening forces the cardiac muscle to perform stronger contractions promoting LV hypertrophy. In addition, myocardial elasticity reduction impacts on diastolic function and on passive coronary blood flow, respectively reducing the total volume ejected for each stroke and reducing the volume of blood that perfuses the heart (Kong et al., 2014).
- Electrical: collagen deposition can disrupt the electrical coupling between cardiomyocytes, increasing the risk of developing a non-coordinated heart contraction, arrhythmias and formation of re-entry circuits (Brown et al., 2005).
- Physiological: collagen deposition around intracoronary arterioles reduces oxygen diffusion towards myocytes increasing cardiomyocytes apoptosis rate. After death, cardiomyocytes are replaced by fibroblasts that increase ECM deposition and fuel a detrimental loop that furtherly exacerbate reduction of coronary reserve and myocyte health (Brown et al., 2005; Galiuto et al., 2006).

Cardiac fibrosis is the final result of an excess of matrix protein deposition due to ECM turnover alteration. On one side, collagen and fibronectin production, regulated by several growth factors, in particular by transforming growth factor-β (TGF-β) (Ignotz and Massague, 1986), increases with age; on the other side aging reduces ECM proteolytic degradation that is regulated by the balance of matrix metalloproteinases (MMPs)/tissue inhibitor of metalloproteinases (TIMPs) (Kong et al., 2014).

Fibroblasts are the major regulators of ECM, controlling protein secretion and degradation. With aging, injury or cardiac hypertrophy, fibroblasts transdifferentiate into myofibroblasts with a more pronounced secretory phenotype (Chen and Frangogiannis, 2010). TGF-β stimulation seems to have a central role in myofibroblasts transdifferentiation (Desmouliere et al., 1993). Myofibroblasts are characterized by α smooth muscle actin (α–SMA) expression and they control several aspects of cardiac remodeling and inflammatory response. Indeed, myofibroblasts show a marked increase in ECM protein and cytokines secretion and elevated susceptibility to chemokine induced migration compared to normal fibroblast (Baum and Duffy, 2011).

MMPs and TIMPs plasma levels also change with aging: MMP-2, MMP-7, TIMP-1, TIMP-2 and TIMP-4 increase and MMP-9 levels decrease. Increased TIMPs concentration is sufficient to inhibit MMPs activity resulting in environment prone to ECM protein accumulation (Bonnema et al., 2007). Indeed, increased TIMP-1 serum levels are associated to increased LV mass and wall thickening in humans and are is a major risk factor for cardiovascular diseases (Hansson et al., 2009).

1.4.4.4. Molecular mechanism of HFpEF: Ang-II and TGF-β signaling pathways

Ang-II is a key factor for cardiac fibrosis, and it is a part of the renin-angiotensin-aldosterone system (RAAS). Ang-II is processed and activated by renin and angiotensin converting enzyme (ACE), both enzymes are produced from activated macrophages and fibroblasts (Kong et al., 2014). Ang-II acts in an autocrine and paracrine manner stimulating fibroblast proliferation, collagen deposition and cardiomyocyte hypertrophy through AT1 activation (Crabos et al., 1994; Sadoshima and Izumo, 1993). Furthermore, Ang-II directly stimulates TGF-β expression and potentiates its signaling (Sadoshima and Izumo, 1993). Blockage of AT1 and ACE-inhibitors treatments were beneficial in pressure-overload hypertrophy models and in HFpEF patients, underlining the importance of this pathway for reducing fibrosis and mortality (Fu et al., 2012; Regan et al., 1997).

TGF-β is one of the most important factors for fibroblast activation and ECM accumulation. TGF-β is markedly associated to cardiac fibrosis indeed, it is responsible for myofibroblast transdifferentiation, increased synthesis of ECM proteins, protease inhibitors like TIMPs or plasminogen activator inhibitor-1 (PAI-1) and decreased expression of MMPs (Desmouliere et al., 1993; Ignotz and Massague, 1986; Kong et al., 2014).

TGF-β is normally present in the ECM in its latent form and, as reviewed in (Annes et al., 2003), the latent complex itself could be described as a sensor that regulates TGF-β release in response to several stimuli like ECM degradation, oxidative stress or acidic environment. TGF-β ligand binds exclusively a tetramer receptor composed by a first homodimer of TGF-β receptor type II (TGFβRII) and second homodimer of TGFβRI (also known as activin-like receptor kinase 5 (ALK5)). After receptor formation and ligand binding, the canonical TGF-β pathway is activated by type I receptor that phosphorylates SMAD2/3 that recruit SMAD4 and translocate in the nucleus to modulate expression of hundreds of genes (Leask, 2015). Canonical TGF-β pathway seems play an important role into fibrotic process. Indeed, TGF-β neutralizing antibody shows marked reduction in ECM deposition and improved wound healing (Shah et al., 1994) and SMAD3 KO mice show marked fibrosis reduction although density of infiltrated myofibroblast at injury site was significantly increased (Bujak et al., 2007). SMAD3-KO-dependent reduction in cardiac remodeling is probably due to lower cytokine, chemokine expression and decrease in fibroblast production of collagen and tenascin-c (Bujak et al., 2007). Interestingly, TGF-β canonical pathway could be modulated by crosstalk of non-canonical pathways as ERK, AKT, TGF-β activated kinase 1 (TAK1)/JNK/p38 MAPK affecting the outcome of fibrosis process (Leask, 2015).

However, non-canonical pathways have not been extensively studied in cardiac fibrosis and, probably due to elevated system complexity, some proteins have contrasting results. As example, TAK1 has been considered cardioprotective from Liu group (Li et al., 2015), but results from Schneider group show that TAK1 activation after pressure-overload result is sufficient to induce HF (Zhang et al., 2000). Probably, age of animals, different promoter and treatment timing could be the explanation for these results discrepancy.

1.4.4.5. Molecular mechanism of HFpEF: Oxidative stress and aged mitochondria

Heart and vasculature have an increase of oxidative stress during aging (Judge et al., 2005; Ungvari et al., 2007). Oxidative stress is caused by unbalanced production and degradation of reactive oxygen species (ROS) that are able to interact and damage all type of cellular macromolecules. Mitochondria are main cellular source of ROS and reducing mitochondrial ROS exposure overexpressing mitochondrial targeted catalase has proved to prolong mice life span, improving diastolic function and reducing cardiac fibrosis (Dai et al., 2009; Schriner et al., 2005). Furthermore, ROS can interact with mitochondrial DNA (mtDNA)

causing random point mutation and deletion leading to an accelerated aging process and impaired respiratory chain function (Trifunovic et al., 2004; Vermulst et al., 2008). Similarly in humans, dysfunctional mitochondria and mtDNA mutations accumulate with age (Corral-Debrinski et al., 1992). Dysfunctional mitochondria have inefficient respiratory chain electron transfer that simultaneously decrease oxidative phosphorylation and increase ROS production through electron leakage as reviewed by (Dai et al., 2012). Heart is an extremely active organ and cardiomyocyte need elevated and constant ATP concentration mitochondria. Thus, damaged mitochondria has to be removed and replaced in a continuous turnover to grant adequate energy levels and low ROS production but efficient macroautophagy decrease with age (Dai et al., 2012; Rubinsztein et al., 2011). As explained in the mitochondrial-lysosomal axis theory of aging, if damaged mitochondria are not repaired properly could undergo to clonal expansion and displace the healthy mitochondria population (Terman et al., 2010). In this scenario, cardiomyocytes are gradually left with an increasing number of dysfunctional mitochondria that are not able to provide enough energy for contraction and homeostasis exacerbating cardiomyocyte stress and promoting cardiac hypertrophy and HF as reviewed in (Goffart et al., 2004). Furthermore, increased oxidative stress is also associate with increased activation of MMPs and decrease collagen expression (Siwik et al., 2001). Increased ECM degradation is not the only effect of activated MMPs on cardiac remodelling: their protease activity could activate others signalling precursors or indirectly, could release cytokine and growth factors entrapped in ECM as described in (Lu et al., 2011).

One of these factors entangled in ECM is TGF-β and it play an important role in regulating fibroblast oxidative stress. Indeed, TGF-β signalling stimulates expression of NADPH oxidase 4 (Nox4) and its superoxide production in cardiac fibroblast (Cucoranu et al., 2005). Nox4 increase intracellular oxidative stress and modulate long-term phosphorylation of SMAD 2/3 inducing irreversibly fibroblast to myofibroblast transdifferentiation (Cucoranu et al., 2005). Interestingly, Nox4-induced cardiac remodelling and hypertrophy seems to be modulated through AKT/mTOR and NFκB pathways activation (Zhao et al., 2015).

1.4.4.6. Molecular mechanism of HFpEF: Calcium signalling and diastolic relaxation

As already mentioned in paragraph 1.4.2 diastolic dysfunction is associated to an impaired LV filling and reduced coronaries perfusion, principally because the heart is unable to relax

properly. Impaired calcium reuptake, together with cardiac stiffening, are the main reasons for reduced and delayed cardiomyocytes relaxation.

Cardiomyocytes, as other muscular cells, undergo through contraction when Ca^{2+} is released from sarcoplasmic reticulum activating myosin-actin interaction and force generation. Subsequently cytoplasmic Ca^{2+} concentration has to decrease rapidly allowing fibers to slide back and assume relaxed position before another contraction cycle could start. SERCA and Na^{+}/Ca^{2+} exchanger (NCX) are the main channel responsible for cytoplasmic Ca^{2+} clearance, the former confine the Ca^{2+} into the sarcoplasmic reticulum restoring its Ca^{2+} content necessary for successive contractions and the latter transport Ca^{2+} extracellularly and Na^{+} intracellularly (Loffredo et al., 2014).

Age-dependent impaired calcium handling could be, at least partially, due to age-dependent decrease of cardiac SERCA2a protein (Cain et al., 1998) although some other groups affirm that there is no age-dependent decrease (Isenberg et al., 2003). Besides SERCA2a amount, its pumping activity is modulated by a second protein called phospholamban (PLN) (Loffredo et al., 2014). It is known that unphosphorylated PLN can interact with SERCA2a decreasing its affinity for Ca^{2+} ions. However, PLN phosphorylation by PKA or CaMKII is thought to alter this interaction stimulating and increasing SERCA pump activity as reviewed in (MacLennan and Kranias, 2003). Age-dependent changes affect also PLN regulator, indeed both PKA activation and CaMKII (δ-isoform) amount seems to decrease with age increasing the unphosphorylated/phosphorylated PLN ratio and decreasing SERCA activity (Jiang et al., 1993; Xu and Narayanan, 1998). Increasing SERCA levels or restoring SERCA/PLN balance has been proved to be beneficial for diastolic function confirming SERCA involvement in age-related diastolic dysfunction (Pathak et al., 2005; Schmidt et al., 2000). Interestingly, even reduction of oxidative stress could directly improve SERCA activity and improve diastolic function (Qin et al., 2013).

Differently from SERCA, studies on NCX channels show more contrasting results. NCX protein amount seems to increase, remain constant or decrease with age (Lim et al., 1999; Schmidt et al., 2000; Walton et al., 2016). However, the prevailing hypothesis is that increased activity of NCX compensate for an increased Ca^{2+} cytoplasmic concentration due to reduced SERCA activity and increased activity of L-type calcium channels (Janczewski and Lakatta, 2010; Piacentino et al., 2003).

1.4.4.7. Mouse model of pressure overload-induced cardiac hypertrophy

Transverse aortic constriction (TAC) is a surgical procedure that induces a stable pressure overload stress in animal hearts leading to cardiac hypertrophy (Rockman et al., 1991). TAC consists in physical bandage of the aorta that reduces its normal diameter (deAlmeida et al., 2010). This alteration increases both LV stress and cardiac hypertrophy recapitulating the effects of aortic stenosis and, if prolonged in time, can progress into HF (deAlmeida et al., 2010).

1.5. Blood factors modulate the aging process

Since ancient times, blood was considered essential for life and modulating its composition was thought to be a way to recover from a disease. With that in mind, for centuries, physicians and surgeons performed bloodletting with the aim of removing "evil humors" from blood. This approach was used to treat almost every kind of diseases and it is easy to imagine that often these treatments did more harm than good to patients. However, from the last century, researchers went towards a more scientific and rigorous approach to investigate blood properties of young and old animals. Heterochronic parabiosis is the most direct and easy experimental approach that allows a shared circulation between two animals with different age (Lunsford et al., 1963). This technique consists in joining surgically two animals, at different ages, in order to allow a shared blood circulation. Indeed, the technique's name derives from Greek and it means literally "life alongside with different ages" (Scudellari, 2015).

The first time this technique was performed in an aging study, it recovered bone weight and density in the aged rats exposed to a young circulation (McCay et al., 1957). Further heterocronic parabiosis experiment showed that shared circulation might also increase life span of animals and improve functionality of aged progenitor cells (Conboy et al., 2005; Ludwig and Elashoff, 1972). These initial studies confirmed the fact that blood carries factors that may modulate tissue aging, however in few cases they have been identified and their mechanism explained. In the following years, an intense research was done in the aging field and, to date, only few of these circulating factors have been identified and characterized, among them growth differentiation factor 11 or GDF11.

1.5.1. Growth differentiation factor 11 (GDF11)

1.5.1.1. Identification as an aging modulator factor

GDF11 was identified, by comparing the abundance in serum of young and old mice using an aptamer-based approach, as a circulating factor that decreases with aging and reverses age-related cardiac hypertrophy (Loffredo et al., 2013). Further experiment confirmed that heterocronic parabiosis increased GDF11 levels in the old parabiont of the pair when compared to the old isochronic control animal (Loffredo et al., 2013). Daily supplementation of recombinant GDF11 recapitulated some of the effects produced by heterochronic parabiosis in heart, skeletal muscle and brain of aged animals (Katsimpardi et al., 2014; Loffredo et al., 2013; Sinha et al., 2014).

1.5.1.2. Protein structure and maturation

GDF11 is a protein member of the activin/inhibin subfamily of the TGF-β superfamily. TGF-β superfamily proteins are produced as pre-pro-proteins that become active after protease cleavage on the C-terminus that releases the ligand, a disulphide linked homo- or heterodimer (Weiss and Attisano, 2013). Indeed, GDF11 is initially translated as a pre-pro-protein and probably the signal peptide is cleaved co-translationally as in other TGF- β proteins (Gentry et al., 1988). During protein synthesis, the prodomain is important for the proper folding of protein in order to obtain a correct maturation of the final dimeric ligand (Gray and Mason, 1990; Harrison et al., 2011). Post-translational modifications are another crucial step: pro-protein sequence contains several cysteines, two N-glycosylation signals and two additional protein cleavage sites. In mature C-terminal region nine cysteines are present forming four intra-chain disulphide bonds plus an extra-chain disulphide bond that assembly the antiparallel homodimer (Walker et al., 2017). A N-glycosylation site is present in the prodomain region of GDF11 (Nakashima et al., 1999) and, at present, there are no studies linking glycosylation to bioactivity of GDF11. Indeed, GDF11 mature protein has no glycosylation sites while proteins belonging to the same subfamily of GDF11, like Inhibin A and Inhibin B, have bioactivity affected by N-glycosylation (Makanji et al., 2008). The two endoproteases sites are processed by two different class of protease: furin-like proteins and BMP1/Tolloid like (TLD) metalloproteinases, respectively at C-terminus and N-terminus. Furin cleavage site has a RSRR consensus sequence and allows a physical separation between prodomain and mature protein (Walker et al., 2017). This post-

translational modification occurs mainly in the trans Golgi network (Takahashi et al., 1995; Walker et al., 2016), but it is know that it could also occur after secretion, in the extracellular space (Cotton et al., 2018; Walker et al., 2017). It is known that similarly to other TGF-β proteins, GDF11 prodomain once cleaved stays bound to the mature peptide through noncovalent interactions (Ge et al., 2005). This complex, called inactive latent complex, blocks the physical interaction between GDF11 mature peptide and the receptors, inhibiting GDF11 bioactivity. In order to release GDF11 protein and increase its bioactivity, an additional post-translational modification has to occur: extracellularly, the BMP1/TLD metalloproteinases cleaves the GDF11 prodomain. This cleavage results in a destabilization of GDF11 inactive latent complex that release the active GDF11 dimer and leads to prodomain degradation (Ge et al., 2005; Poggioli et al., 2016).

1.5.1.3. Protein function and tissue expression

GDF11 is crucial during mammalian development, it is expressed in several tissues and it regulates organs formation and anterior/posterior patterning (McPherron et al., 2009; McPherron et al., 1999). The importance of GDF11 is furtherly recognized by the effects of GDF11 absence, indeed GDF11 KO mice quickly dies within 24 hours after birth with several abnormalities (McPherron et al., 1999).

GDF11 is expressed in the primitive streak and tail bud formation, and it plays an important role in mesodermal cells formation during the early phase of mouse embryogenesis (Gamer et al., 1999; McPherron et al., 1999). Lack of GDF11 dysregulates Hox genes spatial expression, causing a more caudally shifted expression of those genes compared to wild-type (WT) animals (McPherron et al., 1999). Hox gene cluster contains genes responsible for the proper growth and morphogenesis of the embryo and theirs fine-tuning is crucial for a normal development (reviewed in (Favier and Dolle, 1997)).

GDF11 affects some Hox genes through SMAD2 pathway activation, this change seems to be responsible for altered axial patterning that results in several skeletal and neural alterations especially in the posterior region of the body (Liu, 2006). Indeed, the total number of both thoracic and lumbar vertebrae increases with an inverse GDF11 dose-dependent trend, with the $GDF11^{-/-}$ mice showing the most severe abnormalities and $GDF11^{+/-}$ showing a milder phenotype (Table 5) (McPherron et al., 1999).

	Genotype								
Mstn	+/+	+/+	+/+	+/-	+/-	+/-	-/-	-/-	-/-
Gdf11	+/+	+/-	-/-	+/+	+/-	-/-	+/+	+/-	-/-
N° of thoracic vertebrae	N° of animals								
13	10	-	-	10	-	-	10	1	-
14	-	10	-	-	10	-	-	9	-
15	-	-	-	-	-	-	-	-	-
16	-	-	-	-	-	-	-	-	-
17	-	-	-	-	-	-	-	-	-
17+18	-	-	1	-	-	-	-	-	-
18	-	-	8	-	-	7	-	-	-
18+19	-	-	-	-	-	1	-	-	-
19	-	-	1	-	-	2	-	-	1
19+20	-	-	-	-	-	-	-	-	1
20	-	-	-	-	-	-	-	-	11
20+21	-	-	-	-	-	-	-	-	4
N° of lumbar vertebrae	N° of animals								
5	3	-	-	3	-	-	-	-	-
5+6	1	-	-	-	-	-	-	-	-
6	6	10	-	7	10	-	10	9	-
6+7	-	-	-	-	-	-	-	-	-
7	-	-	1	-	-	1	-	1	-
7+8	-	-	1	-	-	-	-	-	-
8	-	-	5	-	-	5	-	-	-
8+9	-	-	2	-	-	-	-	-	-
9	-	-	1	-	-	3	-	-	-
9+10	-	-	-	-	-	1	-	-	-

Table 5: Total number of thoracic and lumbar vertebrae of newborn mice with different combination of Mstn and Gdf11 genotype.
Some mice displayed rib asymmetry of the most posterior thoracic and lumbar vertebrae. The + sign between two numbers represents the different number of ribs on each body side. Table adapted from (McPherron et al., 2009).

In addition, lack of GDF11 activity induces abnormalities in the rostrocaudal patterning affecting spinal cord and in motoneurons formation (Liu, 2006). GDF11 is also important for organ and tissue formation: olfactory epithelium, retina, kidney, pancreas, stomach and spleen are all affected by changes in GDF11 protein activity. In olfactory epithelium, GDF11 cause cell cycle arrest in immediate neuronal precursors and it inhibits the development of progenitor cells responsible for olfactory receptor neurons formation (Wu et al., 2003). Differently, in retina, GDF11 regulates differentiation of retinal progenitors through

precisely time-regulated expression of genes responsible for cell fate determination (Kim et al., 2005). Most of GDF11$^{-/-}$ mice showed complete renal agenesis, showing that GDF11 plays an important role for ureteric bud formation a crucial step for kidney formation (Esquela and Lee, 2003).

In pancreas development, GDF11 absence decreases the total pancreas cell number, it induces an increase of NGN3^{+} islet progenitor cells and it seems to stimulate β-cells differentiation (Harmon et al., 2004). However, contrasting results on pancreas development rose from another paper: they claim that GDF11$^{-/-}$ mice are characterized by hypoplasia of exocrine pancreas rather than a hyperplasia of endocrine pancreas and that there is no change in ratio between α- and β-cells (Dichmann et al., 2006). Furtherly, absence of GDF11 lead to alteration of gastric wall thickness, gastric fold characteristics and impaired spleen development (Harmon et al., 2004).

GDF11 may plays also a role in erythroid maturation, in β-thalassemia overexpression of GDF11 induces a block of terminal differentiation in thalassemic erythroblasts. Decreasing GDF11 levels or inhibiting its receptor reduce immature erythroblasts number and improve disease conditions in mouse model (Dussiot et al., 2014). More recent data shows that however GDF11 KO does not improve or reduce the activity of a erythroid maturation agent (Luspatercept) (Guerra et al., 2019).

In adult age, GDF11 functions are less characterized: postnatally, GDF11 continue to be produced by spleen, kidney, olfactory epithelium and skeletal muscle (Poggioli et al., 2016; Wu et al., 2003). While some reports have shown an age dependent decrease of circulating GDF11 in mouse, rat, horse and sheep (Loffredo et al., 2013; Poggioli et al., 2016), this age-dependent decrease seems not to be retained in humans (GDF11 serum concentration ranging from 224 to 841 pg/mL) (Schafer et al., 2016).

In the last years, several studies were performed in order to investigate the effects of elevated GDF11 concentration in mice serum and to measure GDF11 levels in human populations. Most relevant GDF11's findings are listed in the following table. Contrasting results could be explained by different experimental approaches used by investigators such as: mice strain, animals age, recombinant GDF11 protein dose and GDF11 detection system (Harper et al., 2016; Schafer et al., 2016; Walker et al., 2016).

Target	Approach/Detection method	Phenotype
Heart	Injection of recombinant GDF11 protein (0.1 mg/kg/day, but it might be different (Poggioli et al., 2016) for 28 days.	Reverses age-related cardiac hypertrophy but does not prevent cardiac hypertrophy induced by pressure overload (Loffredo et al., 2013).
Heart	Injection of recombinant GDF11 protein (0.1-0.5-5 mg/kg/day) for 14 days.	GDF11 was able to reduce cardiac hypertrophy and fibrosis induced by pressure overload in mice (Harper et al., 2018).
Heart	Injection of recombinant GDF11 protein (0.1-0.2-0.5-1 mg/kg/day) for 9 days.	Induces atrophy of cardiac muscle in young and old animals. Significant decrease in cardiac mass only for concentration higher than 0.5 mg/kg/day (Poggioli et al., 2016).
Heart	Injection of recombinant GDF11 protein (0.1 mg/kg/day) for 28 days.	GDF11 treatment does not rescue age-related cardiac hypertrophy and it has no effect on cardiac function (Smith et al., 2015).
Heart	AAV8-GDF11 with α-antitrypsin promoter (estimated serum concentration ~60 mg/mL).	Induces atrophy of cardiac muscle (Hammers et al., 2017).
Heart	Stable expressing CHO cells were intramuscularly injected in nude mice for 13 days.	GDF11 reduces cardiac mass and cardiomyocyte size (Zimmers et al., 2017).
Skeletal muscle	Stable expressing CHO cells were intramuscularly injected in nude mice for 13 days.	GDF11 treatment decreased skeletal muscle mass and strength (Zimmers et al., 2017).
Skeletal muscle	AAV8-GDF11 with α-antitrypsin promoter (estimated serum concentration ~60 mg/mL).	Induces atrophy of skeletal muscle (Hammers et al., 2017).
Skeletal muscle	Injection of recombinant GDF11 protein (0.1 mg/kg/day published, but it might be different (Poggioli et al., 2016)) for 28 days and an additional 7 days of GDF11 treatment post injury or 14 days following transplantation.	GDF11 treatment in aged mice leads to: increased function and health of satellite cells, improved skeletal muscle repair, physiology and physical function (Sinha et al., 2014).
Skeletal muscle	Systemic hydrodynamic injection of GDF11 DNA, uptaken and expressed by the liver.	GDF11 induced a 11-18% of weight loss in gastrocnemius skeletal muscle (Jones et al., 2018).

Target	Approach/Detection method	Phenotype
Skeletal muscle	Injection of recombinant GDF11 protein (0.3 mg/kg/day) for 3 days and an additional 14 days of GDF11 treatment post injury.	GDF11 treatment in 16-months old mice leads to inhibition of muscle regeneration and satellite cells expansion (Egerman et al., 2015).
Skeletal muscle	Injection of recombinant GDF11 protein (0.1-0.5-5 mg/kg/day) for 14 days.	GDF11 induces severe atrophy on skeletal muscle tissue mimicking the effects observed by high levels of MSTN (Harper et al., 2018).
Body weight	Injection of recombinant GDF11 protein (0.1-0.2-0.5-1 mg/kg/day) for 9 days.	Induces reduction of total body weight in young and old animals. Old animals were sensitive to lower doses, however treatment at 1 mg/kg/day induces significant weight loss in both young and old mice (Poggioli et al., 2016).
Body weight	Injection of recombinant GDF11 protein (0.1 mg/kg/day) for 28 days.	GDF11 treatment does not induces changes in body weight (Smith et al., 2015).
Body weight	AAV8-GDF11 with α-antitrypsin promoter (estimated serum concentration ~60 mg/mL).	Induces reduction of body weight (Hammers et al., 2017).
Body weight	Injection of recombinant GDF11 protein (0.1-0.5-5 mg/kg/day) for 14 days.	GDF11 induce a marked body weight reduction associated to liver, kidney and spleen weight loss (Harper et al., 2018).
Body weight	Systemic hydrodynamic injection of GDF11 DNA, uptaken and expressed by the liver.	GDF11 produces reduced food intake, anorexia and severe loss of body weight (Jones et al., 2018).
Body weight	Stable expressing CHO cells were intramuscularly injected in nude mice for 13 days.	GDF11 treatment reduces significantly body weight and organ weight (liver and kidney) (Zimmers et al., 2017)
Endothelium	AAV2-GDF11 and recombinant GDF11 protein (0.1 mg/kg/day) for 28 days.	Improved endothelial dysfunction, decreased endothelial apoptosis, inflammation and atherosclerotic plaques formation (Mei et al., 2016).
Humans	GDF11/MSTN detection was performed with SOMAscan aptamer-based method from patients' serum sample.	Higher GDF11/MSTN levels were associate to a lower risk of cardiovascular events or death (Olson et al., 2015).

Target	Approach/Detection method	Phenotype
Humans	GDF11 detection was performed using a LC-MS/MS assay from patients' serum sample.	Higher GDF11 levels are associate with frailty, comorbidities and negative outcome (Schafer et al., 2016).
Humans	GDF11 detection was performed using an ELISA method.	Higher GDF11 levels were associated to a lower mineral density in postmenopausal Chinese women (Chen et al., 2016).

Table 6: Schematic representation of GDF11 findings from in vivo experimentations and studies on human population.

1.5.1.4. Receptor usage and pathway activation

GDF11 dimer is able to signal using specific transmembrane serine/threonine kinase receptors of the canonical TGF-β pathway (reviewed in (Yadin et al., 2016)). GDF11 binds type II receptor dimers like activin receptor kinase IIA (ACVR2A) and ACVR2B and by type I receptor dimers ALK4, ALK5 and ALK7 (Andersson et al., 2006). The exact mechanism of this interaction has not been clarified yet, but it seems that the initial interaction could be started from type II receptor dimer that allow a first ligand stabilization. Subsequently, a type I receptor dimer completes the receptor creating an active hetero-hexameric complex that phosphorylate SMAD2/3 (Yadin et al., 2016). Downstream cascade of SMAD2/3 in TGF-β pathway involves a relative low number of effectors but it has an enormous number of targets even with opposing effects. Indeed, the final outcome of these effects depends on the cell type and cell conditions as reviewed in (Massague, 2012). An example of that was published recently showing as GDF11 induces a different SMAD2/3 activation in presence of different type I TGF-β receptors. Additionally, myostatin (MSTN, also known as GDF8) a protein that share more than 90% of homology with GDF11, showed a different behavior in presence of the same receptors (Walker et al., 2017). These results confirm the complexity of TGF-β pathway and how different combination of receptors could induce different responses in presence of the same ligand.

GDF11-dependent modulation of cardiac and skeletal muscle mass appears to be secondary to two separate events both induced by SMAD2/3 activation. SMAD2/3 activation was already known to reduce skeletal muscle mass and myocyte cross-sectional area in adult mice (Sartori et al., 2009). Furthermore, new studies on neonatal rat cardiomyocytes highlighted that GDF11-depended SMAD2/3 activation was controlled by

an increased intracellular Ca^{2+} due to IP_3 pathway activation and that this effect was able to contrast hypertrophic stimuli (Duran et al., 2018). In addition, among the targets of activated SMAD2/3 cascade, GDF15 expression was increased by GDF11. GDF15, which is also capable to activate SMAD2/3, is associated to lower food intake, higher insulin sensitivity, lipolysis and oxidative metabolism (Chung et al., 2017; Jones et al., 2018). Moreover, GDF15 overexpression was able to contrast the hypertrophic response due to pressure overload in mice and was found protective in case of ischemia/reperfusion injury (Kempf et al., 2006; Xu et al., 2006).

However GDF11 signaling is not only relying on SMAD2/3 cascade, indeed GDF11 has been shown also to activate SMAD 1/5/8 cascade (Zhang et al., 2016), typical of BMP factors, and to signal through non-SMAD pathway, such as ERK, JNK, and p38 MAPK (Egerman et al., 2015).

To summarize, GDF11 signaling depends on multiple, pleiotropic and promiscuous pathways which are difficult to isolate and with a balance that is different in each cell type. It is clear that GDF11 targets many tissues and organs and its therapeutic potential requires a better understanding of its mechanism of action together with a fine regulation of its potency.

1.5.1.5. GDF11 extracellular inhibitors

GDF11 activity is limited by the inactive latent complex, indeed increasing the concentration of GDF11 prodomain has been linked to increased skeletal muscle mass, counteracting the sarcopenic effects of GDF11 and MSTN (Jin et al., 2019). In addition to its own prodomain GDF11 has also several other extracellular inhibitors shared with other TGF-β ligands. These antagonist are follistatin (FST), FST288, FST-like 3 (FSTL3), GDF associated protein 1 (GASP1) and GASP2 (Hill et al., 2002; Hill et al., 2003; Lee and Lee, 2013; Sidis et al., 2006).

FST and FST related proteins contain a N-terminal domain able to mimic a universal type I TGF-β receptor motif blocking the direct interaction between ligand and receptor (Thompson et al., 2005). X-ray crystal of GDF11 bound to an FST inhibitor confirm strong similarities with other activin ligands. GDF11 is recognized and bound by FST288 surrounding the protein. In fact, the N-terminal domain FST288 occupies the site for type I receptor and, on the opposite side, the follistatin domains 1 and 2 interact overlapping the

type II receptor site (Walker et al., 2017). In the mechanism of FST-mediated inhibition it is important to keep in consideration that different FST related genes showed different affinity in binding the activin ligand (Thompson et al., 2005). Additionally, it is important to consider the differential peptidoglycan binding preference of these FST related genes. Presence of heparin binding site on FST can create an isoform compartmentalization between different tissues possibly influencing biological functions and ligand degradation (Cash et al., 2009; Lerch et al., 2007; Schneyer et al., 2004). However, not all FST related proteins have the same properties, indeed FSTL3 does not contain a heparin binding domain and it should not be influenced by the presence of glycan on the cell surface (Sidis et al., 2005).

GASP1 and 2 proteins contain multiple protease inhibitor domains and they are also known as WAP Follistatin/Kazal Immunoglobulin Kunitz and Netrin Domain Containing 2 (WFIKKN2) and WFIKKN1 (Hill et al., 2003). Besides their protease-inhibitor domains, they contain also a 10 cysteine repeat, typical of FST domain, that is primarily responsible for binding and inhibiting the mature protein of GDF11 (Kondas et al., 2008; Shimasaki et al., 1988). Notably, GASP1 and GASP2 show different binding affinity for GDF11 and different tissue-specific expression (Trexler et al., 2002; Walker et al., 2017) (Hill et al., 2003). Another interesting aspect of GASP proteins is to understand if the direct MSTN prodomain binding by the netrin like domain of GASP1/2 is conserved also in GDF11 prodomain (Kondas et al., 2008).

In summary, GDF11 mature protein can be bound by several inhibitors that are differentially expressed among tissues, they can be differentially localized according to glycan composition of cell membrane and each of these antagonists can bind different other proteins, adding ligand competition issues to a mosaic expression of inhibitors. Indeed, in Walker et al. (Walker et al., 2017) similar proteins (GDF11 and MSTN) in presence of the same class of inhibitors (FST or GASP) can exhibit profound difference in ligand:antagonist interactions, underlying the need of extremely controlled experiments with side-to-side comparison in order to produce reproducible results.

1.5.2. Myostatin (MSTN)

In order to clarify some controversy regarding unique/shared functions between GDF11 and MSTN, in the following chapter MSTN biology is described.

1.5.2.1. Protein structure and maturation

MSTN is a protein of the activin/inhibitin subfamily that belongs to TGF-β superfamily. MSTN is produced as other members of TGF-β superfamily as already described for GDF11 in paragraph 1.5.1.2. Post-translational modifications are also similar to GDF11: four intramolecular and one transmolecular disulphide bonds assembly the antiparallel homodimer (Walker et al., 2017). As GDF11, MSTN is cleaved at C-terminus and N-terminus respectively by furin-like proteases and BMP1/TLD metalloproteinases (Walker et al., 2016), process that could occur intracellularly and extracellularly (Lee, 2010; McFarlane et al., 2005). Similarly to GDF11, MSTN prodomain binds to mature peptide creating the inactive latent complex, even if the prodomain is physically separated from mature peptide (Gleizes et al., 1997; Lee and McPherron, 2001). Specific region of MSTN prodomain are required to maintain the inactive latent complex stability. These prodomain inhibitory regions are conserved also in GDF11 prodomain and they consist in three separate elements: the α1-helix, the fastener and the latency lasso (Walker et al., 2018). Interestingly, these MSTN prodomain structures remain stable after FURIN cleavage but not after BMP1/TLD cleavage. Furthermore, even after tolloid activity, BMP1-cleaved prodomain is still able to maintain the inactive latent complex assembly. However, prodomain:ligand interface stability is deeply affected and this instability primes complex dissociation and the release of the mature ligand (Le et al., 2018). MSTN prodomain α1-helix can modify prodomain conformation and re-create this complex instability, even without BMP1-TLD cleavage, and enhance ligand release (Walker et al., 2018). In addition, MSTN prodomain has also a N-glycosylation site but it seems not essential, indeed it is not necessary for prodomain inhibitory activity nor protein production (Jiang et al., 2004).

1.5.2.2. Protein function and tissue expression

MSTN was identified as a protein expressed in developing and adult mice skeletal muscle (McPherron et al., 1997). During embryogenesis, MSTN is expressed in myotomes of developing somites, starting from rostral area, and later in developing skeletal muscle (McPherron et al., 1997). Abolishment of MSTN expression in mice does not lead to skeletal alteration as in GDF11 KO mice, even if these proteins share high level of homology (Gamer et al., 1999; McPherron et al., 1997, 1999). However, crossings that generate a double MSTN and GDF11 mutant mice enlighten some redundant function between these two

proteins (McPherron et al., 2009). $MSTN^{-/-}$ $GDF11^{-/-}$ mice presents more pronounced axial skeleton transformation with additional alteration not observed in the $GDF11^{-/-}$ mutant as an extra bone emerged from shoulder, a third limb and extra digit formation in normal forelimbs (McPherron et al., 2009). The increased transformation level of the double mutant seems to be due to simultaneous expression of both GDF11 and MSTN in the posterior primitive streak (Amthor et al., 2002). This transient expression of MSTN can slightly reduce the axial skeletal alteration induced by lack of GDF11 expression during embryonic development, probably acting on the same receptors (McPherron et al., 2009). In adult animals, MSTN continues to be expressed by several skeletal muscles even if the total mRNA produced is different among muscle type. In all other tissues, except for adipose tissue, it was not possible to detect MSTN expression (McPherron et al., 1997). $MSTN^{-/-}$ animals were viable and fertile although they showed an abnormal body shape and heavier compared to WT animals (McPherron et al., 1997). Phenotype was explained by a significant increase of skeletal muscle mass (2-3 folds compared to WT) due to both hyperplasia and hypertrophy of myofibers (McPherron et al., 1997). These observations suggest that MSTN acts as postnatal negative regulator of skeletal muscle growth (McPherron et al., 1997). MSTN function is evolutionary conserved, indeed inactivating MSTN mutations lead to similar hypermuscular phenotype among mammals, humans included. (Gu et al., 2016; McGivney et al., 2012; McPherron and Lee, 1997; Mosher et al., 2007; Schuelke et al., 2004). MSTN is involved in muscular fiber type switch, where loss of MSTN is associated to reduction of oxidative and endurance fibers (type I and type IIA) and increment of fast glycolytic fibers IIB (Hennebry et al., 2009). However, downstream of MSTN signaling, fiber switch is furtherly modulated by JNK activity that regulates SMAD2 phosphorylation between canonical SMAD2 pathway and JNK-SMAD2-linker pathway (Lessard et al., 2018).

In addition, MSTN deficient mice showed resistance to obesity and type 2 diabetes confirming MSTN role in adipogenesis and glucose metabolism (McPherron and Lee, 2002). Interestingly, these metabolic protective mechanisms induced by lack of MSTN depend on skeletal muscle and not on adipose tissue (Guo et al., 2009) suggesting that myokines secreted during muscle growth or increased skeletal muscle glucose uptake are the effectors of adipose tissue mass reduction (Guo et al., 2009; Pedersen and Febbraio, 2012). Of note, MSTN signaling inhibition induces browning of white adipose tissue (WAT)

stimulating energy expenditure, fatty acid oxidation and increasing expression of peroxisome proliferator-activated receptor gamma coactivator 1α (PGC-1α) and irisin (Dong et al., 2016). On the other hand, MSTN is overexpressed in skeletal muscle and adipose tissue of obese mice and humans showing that metabolism alteration and increased fat deposition can induce mechanism that reduces muscle growth helping the obesity state to persist (Allen et al., 2008; Hittel et al., 2009).

Aside from an extended and coherent literature describing MSTN effects on skeletal muscle or adipose tissues, few works investigated MSTN activity on cardiac muscle as reviewed by Springer (Springer et al., 2010). Among the available publications, MSTN cardiac-specific overexpression was able to reduce cardiac mass in healthy and HF conditions (Biesemann et al., 2014; Heineke et al., 2010) but conversely, cardiac specific MSTN KO was not affecting cardiac mass (Cohn et al., 2007). In order to clarify and characterize the MSTN effects on the heart, further studies are required.

1.5.2.3. Receptor usage and pathway activation

MSTN active ligand can bind serine/threonine kinase receptors of canonical TGF-β pathway (reviewed in (Yadin et al., 2016)), mechanism of interaction and SMAD2/3 pathway activation have been described in paragraph 1.5.1.4. MSTN recognizes type II receptor dimers ACVR2A and ACVR2B and then it binds type I receptor dimers ALK4 and ALK5 (Rebbapragada et al., 2003). Differently from GDF11, ALK7 binding seems not to be recapitulated by MSTN, but results are not conclusive (Walker et al., 2017).

MSTN effects on skeletal muscle tissue can be explained by SMAD2/3 decrease of AKT / mTOR signaling pathway reducing the total protein synthesis and promoting expression of several genes involved in de-differentiation (Amirouche et al., 2009; Trendelenburg et al., 2009). Involvement of AKT/mTOR pathway seems to be confirmed because treatment with IGF-1, that reactivate AKT protein, can block MSTN effects on myocytes (Trendelenburg et al., 2009).

On the other hand, the pathway that confers MSTN mediated protection from obesity and insulin resistance in mice has not been clarified yet (Guo et al., 2009). An indirect effect of the increased muscle mass itself or the increased myokines secretion could partially explain the increased insulin sensitivity as reviewed in (Demontis et al., 2014). MSTN signaling inhibition could also alter hormones levels or nutrients availability that will

directly or indirectly act on the central nervous system altering behaviors like food intake (Guo et al., 2012; Henry and Clarke, 2008). Furthermore, MSTN is able to activate signaling pathways different from SMAD like RAS/MEK/ERK pathway, TAK1/MEK4/JNK pathway and TAK1/MEK3-6/p38 MAPK (Biesemann et al., 2015; Huang et al., 2007; Yang et al., 2006). These pathways, also modulated by GDF11, are involved in fibrosis, cardiac hypertrophy and myocytes differentiation underling how much these pathways are intertwined and complex to modulate.

1.5.2.4. MSTN extracellular inhibitors

Most of circulating MSTN (>70%) is bound to its prodomain regulating protein bioactivity (Hill et al., 2002). As for GDF11 this prodomain binding regulate the activity of MSTN ligand through inactive latent complex formation. Thus, several results confirmed that increasing the amount of circulating MSTN prodomain can lead to muscle hypertrophy in a similar extent as obtained with MSTN neutralizing antibodies (Latres et al., 2015; Yang et al., 2001). Recent findings have shown that GDF11 prodomain is able to inhibit MSTN activity (Jin et al., 2019). In addition to GDF11 and MSTN prodomain, MSTN activity is regulated by several other extracellular inhibitors as FST, FST288, FSTL3, GASP1, GASP2 (Amthor et al., 2004; Hill et al., 2003; Sidis et al., 2006). These inhibitors are shared with GDF11 and properties and mechanism of these factors have already been described in paragraph 1.5.1.5.

Another MSTN inhibitor is DECORIN a small leucine-rich glycosylated protein (Miura et al., 2006). DECORIN is often bound on collagen fibers and can play an important role in cell growth modulating bioactivity of growth factors as epidermal growth factor (EGF) and TGF-β (Iozzo, 1999; Santra et al., 2002; Schonherr et al., 1998). Interestingly, glycosaminoglycan removal from DECORIN does not affect binding of MSTN, probably because glycan are involved only in DECORIN-ECM interaction and not in growth factor binding (Iozzo, 1999; Miura et al., 2006).

1.5.3. GDF11/MSTN therapeutic avenues

MSTN and its pathway have been extensively investigated as a possible therapeutic target while GDF11 pharmacological applications are still debated. MSTN KO mouse shows a hyper-muscular phenotype and MSTN inhibition is an attractive strategy for numerous therapeutic conditions associated to muscle wasting (Smith and Lin, 2013). Overexpression

of MSTN prodomain, soluble ACVR2 receptors, inhibition of MSTN extracellular maturation and usage of neutralizing antibodies are all strategy successfully attempted to increase muscle mass in healthy and several muscle wasting models (Latres et al., 2015; O'Connell et al., 2015; Pirruccello-Straub et al., 2018; Yang et al., 2001). However, few of these treatments were really MSTN-specific and most involved also GDF11 and other TGF-β ligands. Surprisingly, positive results obtained in pre-clinical studies were not recapitulated as expected by clinical trials results as listed in table 7 where only few treatments were capable to increase muscle mass in humans without inducing adverse effects. Together, results from all these clinical trials suggest that unspecific blocking of circulating MSTN and GDF11 or not-finely regulated ACVR2A/B signaling, probably because of promiscuity of ligands and inhibitors, is not sufficient to treat muscle wasting conditions and is associated to several adverse effects.

On the other hand, modulation of GDF11/MSTN signaling may be considered to induce a reduction of muscle mass. More specifically, GDF11 has been suggested as a drug that can reverse age-related cardiac hypertrophy or other forms of pathological cardiac hypertrophy. This approach is still in its preliminary phase if compared to MSTN blocking strategy but is intensively investigated (Harper et al., 2016; Walker et al., 2016). GDF11 can indeed reverse cardiac hypertrophy but can also induce sarcopenia and cachexia and thus a more specific characterization is needed (Harper et al., 2016). Fine GDF11 circulating levels modulation could be exploited to have milder but more specific SMAD2/3 pathway activation only in cardiac tissue reducing undesired systemic side effects (Walker et al., 2017). Moreover, ligand activity could be furtherly modulated by injection of recombinant inactive latent complex, as a novel therapeutic agent. Indeed, several previous *in vivo* experiments used commercially available GDF11 recombinant protein that consisted in pure mature and active form (listed in table 6). For MSTN ligand, the difference in potency between mature protein and its inactive latent complex is in the order of hundred-fold difference (Cotton et al., 2018). It easy to speculate that this difference could be applied to GDF11 and that lower potency will allow a more gradual and less intense SMAD2/3 activation that could limit adverse effects.

Aside of treatments aiming to increase GDF11 serum levels, GDF11 was also investigated as novel marker for several conditions but more studies are necessary to clear the divergent conclusion. Indeed, high serum GDF11 concentration has been linked to higher risk of

rehospitalization and comorbidity (Schafer et al., 2016) but from a previous study enrolling almost 2 thousand patients, higher GDF11/8 concentration levels were protective against cardiovascular events (Olson et al., 2015). Considering both results, on one hand Schafer et al. were more specific than Olson et al. using mass spectrometry to differentiate circulating GDF11 from MSTN. On the other hand, Schafer quantification analyzed a relatively small number of patients already suffering from heart conditions (55 men and 41 women) and data obtained from this cohort may not be representative for the entire healthy population. Moreover, the simple association between increased GDF11 serum concentration and frailty in cardiovascular patients does not clarify if GDF11 is a causative or protective factor in end-stage valvular heart disease (Schafer et al., 2016).

Aiming at evaluating GDF11 therapeutic potential, future studies must be carefully designed to quantify and compare GDF11 and MSTN circulating levels, to assess their side effects and to observe the changes on the cardiovascular system (McPherron, 2013).

Name	**Target**	**Muscle-related effects**	**Clinical trial conclusions**
LY2495655	anti-MSTN antibody	No changes in muscle mass or muscle function.	Phase 2 clinical trial was terminated prematurely because treatment was not conferring clinical benefits in pancreatic cancer patients (Golan et al., 2018).
LY2495655	anti-MSTN antibody	Some muscle physical performances were improved.	Phase 2 clinical trial increased lean body mass and muscle performance in older weak fallers (Becker et al., 2015).
ACE-031	ACVR2B soluble receptor	Positive trend of lean body mass and bone mineral density.	Phase 2 clinical trial, on patients affected by Duchenne muscular dystrophy, was terminated prematurely because of non-muscle related adverse (Campbell et al., 2017).
Bimagrumab	Competitive antagonist for ACVR2A/B	No significative changes in 6 minutes walking distance test or muscle strength.	Phase 2 clinical trial on patients with inclusion body myositis showed good safety profile to Bimagrumab treatment (Hanna et al., 2019).

ACE-083	Follistatin-based inhibitor for TGF-β family ligands	ACE-083 induce significant muscle growth in targeted muscles. No changes in muscle strength was registered.	Phase I clinical trial was well tolerated in healthy women (Glasser et al., 2018). Phase II clinical trial is ongoing (clinical trial identifier: NCT03943290).
Sotatercept	ACVR2A soluble receptor	Non investigated.	Phase 2 clinical trial on patients with myelodysplastic syndromes. Treatment was well tolerated and improved anemia condition (Komrokji et al., 2018).
Luspatercept	ACVR2B soluble receptor	Non investigated.	Phase 2 clinical trial on patients affected by β-thalassemia showed improved erythropoiesis (Piga et al., 2019).

Table 7: List of clinical trial aimed to neutralize circulating GDF11/MSTN or inhibit ACVR2A/B receptors activity.

2. MATERIALS AND METHODS

2.1. Materials

2.1.1. Chemical and cell culture reagents

Unless otherwise stated, general chemicals and cell culture reagents were purchased from Sigma-Aldrich, Merck, Honeywell, Diapath, InvivoGen, Thermo Fisher Scientific (Life Technologies, Gibco, Invitrogen, Applied Biosystems, Novex) and Corning.

2.1.2. Standard solutions

All the solutions are described in the text, except for the following:

- PBS: 137 mM NaCl, 2.7 mM KCl, 10 mM NaH_2PO_4, pH 7.4.
- TBE: 89mM Tris base, 89 mM Boric acid, 2 mM EDTA, pH 8.3.
- TBST: 50 mM Tris base, 150 mM NaCl, 0.1% tween, pH 7.4.
- LB medium (1 liter): 10 g Tryptone, 10g NaCl, 5g yeast extract, pH 7.0, sterilized by autoclaving.
- CBFHH: NaCl (136 mM), Hepes (20 mM), Glucose (5.55 mM), KCl (5.36 mM), $MgSO_4$ (0,81 mM), KH_2PO_4 (0.44 mM), NaH_2PO_4 (0.34 mM), pH 7.4.
- HBS 2X: NaCl (280 mM), KCl (10 mM), Na_2HPO_4 (1.5 mM), dextrose (12 mM), 50 mM HEPES, pH 7.13, sterilized by 0.22 µm filtration.
- PFA 4% (1 liter): 40 g of Paraformaldehyde (PFA) in PBS, pH 7.4, 0.45 µm filtered.
- Binding Buffer (0.5 liter): 6 mL of NaH_2PO4 (0.2 M), 44 mL of Na_2HPO4 (0.2M), 50 mL of NaCl (5M), pH 7.4, H_2O to volume, 0.22 µm filtered.
- Elution Buffer (0.1 liter): 1.2 mL of NaH_2PO4 (0.2 M), 8.8 mL of Na_2HPO4 (0.2M), 10 mL of NaCl (5M), 10 mL of Imidazole (5M, BioUltra, Sigma-Aldrich), pH 7.4, H_2O to volume, 0.22 µm filtered.

2.1.3. Synthetic oligonucleotides

Small synthetic DNA oligonucleotides (<80 bp) used for PCR and cloning purposes were all purchased from Sigma-Aldrich.

Larger synthetic DNA fragments were synthetized by Genewiz cloned in pUC plasmid.

2.1.4. Commercial proteins

All commercial proteins used in this work are listed in the table below.

Protein name:	Code	Supplier
GDF11	120-11	PeproTech
MSTN	120-00	PeproTech
MSTN Prodomain	1539PG	RnD
TGF-β1	100-21	PeproTech
BSA	10735086001	Sigma-Aldrich
Cytochrome C	C3131	Sigma-Aldrich

Table 8: List of commercial recombinant proteins.

2.1.5. Plasmids

pZac 2.1 plasmid (gently donated by Prof. Giacca's laboratory), containing CMV promoter and AAV ITR were used for transient transfection and AAV6/9 vector production. A modified version of pZac2.1, capable of expressing sgRNAs under the control of U6 promoter, was gently donated by Dr. Elena Chiavacci from Prof. Giacca Laboratory.

In order to obtain stable eukaryotic clones, selected ORF were cloned in pcDNA 3.1+ (Invitrogen) containing Puromycin, Geneticin or Zeocin resistance. WT GDF11 and WT MSTN ORFs were modified by site-directed PCR mutagenesis. WT signal peptides were substituted with BM40 signal peptide (MRAWIFFLLCLAGRALA) in order to allow efficient protein expression and secretion (Mayer et al., 1993). Then, downstream to BM40 signal peptide, an hexa histidine tag (His6) and three glycines were added to the protein for subsequent purification (Kimple et al., 2013).

All CAGA12 reporter plasmid were developed from a pGL3-Basic (Promega) vector. For AAV8-hAAT vectors productions a pGG2 plasmid was used, gently donated by Prof. Muro's Laboratory. pGG2 plasmid contained ITR regions and a human anti-trypsin promoter that granted sustained and elevated expression in hepatocytes (Bortolussi et al., 2014).

2.1.6. Enzymes

All enzymes used in this work were purchased from New England Biolabs (NEB), unless otherwise stated.

2.1.7. Antibodies

All antibodies used in this work are listed in the table below showing target, usage conditions and supplier.

Target	Application	Dilution	Code	Supplier
GDF11/MSTN	WB	1:1000	ab124721	Abcam
MSTN	WB, Co-IP	1:2000	BAF788	RnD
GDF11	WB, Co-IP	1:1000	MAB19581	RnD
His6-Tag	WB	1:1000	ab18184	Abcam
HSC70	WB	1:1000	1B5	Enzo Life Sciences
MSTN Prodomain	WB	1:2000	AF1539	RnD
Activin A Receptor Type IB/ALK-4	WB	1:1000	ab109300	Abcam
TGF β Receptor I/ALK-5	WB	1:1000	ab31013	Abcam
Activin A Receptor Type IC/ALK-7	WB	1:1000	ab77051	Abcam
Sarcomeric Alpha Actinin	IF	1:400	ab9465	Abcam
Mouse Immunoglobulins, HRP	WB	1:2000	P0447	Agilent
Rabbit IgG (H+L), HRP	WB	1:5000	31460	Thermo Fisher Scientific
Sheep IgG (H+L), HRP	WB	1:5000	31480	Thermo Fisher Scientific
Rat IgG (H+L), HRP	WB	1:2000	31470	Thermo Fisher Scientific
Rabbit IgG (H+L), Alexa Fluor 488	IF	1:500	A-11034	Thermo Fisher Scientific

Table 9: List of antibodies.

2.1.8. Adeno Associated Virus (AAV)

All viral vectors used in this work were produced by the AAV Vector Unit (AVU) at International Centre for Genetic Engineering and Biotechnology (ICGEB), Trieste (https://www.icgeb.org/avu-core-facility/).

2.2. General molecular biology techniques

2.2.1. PCR

PCR technique was performed on plasmid DNA, amplicons and genomic DNA following GoTaq DNA Polymerase (Promega) or Pfu DNA Polymerase (Promega) manufacturer's instruction. DNA template amount was in a range from 0.1 to 10 ng for plasmids and amplicons, 50/500 ng in case of genomic DNA. Annealing temperature was determined according to the lower melting temperature (Tm) calculated from the 3' 20 bp for each primer. Elongation time was calculated according to DNA amplificated length divided by polymerase speed (bp/min). Standard PCR cycles were used for most cloning purpose, whereas for genotyping analysis protocol is described in detail in paragraph 2.9.2.

2.2.2. DNA extraction from cultured cells

Cultured cells were washed with PBS, detached using trypsin and centrifuged (5 min, 100 g). Supernatant was removed and cells were washed again with pbs and re-centrifuged (5 min, 100 g). For a 24 well, 50/100 µL of NaOH (50 mM) was added to cellular pellets and heated for 10 min at 85°C. Then, 5/10 µL Tris-HCl (1M, pH 8.5) were added and obtained solution could be directly used for PCR or stored at -20°C.

2.2.3. RNA extraction protocol

2.2.3.1. RNA extraction from cell culture

Cultured cells were washed with PBS and then RNA TRIzol was added into the well/plate for 5 minutes on a rocking plate. Then chloroform extraction was performed according to manufacturer. DNase/RNase free water was used to resuspend pellet and stored at -80°C. RNA concentration and quality was evaluated using Nanodrop 1000 Spectrophotometer (Thermo Fisher Scientific) and agarose gel electrophoresis.

2.2.3.2. RNA extraction from animal tissue

Tissues were weighted and 1 mL of TRIzol (Invitrogen) was added to every 100 mg of tissue. Maximum weight of tissue processed was 150 mg. Mechanical sample homogenization was achieved using "Lysing Matrix D" (MPBio), for two 30 seconds cycles (6500 speed units) using a MagNA Lyser (Roche). Between cycles, samples were chilled in ice, and after

homogenization, samples were always kept on ice unless stated otherwise. Supernatant was separated from tissue debris and phenol/chloroform extraction was performed.

2.2.4. cDNA synthesis

cDNA was obtained using "High-Capacity cDNA Reverse Transcription Kit with RNase Inhibitor" (Applied Biosystem) according to manufacturer's instructions. cDNA samples were diluted 1:10/1:20 with DNase/RNase-free water and used for qPCR analysis.

2.2.5. qPCR

Diluted cDNAs were used for quantitative assessment of RNA expression of selected genes and results were normalized by the expression of housekeeping genes. TaqMan (Applied Biosystem) system was used to quantify levels of gene expression using TaqMan probes listed in the table 10 and following manufacturer's instruction. For each experimental condition, at least three biological replicates and two technical replicates were used. Fold change between control and treated samples was identified with $2^{-\Delta\Delta CT}$ method.

Gene target	Probe ID
Acvr1b (Alk4)	Mm00475713_m1
Tgfbr1 (Alk5)	Mm00436964_m1
Acvr1c (Alk7)	Mm03023957_m1
Gapdh	Mm99999915_g1

Table 10: List of TaqMan probes.

2.2.6. Protein extraction protocols and protein lysates quantification

2.2.6.1. Conditioned cell culture medium harvesting

Cultured transfected cells have been used to produce and secrete protein of interest in culture medium. In order to avoid confounding effects due to fetal bovine serum (FBS) presence, after 16/24h since transfection, cells were washed with PBS and medium was replaced with serum free Optimem (Gibco) medium. When needed, 4 mM NaB (Sigma-Aldrich) or 100 µM biotin (Sigma-Aldrich) were added to Optimem medium. The former is a histone deacetylase inhibitor capable of enhancing protein production (Palermo et al., 1991) and the latter was used to induce protein biotinylation through BirA system (Predonzani et al., 2008). In case of neonatal rat cardiomyocytes cultures Optimem medium

was not used but the neonatal rat cardiomyocytes medium (described in paragraph 2.5) was modified adding 0.1% FBS. Medium was harvested and centrifuged at 4°C for 15 min at 15600 g. Supernatant was transferred in a new tube and used for following studies or stored at -80°C.

2.2.6.2. Protein extraction from cell culture

RIPA buffer was prepared and chilled before starting protocol. 5X RIPA buffer (Cell Signaling Technologies) was supplemented with "PhosSTOP" (Roche), "cOmplete, Mini, EDTA-free Protease Inhibitor Cocktail" (Roche) and PMSF according to manufacturer instruction. Cultured cells were washed with PBS, plate was positioned on ice and then 1X RIPA buffer was added to the well/plate (400 µL for a 10 cm dish or 10^7 cells). Cells were kept 10 min in cold room on a rocking plate, then detached using a cell scraper. Samples were sonicated and stored at -80°C or used for further analysis.

2.2.6.3. Protein extraction from animal tissues

RIPA buffer was prepared as described in previous paragraph. Harvested tissues were weighted and 1 mL of 1X RIPA buffer was added to every 100 mg of tissue. Maximum weight of tissue processed was 150 mg. Mechanical sample homogenization was achieved as described in paragraph 2.2.3.2. Samples were chilled on ice between cycles, and, after homogenization, were always kept on ice unless stated otherwise. Then samples were centrifuged at 4°C for 10 min at 15600 g and transferred in a new tube, sonicated and stored at -80°C or used for further analysis.

2.2.6.4. Estimation of protein lysate concentration

Protein sample concentration was determined by Bradford Protein Assay Dye Reagent Concentrate (Bio-Rad) according to manufacturer instructions. Standard curve was prepared at each measurement with various amount of commercial BSA.

2.2.7. SDS-PAGE and western blot

2.2.7.1. SDS-PAGE

SDS-PAGE is an electrophoresis method used for protein separation by mass. Pre-cast gradient polyacrylamide gels "Bolt 4-12% Bis-Tris Plus" (Life Technologies) were used in this

work for protein analysis. Protein samples were prepared adding "Bold Loading Dye" (Life Technologies) and β-mercaptoethanol (Sigma-Aldrich) at 5/20 and 1/20 fractions of total volume, respectively. Samples were denatured for 10 min at 70°C and loaded onto a gel. In order to estimate protein size, "Prestained Protein Ladder (10 - 180 kDa)" (Abcam) or "SeeBlue Plus2 Pre-stained Protein Standard" (Invitrogen) were loaded in parallel with samples. For samples obtained from cell or tissue lysate, 20 to 35 µg of total protein were loaded in each line. Conditioned medium was normalized by volume, as for serum samples where 1 µL of serum was diluted in 20 µL of loading volume. Gels were run in 1X "Bolt MES SDS Running Buffer" (Life Technologies) for initial 5 min at 150V constant, then 200V constant until desired separation was obtained. Once run was terminated gel was either stained with Coomassie staining or transferred on PVDF membrane.

2.2.7.2. Coomassie staining

SDS-PAGE gels were stained with Coomassie in order to visualize and quantify separated proteins. BSA and Cytochrome c proteins were prepared and loaded in order to compare samples to known amount of proteins.

In this work two different Coomassie were used:

- *In-house prepared Coomassie:*

  100 g ammonium sulfate, 5 mL of Coomassie Brilliant Blue G250 (6%, aqueous solution), 30 mL of phosphoric acid (85%, aqueous solution), 200 mL of ethanol and 550 mL of deionized water. Gel was stained ON, then destained with water until background was transparent.

- *Commercial Coomassie:*

  "InstantBlue" (Expedeon) was used according manufacturer's instructions.

2.2.7.3. Western blot

Proteins into polyacrylamide gel were transferred on "Amersham Hybond P 0.2 PVDF membrane" (GE Healthcare) using the "Mini Blot Module" (Invitrogen) system. PVDF membrane was activate in pure methanol, then washed in water and transfer buffer before transfer process. Transfer buffer was prepared according manufacturer's instruction, "Bolt Transfer Buffer (20X)" was diluted with water to final volume after addition of 10% methanol (Sigma-Aldrich), 0.1% Bolt Antioxidant. 3MM Chr (Whatman) paper was used for

sandwich gel assembly. Transfer process used a constant 20V tension for 60 min. Once transfer was completed, protein transfer was checked using Ponceau Ruby Protein Gel Stain (Invitrogen) and then membrane was cleaned by repeated washing with TBST. Subsequent membrane blocking step was executed at RT with 5% Non-Fat Dry Milk (NFDM) or 5% BSA in TBST for 60 to 90 min on a tube roller and incubated with selected antibody (diluted in the appropriate blocking solution) ON at 4°C on a tube roller. The day after, membranes were washed 5 times for 6 min with TBST and incubated with the corresponding secondary antibody for 60 min. A second round of 5 washes (6 minutes each) was performed and HRP chemiluminescence was produced using "ECL Western Blotting Analysis System" (Ge Healthcare) or "Clarity Max Western ECL Substrate" (Bio-Rad), in case of normal or faint bands, respectively. Signal detection was achieved using "Amersham Hyperfilm ECL" (Ge Healthcare) photosensitive films or with "ChemiDoc Touch" Imaging System (Bio-Rad). Intensity band quantification was assessed using ImageJ or Image Lab (Bio-Rad) software.

2.2.7.4. Membrane stripping

Occasionally membrane was stripped from previous incubated antibodies and re-probed with a new antibody. Briefly, a stripping solution composed by 20 mL of Tris (pH 6.8), 5 mL of SDS 10% and 175 µL of β-mercaptoethanol was prepared and heated at 60°C. Membrane was incubated in stripping solution for a time ranging from 10 to 20 min at 60°C in a rocking plate. Then, blocking and antibody incubation was performed as described in the previous paragraph.

2.3. Bacterial culture procedures

2.3.1. General bacterial handling

The *E. coli* XL10-Gold strain was used in this study for cloning and plasmid amplification purposes. Bacteria were grown, at 37°C, in Luria Bertani (LB) medium in liquid culture or solid agar plate (if 15 g/L of agarose was added to LB medium recipe). For selection, ampicillin or kanamycin was added to growth medium at a final concentration of 100 µg/mL or 50 µg/mL, respectively. Colonies on agar plate were maintained at 4°C for short term conservation, but for long term storage glycerol bacterial stocks were prepared mixing

bacterial culture (600 µL) and sterile glycerol (400 µL) then stored at -80°C and used for future inoculations.

2.3.2. Competent XL10-Gold cell preparation

Bacterial competent cells were prepared in-house following the protocol described by Sambrook (Sambrook and Russell, 2006). Briefly, a glycerol stock of XL10-Gold was inoculated into a fresh culture medium. After 12/16h, 4 mL of culture medium were added to 400 mL of fresh LB, with no antibiotics, and grown until OD_{600} reached a value of 0,4. Then bacteria were chilled on ice and centrifuged (4°C, 2000 g for 15 minutes). Supernatant was discarded and pellet was resuspended with 80 mL of sterile, ice-cold $CaCl_2$ 0.1 M. Bacteria solution was incubated at 4°C for 30 min and centrifuged again as described before. Pellet was resuspended in 15/20 mL of sterile, ice-cold $CaCl_2$ 0.1M with 15% of glycerol and aliquoted (200/400 µL) in ice cold tubes and stored at -80°C. Bacteria competence was checked by performing transformation with 0.1 ng of a control plasmid.

2.4. Cloning procedures

2.4.1. DNA restriction endonuclease digestion

DNA endonuclease digestion was performed following manufacturer's instructions. Enzymes' buffer compatibility was determined using the NEBCloner tool (https://nebcloner.neb.com/). For analytical digestions 500 ng of plasmid DNA were digested for 30/60 min (37°C) with 5 U of specific restriction enzymes. For preparative digestions 2 µg of plasmid or PCR amplificated were digested for 2/3 hours (37°C) with 10U of specific restriction enzymes.

2.4.2. Site-directed mutagenesis by PCR

In order to expand cloning possibilities, DNA fragment were modified using PCR overhanging and/or overlapping primers designed to contains new restriction sites or change short DNA sequence. Briefly, modified DNA template was amplificated by Pfu DNA Polymerase and purified from agarose gel. DNA was digested using restriction enzymes or used as target to perform a novel round of site-directed mutagenesis.

2.4.3. DNA inserts ligation into plasmid vectors

Plasmid ligation was performed using T4 DNA ligase (NEB) that catalyzes the formation of a phosphodiester bond between 3' hydroxyl and 5' phosphoryl DNA extremities using ATP. Briefly, 25 ng of digested backbone plasmid were added to 1:3 or 1:6 molar ratio of purified digested DNA fragments (insert). Plasmid+Insert solution was supplemented with 1X T4 DNA ligase buffer and 0.5/1U of T4 DNA ligase, as stated in NEB's instructions. Negative control reaction (linearized plasmid backbone + water + T4 DNA ligase) was always carried out in order to determine the number of self-ligating plasmid events. Reaction was carried out at RT for 1h to 3h (sticky ends ligation) otherwise at 16°C ON (blunt ends ligation). Occasionally, small synthetic ds oligonucleotide (<80 bp) were also used as DNA insert. In this scenario, Calf Intestinal Phosphatase (CIP) (NEB) was used to remove plasmid 5' phosphate group and reduce the chance of self-ligating plasmid event. Furthermore, several molar ratios were attempted ranging from 1:25 to 1:250 molar ratio between linearized backbone plasmid and synthetic insert, then, ligation proceeded as for blunt end ligations.

2.4.4. Enzyme free DNA ligation into plasmid vectors (AQUA cloning)

Aiming to clone a multicistronic plasmid, as in the case of pGL3-CAGA12+PuroR-P2A-hRenilla-T2A-EGFP standard cloning procedure were not feasible because of absence of unique restriction site. In order to overcome these difficulties AQUA cloning method was performed. Protocol is described by Beyer and colleagues (Beyer et al., 2015), briefly, 12 ng of linearized plasmid backbone and DNA fragment were incubated at RT for 1h in a 10 µL volume (1:3 molar ratio, if occurred, water was added to volume) and then used for bacterial transformation. The only requirement needed was the necessity of a sequence homology region (16-32bp) present in both plasmid backbone and insert. Ligation events was totally mediated by competent cells intrinsic ability to process linear DNA fragments.

2.4.5. Transformation of XL10-Gold bacterial competent cells

Competent cells were thawed slowly in ice and divided in several ice-cold tubes (45 µL each). Competent cells received 5 µL of the previously obtained DNA ligation reaction and competent cells/DNA mixture was incubated in ice for 15/30 min. After this first incubation step, cells were heat-shocked at 42°C for 60 sec in a water bath and re-incubated for

5 minutes on ice. Transformed bacteria were occasionally plated immediately or they were added with 200 µL of LB and kept for 60/120 min at 37°C before plating. Transformed competent cells were spread on LB-agar plates containing the selected antibiotic, and grown ON at 37°C.

2.4.6. Small- and large-scale plasmid DNA preparation

Colonies obtained after transformation process were expand in LB medium + antibiotics. Single colonies were picked using a sterile disposable inoculating loop (Nunc) and bacteria were inoculated into 6 mL of LB medium and incubated ON. After ON culture growth, small- or large-scale plasmid DNA purification protocols were performed.

2.4.6.1. Small-scale plasmid preparation

Bacterial cultures (5/6 mL) were centrifuged at 5000 g for 15 min to aggregate bacterial cells into a pellet. "Wizard Plus SV Minipreps DNA Purification System" (Promega) kit was used following manufacturer's instructions. Plasmid DNA were checked by restriction enzyme digestion and sequence.

2.4.6.2. Large-scale plasmid preparation

Bacterial culture (1/3 mL) was inoculated ON in 200/400 mL of LB medium at 37°C. On the following day, bacterial culture was pelleted as in previous paragraph. Then large-scale plasmid preparation was performed using "NucleoBond® Xtra Maxi" (Macherey Nagel) kit following manufacturer's instructions. Plasmid DNA were checked by restriction enzyme digestion.

2.4.7. Sequencing service for cloning purposes

DNA sequence analysis was performed after each cloning procedure. Briefly, at least 2 small-scale plasmid preparation was obtained from each ligase reaction and tested by restriction enzyme digestion. If digested DNA fragments were matching the DNA fragments expected sizes, 15 µL of mini-prep plasmid DNA (50/100 ng/µL) were added with 2 µL of desired sequencing primers (10 µM) according to "Mix2Seq kit" (Eurofins) protocol.

2.4.8. Generation of CAGA12 reporter constructs

2.4.8.1. pGL3-CAGA12 reporter construct

CAGA12 reporter construct was cloned according to Dennler et al. (Dennler et al., 1998). Briefly, a dsDNA oligo containing 12 times the "AGCCAGACA" sequence (CAGA box) interspaced by "AAA" or "TTT" every other time and followed by Adenovirus 2 Major Latent Promoter (MLP) was synthetized by Genewiz. Below the full synthetized sequence can is shown with NheI and HindIII restriction sites in bold, the CAGA box highlighted in yellow and the MLP underlined:

T**GCTAG**CCCGGGAGCCAGACAAAAGCCAGACATTTAGCCAGACAAAAGCCAGACATTTAGCCAG
AAAAAGCCAGACATTTAGCCAGACAAAAGCCAGACATTTAGCCAGACAAAAGCCAGACATTTA
GCCAGACAAAAGCCAGACACTCGAGATCTGGGCTATAAAAGGGGGTGGGGGCGCGTTCGTCCTCA
CTCTCTTCC**AAGCTT**GGCATT

After preparative digestion, synthetic DNA insert was cloned in the multicloning site of pGL3-Basic (Promega) using respective restriction sites.

2.4.8.2. pGL3-CAGA12-NeoR reporter construct

In order to create a stable reporter cell line, an antibiotic resistance gene was inserted. Neomycin resistance (NeoR) gene, its SV40 promoter and its SV40 PolyA were amplificated using PCR, adding desired restriction sites at the extremities, from pcDNA 3.1+ construct. Digested PCR products was cloned in a linearized (BamhI-SalI) pGL3-CAGA12 reporter construct.

2.4.8.3. pGL3-CAGA12-PuroR-P2A-hRenilla-T2A-EGFP construct

In order to create stable cell lines expressing also the luciferase hRenilla normalizator and EGFP to accelerate the selection process, a new pGL3-CAGA12 reporter construct was cloned. Briefly, the insert was obtained by several steps of PCR amplification:

- SV40 promoter and Puromycin resistance (PuroR) gene were amplified from pcDNA 3.1+ vector adding a pGL3, 32bp, homology region its 5' and partial P2A sequence at its 3'
- hRenilla sequence was amplified from psi-CHECK2 vector (Promega) and modified at 5' and 3' with partial P2A and T2A sequences, respectively.

- EGFP gene and SV40 polyA were amplified from pZac-EGFP construct (gently offered by Prof. Giacca Laboratory) with partial T2A sequence at its 5' and a pGL3, 32bp, homology region its 3'.

A unique 3 kb PCR amplicon was generated using the 3 templates and it was inserted in a linearized (BamhI-SalI) pGL3-CAGA12 reporter construct using AQUA cloning method. P2A and T2A sequences were obtained from the Liu et al. published work (Liu et al., 2017).

2.4.9. Generation of sgRNAs constructs

In order to generate sgRNAs able to target specific receptor an informatic prediction tool "CHOPCHOP" was used (https://chopchop.cbu.uib.no/). Best score hits were furtherly screened using ENSEMBL database to choose sgRNA targeting the most upstream and common sequence among all gene isoforms. Presence of SNP was also checked, in case of SNP presence the relative sgRNA was discarded. For each targeted receptor 2 different sgRNAs were selected and, for each sgRNA, two 25bp ssDNA oligonucleotide were synthetized. Annealing of ss DNA oligonucleotides in a dsDNA oligonucleotide with overhanging ends compatible for sticky end ligation was performed using thermocycler starting from a 95°C denaturation step and decreasing progressively to 25°C in a period of 20 minutes. Backbone plasmid pZac2.1-U6sgRNA-CMV-ZsGreen was digested with BbsI, then 50 ng of linearized plasmid were ligated with 2 µL of annealed oligonucleotide mixture (10 µM) as described before in paragraph 2.4.3.

2.5. Cell culture procedures

2.5.1. General cell culture conditions

In this work, several cell lines were cultured according to the following conditions:

- HEK-293T: cells were cultured in Dulbecco's modified Eagle's medium, high glucose (DMEM-HG, Gibco) supplemented with 10% FBS, and penicillin/streptomycin (P/S, 100 U/mL and 100 g/mL) unless stated differently.
- NIH/3T3: cells were cultured in DMEM-HG supplemented with 10% FBS, and P/S unless stated differently.
- A204: cells were cultured in McCoy's 5a Medium Modified supplemented with 10% FBS, and P/S unless stated differently.

- CHO: cells were cultured in Ham's F-12 Nutrient Mix supplemented with 10% FBS, and P/S unless stated differently.
- HL-1: cells were cultured in Claycomb Medium supplemented with 10% FBS, glutamine 2mM and P/S unless stated differently. “Primaria” (Corning) plates were required for cell adhesion.
- Neonatal rat cardiomyocytes: cells were cultured in DMEM-HG supplemented with 5% FBS, B12 vitamin (2 mg/L) and P/S unless stated differently. “Primaria” (Corning) plates were required for cell adhesion.

All cell lines were maintained in a humidified environment at 37°C and 5% CO_2.

2.5.2. Isolation of neonatal rat cardiomyocytes:

Ventricle from 1-2 days old Wistar rats were separated from the atria, minced into small pieces and digested at RT using CBFHH buffer supplemented with Trypsin (1.75 mg/mL) and DNase I (10 µg/mL). Ventricular cardiomyocytes were detached through pipetting and collected in supernatant, then cells were centrifuged and re-suspended in neonatal rat cardiomyocyte medium. Recovered primary cells were passed through a cell strainer (40 µm) and then seeded onto standard plastic dishes and incubated for 2h. After this pre-plating steps, most fibroblast adhered to plastic surface and cardiomyocytes were collected from supernatant. Then cardiomyocytes were counted and seeded at desired density on “Primaria” plates (Corning).

2.5.3. Transfection protocols

In this work, several cell lines were transfected according to the following protocols:

- HEK-293T: cells were transfected using calcium phosphate method described by Jordan (Jordan et al., 1996). Briefly, when cellular confluence reached 40-60%, culture medium was replaced with fresh medium and after 1/2h transfection mix was prepared. For $5*10^5$ cells, 2.5 µg of plasmid DNA was added to sterile water to a final volume of 90 µL and supplemented with 10 µL of $CaCl_2$ (2.5 M). After mixing, solution was added to an equal volume of HBS 2X and vortexed vigorously for 45 sec. Shortly after, transfection mix was added drop by drop to culture medium. Cells were left growing ON and medium was replaced on the following day.

- NIH/3T3: cells were transfected following Lipofectamine 2000 (Invitrogen) manufacturer's protocol. Briefly, when cellular confluence reached 70-80%, culture medium was replaced with 50 µL of fresh Optimem without antibiotics (96-well) and transfection mix was prepared. 25 µL Optimem-Lipo2000 mixture was prepared (100:1 or 50:1 ratio), and after 5 minutes, 25 µL of Optimem-DNA (from 10 to 40 ng/µL) was added and incubated for 20-30 minutes. After this step, transfection mix was added to cells and incubated for 4-6h. Finally, medium was removed and replaced with fresh medium without antibiotics.
- A204: cells were transfected following a using Lipofectamine 2000 manufacturer's protocol as already described above (NIH/3T3 cells).
- CHO: cells were transfected following Lipofectamine 2000 manufacturer's protocol as already described above (NIH/3T3 cells).
- HL-1: cells were transfected following FuGENE HD (Promega) manufacturer's protocol. Briefly, when cellular confluence reached 70-80%, culture medium was replaced with 95 µL of fresh medium (96-well) and transfection mix was prepared. 4.5 µL of Optimem-DNA mixture (20 ng/µL) were supplemented with 0.5 µL of FuGENE HD, mixed and incubated for 10 minutes. After this step, transfection mix was added to cells and incubated ON.
- Neonatal rat cardiomyocytes: cells were transfected following Lipofectamine 2000 manufacturer's protocol as already described above (NIH/3T3 cells).

In each transfection process, EGFP- or mCherry-transfected cells were used as positive control for transfection.

2.5.4. AAV infection protocols

In this work, HL-1-CAS9 and HEK-293T were infected using AAV9 or AAV6 vectors at a concentration of $5*10^4$ GC/cell. Briefly, cell's medium was removed and fresh medium supplemented with desired viral titer was added for 24/48h. Infectivity could be enhanced by MG132 supplementation as described in Nonnenmacher work (Nonnenmacher and Weber, 2012). Successful transduction was checked using EGFP-expressing AAVs.

2.5.5. Generation and selection of stable clones

Stable clones were generated from an initial mix of transfected cells with a plasmid co-expressing an antibiotic resistance gene. After transfection, cells were re-plated and exposed to single or to a combination of different antibiotics (InvivoGen) at the following concentrations: Geneticin (1 mg/mL), Zeocin (0.75 mg/mL), Puromycin (5 µg/mL). After 1 week, cells were detached and subjected to limiting dilution as shown in fig. 6. Briefly, approximately 4000 cells were plated in "A1" well (96-well plate), then sequential 1:2 dilutions were performed in each well of the first column. Subsequently, using a multi-channel pipette, a second series of 1:2 serial dilution was performed from row 1 to row 12. Following days wells were carefully checked and wells with only a single colony were selected.

In one case, HEK-293T-CAGA12-hRenilla-EGFP clones, selection process was remarkably accelerated using a fluorescence activated cell sorting (FACS) with cells co-expressing an EGFP transcript in frame with a P2A peptide and the antibiotic resistance gene.

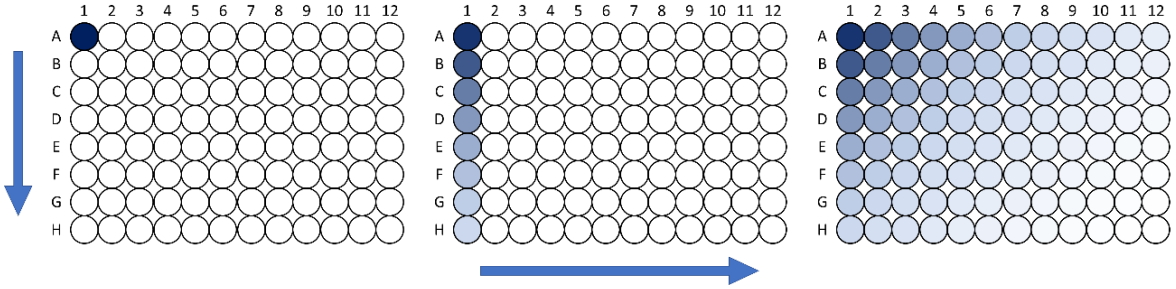

Figure 6: Schematic representation of cell limiting dilution protocol.

2.6. CAGA12-luciferase assay

2.6.1. Assay settings

Stable reporter cells or transient transfected cells grew until they reached an average confluency of 80-90%, then complete medium was removed, and cells were washed with PBS to remove FBS contaminations. Serum-free Optimem medium was added to each well for a period of 8h before inducing signaling with recombinant proteins. Recombinant proteins were thawed in ice and diluted in serum-free Optimem medium in order to have desired concentration for recombinant protein stock solution. This stock solution was then serially diluted by 1/3 factor in order to cover a wide range of tested conditions. When GDF11 or MSTN activity was investigated, dilutions were performed using serum-free Optimem medium, but in case of prodomain bioactivity testing, dilutions were performed

using serum-free Optimem medium supplemented with a fixed amount of GDF11/MSTN. At the end of the incubation time, stock solutions and/or diluted treatments were then added to each well ON (n=2-3). On the following day, SMAD3/4 activity was measured as described in the next paragraph.

2.6.2. Firefly and Renilla luciferase measurements

Luciferase assays were performed according to manufacturer's instruction of Glo-Lysis buffer (Promega) followed by ONE-GLO or DUAL-GLO Luciferase Assay System (Promega). ONE-GLO system was used in case of stable CAGA12 reporter cell line, whereas DUAL-GLO system was used in case of transient CAGA12 transfection or in case of HEK-293T-CAGA12-hRenilla-EGFP stable cell line. Briefly, cells were washed with PBS and then 50 µL of Glo-Lysis buffer were added to each 96-well and incubated for 10 minutes. Then lysate was recovered and mixed in a 1:1 ratio with respective GLO-luciferase substrates and after 10 minutes luciferase activity was detected with a EnVision Multilabel Plate Reader (PerkinElmer, 1 second integration signal). Results obtained were expressed as fold change over control treatment. EC50 and IC50 values were calculate importing the luciferase activity data into GraphPad Prism software and using a non-linear regression curve fit with a variable slope (four parameters).

2.7. Protein purification procedures from culture medium

2.7.1. Inactive latent complex purification through streptavidin beads

"Streptavidin Mag Sepharose" beads (GE Healthcare) were used in the preliminary studies to purify protein from small volume of medium. Briefly, biotinylated proteins were produced through BirA system (Predonzani et al., 2008) and secreted into conditioned culture medium. Excess of biotin was removed from culture medium using a centrifugal filtering unit (10 kDa cutoff). Then, 2 to 6 mL of filtered culture medium were incubated with equilibrated streptavidin beads (from 40 to 100 µL) for 3 h, at 4°C on a roller tube. Beads were washed 3 times with ice-cold PBS and treated with different denaturing conditions for 1 h, at 4°C on a roller tube. After incubation, supernatant was collected for further quantification and beads were washed 3 times with PBS. Streptavidin beads were

recovered and loaded as control to quantify the amount of mature protein still entrapped in the inactive latent complex.

2.7.2. Immobilized metal affinity chromatography (IMAC) protein purification

Protein purification process from medium volumes larger than 50 mL was performed by IMAC. HiTrap Chelating HP IMAC 5 mL columns (GE Healthcare) were loaded with $NiSO_4$ (0.1 M) using an ÄKTA FPLC system (GE Healthcare). Conditioned medium was prepared as described in paragraph 2.2.6.1, supplemented with NaCl (0.5 M final concentration), filtered (0.22 µm) and adjusted to a pH of 7.4.

A small fraction of filtered medium was stored for further analysis (Input), the rest was loaded into equilibrated HiTrap 5mL column at 2.5 mL/min. Flow-through (FT) was collected until all medium was loaded on the column (FT1), then column was washed using binding buffer until UV absorption reached baseline (FT2). Elution was performed with an elution buffer gradient and fractions were collected according to λ_{280} absorption. Subsequently, fractions were investigated for protein of interest presence using WB. Fractions showing the highest purity and protein concentration were mixed together and concentrated using centrifugal filter units: Amicon Ultra-0.5 (10 kDa cutoff, Sigma-Aldrich) or Vivaspin 6 (10 kDa cutoff, Sartorius). Concentrated samples were then quantified using Coomassie staining.

2.7.3. HPLC C4 reverse phase protein purification

Protein samples obtained from previous IMAC purification were equilibrated with 0.1% trifluoroacetic acid (TFA) and loaded into an equilibrated Jupiter 5 µm C4 300 Å, LC Column 250 x 4.6 mm, (Phenomenex) using an Agilent 1100 HPLC system (Agilent Technologies). Liquid phase composition was changed with a linear gradient from 0.1% TFA in water to a 0.1% TFA in acetonitrile (ACN) in 60 min (1 mL/min). UV absorption at 280 nm was constantly measured during the separation process and it was used to identify and collect protein peaks eluting from the column. Eluted fractions were then frozen on dry ice and sublimated using SpeedVac SC110 (Savant). Lyophilizated proteins were then resuspended in an appropriate volume of PBS 4mM HCl and used for further analysis or stored at -80°C.

2.8. Histology

2.8.1. Periodic Acid Shift (PAS) stain and cross-section area measurement

PFA fixed tissues were washed for two consecutive days with a solution of 50% ethanol, in H_20 at 4°C. Tissues were embedded in paraffin following manufacturer's protocol using an Automatic Tissue Processor TP1020 (Leica). Staining for PAS was performed as described in PAS staining system (Sigma-Aldrich).

PAS-stained heart and tibialis muscles sections images were acquired using a Leica ICC50W microscope (HI Plan 20×/0.40 NA objective, Leica), and cross-sectional area was measured using ImageJ software (NIH). Both procedures were performed by an operator that was blinded. For each tissue, three consecutive sections taken at a distance of 150/200 µm from each other were analyzed. Among these sections, a minimum of 150 cells per sample were selected and measured.

2.9. In vivo experimental procedures

2.9.1. Animal housing and mice strains used

Housing and handling of mice were performed in accordance to institutional guidelines and all the experimental procedures were approved by International Centre for Genetic Engineering and Biotechnology (ICGEB) board, with the full respect of the EU directive 2010/63/EU for animal experimentation. The study was authorized by the Italian Ministry of Health, "ICGEB PPR n. PPR2/14". Animals were kept in the ICGEB Bio-experimentation Facility in a temperature-controlled environment with a 12/12 hours light-dark cycles. All animals received a standard chow diet and water ad libitum.

In this work two different mice strains were used:

- C57Bl/6 WT strain: initially purchased from Envigo (exact strain name: C57BL-6JOlaHsd), mice were interbred to expand the colony. Females did not undergo through more than 4 delivery.
- Myh6-Cas9-C57Bl/6 strain: gently donated by Prof. Mauro Giacca laboratory (exact strain name C57-Myh6-Cas9-2A-TdTomato, described in Carrol published work (Carroll et al., 2016)). Mice were crossed with C57Bl/6 WT mice to expand and

maintain the colony. Females did not undergo through more than 4 delivery.

2.9.2. Animals genotyping from tail biopsies

In order to genotype animals, tail biopsies were performed to obtain genomic DNA. Approximately 5mm of tail was processed according "Extract-N-Amp Tissue PCR Kit" (Merck) manufacturer's protocol. Primers used for PCR amplification are listed in table 11, amplification conditions are illustrated in fig. 7. PCR products were separated and analyzed after run in a 1% agarose gel. Expected transgenic band was 689 bp, WT animals genomic DNA was not amplified.

Primer Name:	**Sequence (5'-3'):**
Td-Tomato Fw	ACATGGCCGTCATCAAAGA
Td-Tomato Rev	CTTGTACAGCTCGTCCATGC

Table 11: List of primers used during genotyping process.

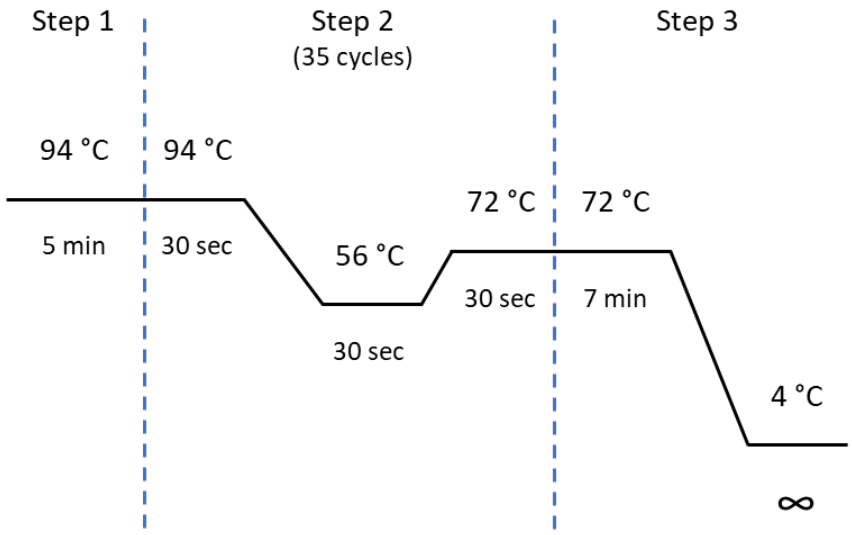

Figure 7: Schematic representation of genotyping PCR protocol.

2.9.3. Surgical anesthesia and post-surgery analgesia

Animals undergoing invasive procedures (minor or major surgeries) were always anesthetized using a mixture of oxygen gas and isoflurane. A 2% to 4% isoflurane concentration was used to induce, within 2-3 minutes, a non-responsive state in mice. Then mice were moved to surgical plane and a nose cone or endotracheal tube was positioned to maintain anesthesia by gas mixture inspiration. Mice pain-awareness was checked by

tail-pinch method. Animal temperature was maintained using a heating pad at 37°C. Once surgical procedure was finished, mice received 0.1 mg/kg/12h buprenorphine subcutaneous injection and recovered in a heated (37°C) clean cage. Post-surgery analgesia was maintained for 24h in case of minor surgery or 48h in case of major surgery (0.1 mg/kg buprenorphine every 12 hours).

2.9.4. AAV vector injections and animals' follow-up

Investigation using AAV vector administration were performed using two different injection methods:

- Intramyocardial delivery: two separate injections (20 µL each) were performed directly into the left ventricle anterior wall and locally delivered a total of 10^{11} GC/animal. For this approach 2 months old, male, WT C57Bl/6 animals were used.
- Intravenous delivery: a single retro-orbital sinus venous injection (50 µL of volume) was performed using up to $2*10^{12}$ GC/animal. In this case, 3 months old, male, WT C57Bl/6 animals were used. Dose finding studies were performed using untreated animals. In case of experiments using the pressure overload mouse model, AAV injection was performed 1 week after the TAC procedure.

Both injections methods were performed using an insulin syringe (30 gauge). Control treatments were performed using AAV-GFP vector or PBS. All treatments were administered by a blinded operator on randomized animals.

During the experimental period, animals were weighted twice a week and its percentual body weight change was calculated according to their initial weight before the AAV injection or surgical procedure. If percentual body weight reduction was more than 25%, animals were euthanized, and tissue harvested.

2.9.5. Blood withdrawal procedures

Blood samples were collected at different timepoints during experimental procedures. Submandibular bleeding or terminal bleeding were performed as described by Golde and Parasuraman respectively (Golde et al., 2005; Parasuraman et al., 2010). Blood was collected in 1.5 mL tubes, clotted at RT for 1 hour and centrifuged 10 min at 5000g. Serum was stored at -80°C for future analysis.

2.9.6. Sacrifice and tissue harvesting

At the end of the experimental period, animals were anesthetized and sacrificed by intravenous injection of potassium chloride (150 mg/kg) or by cervical dislocation. Terminal blood withdrawal was performed at this point, then skin was incised, and organs harvested. Each organ was weighted before further processing. Heart was cut in 3 different parts that were used respectively for RNA isolation, protein extraction and histology. Liver quadrate lobe was used for RNA/protein extraction and the remaining was fixed for histology. Tibialis anterior, gastrocnemius and quadriceps femoris were identified, isolated and harvested. All tissues designed for histology were fixed in PFA 4% ON. All tissues for RNA and protein extraction were immediately frozen in liquid nitrogen after harvesting. Tibia length was measured for normalization purposes. All sacrifice procedures were performed by two blinded operators.

2.9.7. Transverse aortic constriction (TAC)

Mice underwent either a sham operation or were subjected to pressure overload induced by TAC. The transverse aortic arch was ligated (6-0 silk) between the innominate and left common carotid arteries with an overlying 27-gauge needle, and then the needle was removed. TAC pressure gradients were determined by Doppler echocardiography to exclude from the study mice with a right carotid/left carotid flow ratio (Hartley et al., 2008). All surgical procedures were performed by a single operator blinded to the experimental conditions.

2.9.8. Echocardiography

Trans-thoracic two-dimensional echocardiography was performed one day before animals' sacrifice. Mice were anesthetized using 1-2% isoflurane and imaged using a Vevo 2100 Ultrasound (VisualSonics), equipped with a 30-MHz linear array transducer. M-mode tracing was used to measure ejection fraction, fractional shortening, left ventricular anterior wall thickness, left ventricular posterior wall thickness and internal chamber diameter at end-systole and end-diastole. All echocardiography imaging and data analysis was performed by a single operator blinded to the experimental conditions.

2.9.9. Terminal hemodynamic assessment

Mice that underwent to TAC or Sham operated mice were subjected to a terminal hemodynamic study as previously described (Pacher et al., 2008). A 1.4F, high-fidelity, manometer-tipped catheter (SPR-839, Millar Instruments) was introduced into the left ventricle through the right common carotid artery. Data was acquired at steady states and during acute inferior vena cava occlusions (variable loading conditions). Data analysis was performed by PVAN software (AD Instruments, Inc). The end-systolic and end-diastolic pressure-volume relationships during inferior vena cava occlusions were used to calculate end-systolic and end-diastolic stiffness (slope of linear fit of end-diastolic pressure-volume relationship). Measurement of the diastolic properties of the left ventricle were also estimated from indices such as the maximal rate of pressure decay (dP/dt_{min}), or isovolumic relaxation constant (Tau).

2.10. GDF11/MSTN quantification from culture medium and serum

In this study, GDF11/MSTN quantification from serum or culture medium samples was achieved following two different protocols:

2.10.1. Western blot

Western blot was used prevalently to estimate GDF11 and MSTN concentrations in culture medium and in serum samples. Western blot protocol is described in paragraph 2.2.7. Primary antibody was the Rb MAB antiGDF11/8 (Abcam, code: ab124721). This antibody was able to bind both GDF11 and MSTN recombinant proteins with the same affinity as showed in fig. 8A. Other, more specific antibody against GDF11 or MSTN were also used: anti-GDF11 antibody (RnD, code MAB19581) or anti-MSTN antibody (RnD, BAF788). However only the former was adequately specific, the latter showed a 10-15% of cross reactivity with GDF11 protein (Fig 8A).

For our purposes, the Rb MAB antiGDF11/8 was selected for the quantification method because it is able to compare directly GDF11 and MSTN without bias of affinity but cannot distinguish the two proteins.

2.10.2. Mass spectrometry

Unspecific GDF11/MSTN detection represents a major issue that has been addressed by Schafer and colleagues by developing a highly specific liquid chromatography tandem mass spectrometry (LC-MS/MS) assay to quantify GDF11 and MSTN concentration in human serum (Schafer et al., 2016). In collaboration with Dr. Olga Shevchuk (Leibniz Institut für Analytische Wissenschaften, ISAS Campus, Dormund) we have developed a parallel reaction monitoring (PRM) LC-MS/MS based assay combined with immunoprecipitation where, using stable isotope labeled (SIL) peptides, we could reliably distinguish MSTN, GDF11 and also determine their endogenous concentrations in murine serum. The development of the assay was entirely performed by Dr. Olga Shevchuk while we developed the immunoprecipitation steps and provided murine serum.

2.10.2.1.GDF11/MSTN immunoprecipitation (IP)

Previous analyses have shown that MSTN and, in particular, GDF11 are present at very low concentration in human serum (Schafer et al., 2016). We performed IP of GDF11 and MSTN from serum of WT mice before mass spectrometry analysis. This step is not crucial for the method itself, but it is necessary if GDF11 and MSTN concentration are lower than detection limits. Indeed, in paragraph 4.5.1 after AAV infection, GDF11 and MSTN enriched serum samples do not required IP step and they were directly measured as described in the following chapter.

Briefly, antibody biotinylation of anti-GDF11 antibody (RnD, code MAB19581) was performed following manufacturer's instructions of "Biotin Conjugation Kit (Fast, Type B)" (Abcam). Biotinylation process does not affect its binding capacity (Fig. 8A). IP was carried out starting from 50 µL of C57Bl/6 WT serum. Samples (S1) were incubated with 5 µg of selected biotinylated antibody ON, at 4°C on a tube roller. On the following day, "Streptavidin Mag Sepharose" beads (GE Healthcare) were equilibrated and added (40 µL) to each serum sample for an additional 20 min at 4°C on a tube roller. Immunoprecipitated serum (S2) was collected for subsequent WB analysis. Recovered beads were gently washed with ice-cold PBS (400 µL) for three times and washing solutions were collected for further analysis (W1, W2, W3). The elution was performed twice with 10% SDS solution (25 µL) at 95°C for 3 min (E1, E2) or twice with 20 µL of 0.1M glycine followed by neutralization with 40 µL of ammonium bicarbonate buffer, in case of WB or LC-MS/MS analysis

respectively. Eluted beads (B1) were recovered and loaded as control for complete elution (Fig. 8B-C).

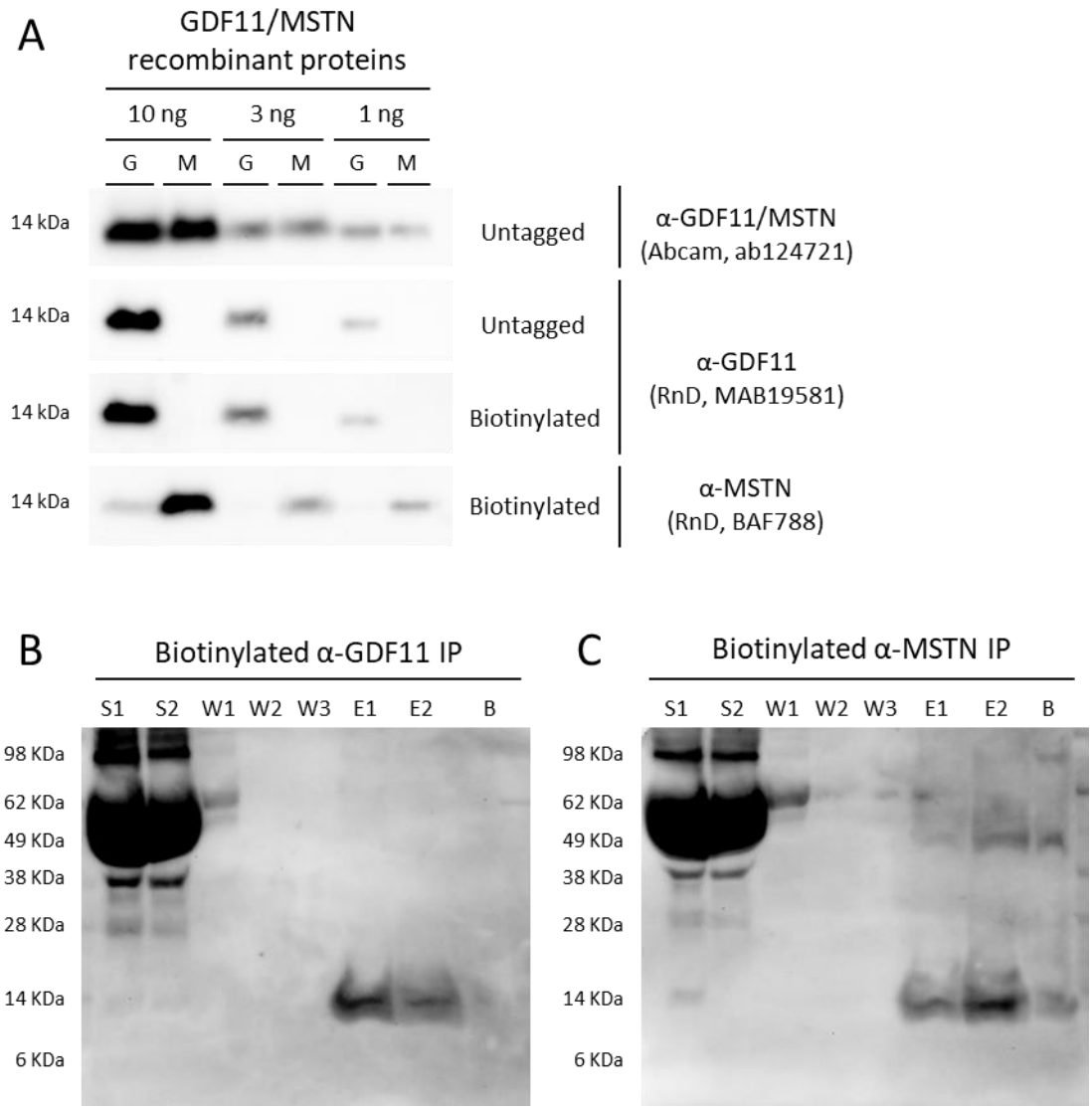

Figure 8: Immunoprecipitation of GDF11 and MSTN from mouse serum.
(A) Comparison of GDF11/MSTN detection specificity and threshold of commercial antibodies. Binding capacity of unlabeled and biotinylated antibodies were compared. GDF11 and MSTN recombinant protein are marked as "G" or "M", respectively.
(B, C) IP from mouse serum: both anti-GDF11 (B) and anti-MSTN (C) were able to precipitate GDF11 and MSTN from serum. Lanes legend is described in paragraph 2.10.2.1.

2.10.2.2. Trypsin digestion of C57Bl/6 WT serum

Serum digestion was performed starting from 5 µL of fresh C57Bl/6 WT serum, 28.7 µL of 50 mM ammonium bicarbonate buffer and 20 µL of 10% sodium deoxycholate. Then solution was supplemented with 20 µL of 50 mM TCEP and incubated at 60°C for 30 min. Reduced proteins were alkylated using 20 µL of 100 mM iodoacetamide (IAA) at 37°C for 30 min, followed by supplementation with 20 µL of 100 mM dithiothreitol (DTT) to quench

the unreacted IAA (37°C for 15 min). Trypsin (Promega, enzyme:substrate ratio of 1:10) digestion was performed at 37°C for 16h in agitation and blocked by addition of TFA to a final concentration of 1%. Serum peptide digestion was then vortexed and centrifuged at 18000g for 5 min. Supernatant was recovered and collected in LowBind tubes (Eppendorf) and desalted using C18 solid phase extraction cartridges (SPEC, 4 mg, Varian) following manufacturer's instructions. Eluted digestions were lyophilized using the SpeedVac system and resolubilized in 0.1% TFA.

2.10.2.3.Generation of calibration curves with SIL peptides in digested serum

In order to perform GDF11 and MSTN quantification from serum a ten-point response calibration curve was generated using three distinct unique isotope labeled peptides. More in detail, GDF11 or MSTN specific SIL-peptides are enlisted in table 12 and represented in fig. 9 on their respective ligand aminoacidic sequence.

Protein	Peptide	Precursor Charge	Isotope Label Type	Precursor Mz
GDF11	IPGMVVDR	2	Light	443.7444
	IPGMVVDR	2	Heavy	448.7485
MSTN	DFGLDCDEHSTESR	3	light	556.5583
	DFGLDCDEHSTESR	3	heavy	559.8943
	IPAMVVDR	2	light	450.7522
	IPAMVVDR	2	heavy	455.7563

Table 12: Peptides and precursor selected for the assay.

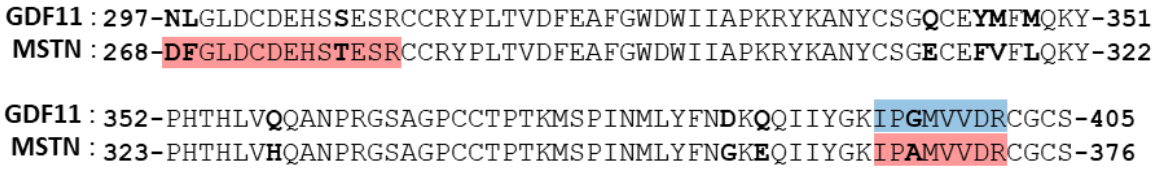

Figure 9: Schematic representation of GDF11 and MSTN aminoacid sequences and of the selected peptides used in the assay.

Only mature protein sequence is represented. Amino acid difference between the two ligands are represented in bold. Selected peptides are highlighted in blue (GDF11) or in red (MSTN).

Briefly, serial dilutions of each SIL-peptides were performed in a digested serum matrix prepared as described in 2.10.2.2 paragraph. Multipoint calibration curve had

concentration of SIL peptides starting from 3.33 nM to 1 pM, diluted progressively in the same serum matrix (200 ng each sample). Peptide samples were then separated on an Ultimate 3000 Rapid Separation Liquid Chromatography (RSLC) nano system (Thermo Scientific) with ProFlow flow control device coupled to a Q Exactiv HF mass spectrometer (Thermo Scientific). Data obtained from this calibration curves allowed to identify the optimal amount of SIL-peptide (2 fmol corresponding to 0.13 nM of each peptide) to add in each serum sample for a reliable GDF11/MSTN quantification.

In order to further optimize the method and assess its sensitivity, new calibration curves with lower SIL peptides concentration and with both light and heavy SIL peptides are going to be performed and evaluated.

2.10.2.4.(PRM) LC-MS/MS of GDF11/MSTN IP samples from C57Bl/6 WT serum

For each IP eluate, 30 µL of sample were reduced using 10 mM DTT at 56°C for 30 min, alkylated using 20 of 30 mM iodoacetamide (IAA) at 37°C for 30 min followed by ethanol precipitation (1:10 ratio using ice cold ethanol). After 60 min at -80°C, samples were thawed during centrifugation (4°C, 20000 g for 40 min) and supernatant discarded. Pellet was resuspended in 30 µL of digestion buffer (0.2 M guanidinium chloride, 50 nM ammonium bicarbonate buffer, 2 mM $CaCl_2$ and 100 ng of trypsin) and incubated at 37°C for 16h in agitation and blocked by addition of TFA to a final concentration of 1%. Samples were spiked with 2 fmol of each SIL peptide and analyzed using an Ultimate 3000 RSLC system coupled to a Q Exactive HF orbitrap (Thermo Scientific). Raw data were analyzed with Proteome Discoverer 2.2 (Thermo Scientific) using Mascot 2.6 as search algorithms. MS/MS spectra were searched against murine UniProt database with a fragmented ion tolerance of 0.02 Da.

2.10.2.5.(PRM) LC-MS/MS of GDF11/MSTN serum samples from AAV treated animals

Animal with supraphysiological levels of GDF11 or MSTN do not required an immunoprecipitation step to increase their ligand concentration in the serum samples. Indeed, serum sample of animals described in paragraph 4.5 were digested and resuspended as described in paragraph 2.10.2.2. After resuspension, samples were spiked with 2 fmol of SIL peptides and quantified as described in the previous paragraph.

2.11. Statistical analysis

All the results are expressed as mean ± standard deviation. Student's T-test, one-way ANOVA or two-way ANOVA tests were calculated using GraphPad Prism 6 (GraphPad Software, La Jolla California USA). Student's T-test was used to compare two groups, one-way ANOVA followed by Dunett's multiple comparison was used to compare multiple sample groups with one control, two-way ANOVA was used to compare multiple measurements of distinct sample groups. Statistical significance against control treatment was highlighted with "*" symbols as listed in table 13. EC50 and IC50 values were calculated using nonlinear regression curve with variable slope (four-parameter) in GraphPad Prism 6.

Statistical significance	Symbol
$P > 0.05$	n.s.
$P \leq 0.05$	*
$P \leq 0.01$	**
$P \leq 0.001$	***
$P \leq 0.0001$	****

Table 13: Schematic representation of statistical significance thresholds and their respective symbols.

3. AIMS OF THE STUDY

GDF11 and MSTN share 90% structural homology and receptor use, however, overlapping and unique effects are still unclear, limiting their use as pharmacologic targets. Indeed, GDF11 has shown a more potent effect in reversing cardiac hypertrophy when compared to MSTN.

Aim 1. *To test the hypothesis that GDF11 and MSTN are redundant in activating SMAD2/3 in cardiomyocytes and the differential effect can be explained by differences in potency*. In this part of the thesis we will produce recombinant proteins, test their bioactivity and perform *in vitro* experiments by selectively knocking out type I TGF-β receptors in cardiomyocytes.

Aim 2. *To test the hypothesis that cardiac specific increase of GDF11 and MSTN levels using an AAV vector can reverse pathological cardiac hypertrophy in vivo without systemic adverse effect.*

In this part of the thesis we will perform *in vivo* studies to evaluate the effect of targeting specifically cardiomyocytes by AAV vectors. We will also evaluate the dose-dependent effect of both GDF11 and MSTN in reducing cardiac mass in physiological conditions and in a model of pathological cardiac hypertrophy. Finally, we will evaluate if reversal of pathological cardiac hypertrophy translates in improvement of diastolic function.

4. RESULTS

4.1. Regulation of GDF11/MSTN production and signaling

In order to understand the differences between GDF11 and MSTN signaling in cardiomyocytes, we decided to investigate how these two proteins activate their canonical pathway using several immortalized cell lines. Activation of canonical TGF-β pathway involves nuclear assembly of different proteins: SMAD2, SMAD3 and SMAD4, that form a heterotrimeric complex able to regulate gene expression (Yang et al., 2015). In order to study this pathway, we took advantage of the CAGA12 luciferase reporter system developed by Dennler and colleagues (Dennler et al., 1998), that is sensitive to SMAD3/4 activation. Luciferase measurements allowed us to quantify GDF11 and MSTN bioactivity, potency and how their signaling is modulated by respective prodomains.

4.1.1. GDF11/MSTN transfected HEK-293T conditioned media do not increase SMAD3/4 signaling

GDF11 and MSTN are both secreted proteins. Our first approach to study their properties was obtaining conditioned media from transiently transfected HEK-293T cells. HEK-293T were transfected using standard calcium phosphate method and, after 24 hours, cells were placed in serum free medium for 48 hours. Then, conditioned medium was harvested for bioactivity experiments.

In parallel, a second set of experiments using HEK-293T co-transfected with CAGA12 reporter plasmid and renilla luciferase plasmid were used to quantify GDF11 and MSTN conditioned media bioactivity. As shown in fig. 10A, both GDF11 and MSTN conditioned media did not produce any significant change in luciferase activity when compared to control medium.

Interestingly, the concentration of GDF11 mature ligand in conditioned medium, detected by western blot (Fig. 10B), was estimated in the range of 1-5 nM. This concentration would have been sufficient to induce the activation of CAGA12 reporter when compared to a parallel CAGA12 assay obtained using GDF11 recombinant protein (Fig. 10C, EC50: 0.11 nM). We speculate that the presence of the prodomain was preventing GDF11 and MSTN activity.

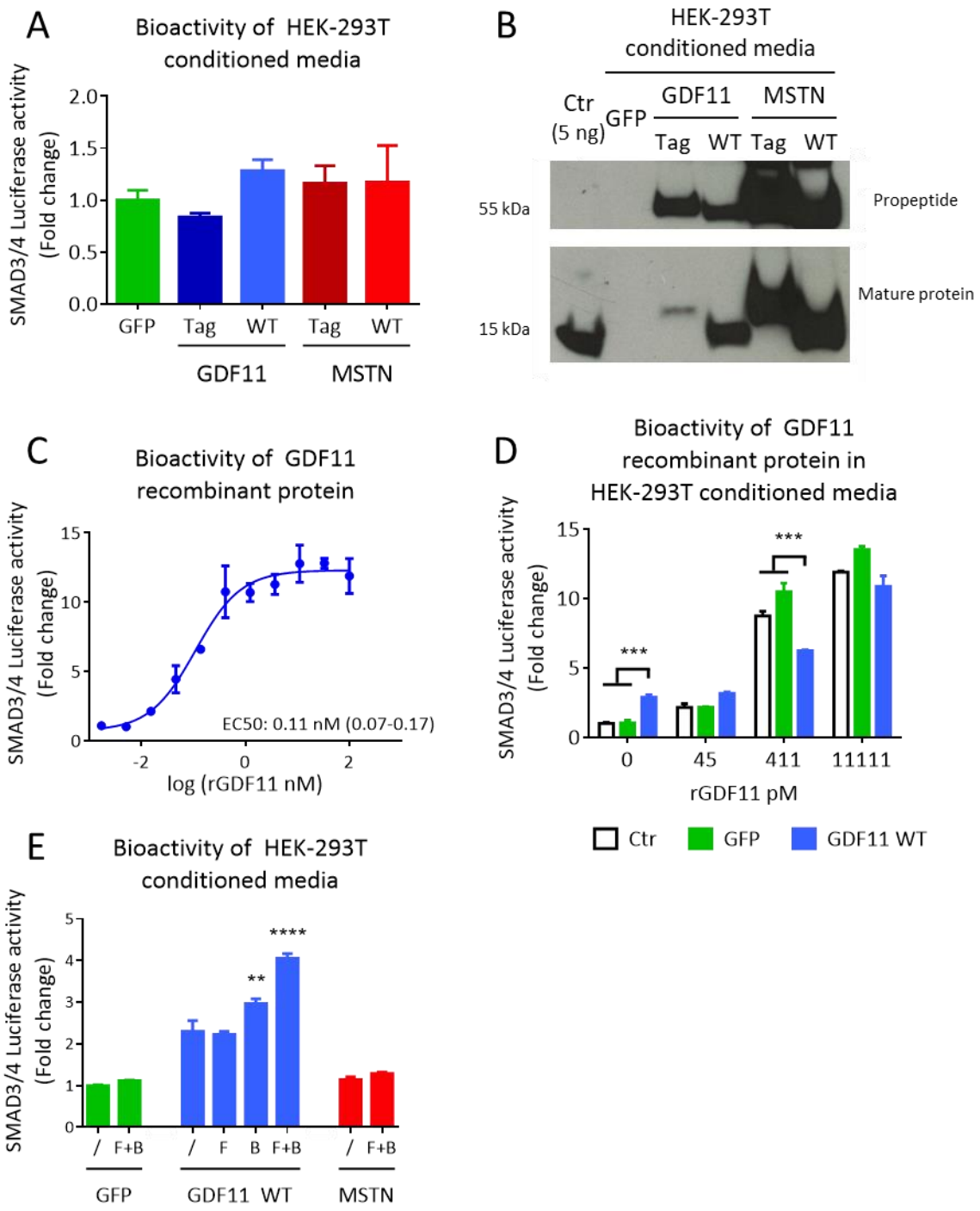

Figure 10: Biological activity of GDF11 is controlled by post-translational processing in HEK-293T conditioned media.

(A) CAGA12 luciferase assay does not reveal significant difference among GDF11/MSTN conditioned media when compared to GFP conditioned media. A C-terminus, 3 kDa Myc-Flag-tag, above mentioned as "Tag" was used in the initial part of the studies aiming to discriminate the transfected GDF11/MSTN proteins from the endogenous produced ligands. Activity assays revealed that Tag protein was inactivating both GDF11 and MSTN and thus this strategy was no longer pursued.

(B) WB analysis showed that HEK-293T conditioned media used in CAGA12 assay contains GDF11 and MSTN mature proteins. Estimated rGDF11 concentration is between is 1-5 nM. Abcam GDF11/MSTN (ab124721) was used as primary antibody. GDF11 recombinant protein (Ctr, 5 ng) were added as reference for quantification.

(C) CAGA12 luciferase assay performed with commercial recombinant protein. EC50: 0.11nM. (D) CAGA12 luciferase assay performed with different amounts of recombinant GDF11 added to fresh medium (Ctr), GFP conditioned medium or GDF11 conditioned medium. GDF11 conditioned medium spiked with 411 pM GDF11 showed a lower SMAD3/4 activation when compared to fresh medium of GFP conditioned medium.
(E) Co-transfection of GDF11 and BMP1 (represented by letter "B") with or without FURIN (represented by letter "F") increased SMAD3/4 activation in GDF11 conditioned medium.
Data are representative of two separate experiments with n=2/3 biological replicates. Data shown as mean ± SD.

4.1.2. GDF11 conditioned medium but not GFP conditioned medium can blunt GDF11 signaling

In order to test the hypothesis that HEK-293T conditioned media contains some unidentified factor that could inhibit GDF11 signaling I performed an additional experiment where I spiked the following media with commercial recombinant mature GDF11: control medium (Optimem), GFP-transfected conditioned medium and to GDF11-transfected conditioned medium (Fig. 10D). The results of this experiments show that conditioned medium from GDF11 transfected cells was significantly decreasing the activity of exogenously added GDF11 when compared to control medium and GFP medium. We confirmed that the presence of the prodomain was responsible for the inhibitory effect observed. Indeed, co-transfection with BMP1, the protease that by cleaving the prodomain releases the mature protein of GDF11 from the inactive latent complex, was sufficient to significantly increase signaling (Fig. 10E). Because of the issues observed with conditioned medium we changed our strategy and moved to produce and purify GDF11 and MSTN using a eukaryotic expression system (paragraph 4.1.4). When possible, commercial recombinant GDF11 and MSTN proteins were used in parallel to furtherly confirm our findings.

4.1.3. Development of stable SMAD3/4 luciferase reporter cell lines

In order to overcome the variability that derives from transient reporter plasmid transfections, we generated stable CAGA12 reporter cell lines using HEK-293T, NIH/3T3 and A204 cells. All these three stable cell lines were obtained as described in the paragraph 2.5.5 and they were used in the following experiments. As shown in fig. 11A-C, GDF11 was able to activate the reporter in a dose dependent manner with a EC50 that was 0.39 nM, 0.52 nM, 0.41 nM, for NIH/3T3, A204 and HEK-293T respectively. We also tested the activity of MSTN and a reliable EC50 was obtained only when using HEK-293T cells (Fig. 11C, 2.71

nM). Indeed, the range of MSTN used was not sufficient to reach the plateau phase when using NIH/3T3 and A204. As expected, GDF11 is more potent than MSTN in activating the SMAD3/4 signaling. As previously reported, A204-CAGA12 cells did not show luciferase activity in response to rTGF-β1 ligand at the concentration tested (Fig. 12) because of the lack of TGFβRII (Zhu et al., 2004). This feature makes this reporter cell line particularly useful to study GDF11/MSTN signaling removing the possible confounding effects induced by the more potent TGF-β1 ligand.

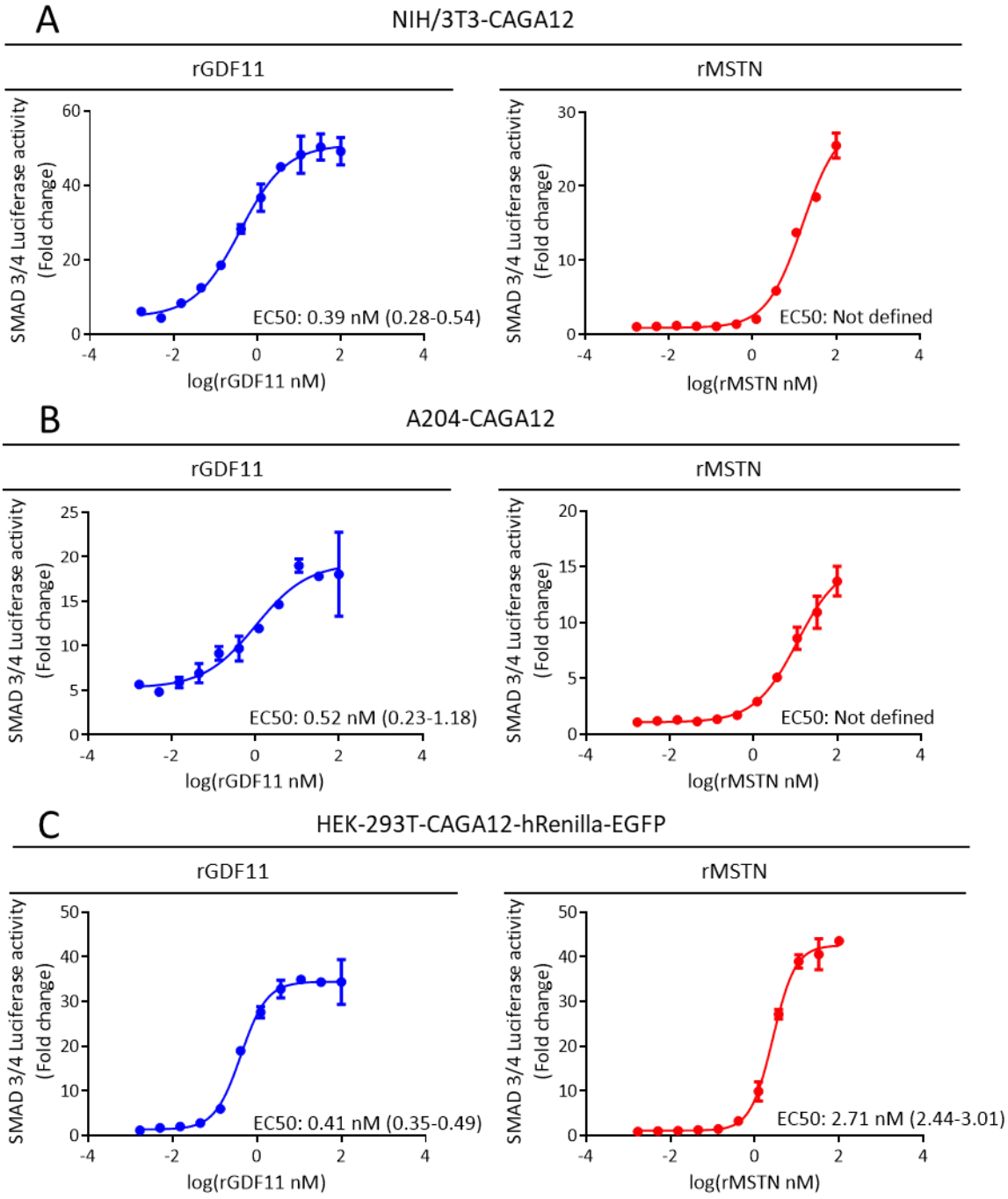

Figure 11: Comparison of GDF11/MSTN dose response curves in NIH/3T3, A204 and HEK-293T CAGA12 stable clones.

(A, B, C) In all three stable reporter cell lines recombinant GDF11 was more potent than MSTN with HEK-293T clone presenting the higher sensitivity to MSTN signaling.
Data are representative of two separate experiments with n=2/3 biological replicates. Data shown as mean ± SD.

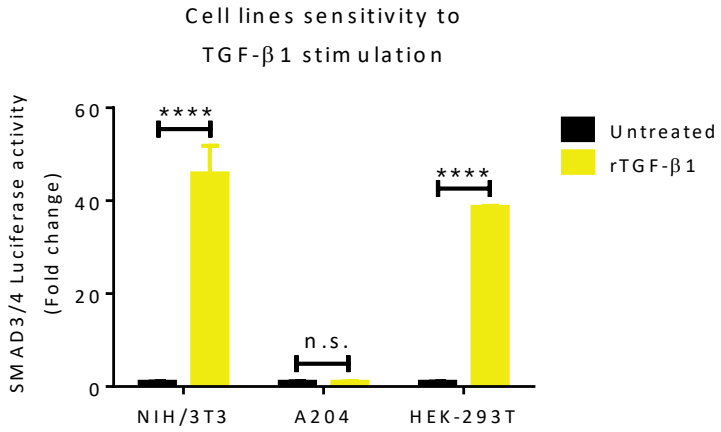

Figure 12: A204 CAGA12 reporter cells do not respond to TGF-β1.
A204, as expected, is the only cell line that is unresponsive to TGF-β1 stimulation (2.73 pM). Data are representative of two separate experiments with n=2/3 biological replicates. Data shown as mean ± SD.

4.1.4. Development and optimization of recombinant protein production strategy

Preliminary results using conditioned media and the CAGA12 assay showed that it is possible to produce bioactive proteins and to measure their biological activity. However, the intrinsic variability of the conditioned media obtained from transiently transfected cells was a critic point and was a hurdle to characterize GDF11 signaling and regulation *in vitro*. Moving our strategy towards an approach based on recombinant proteins allowed us to obtain more controlled and reproducible experimental condition together with a higher concentration and purity of the factors involved.

4.1.4.1. GDF11 and MSTN proteins are not produced at the same levels in vitro

The analysis by western blot of conditioned medium shows that the amount of MSTN was consistently higher when compared to GDF11. The average difference in protein concentration was about 5-folds, a considerable difference considering their high homology and that they share the same experimental conditions (Fig.13A-B, lanes 1 and 2). GDF11 and MSTN share 90% of homology in their mature protein while only 52% in their prodomain (Walker et al., 2016). We hypothesized that this was sufficient to explain the differences in protein production and to test our hypothesis we developed chimeras of both GDF11 and MSTN (Fig. 13C). We also speculated that codon optimization may be

relevant in increasing GDF11 protein production (Fig. 13D-E). This strategy allowed us to understand biology of these two homologous proteins and to optimize recombinant protein production.

4.1.4.2. MSTN prodomain significantly improves GDF11 protein synthesis

To test our hypothesis, we generated two different constructs: GDF11-chimera (GDF11-Chim) and MSTN chimera (MSTN-Chim), by swapping the prodomains. The former is formed indeed by MSTN prodomain and GDF11 mature protein, the latter has GDF11 prodomain and MSTN mature protein (Fig. 13C).

The two wild type constructs and the two chimeras were tested in HEK-293T. Cells were co-transfected with a Furin expressing plasmid to improve intracellular processing. After transfection, cells were switched to serum free medium and after 48h conditioned media was harvested and used for western blot quantification. Different volumes of conditioned media were used in each well in order to improve comparison between samples. As shown in fig. 13A-B switch of prodomains is associated to strong changes in protein production of both GDF11 and MSTN. While MSTN prodomain increases GDF11 production about 7 folds when compared to WT GDF11, GDF11 prodomain produced a decrease in MSTN production of approximately 5 folds when compared to WT MSTN.

4.1.4.3. Development of stable clones for protein productions

The complexity of TGF-β family members biology, including post-translational processing and promiscuity of ligands, receptors and inhibitors, is a major limitation for the use of conditioned media. Thus, our strategy moved and focused on production and purification of recombinant proteins. Our initial strategy was based on transient transfection of the construct of interest in HEK-293T. However, in order to scale up protein production, we moved to selecting high-expressing stable clones using CHO cells. Both GDF11 and MSTN proteins are characterized by two biologically active parts: the inhibitory prodomain and the active mature protein. While the recombinant prodomain can be successfully produced in eukaryotic systems, the mature protein requires the presence of the prodomain for efficient synthesis and proper folding (Walker et al., 2016).

Our approach for recombinant expression of prodomains is shown in fig. 14 and yielded standard, single, stable transfected clones. In the case of recombinant mature proteins, a

full-length propeptide-expressing vector was required. Furthermore, in order to enhance GDF11/MSTN post-translational processing, that requires the presence of furin activity, we first developed a Furin expressing stable CHO clone (Fig. 14). This clone was used afterwards to develop stable clones transfected with using the full-length propeptide-expressing vectors, named double stable transfected clones.

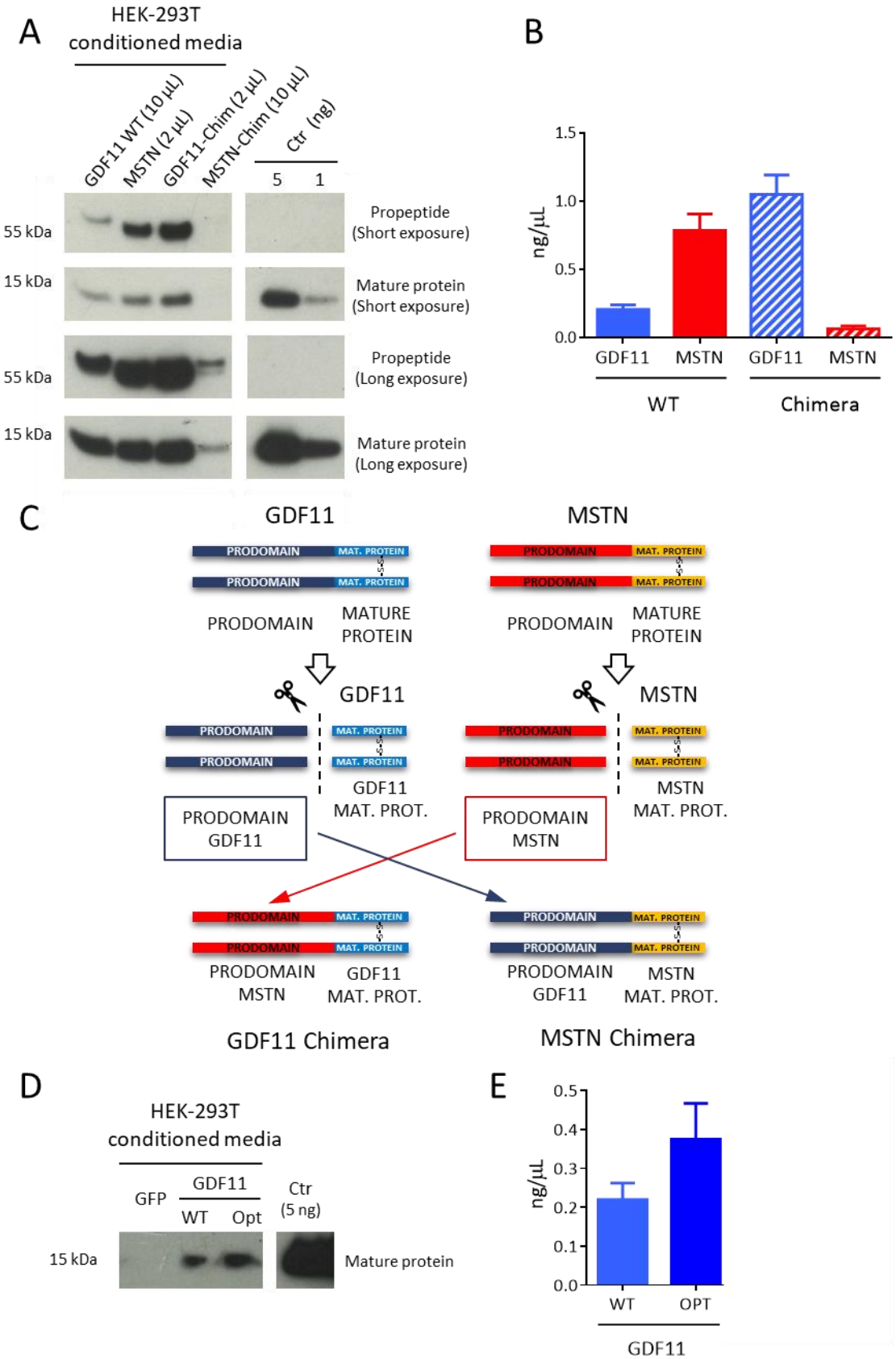

Figure 13: GDF11 and MSTN protein production is regulated by prodomain sequence. *(A) Different volumes of conditioned media were loaded. Abcam GDF11/MSTN (ab124721) was used as primary antibody. GDF11 prodomain is associated with poor protein production of GDF11 mature protein, however efficient protein production can be recovered if GDF11 prodomain is substituted*

with MSTN prodomain. In line with these observation, MSTN protein production was decreased by GDF11 prodomain.
(B) Western blot quantification. Bands intensity was measured using ImageJ software.
(C) Schematic representation of GDF11 and MSTN chimera.
(D) Same volumes of GDF11-WT and GDF11-Opt HEK-293T conditioned media were compared side by side. GDF11 mature protein production was enhanced by codon optimization process but surprisingly, codon optimization was less effective than MSTN prodomain chimera.
When necessary different amounts of GDF11 recombinant protein (Ctr, ng) were added as reference for quantification. Data are representative of two separate experiments with n=2/3 biological replicates. Data shown as mean ± SD.

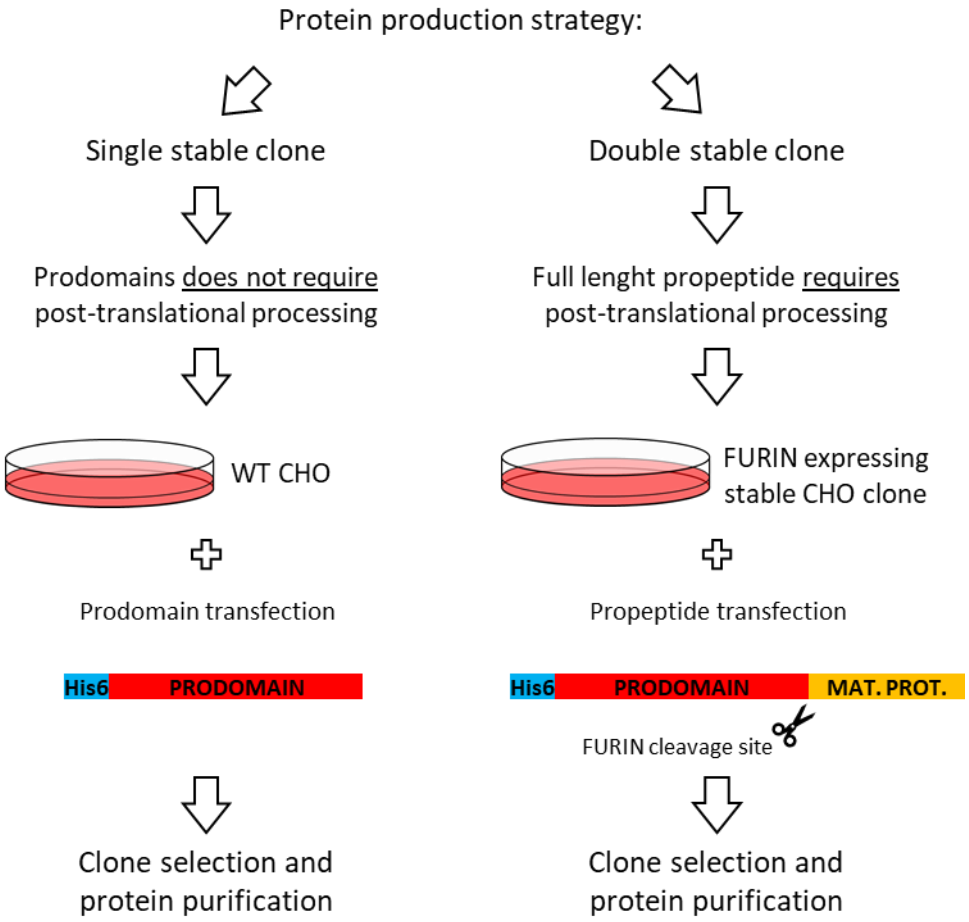

Figure 14: Schematic representation of protein production strategy.
Single transgene expressing clones were used for prodomain production. In case of full-length protein production, double transgene expressing clones were used to increase Furin post-translational processing.

- *Single stable transfected clones*

  Single stable transfected clones were developed to produce proteins that do not require further post-translational processing. This was the case of GDF11 and MSTN prodomains. Stable transfected clones were generated using selection antibiotics, isolated in single clones using the limiting dilution approach and screened for their

protein production levels by western blot (Fig. 15A-B). The clone identified as the highest producer was isolated and expanded for future application and in order to further optimize clone-specific protein production protocols. The selection of the highest expressor was performed by evaluating media harvesting timing and sodium butyrate (NaB) media supplementation (Palermo et al., 1991) (Fig. 15C-D).

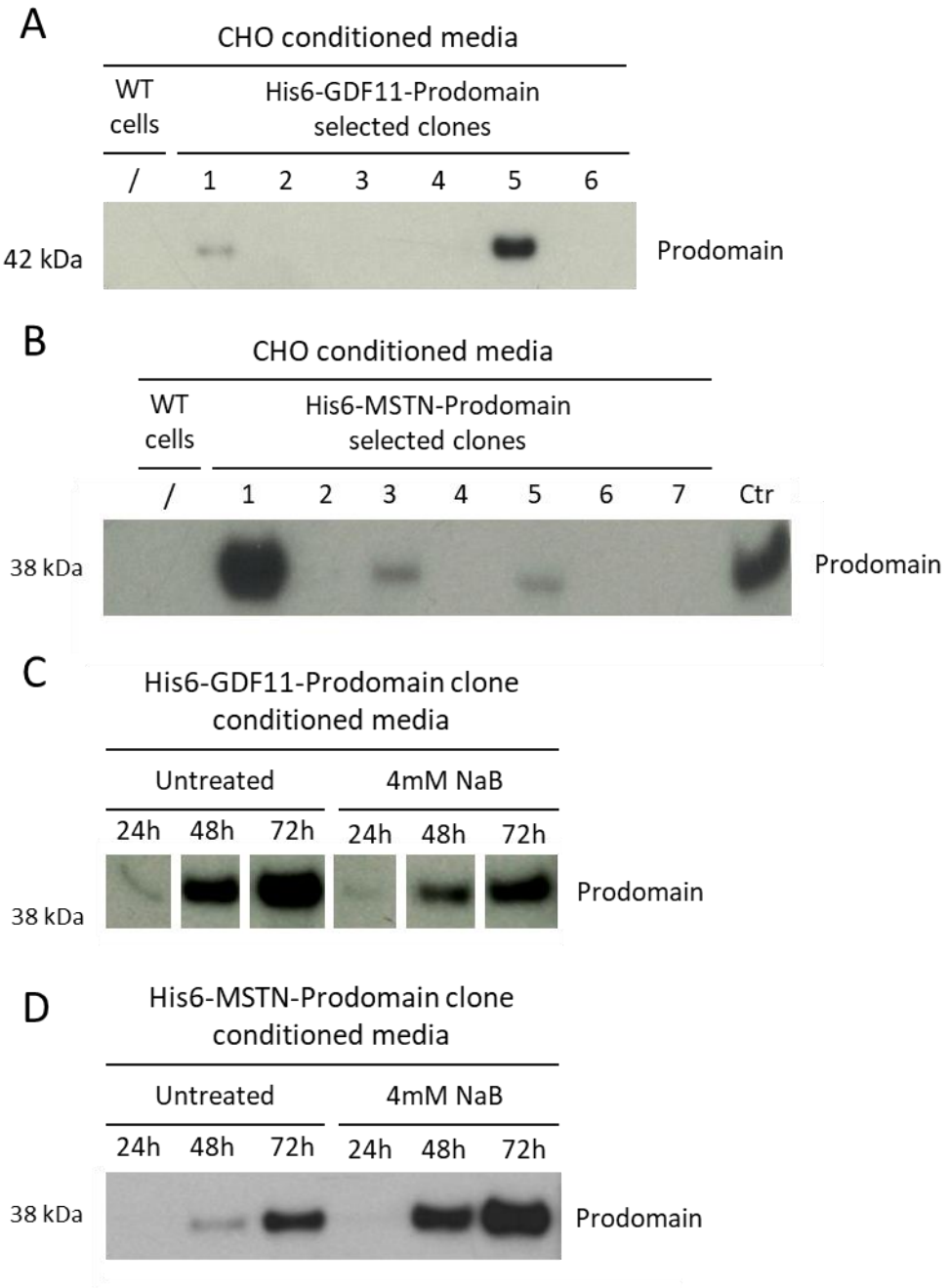

Figure 15: Single stable clone selection and protein production optimization.
(A, B) Screening for high expressing clones for GDF11 and MSTN prodomain, respectively. When available, 10 ng of recombinant protein was used as positive control (Ctr).
(C, D) Comparison of protein production methods between CHO selected clones. NaB supplementation was effective to increase MSTN prodomain production but not GDF11 prodomain.

- *Double stable transfected clones*

  As mentioned before both GDF11 and MSTN proteins needed Furin processing to improve protein maturation. To do so, a Furin stable expressing clone was developed, and clones were screened for their GDF11-Chim cleavage activity (Fig. 16). Once identified the most efficient Furin expressing clone, it was used for subsequent double stable clones development of GDF11-WT, MSTN and GDF11-Chim transgenes. Similar as performed in the previous paragraph, the highest producing clones were identified, and their protein production was optimized for harvesting timing and NaB supplementation (Fig. 17).

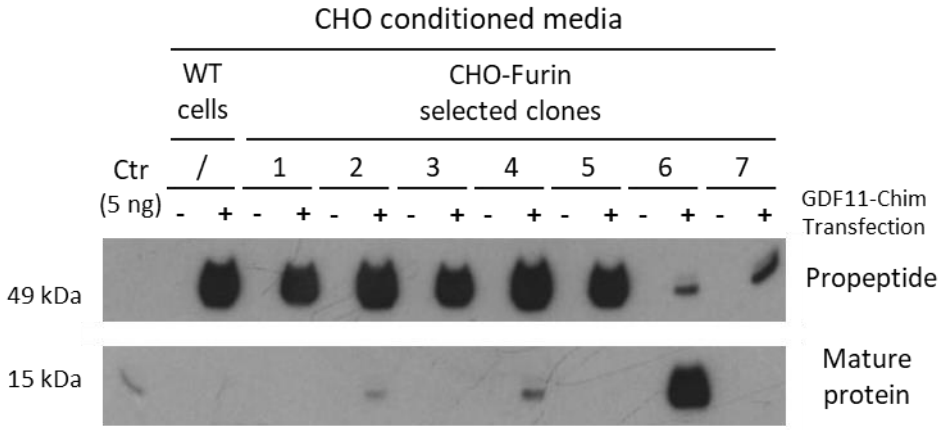

Figure 16: Furin stably expressing clone selection.
Stable clones were indirectly screened for Furin expression by evaluating their post-translational processing. Clone 6 was selected as the most efficient in processing GDF11 and used for development of double stable clones. GDF11 recombinant protein (5 ng) was used as control (Ctr).

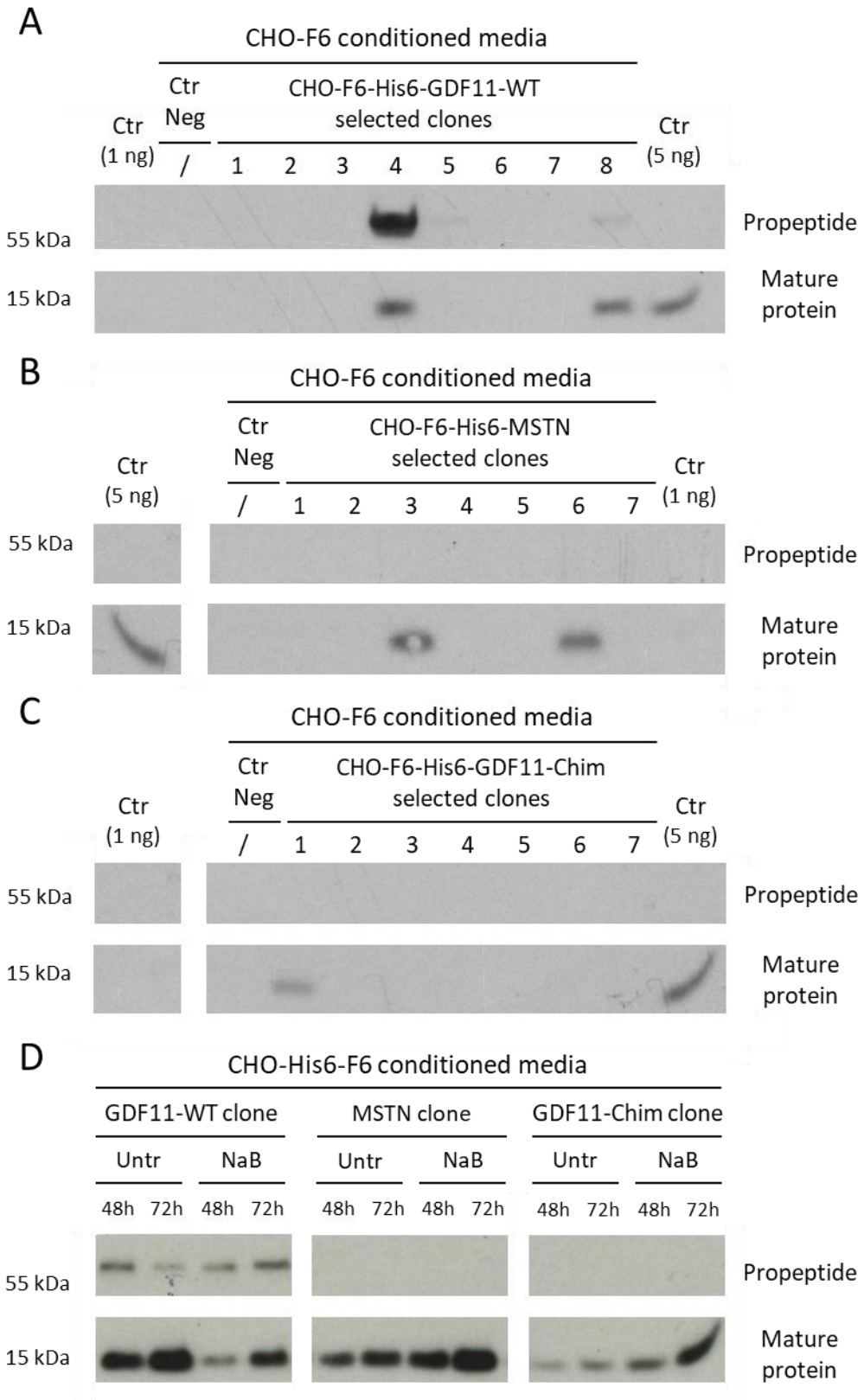

Figure 17: Double stable clone selection and protein production optimization.
(A, B, C) Screening for high expressors clones for GDF11-WT, MSTN AND GDF11-Chim, respectively. (D) Comparison of protein production methods between CHO selected clones. NaB supplementation (4 nM) was effective in increasing MSTN and GDF11-Chim but not WT GDF11.
GDF11 recombinant protein (1 or 5 ng) was used as quantification control (Ctr).

4.1.5. Recombinant His6-tagged proteins can be recovered from culture media using IMAC

One of the most common and simple strategy for protein purification consists of cloning a purification tag at the carboxi- or amino-terminus of the protein of interest. Our purification strategy employed a His6 tag at the amino-terminus of both GDF11 and MSTN prodomains and full-length constructs. CHO stably expressing prodomains were harvested at 48/72h, centrifuged, filtered and loaded on a nickel purification column as described in paragraph 2.7.2. Production and purification efficiency were evaluated comparing the amount of recombinant protein obtained to the volume of the conditioned medium used. In this analysis, GDF11 prodomain production and purification resulted more efficient than MSTN prodomain with a yield of 70/80 µg/L, vs. 40/50 µg/L, respectively (Fig. 18).

4.1.6. GDF11 and MSTN prodomains inhibitory activity is not limited to their respective ligands

In order to evaluate the biological activity of the recombinant prodomains we tested their ability to inhibit GDF11 and MSTN activity using the A204-CAGA12 reporter cell line. It has been shown that GDF11 and MSTN prodomains can inhibit their respective ligands activity by forming the inactive latent complex (Ge et al., 2005; Lee and McPherron, 2001). Our hypothesis was to confirm that prodomains inhibiting activity is not confined to their respective ligands, but, due to their high level of ligand homology, can be extended also to their opposite ligands. As shown in fig. 19A-B each recombinant prodomain is biologically active and able to inhibit both recombinant GDF11 and recombinant MSTN mature ligands. Interestingly, GDF11 prodomain shows higher inhibitory activity for both GDF11 and MSTN signaling when compared to MSTN prodomain. Calculated IC50 showed a difference of approximately 10-fold between GDF11 prodomain and MSTN prodomain in inhibiting both GDF11 and MSTN ligands. Commercial recombinant MSTN prodomain was used as a control showing an activity comparable to recombinant MSTN prodomain purified in our laboratory. Commercial recombinant GDF11 prodomain is not available and thus we could not perform this additional control.

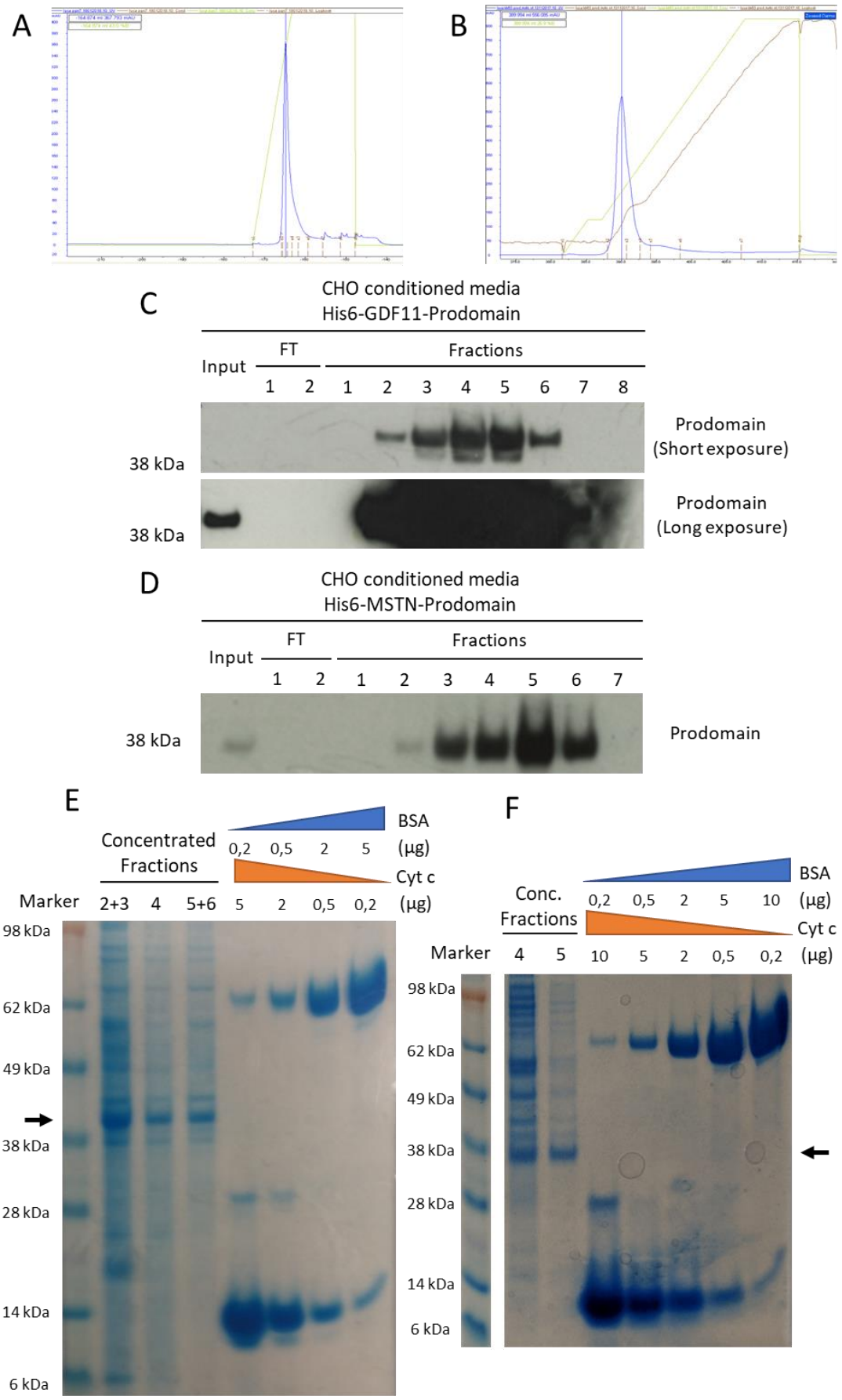

Figure 18: GDF11 and MSTN prodomains production and purification.

(A, B) IMAC chromatogram during elution phase of, respectively, GDF11 and MSTN prodomains. (C, D) Western blot of eluted fractions obtained during conditioned media purification. Both

GDF11 (C) and MSTN (D) prodomains were detected by the same antibody recognizing His6 tag (anti-His6, ab18184). Fractions showing the highest purity and concentration of recombinant protein were combined and concentrated.
(E, F) Concentrated fractions with GDF11 (E) and MSTN (F) prodomains were tested for quantification and purity by Coomassie staining. Arrows on the side of the gels indicate GDF11 (E) and MSTN (F) prodomains with an expected molecular weight of 31.3 kDa and 28.7 kDa, respectively. Fraction 4 for GDF11 prodomain and fraction 5 for MSTN prodomain were used for bioactivity assays. Figure F was digitally cropped to remove 9 lanes of an unrelated experiment without altering the migration pattern.

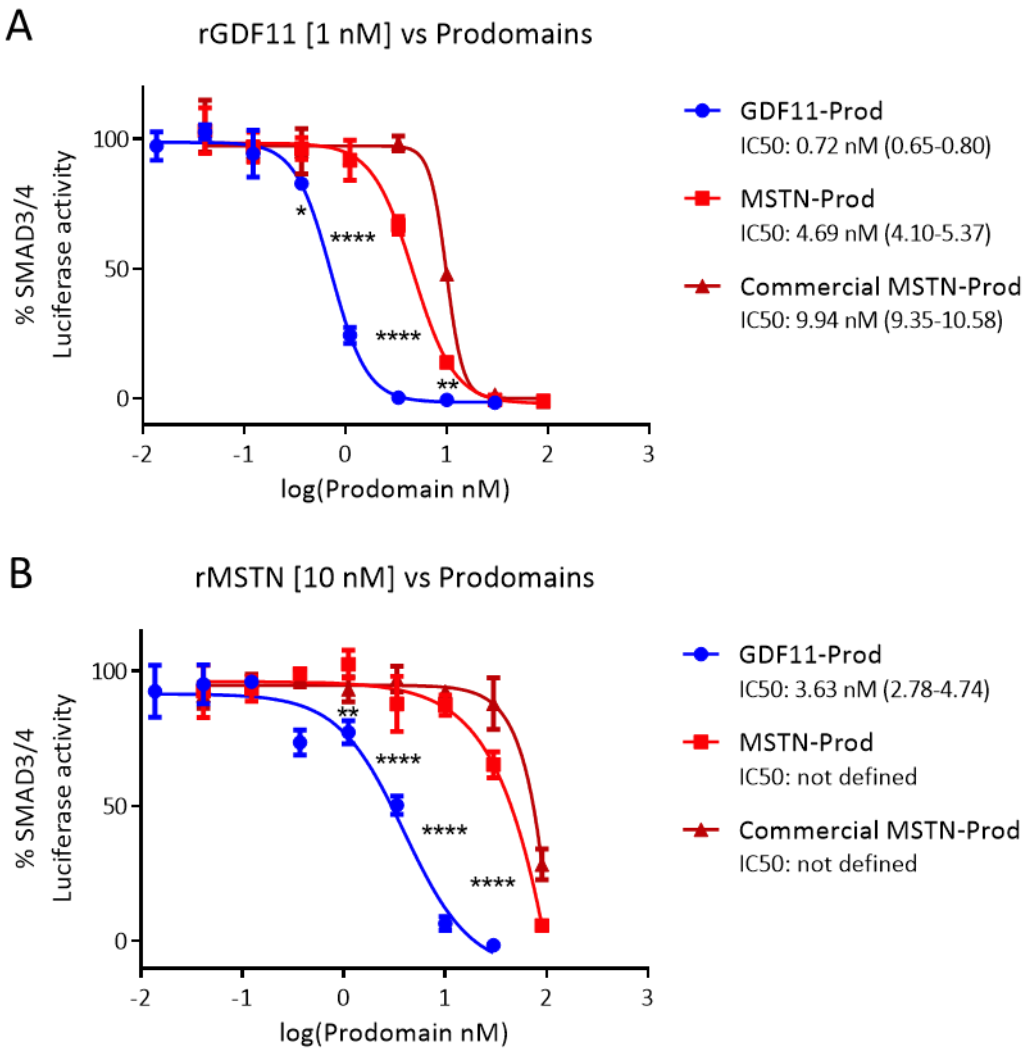

Figure 19: GDF11 prodomain is more potent than MSTN prodomain in inhibit both GDF11 and MSTN ligands.
(A, B) A204-CAGA12 reporter cell line was placed in serum free medium for 8h, then the medium was changed adding serum free medium containing rGDF11 (1 nM) or rMSTN (10 nM). For each ligand, it was also added a separate 8-point dilution curve (1/3 serial dilutions, starting from 90 nM for MSTN prodomain or 30 nM for GDF11 prodomain) and incubated for 14h. Subsequently, luciferase activity was measured and GDF11 prodomain showed a higher inhibitory potency compared to MSTN prodomain. Commercial MSTN prodomain inhibitory activity was comparable with our purification of MSTN prodomain furtherly demonstrating that our method maintained prodomain biological activity.

Data are representative of two separate experiments with n=2/3 biological replicates. Data shown as mean ± SD.

4.1.7. Simultaneous purification of GDF11/MSTN prodomain and mature ligand can be achieved exploiting the inactive latent complex formation

The presence of prodomains is required for proper folding and maturation of mature proteins for both GDF11 and MSTN (Walker et al., 2016), forming a non-covalently bound latent complex. Thus, our strategy was to exploit the presence of the latent complex to copurify both prodomain and mature protein through the N-terminus His6 tag. Of note, we performed a small experiment to evaluate the efficiency of a different approach by replacing the His6 tag with a Biotin Acceptor Peptide sequence (BAP) tag, capable of the extremely stable biotin-streptavidin binding (Kimple et al., 2013; Predonzani et al., 2008). The data confirmed the stability of the latent complex even in mildly denaturing conditions proving feasibility of latent complex purification (Fig. 20). However, because of difficulties in removing the unbounded biotin from large volumes of medium, the scaling up process was pursued using a His6 tag approach.

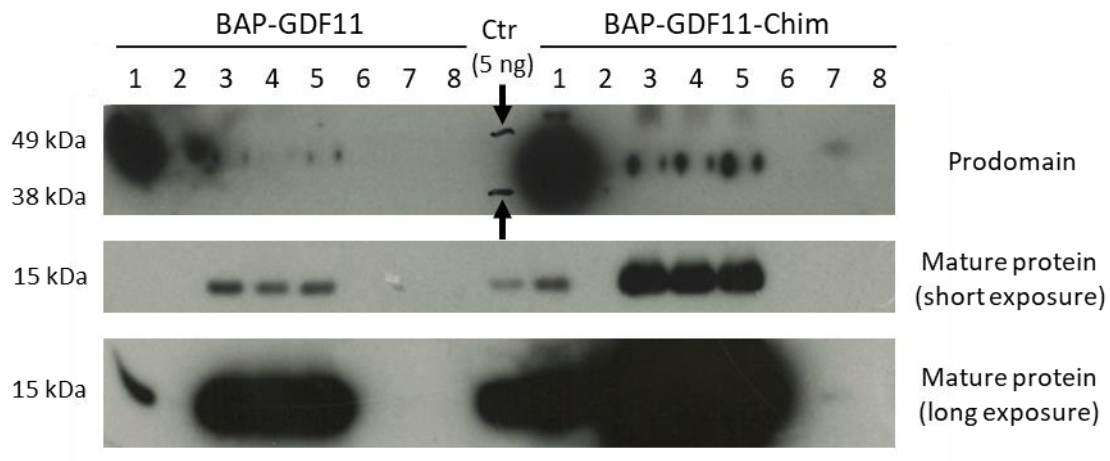

Figure 20: Latent inactive latent complex purification.
Conditioned media containing biotinylated GDF11 and GDF11-Chim were collected after 48h and processed to remove not-bound biotin (lane 1). Streptavidin beads were added to the processed culture media and incubated for 2h at 4°C. Supernatant was removed (lane 2) and beads were incubated in mild denaturing condition. Beads were incubated for 2h in PBS, pH 2.7 or in 1% NP40 and beads (respectively lanes 3, 4, 5) were separated from supernatant (lanes 6, 7, 8), showing that GDF11 mature protein was not released. Black arrows indicate ink-marker signs corresponding to 49 kDa and 38 kDa of SeeBlue Plus2 Pre-stained Protein Standard ladder.Data are representative of two separate experiments with n=2/3 biological replicates. GDF11 recombinant protein (5 ng) was used as control (Ctr). Data shown as mean ± SD.

4.1.7.1. N-terminus His6-tag latent complex purification from transiently transfected HEK-293T media

In order to produce and purify GDF11 and MSTN mature protein, HEK-293T were transiently transfected with GDF11-Chim or MSTN. WT GDF11 construct was not used because of its *in vitro* low protein production efficiency (Fig. 13A-B). We have previously shown that MSTN prodomain can efficiently bind mature GDF11 thus we hypothesized that using the GDF11 chimera construct can be a suitable approach (Fig. 20). 48h/72h post transfection medium was harvested, processed and loaded on a nickel purification column as described in paragraph 2.7.2. Both GDF11-Chim and MSTN purification where subjected to identical purification steps and they are shown side by side (Fig. 21). Fractions containing the latent complex showing the highest purity and protein concentration were pulled together, concentrated through centrifugation using size exclusion columns and subsequently quantified by Coomassie staining (Fig. 21C). Since our purification strategy was targeting the entire inactive latent complex, both mature protein and His6-tagged prodomain are visible. Quantification of mature ligands revealed that, for both GDF11-Chim and MSTN, final recombinant protein yield was in a range of 70-90 µg per liter of conditioned medium.

In order to separate the inactive latent complex components, a further purification step requiring HPLC was performed and described in the following paragraph.

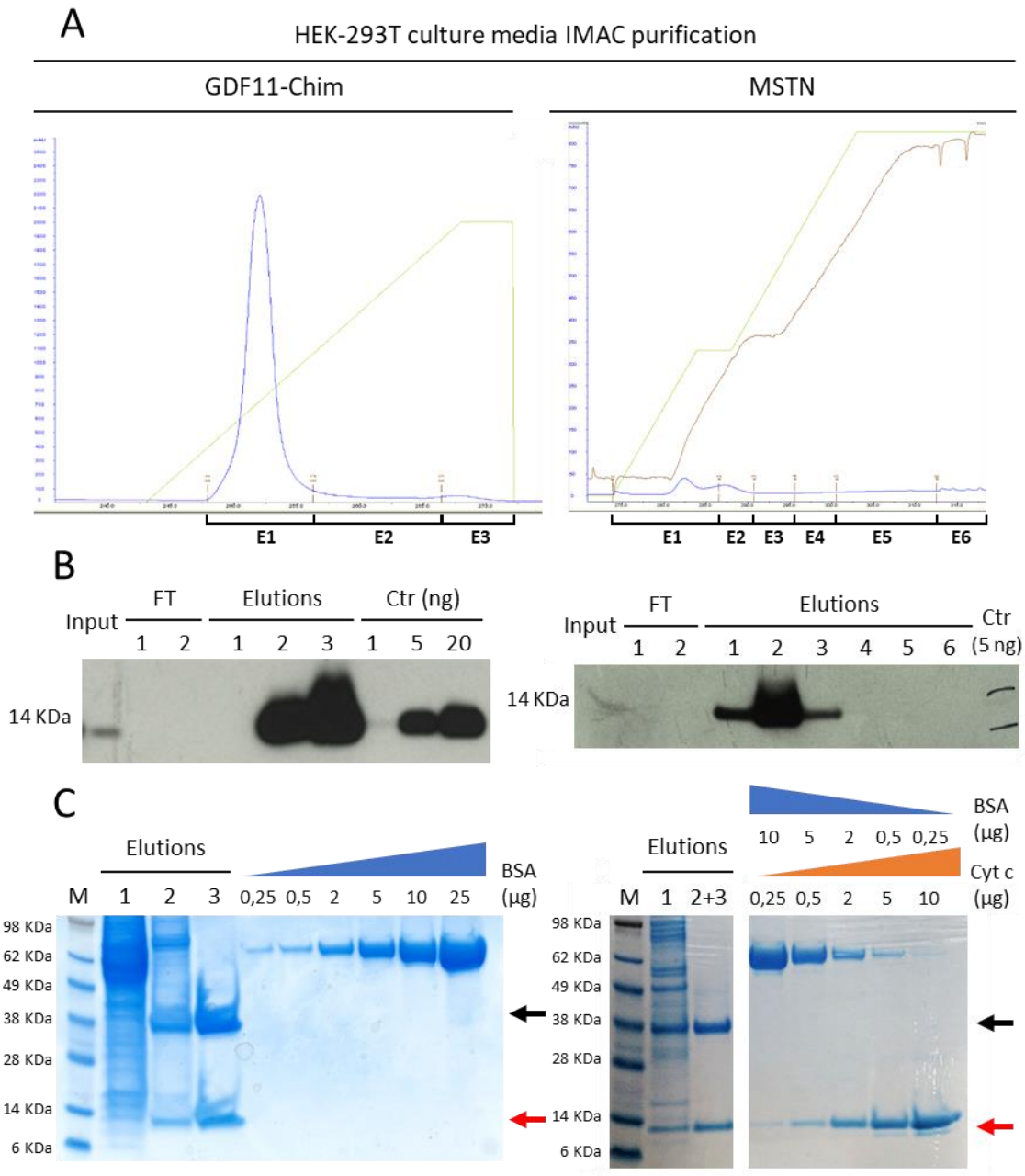

Figure 21: GDF11-Chim and MSTN inactive latent complex purification.
(A) IMAC chromatogram during elution phase of GDF11-Chim and MSTN full length proteins, respectively. Fractions collected during elution are represented with distinct brackets and named progressively ("E1-6"). All collected fractions were screened for the protein of interest using WB.
(B) Both GDF11 and MSTN mature proteins were detected by the same antibody recognizing both GDF11 and MSTN ligands. GDF11's "E3" and MSTN's "E2" fractions appeared to have the highest amount of purified recombinant protein among all the collected samples. Further analysis showed a low presence of unspecific proteins in MSTN's "E3" sample. For this reason, "E3" fraction was pooled with MSTN's "E2" sample and processed as unique sample called "Elution 2+3".
(C) "Elution 3", GDF11 and "Elution "2+3", MSTN, analyzed by Coomassie staining, contain relatively pure prodomain (~28 kDa) and mature protein (~12.5 kDa). Arrows on the side of the gels indicate the two proteins of the inactive latent complex. Prodomain is indicated by a black arrow and has an expected molecular weight of 28.7 kDa. GDF11/MSTN mature forms are both indicated by a red arrow and both have an expected molecular weight of 12.4 kDa. In both gels is possible to observe a high amount of unspecific proteins present in "Elution 1" indicating that the purification protocol

can be still significantly improved. Further eluting steps improved purity and thus "Elution 3" and "Elution 2+3" of respectively, GDF11 and MSTN inactive latent complex were subsequent purified as described in the following paragraph.Different amounts of recombinant GDF11 (Ctr, ng), BSA and/or Cytochrome c proteins were used as reference for quantification.

4.1.7.2. Mature protein and prodomain separation using reverse-phase HPLC

In order to isolate the two peptides forming the inactive latent complex, we took advantage of a previously published method used to purify MSTN ligand (Lee and McPherron, 2001). This method is based on reverse-phase C4 HPLC column that elute the proteins with an ACN gradient in 0.1% TFA. Considering the high level of homology between GDF11 and MSTN we tested if this method could be adapted also for GDF11 ligand purification. IMAC fractions containing GDF11-Chim ("E3") or MSTN ("E2+E3") were loaded in a reverse-phase C4 HPLC column and samples were separated as described in paragraph 2.7.3. UV absorption at 280 nm was constantly measured during the separation process and it was used to identify and collect protein peaks eluting from the column. In fig. 22A, it is possible to observe a side to side comparison between GDF11-Chim and MSTN HPLC chromatogram. Fraction samples were lyophilized using a Speedvac apparatus and then resuspended in acidic 4mM HCl PBS to improve solubilization. Coomassie staining after HPLC fractionation (Fig. 22B) showed two or three different protein peaks that were respectively mature protein, BSA (if previously added to improve stability) and prodomain in both GDF11-Chim and MSTN purified samples. Retention time of the mature protein was shorter (29-30 minutes) than prodomain (30-32 minutes) allowing proper separation. Coomassie bands were also used to evaluate the amounts of purified peptides (mature protein and prodomain) obtained after HPLC separation and identify their recovery ratio comparing to the total sample input loaded into the C4 column. Known amounts of BSA and cytochrome c that have a similar MW to prodomain and mature protein respectively, were used to determine a more precise concentration of the proteins and reduce the bias due to size differences. Quantification results showed that both protein samples have quite low recovery rate that is approximately 5-15% of the initial input, with GDF11-Chim performing more efficiently than MSTN (Fig. 22B).

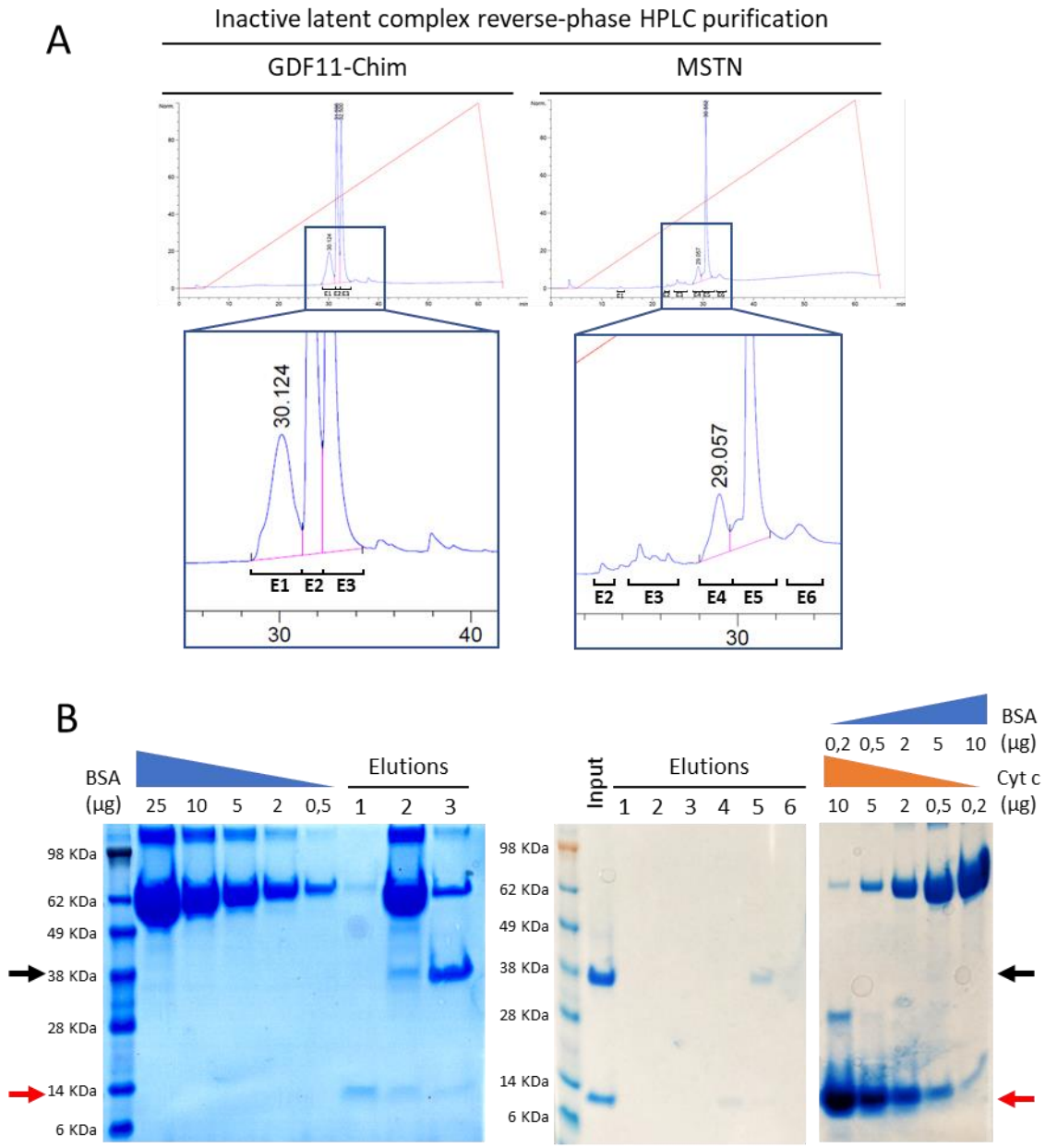

Figure 22: Reverse phase HPLC separates GDF11-Chim and MSTN prodomain and mature protein.
(A) Detail of HPLC chromatogram showing eluted fractions ("E#").
(B) Eluted fractions were lyophilized and protein quantification was performed by Coomassie staining. Arrows on the side of the gels indicate the prodomain (black arrow) and mature protein (red arrow) separated from each inactive latent complex. "Elution 1" and "Elution 4" containing GDF11 and MSTN mature proteins, respectively, were used in the bioactivity assay described in the following paragraph.
Different amounts of recombinant BSA and/or Cytochrome c proteins were used as reference for quantification.

4.1.7.3. Both GDF11 and MSTN separated by HPLC are biologically active

In order to test whether GDF11 or MSTN mature protein maintained their biological activity after HPLC purification, both peptides were tested using A204-CAGA12 reporter cell line,

as described before in paragraph 2.6.1. Commercial rGDF11 and rMSTN were used as a control in a range from 2 pM to 100 nM (Fig. 23A).

Our data indicate that both GDF11 and MSTN are biologically active, with GDF11 showing a EC50 of 1.42 nM, comparable to commercial rGDF11 (1.03 nM). Unfortunately, the lower yield of MSTN and its intrinsic lower potency did not allow to calculate the EC50 (Fig. 23B).

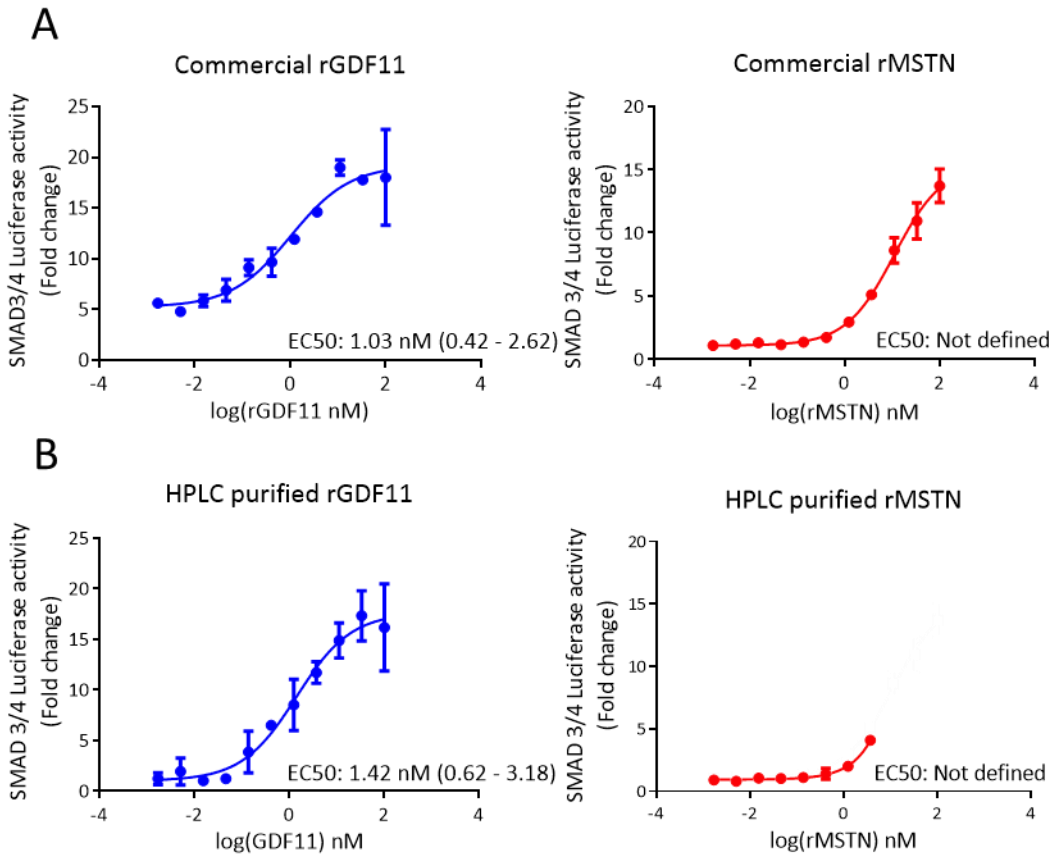

Figure 23: GDF11 and MSTN mature proteins purified by HPLC are biologically active.
(A) Commercial GDF11 and MSTN proteins were used as control.
(B) Biological activity of purified GDF11 was not statistically different from bioactivity of commercially recombinant protein. MSTN low yield did not allow a full dose-response curve.

4.1.8. Specific mutations in GDF11 and MSTN prodomain can modulate protein bioactivity

Recent data have shown that specific mutations on hydrophobic residues of the α-1 helix prodomain of both human GDF11 and MSTN can lead to weak latent complex formation and higher ligand potency (Fig. 24A), independently from BMP1/TLD metalloproteinase processing (Walker et al., 2018). On the other hand, mutations that disrupt BMP1/TLD recognition site reduce GDF11 and MSTN potency. However, it is not known whether these findings can be translated in a murine system. This is particularly important considering

that this approach may facilitate *in vivo* delivery using AAV vectors (paragraph 4.4.1) by modulating local availability without affecting BMP1 maturation. For this purpose, we designed two different constructs introducing the L74E and the I57E mutations in murine codon optimized GDF11 and in MSTN ORFs respectively. We also introduced D120A and D100A mutations in murine GDF11 and MSTN to produce BMP1 protease resistant mutants. In order to improve *in vitro* HEK-293T-CAGA12 reporter cell line were co-transfected with Furin and each of the six different constructs and luciferase activity was measured. As shown in fig. 24B, mutations that reduce the affinity of the latent complex (L74E and I57E), respectively of GDF11-Opt and MSTN, can significantly increase ligand activity approximately by a factor 10 when compared to WT protein. Mutations that disrupt BMP1 cleavage site did not significantly reduce bioactivity of both GDF11 and MSTN, possibly because of the low BMP1 processing activity in this an *in vitro* assay.

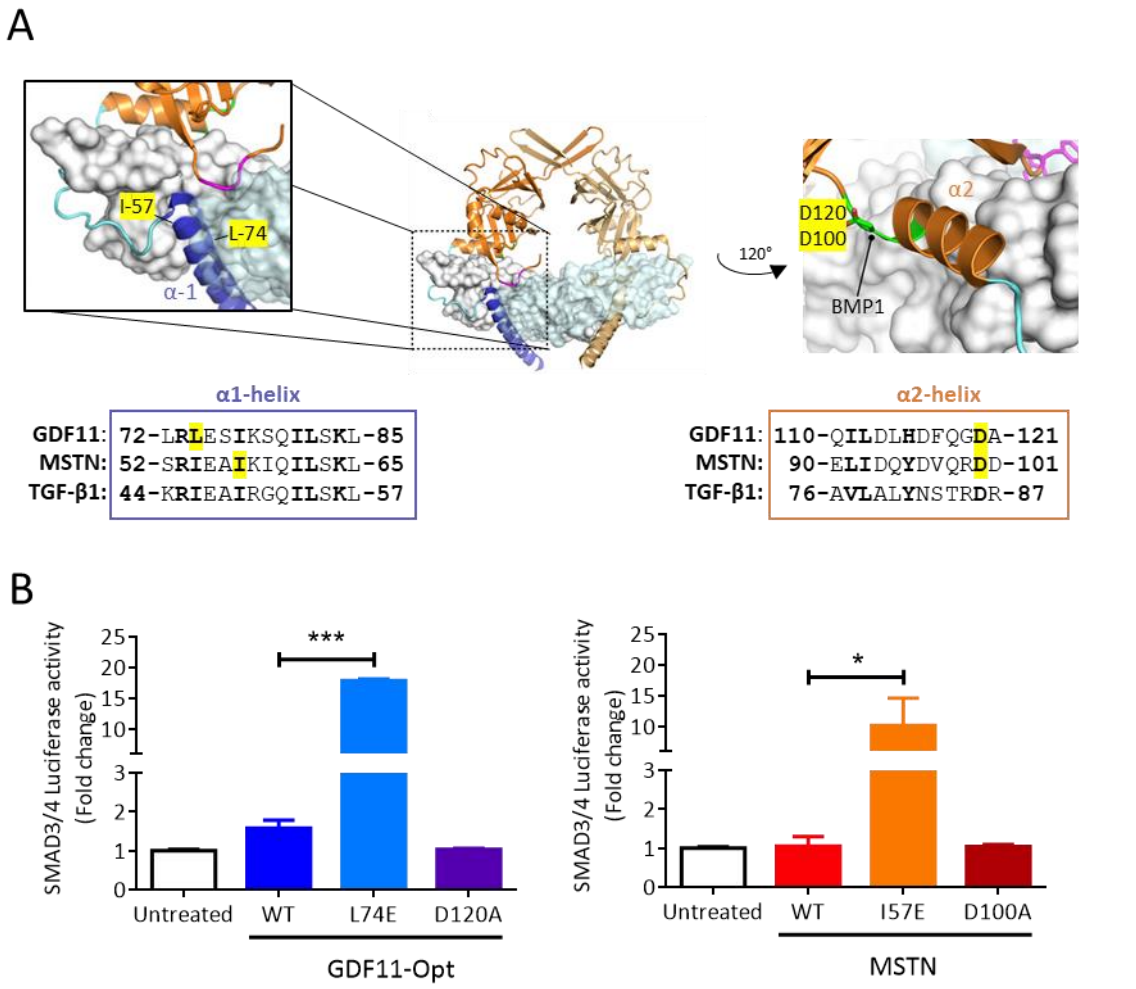

Figure 24: Single mutations in GDF11 and MSTN prodomain can control biological activity of mature proteins.

(A) Graphical representation of Mus musculus conserved residues involved in bioactivity regulation of GDF11 and MSTN proteins. Residues mutation on hydrophobic residues (highlighted in bold) of α1-helix are associated with increased biological activity of GDF11 and MSTN even without BMP1

cleavage. On the other hand, BMP1 cleavage site can be eliminated by D to A mutation in proximity of α2-helix conserved residues. Residues marked in yellow were tested in this thesis. Figure adapted from (Walker et al., 2018).
(B) CAGA12 assay using GDF11 and MSTN mutated proteins. Both L74E and I57E mutations on GDF11 and MSTN prodomains, respectively, were able to increase biological activity of mature proteins without BMP1 co-transfection. Lower, but not statistically significant activity was detected in BMP1-resistent mutants (D120A and D100A) but further experiments in different conditions are required to characterize their biological activity.
Data are representative of two separate experiments with n=2 biological replicates. Data shown as mean ± SD.

4.2. GDF11/MSTN type I TGF-β receptors analysis *in vitro* and *in vivo*

After producing and testing bioactivity of different constructs, as described in the previous section of this thesis, we next focused our attention on elucidating the mechanisms that are responsible for the effect of GDF11 and MSTN on cardiac and skeletal muscle tissue, in particular evaluating the role of differences in TGF-β receptors.

4.2.1. TGF-β receptors mRNA and protein expression in cardiac and skeletal muscle tissue

GDF11 and MSTN activate TGF-β/SMAD signaling pathway binding TGF-β type I and type II receptors, however displaying different relative affinity (Walker et al., 2017). In order to test our hypothesis that a differential representation of TGF-β type I receptors in cardiac and skeletal muscle tissue may contribute to tissue specificity of GDF11 and MSTN, we analyzed gene expression and protein levels of ALK4, ALK5 and ALK7.

Both tissues, cardiac and skeletal muscle, showed a similar pattern of expression, with Alk4 transcript most expressed, followed by Alk5 mRNA and lastly Alk7 (Fig. 25A). Comparing Alk receptors expression levels in cardiac muscle and skeletal muscle showed that, while Alk4 mRNA level are not statistically different, Alk5 expression levels in cardiac tissue are 2-fold higher than in skeletal muscle and conversely, Alk7 expression levels are 4-fold lower when cardiac muscle is compared to skeletal muscle (Fig. 25B). However, RNA expression analysis does not properly match with receptors quantification obtained by WB. Indeed, ALK4 and ALK7 are significantly more abundant in cardiac tissue than in skeletal tissue, whereas ALK5 show a similar trend, but it is not statistically significant (Fig. 25C).

All together, these data showed that cardiac tissue has more ALK receptors than skeletal muscle. This tissue-dependent difference could lead to a distinct signaling activation in response to GDF11 or MSTN stimulation, however further experiments are required to understand the biological relevance of these findings.

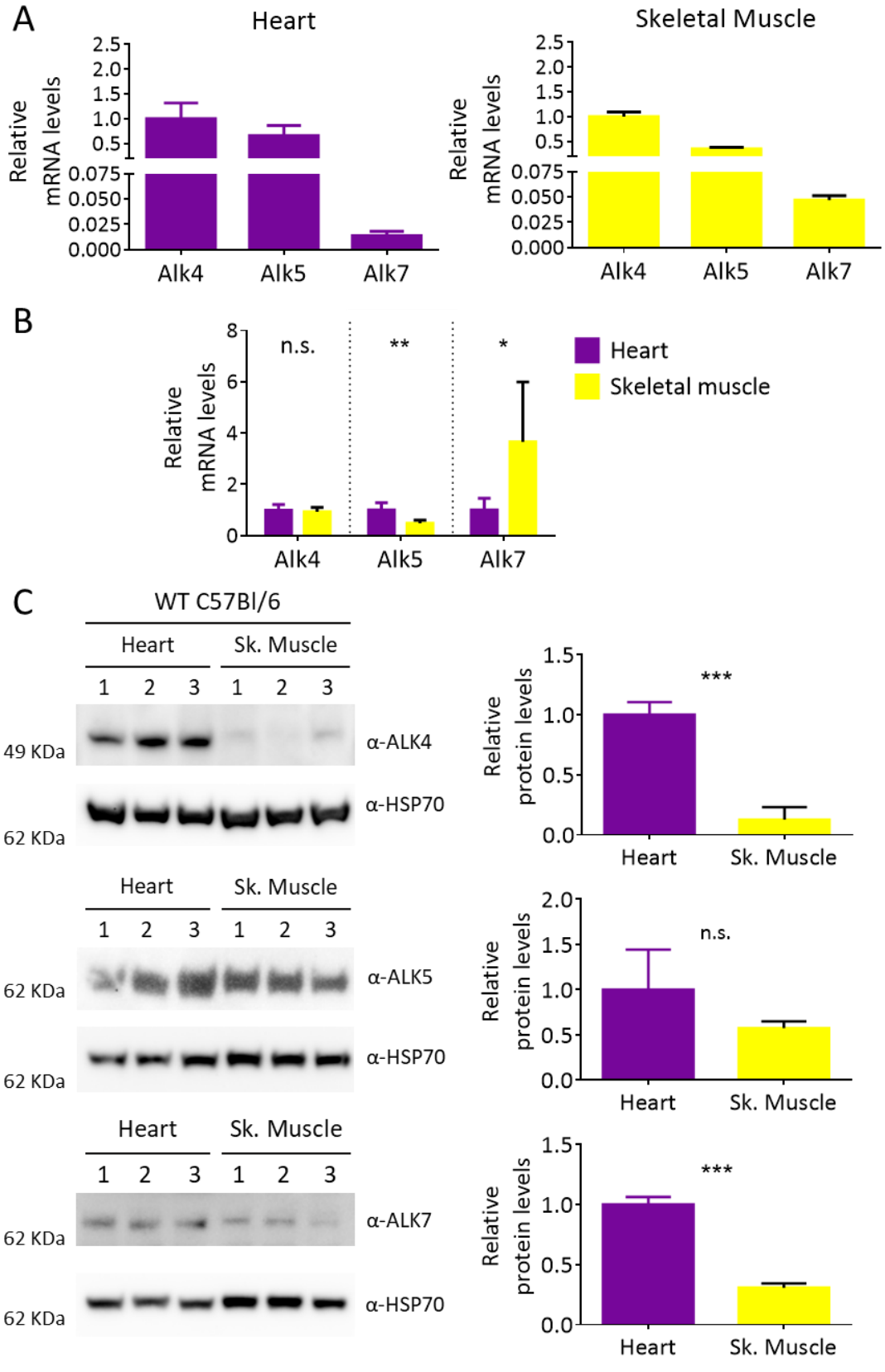

Figure 25: Differential expression and protein levels of TGF-β type I receptors (ALK4, ALK5, ALK7) in cardiac and skeletal muscle tissue.
(A) Intra-tissue comparison of relative mRNA expression levels among Alk4, Alk5 and Alk7.
(B) RNA expression levels of different TGF-β type I receptors in cardiac and skeletal muscle tissue.
(C) Western blot of cardiac and skeletal muscle tissue lysate. Quantification of band intensity was performed using Image Lab software. Discrepancies between gene expression and protein levels may be secondary to post-transcriptional processing and requires further evaluation.
Data are representative of two separate experiments with n=2/3 biological replicates. Results are represented as fold change compared to Alk4 mRNA expression (A) or compared to cardiac tissue (B, C). Data shown as mean ± SD.

4.2.2. CRISPR/Cas9 strategy to induce single type I TGF-β receptor KO

In order to investigate the role of type I TGF-β receptors in determining the differential effect of GDF11 and MSTN on cardiomyocytes we took advantage of CRISPR/Cas9 strategy to induce specific KO of target receptors. We used a mouse atrial cardiomyocyte cell line with a stably integrated construct able to express Cas9 endonuclease under the control of a doxycycline promoter (HL-1-Cas9). This cell line was a kind gift of Dr. Hashim Ali from the Molecular Medicine Laboratory at ICGEB.

In order to direct Cas9 cleavage two different sgRNAs were selected for each gene target. Selection was carried out using *in silico* prediction methods and aimed to gene KO as described in paragraph 2.4.9 and by Zhou et al. published work (Zhou et al., 2014). Indeed, double sgRNAs strategy should increase the amount of INDEL induced in each target thus leading to higher probability to obtain missense mutations and/or to disrupt the proper protein translation (Fig. 26A).

4.2.2.1. Selected sgRNAs couples targeting specific type I TGF-β receptor can induce double strand DNA breaks (DSB) at both targeted sites

In order to verify *in silico* design of sgRNAs, selected sgRNAs were tested for their ability to induce DSB at targeted sites in HL-1-Cas9 cells. Doxycycline-treated cells were transduced with AAV6 vectors carrying two sgRNAs for each receptor and subsequently, DNA was analyzed by PCR to evaluate the presence of cleavage. As shown in fig. 26B, amplicons showed that sgRNAs can produce specific deletion in the selected receptors. Expected size of PCR-amplicons is showed in fig. 26C.

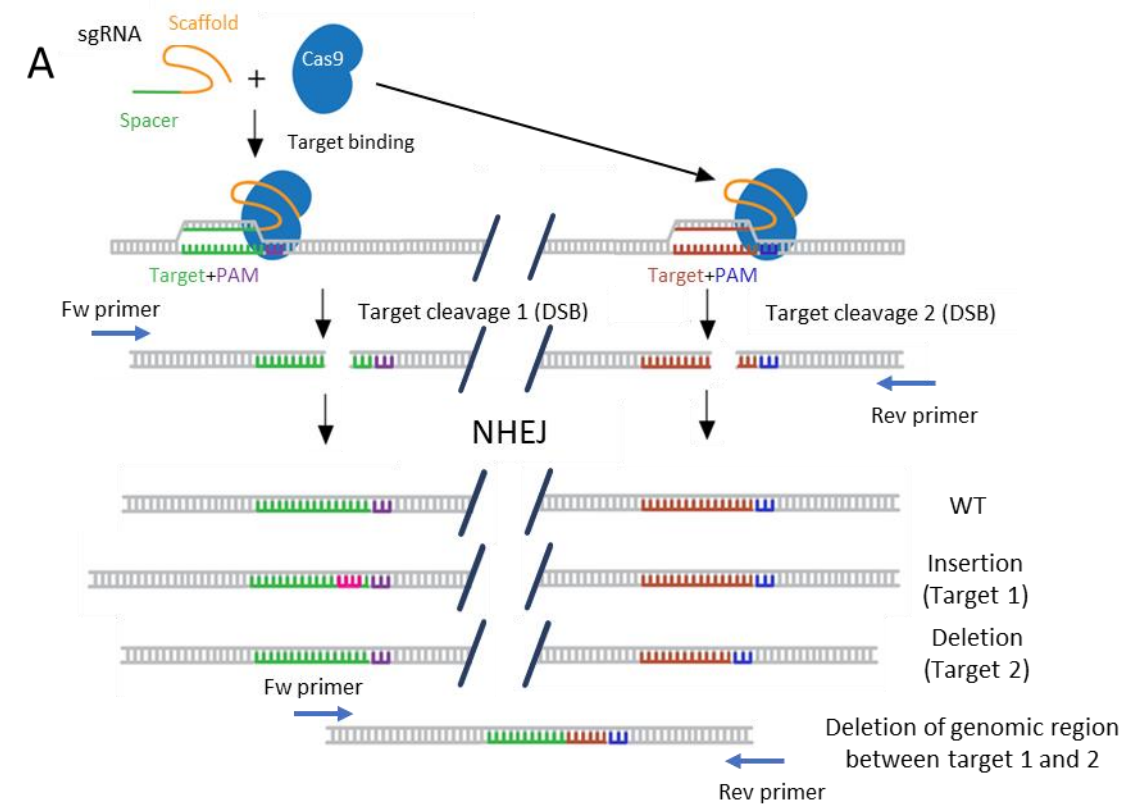

Target	Cleavage sites	WT PCR-amplicon size	Double cleaved PCR-amplicon size
Alk4	Exon 3: +66 bp	397 bp	~312 bp
	Exon 3: +151 bp		
Alk5	Exon 3: +150 bp	3396 bp	~348 bp
	Exon 4: +100 bp		
Alk7	Exon 2: +51 bp	427 bp	~346 bp
	Exon 2: +132 bp		

Figure 26: sgRNAs can targeted specifically TGF-β type I receptors and induce DSB.
(A) Schematic representation of CRISPR/Cas9 strategy for single gene KO and detection by PCR. For each targeted receptor two sgRNAs were simultaneously transfected/transduced into desired cells with a 1:1 ratio. Cas9 endonuclease activity results in DSB that are corrected by non-homologous end joining (NHEJ) mechanism. NHEJ repair process is prone to error by inserting or deleting a variable number of bases. Frameshift mutations likely generate non-functional proteins.
(B) Detection of genomic deletion induced by simultaneous sgRNAs cleavage in HL-1-Cas9 cells. HL-1-Cas9 were transduced with AAV6 carrying 2 sgRNAs targeting Alk4, Alk5 or Alk7 receptors. Agarose gels images are showing specific cleavage of the receptor only where the corresponding sgRNAs were used.
(C) Table of expected PCR-amplicon sizes for each receptor.

4.2.2.2. HL-1-Cas9 are sensitive to both GDF11 and MSTN recombinant proteins

In order to investigate HL-1-Cas9 sensibility to GDF11 and MSTN signaling a CAGA12 assay with recombinant proteins was performed.

As in previous analysis, GDF11 was more potent than MSTN in activate SMAD3/4 phosphorylation (Fig. 27A), however treatments concentration used for MSTN ligand (up to 100 nM) was not enough to induce a clear plateau state in order to calculate its respective EC50.

4.2.2.3. ALK7 KO reduces GDF11 but not MSTN signaling in vitro in HL-1-Cas9 cells

In order to investigate the direct effect of type I TGF-β receptor KO in modulating SMAD3/4 signaling induced by GDF11/MSTN in cardiac cells, we stimulated HL-1-Cas9 cells with GDF11 or MSTN upon transduction with sgRNAs to induce specific KO of Alk4, Alk5 or Alk7. We have performed preliminary experiments showing, as expected, a different sensitivity of HL-1 cells to stimulation with GDF11 and MSTN.

In order to obtain similar levels of SMAD3/4 activation, different concentrations of GDF11 (6 nM) and MSTN (30 nM) were tested using CAGA12 luciferase assay. As shown in fig. 27B, all three couples of sgRNAs (specific for Alk4, 5 and 7), were able to reduce SMAD3/4 signaling after GDF11 stimulation significantly when compared to untreated controls. Down-regulation of ALK4 and ALK5 produced a similar and statistically significant reduction in luciferase activity in both GDF11 and MSTN treated HL-1-Cas9 cells, with ALK5 that appeared to be the most relevant receptor to induce SMAD3/4 signaling for both ligands. Interestingly, down regulation of ALK7 significantly reduced SMAD3/4 activation in GDF11 treated cells but not upon MSTN stimulation. This difference in signal induced by Alk7 KO was suggesting the possibility that ALK7 receptor may be relevant for GDF11 activity in cardiac cells. Different combination of sgRNAs targeting simultaneously different ALK receptors were also tested, but no significative difference among these groups were detected.

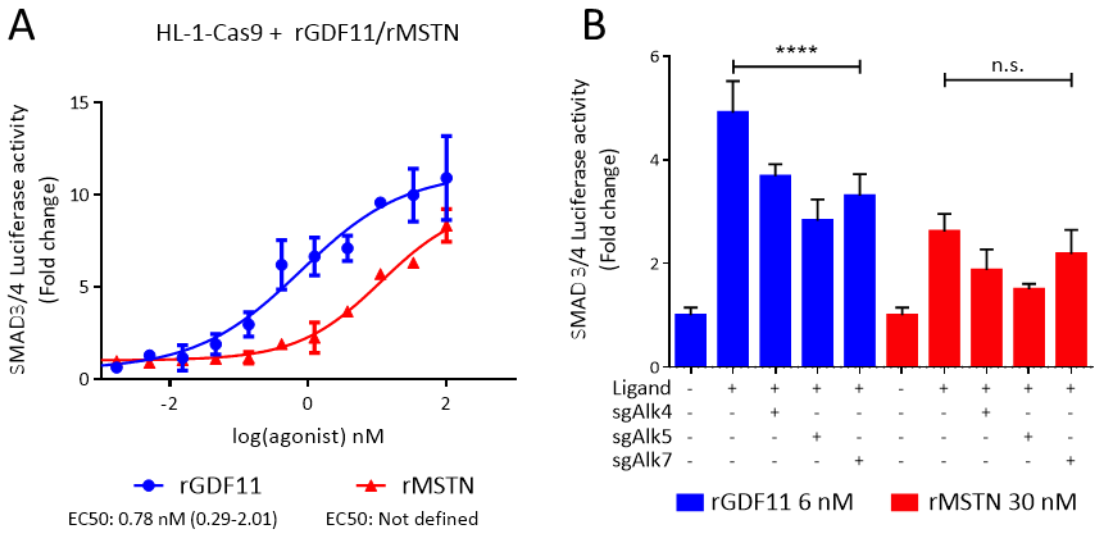

Figure 27: GDF11 but not MSTN signalling is reduced in Alk7 KO cells.

(A) A 12-point dose-response curve for both recombinant GDF11 and MSTN was performed using CAGA12 luciferase assay on HL-1-Cas9 cell line. As expected, GDF11 is more potent when compared to MSTN. In order to have similar SMAD3/4 activation level different amounts of GDF11 (6 nM) and MSTN (30 nM) were selected for subsequent investigations on HL-1-Cas9.

(B) HL-1-Cas9 cells were transduced with control sgRNAs or distinct couples of sgRNAs targeting TGF-β type I receptors. Two days after transfection cells were transfected with CAGA12 reporter plasmid. On the following day, cells were placed in serum free medium for 8h, then stimulated with constant concentration of rGDF11 (6 nM), Mstn (30 nM) or control (PBS). After 14h luciferase activity was evaluated. Alk7 KO significantly reduced SMAD3/4 activation only after GDF11 stimulation. Data shown as mean ± SD.

4.2.2.4. Selected sgRNAs targeting specific type I TGF-β receptors can down-regulate type I TGF-β receptors in vivo at cardiac level

To further confirm sgRNAs ability to KO specific receptor and set the basis for further investigation, an *in vivo* sgRNAs validation was performed. We used C57Bl/6-Myh6-Cas9-2A-TdTomato mice, a transgenic strain expressing Cas9 endonuclease constitutively in mature cardiomyocytes (Carroll et al., 2016). Mice were randomized to receive a single administration of 10^{12} GC of an AAV9 vector carrying sgRNAs that specifically target Alk4, Alk5 or Alk7 genes and compared to the PBS injected group. No phenotypical alterations were observed over 35 days when the animals were sacrificed and heart harvested for further processing. As shown in fig. 28A-B, sgRNAs were able to induce a trend in reduction of total amount of ALK proteins in cardiac tissue when compared to control, however, only Alk4 sgRNA produced a significant effect. Considering the modest results of Alks KO, improvement in AAV delivery and new silencing methods are now under investigation.

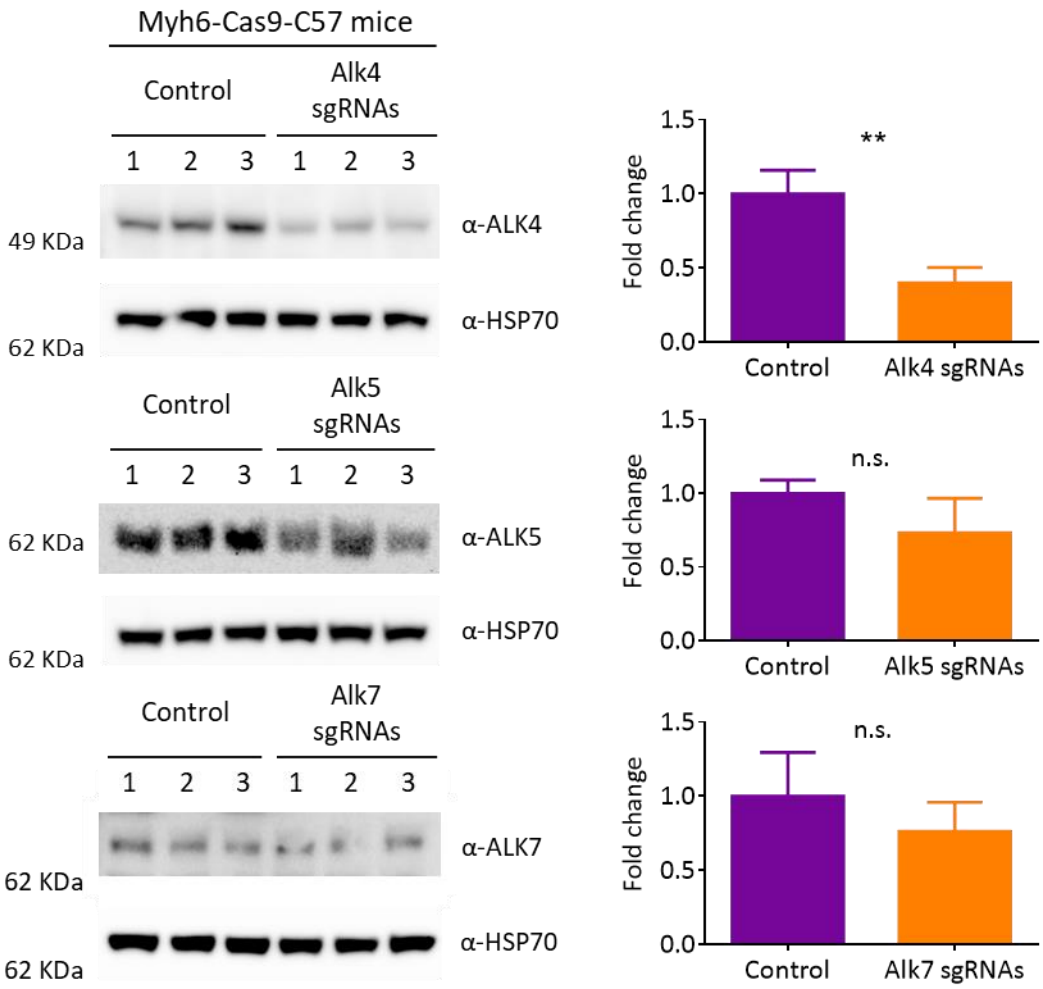

Figure 28: Systemic delivery of sgRNAs in mice have modest effects on ALKs protein levels. *Western blots of PBS treated mice (Control) and sgRNAs treated mice. Three distinct antibodies recognizing ALK4, ALK5 and ALK7 proteins were tested on tissue lysate of control and treated animals. Quantification of band intensity was performed using Image Lab software.*
Data are representative of one experiment with n=3 biological replicates. Data shown as mean ±SD.

4.3. Effect of GDF11 and MSTN *in vivo*

As described in paragraph 4.1.5 and 4.1.7, we have been successful in producing recombinant GDF11 and MSTN and their prodomains. Because of technical issues, in particular the low yield, we were not able to perform *in vivo* experiments. The optimization and scale up of recombinant protein production are ongoing but this goes beyond the scope of this thesis. ICGEB has a long-time experience in production of AAV vectors. We changed our strategy and took advantage of the ICGEB AAV facility to produce vectors and deliver GDF11 and MSTN *in vivo* in mice and study their role and their differences in regulating cardiac mass. We also evaluated the possibility of delivering GDF11 and MSTN to cardiomyocytes to reduce side effects of systemic administration.

4.4. AAV delivery of GDF11 and MSTN *in vivo*

We have developed two different approaches targeting two different districts: the heart and the whole body. The former strategy, described in paragraph 4.4.1, was aiming to increase GDF11 and MSTN concentration directly and only at cardiac level, reducing possible systemic side effects and maximizing its activity on cardiac tissue. The latter strategy, described in paragraph 4.4.2, consisted in using the liver as a protein factory to increase serum concentration of GDF11 and MSTN using AAV vectors with a liver specific promoter. This second approach should grant a more intense and constant GDF11 exposition, but at price of losing cardiac specificity.

4.4.1. Cardiac-localized transduction with AAV9-CMV-GDF11 has no effect on cardiac mass

Our first *in vivo* strategy consisted in increasing GDF11 concentration at cardiomyocytes level using an intraventricular injection of AAV9 expressing a Gdf11 WT and Gdf11-Chim ORF under control of a human cytomegalovirus (CMV) promoter. Localized heart transduction was obtained by taking advantage of AAV9 serotype tropism for the cardiac muscle (Zacchigna et al., 2014) and by a precise and confined intramyocardial virus injection. 2 months old male C57Bl/6 mice were randomized to receive 10^{11} GC/animal through two injections in the left ventricle free myocardial wall (n=5 per group) and compared to AAV9-GFP as a control (Fig. 29A). As shown in fig. 29B, we could not detect any significant difference in changes in heart weight/tibia length ratio (HW/TL) or heart weight/body weight ratio (HW/BW) after 28 days. AAV9 had successfully transduced cardiomyocytes as shown in fig. 29C thus we moved to investigate the possibility that GDF11 and MSTN processing in cardiomyocytes was not efficient.

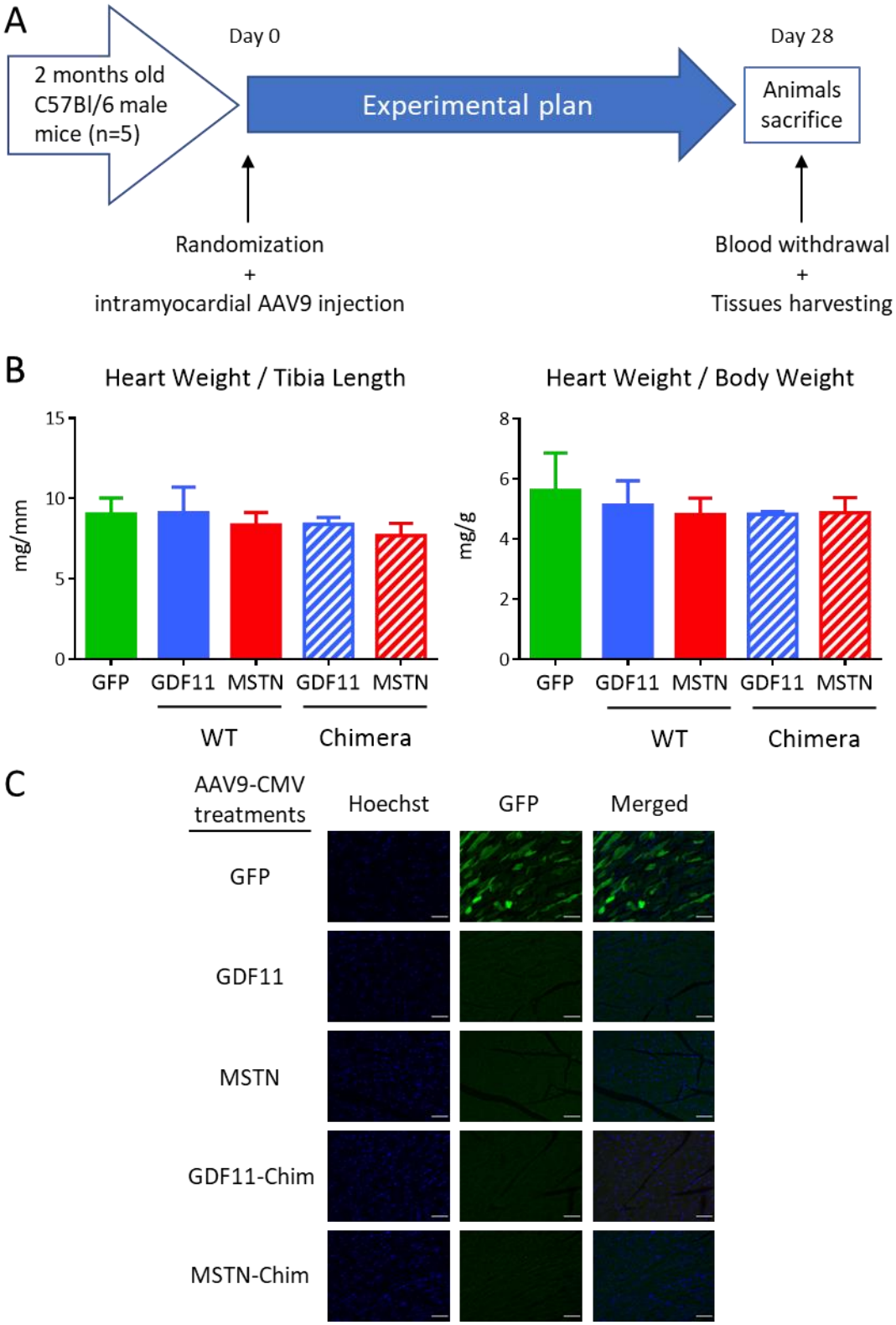

Figure 29: AAV9-GDF11 intramyocardial delivery does not reduce cardiac mass because of inefficient post-translational processing in cardiomyocytes.
(A) Schematic of the experiment.
(B) Heart weight is unchanged 28 days after AAV9-GDF11 intramyocardial delivery when compared to control. Normalization was performed by tibia length and body weight.
(C) Frozen sections of control hearts infected with AAV9-GFP show GFP positive cardiomyocytes indicating efficient AAV9 transduction. The scale bar represents 50 µm.

Data are representative of a single experiment with n=5 biological replicates per group. Data shown as mean ± SD.

4.4.1.1. AAV9-CMV vectors can produce recombinant GDF11 and MSTN in HEK-293T cells

While we could demonstrate that AAV9-CMV was able to transduce cardiomyocytes effectively by analyzing the expression of GFP, it was not clear whether the constructs carrying our protein of interest were functional. HEK-293T cells were transduced using AAV9 vectors expressing GDF11 or MSTN. As shown in fig. 30A all constructs were able to produce and secrete their mature protein. As expected, FURIN overexpression induced a higher degree of mature protein production compared the control. Together, these results showed that AAV9 were functional but GDF11/MSTN protein maturation still remained a bottleneck even in case of AAV transduction.

4.4.1.2. Cardiomyocytes can produce GDF11 and MSTN propeptide but FURIN processing is a limiting factor for ligand maturation

In order to assess if GDF11/MSTN maturation was efficiently performed in cardiomyocytes, neonatal rat cardiomyocytes were co-transfected using GDF11/MSTN transgenes from our *in vivo* experiment, with or without FURIN. We did not use AAV9 because neonatal cardiomyocytes are resistant to transduction with this serotype. As shown in fig. 30B, most of the secreted GDF11 and MSTN were in the form of the immature and inactive propeptide, suggesting that furin-like activity to process and produce the active mature protein was inefficient in cardiomyocytes. Co-transfection with Furin increased post-translational processing as indicated by the detection of the 12.5 kDa band in conditioned media. This experiment indicate that cardiomyocytes are able to produce GDF11 and MSTN propeptides, but at the same time they had a suboptimal protein maturation that resulted in low mature protein production in WT conditions. Since protein maturation process is crucial for GDF11/MSTN bioactivity as described in paragraph 4.1.2, we can speculate that inability of cardiomyocyte in processing GDF11 and MSTN is a major limitation for local delivery.

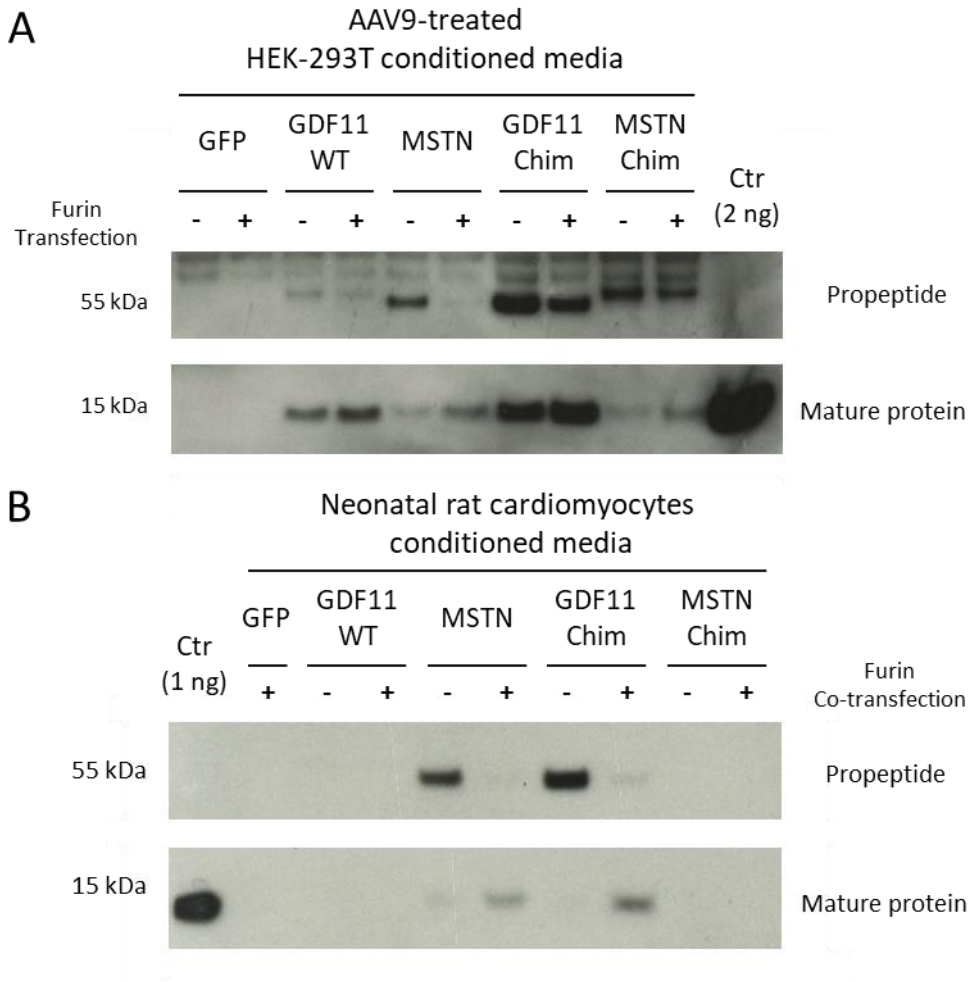

Figure 30: Furin post translational processing of GDF11 and MSTN increases ligand production.
(A) GDF11 and MSTN can be detected in conditioned media of HEK-293T cells infected with AAV9 vectors. Co-transfection of Furin enhances post-processing.
(B) Neonatal rat cardiomyocytes transfected with GDF11 and MSTN constructs show very low post-translational GDF11/MSTN processing that can be rescued by Furin co-transfection.
Data are representative of two separate experiments with n=2 biological replicates. GDF11 recombinant protein (1 or 2 ng) was used as control (Ctr).

4.4.2. High dose AAV8-hAAT-GDF11 or MSTN systemic delivery can reduce cardiac mass in mice after 10 days

In order to evaluate the differential effect of GDF11 and MSTN on cardiac mass, we performed experiments using AAV8 vectors and increase systemic levels of our protein of interest. We developed AAV8 vectors, a serotype that exhibit liver tropism (Zacchigna et al., 2014), together with a human α-1-antitrypsin (hAAT) promoter (Kramer et al., 2003) that grants hepatocyte-specific expression. Liver presents also higher RNA and protein expression levels of FURIN when compared to cardiac tissue (The Human Protein Atlas, 2019) suggesting a more efficient GDF11/MSTN maturation (Hammers et al., 2017).

In order to prove feasibility of this approach C57Bl/6 3 months old male mice were randomized to receive single intravenous injection of $2*10^{12}$ GC/animal (from now on also referred as "High Dose (HD)" (Table 14), n=5/6 per group) of AAV8 carrying GDF11-WT, GDF11-Opt, GDF11-Chim, MSTN or PBS as negative control (Fig. 31A).

Animals weight was measured twice a week from injection until sacrifice, planned 4 weeks later. However, we observed a progressive and severe body weight loss in animals that received GDF11 treatments and thus sacrifice was anticipated at day 10 post-injection.

In all groups treated with GDF11 we observed significant body weight loss when compared to control while MSTN did reduce body weight without reaching significance (Fig. 31C). Cardiac mass expressed as HW/TL ratio was significantly reduced in all GDF11-HD treatments (Fig. 32A). We could translate this finding to cellular level as indicated by the significant reduction in cardiomyocytes cross-sectional area (Fig. 32B). Interestingly, MSTN-HD reduced cardiac mass, although not significantly, independently of body weight reduction, revealing a potential cardiac effect of MSTN. Another interesting observation is the loss of statistical significance for cardiac mass reduction when normalized by body weight (Fig. 32A), implying that GDF11-mediated reduction of cardiac mass may also be secondary to a profound and diffuse change in body mass. We also estimated circulating levels in the different groups by performing western blot analysis on serum harvested at sacrifice. As shown in fig. 31B we could observe a significant increase in both GDF11 and MSTN after AAV8 treatment except for GDF11-WT. As previously shown in our *in vitro* experiments, codon optimization and the presence of MSTN prodomain increased GDF11 production when compared to GDF11-WT.

4.4.2.1. AAV8-hAAT-GDF11/MSTN-HD did not reduce skeletal muscle mass after 10 days

MSTN is the most important negative regulator of skeletal muscle mass and its overexpression has already been linked to skeletal muscle atrophy (Walker et al., 2018). In order to investigate if this effect is shared with GDF11, tibialis muscle weight normalizated on tibia length (TW/TL) and body weight (TW/TL) were evaluated. Interestingly, despite high systemic levels of both GDF11 and MSTN, we did not observe any significant change in tibialis mass when compared to control (Fig. 32C), suggesting that cardiac muscle and skeletal muscle have different time dependent sensitivity to the effect of GDF11 and MSTN.

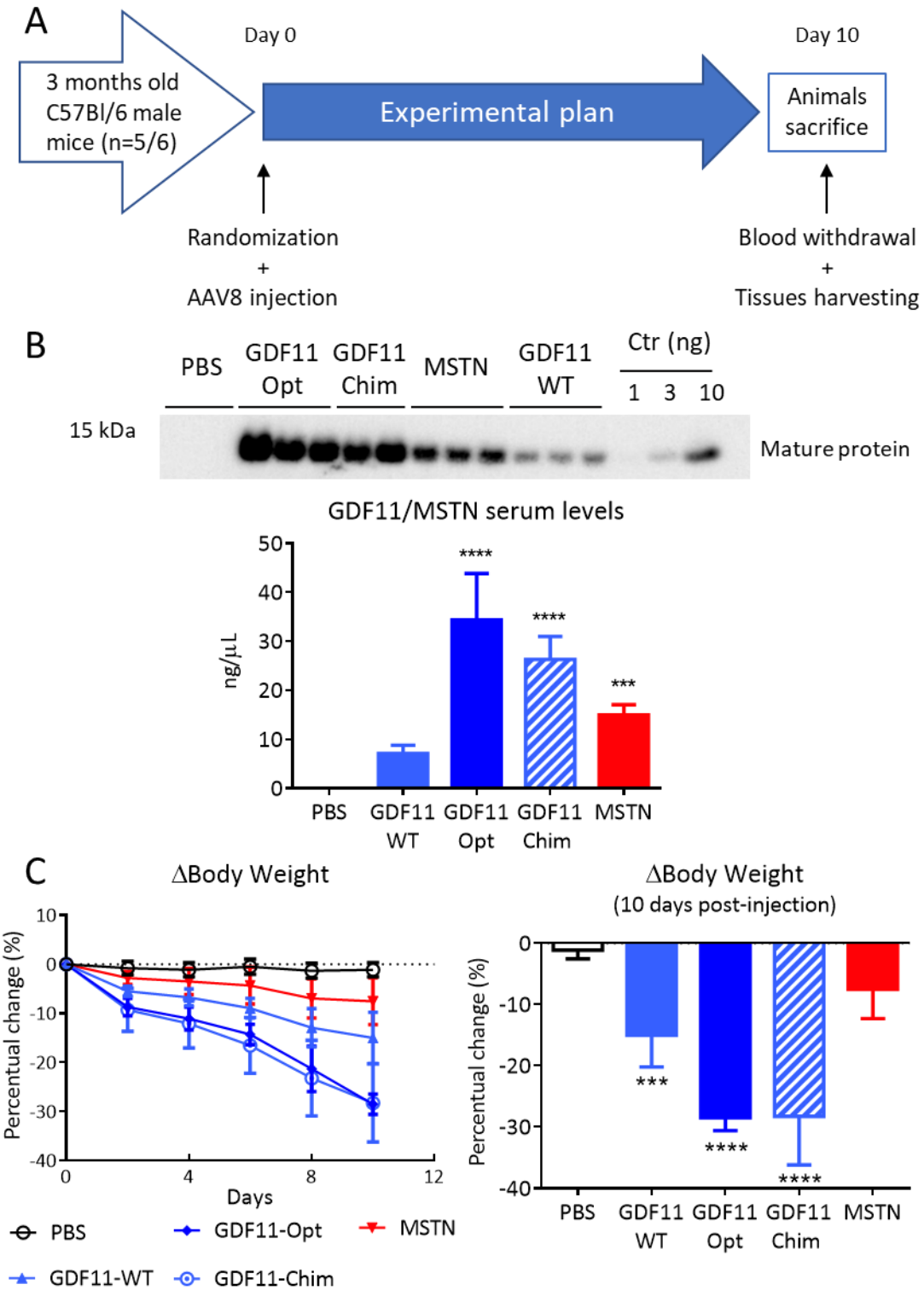

Figure 31: Systemic AAV8 vectors with liver-specific hAAT promoter increase circulating levels of GDF11 and MSTN and is associated to body weight loss.

(A) Schematic of the experiment.

(B) Circulating levels where evaluated by western blot using 1 µL of serum collected at sacrifice.

(C) Increased circulating levels of GDF11 but not MSTN are associated to significant body weight loss when compared to PBS control group.

Data are representative of a single experiment with n=4/6 biological replicates per group. Western blot quantification was performed with Image Lab using a known amount of recombinant GDF11 (n=2/3). GDF11 recombinant protein (1, 3 or 10 ng) was used as quantification control (Ctr). Data shown as mean ± SD.

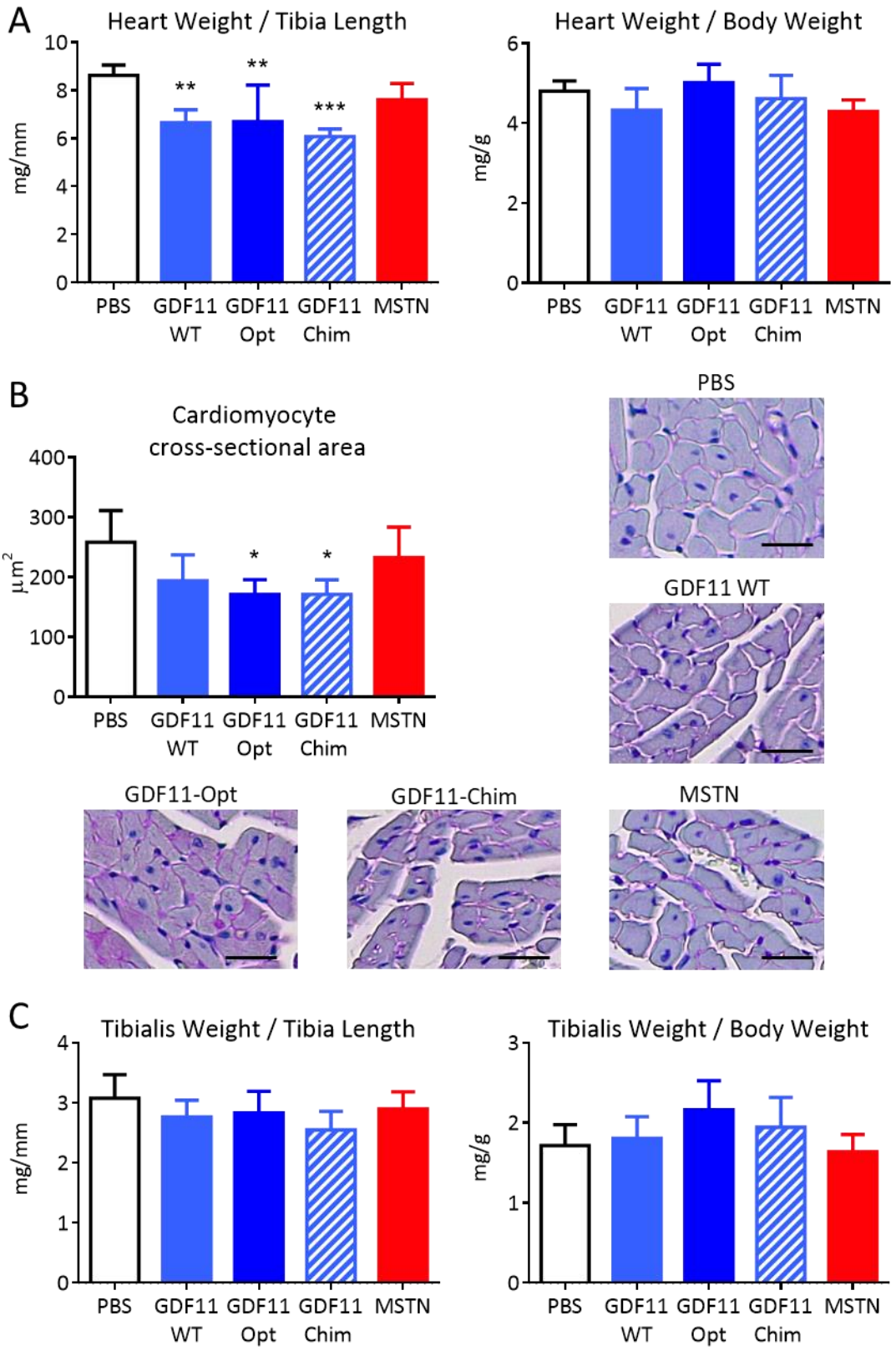

Figure 32: Increasing circulating levels of GDF11 is associated to reduced cardiac mass after 10 days.

(A) Graph representing the HW/TL and HW/BW 10 days after AAV8 injection. The HW/TL was significantly lower in mice injected with AAV8-GDF11 compared to control. A trend towards lower HW/TL can be observed in the MSTN group.

(B) Periodic acid Schiff (PAS) staining of left ventricles. Cardiomyocyte cross-sectional area results

are based on the average of a minimum of 150 myocytes per animal from 4 animals per group. The scale bar represents 25 µm.
(C) No change in skeletal muscle mass was observed 10 days after AAV8 injection when compared to control.
Data are representative of a single experiment with n=4/6 biological replicates. Data shown as mean ± SD.

4.4.3. GDF11-Opt dose response study showed that concentration higher or equal than $2*10^{11}$ GC/animal are associated to poor body conditions

Our previous *in vivo* experiment (paragraph 4.4.2) indicated that high levels of GDF11 produced by AAV8-hAAT treatments, although effective in reducing cardiac mass, were associated to systemic and detrimental changes, specifically a significant body weight loss. In order to determine the optimal dose of AAV8 vector that produces an increase in systemic levels of GDF11 without affecting systemic conditions, we performed a pilot study to evaluate the effect of different viral titers and to determine GDF11-Opt treatment safety rage. We also performed a similar study for AAV8-hAAT-MSTN. Survival, body weight reduction and heart mass reduction were the major endpoints evaluated during these studies. Since numerous and different AAV8-hAAT-treatment titers were tested, we arbitrarily associated virus titer to specific doses ranging from D1 to D7, as described in table 14. We also assigned a Low to High value to specific titers (see table, right column). The results obtained from these dose-effect experiments are critical to compare different titers of AAV8-GDF11-Opt and AAV8-MSTN to modulate GDF11/MSTN serum concentration in mice according to therapeutic needs.

Doses	Corresponding AAV8-hAAT-titer	Second Short Name
D1	$2*10^9$ GC/animal	
D2	$2*10^{10}$ GC/animal	
D3	$6*10^{10}$ GC/animal	
D4	$1.2*10^{11}$ GC/animal	Low Dose (LD)
D5	$2*10^{11}$ GC/animal	Medium Dose (MD)
D6	$6*10^{11}$ GC/animal	
D7	$2*10^{12}$ GC/animal	High Dose (HD)

Table 14: List of AAV8 doses and their corresponding titers.

Three months old C57Bl/6 male mice were injected with 5 different doses, from D1 to D5 (Table 14) and compared to PBS as a control (Fig. 33A). Animals where followed for 35 days, measuring body weight twice a week. Dose D5 produced significant body weight loss that

required euthanasia at day 14 (Fig. 33C). D5 dose was the only one to require premature sacrifice and we could observe a dose dependent effect on body weight loss. The increase of circulating levels of D2, D3, D4 treatments were confirmed by western blot as shown in fig. 33B.

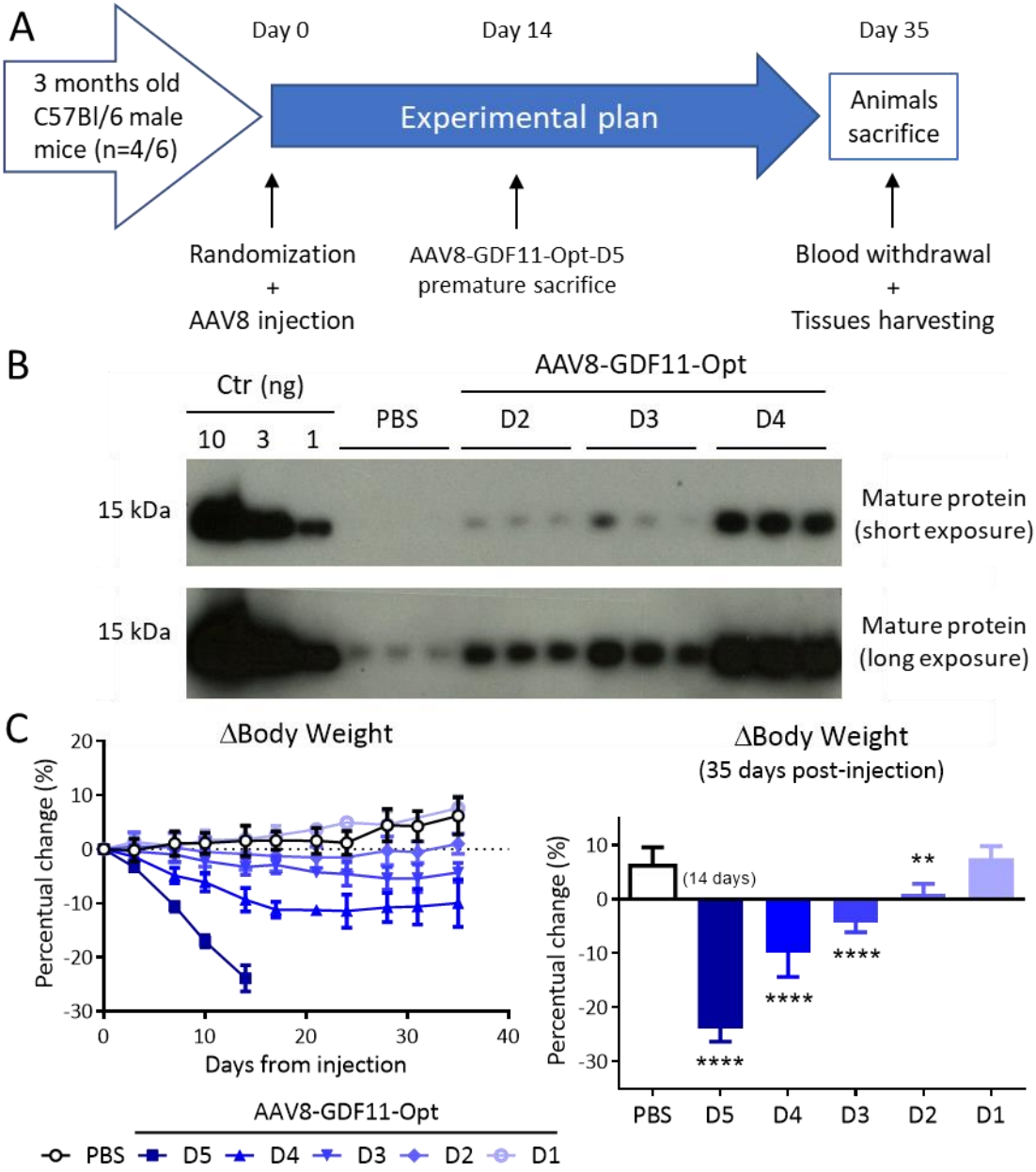

Figure 33: Systemic AAV8-GDF11 produce a dose dependent increase in circulating levels of GDF11.
(A) Schematic of the experiment. Three months old male mice were injected intravenously with increasing doses of AAV8-GDF11-Opt and sacrificed after 35 days. Because of poor body conditions, mice that received the high dose (D5) where sacrificed on day 14.
(B) Western blot analyzing 1 µL of serum collected at sacrifice showing a dose dependent increase in circulating GDF11 after AAV8 injection.
(C) GDF11 delivered with a AAV8 vector carrying a liver specific promoter reduces body weight in a dose dependent manner.
Data are representative of a single experiment with n=4/6 biological replicates. GDF11 recombinant protein (1, 3 or 10 ng) was used as quantification control (Ctr). Data shown as mean ± SD.

4.4.4. GDF11 delivered by AAV8 produces a dose dependent reduction in cardiac mass in mice

We next sought to evaluate the effect of our treatments on cardiac mass, one of the major endpoints of the AAV8-hAAT-GDF11-Opt dose finding experiment. As shown in fig. 34A, GDF11-Opt-D4-treated mice showed a significant reduction in HW/TL (7.46±0.66 mg/mm vs. 8.60±0.80 mg/mm) when compared to control without major deterioration of systemic body conditions. These results were showing that by modulating the dose of delivered vectors, and thus circulating GDF11, the treatment is safe and could be used in the setting of pathologic hypertrophy. On the other hand, as previously shown in 4.4.2 paragraph, GDF11 effects are not confined to cardiac tissue. Indeed, TW/TL of GDF11-Opt-D4 treatment was significantly lower than control group (Fig. 34B), and we observed significant reduction in body weight, a major limitation for systemic delivery (Fig. 33C).

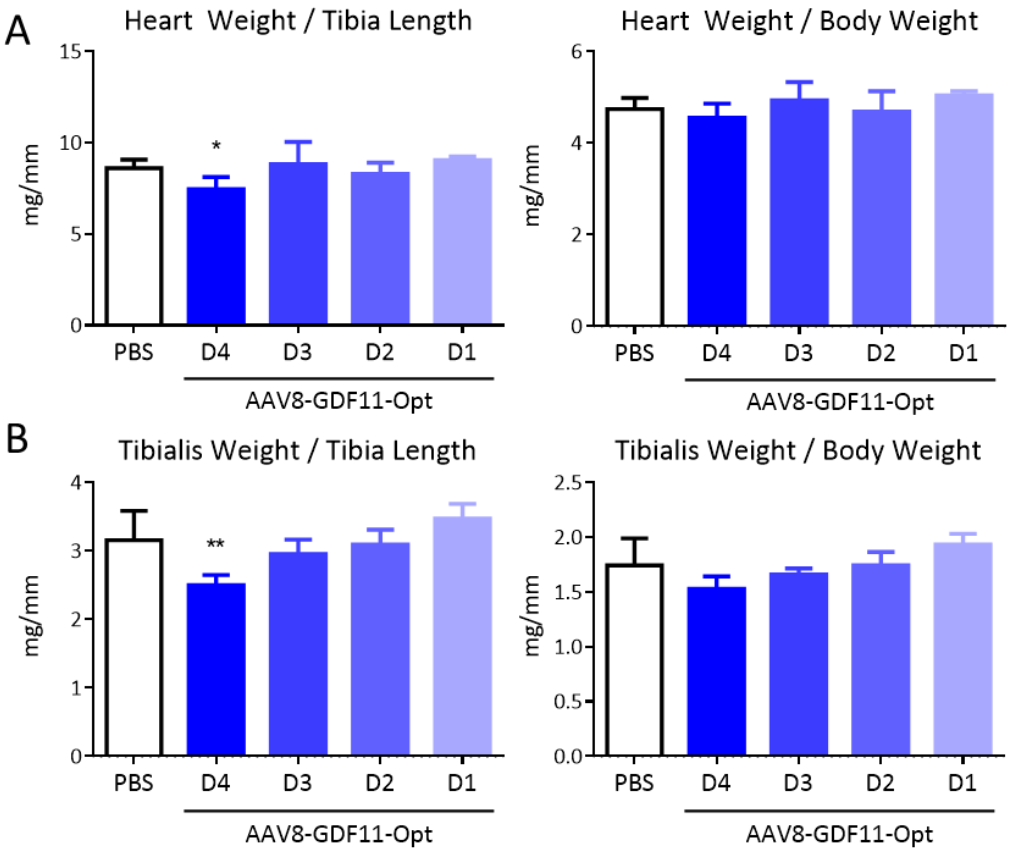

Figure 34: Systemic AAV8-GDF11 produce a dose dependent reduction in cardiac mass. *(A) Graph showing the effect of different doses of GDF11 on cardiac mass calculated as ratio between heart weight and tibia length or body weight.*
(B) The effect of GDF11 was not limited to cardiac mass and is associated to a dose dependent decrease in skeletal muscle mass.
Data are representative of a single experiment with n=4/6 biological replicates per group. Data shown as mean ± SD.

4.4.5. MSTN-D7 (HD, $2*10^{12}$ GC/animal) was safe and showed a trend in HW/TL reduction

We also evaluated, in parallel with GDF11, safety and the effect on cardiac and skeletal muscle mass, of elevating systemic MSTN through AAV8-hAAT-MSTN delivery at different doses. Our data has shown that high levels of MSTN (MSTN-D7 treatment, $2*10^{12}$ GC/animal), were not associated to significant side effects, with no impact on mortality and body condition deterioration after 10 days (paragraph 4.4.2). Thus, we performed a new experiment where we evaluated the effect of different doses of MSTN by modulating the titer of vectors that were delivered (D7, D6, D5, D3 corresponding to $2*10^{12}$, $6*10^{11}$, $2*10^{11}$ and $6*10^{10}$ GC/animal, respectively, n=4 mice per group, table 14).

As for our previous experiments, the major endpoints that we evaluated were body condition, body weight reduction, effect on cardiac and skeletal muscle mass (Fig 35A). After 35 days from vectors delivery, all the animals were in good body condition, suggesting a higher safety profile of MSTN compared to GDF11. We also observed a dose-dependent decline in body weight that however appears more gradual and less severe when compared to equal doses of GDF11 (Fig. 35B-C).

We also observed a trend towards a dose dependent reduction in cardiac mass (Fig. 36A). We speculate that in the setting of pathological cardiac hypertrophy this could be relevant. As observed for GDF11 treatments, elevating systemic levels of MSTN was associated to a significant reduction of skeletal muscle mass (Fig. 36B). We also confirmed the elevation of serum levels of MSTN by western blot, that appears to be higher than GDF11, suggesting and confirming the difference in potency of these two proteins (Fig. 35B). The exact quantification of circulating levels, as for the other experiments, is at the moment under investigation using mass spectrometry (see paragraph 2.10.2). These observations, together with our previous results, showed that GDF11 and MSTN may have overlapping effects on cardiac tissue, skeletal muscle and body weight, that can be explained by the different potency. To further characterize therapeutic application and ligand potency of these two peptides, we evaluated the effect in a model of pathologic hypertrophy, by producing pressure overload in mice.

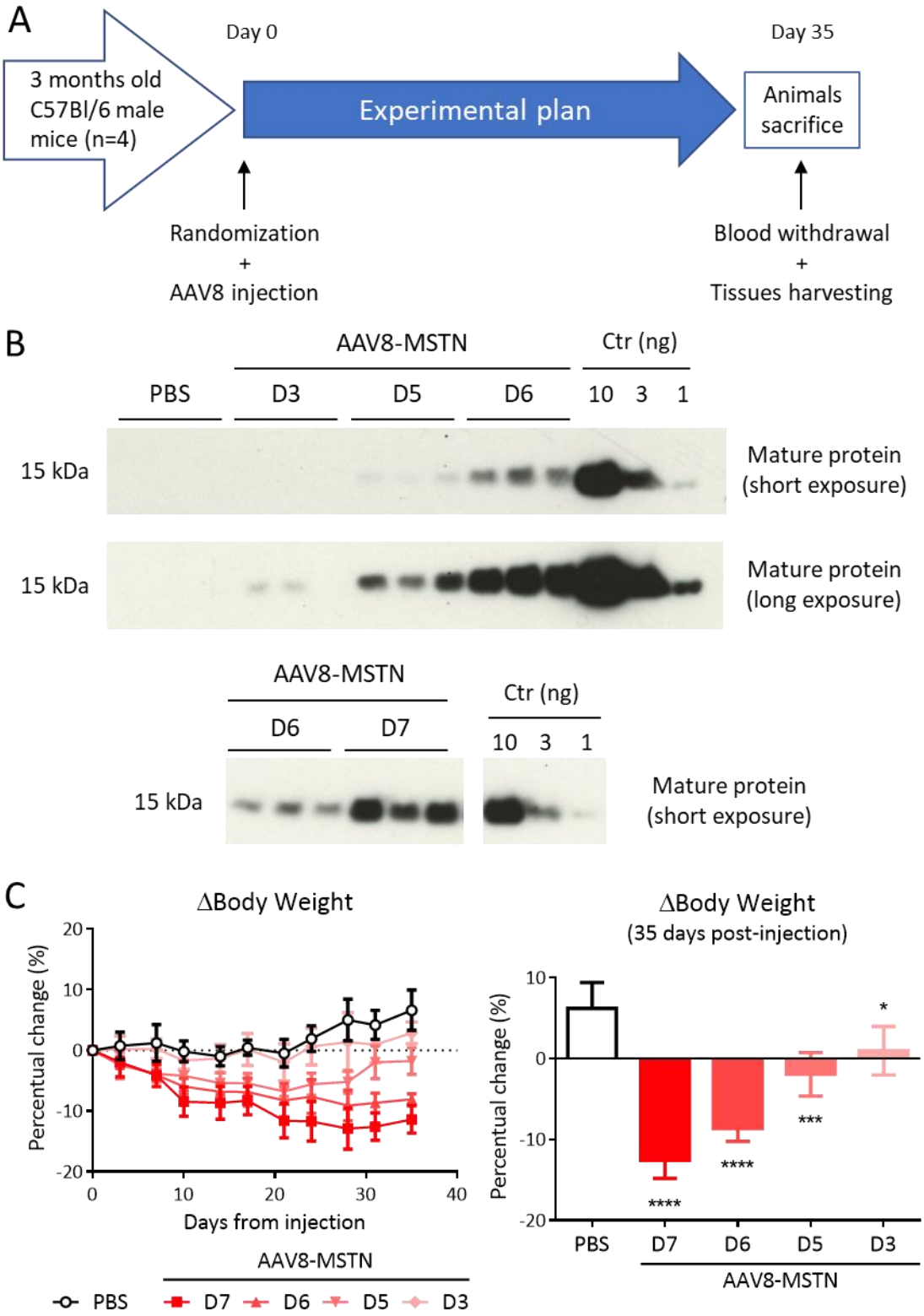

Figure 35: Systemic AAV8-MSTN produce a dose dependent increase in circulating levels of MSTN.
(A) Schematic of the experiment. As for GDF11, 3 months old male mice were injected intravenously with increasing doses of AAV8-MSTN and sacrificed after 35 days.
(B) Western blot analyzing 1 µL of serum collected at sacrifice showing a dose dependent increase in circulating MSTN after AAV8 injection.
(C) MSTN delivered with a AAV8 vector carrying a liver specific promoter reduces body weight in a dose dependent manner.
Data are representative of a single experiment with n=4 biological replicates. GDF11 recombinant protein (1, 3 or 10 ng) was used as quantification control (Ctr). Data shown as mean ± SD.

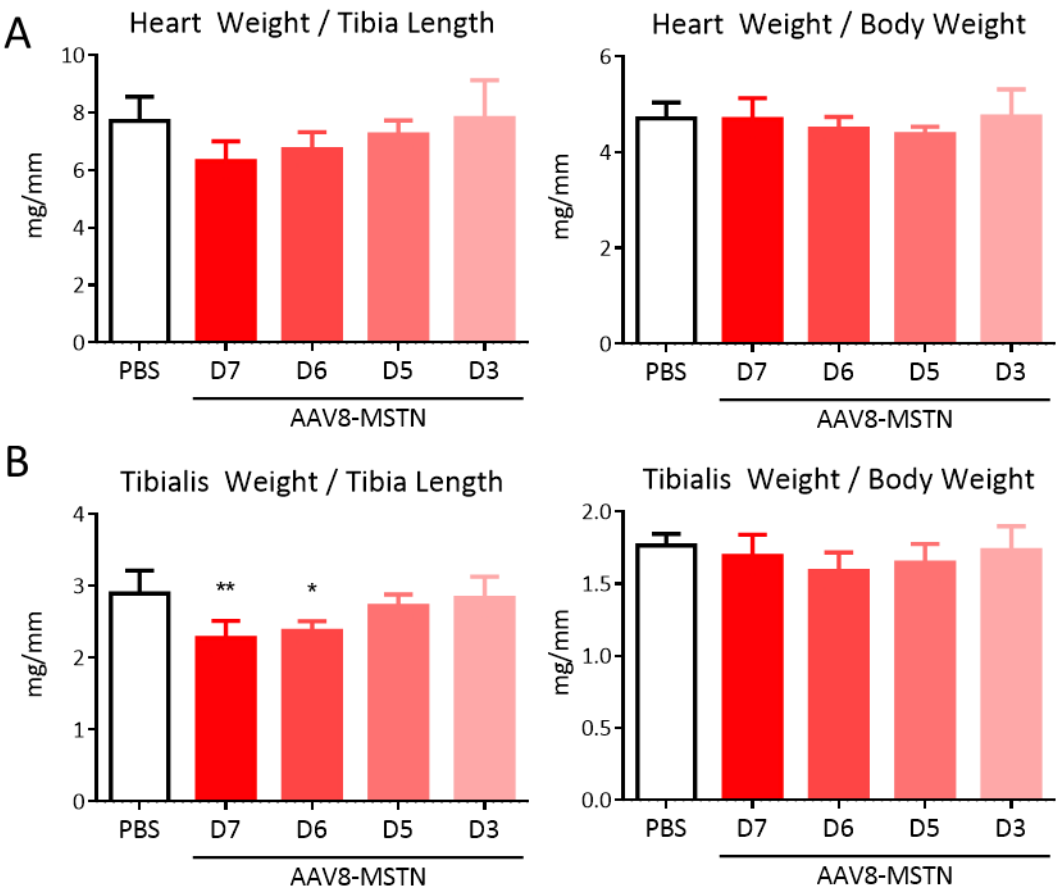

Figure 36: Systemic AAV8-MSTN produce a dose dependent trend in reducing cardiac mass. *(A) Graph showing the effect of different doses of MSTN on cardiac mass calculated as ratio between heart weight and tibia length or body weight. MSTN produced a dose-dependent trend in lower HW/TL when compared to control.*
(B) MSTN is associated to a significant dose dependent decrease in skeletal muscle mass when normalized to tibia length.
Data are representative of a single experiment with n=4 biological replicates per group. Data shown as mean ± SD.

4.5. GDF11 and MSTN can prevent pathological cardiac hypertrophy induced by pressure overload in mice

Our data indicate that GDF11 can reduce cardiac mass in a dose-dependent manner in basal conditions. MSTN, although the data was not significant, has shown a similar trend. While the initial findings have shown that GDF11 is able to reduce cardiac hypertrophy, new studies indicate a powerful effect of GDF11 in reducing cardiac mass also in young animals, possibly by activating atrophy pathways (Hammers et al., 2017). GDF11 has also shown to prevent cardiac hypertrophy after transverse aortic constriction, a common mouse model of pressure overload, however at the expense of a cachectic state that required euthanasia

(Harper et al., 2018). We hypothesize that by finely modulating GDF11 systemic levels it is possible to achieve a therapeutic effect without significant side effects. We also hypothesize that MSTN, which in our previous experiment has shown a broader and safer therapeutic window, may have a similar effect.

3 months old C57Bl/6 male mice were randomized to undergo TAC or sham surgery (Fig. 37A). To confirm successful ligation of the transverse aorta, two days after surgery animals were subjected to Doppler assessment of flow velocity of right and left common carotid arteries. Only mice with a right carotid/left carotid flow ratio > 5 where included in the study. One week after surgery mice that were assessed for successful TAC were furtherly randomized to receive AAV8 intravenous injection or PBS. The experimental groups were: GDF11 low dose (LD) and medium dose (MD), GDF11-Chim-LD, and MD and high dose (HD) of MSTN (Table 14). Sham operated animals were injected only with PBS. Mice were weighted twice a week and monitored until sacrifice. Twenty-five days post AAV8-treatment, mice were subjected to a full echocardiographic evaluation. Subsequently, invasive hemodynamic assessment by left ventricular pressure-volume loop analysis was performed prior sacrifice. GDF11 and MSTN serum concentration was evaluated after animal sacrifice by western blot (Fig. 37B). GDF11/MSTN quantification was also carried out using a specific mass spectrometry assay (described in paragraph 2.10.2) (Fig. 37C). The group that was receiving the medium dose of GDF11 was sacrificed earlier (day 18 after AAV delivery) because of poor body conditions, characterized by significant and severe body weight loss (Fig. 38A). As expected, HW/TL was significantly higher in TAC animals that received PBS when compared to sham operated mice (11.59±1.97 vs. 8.08±1.24 mg/mm) (Fig. 38B). GDF11 prevented the onset of pathological cardiac hypertrophy in a dose-dependent manner (Fig. 38B). Interestingly, despite a shorter exposure to circulating GDF11, HW/TL in the GDF11-MD was significantly smaller than PBS treated animals (6.95±1.89 vs. 11.59±1.97 mg/mm) (Fig. 38B). We speculate that batch to batch variability of AAV vectors, different infectivity, additional stress due to TAC procedure may have contributed to deteriorate body conditions in this group. Our data indicate that GDF11-LD was also effective in preventing cardiac hypertrophy after TAC when compared to PBS (8.10±1.92 vs. 11.59±1.97 mg/mm), with a less severe impact on body weight (Fig. 38A-B). Similarly to GDF11-LD, also GDF11-Chim-LD treatment prevented cardiac hypertrophy after TAC (8.66±1.53 vs. 11.59±1.97 mg/mm). Interestingly, MSTN showed a

dose dependent effect in preventing cardiac hypertrophy after pressure overload. The high dose of MSTN significantly reduced cardiac mass after TAC when compared to PBS (8.96±1.10 vs. 11.59±1.97 mg/mm), without affecting body condition (Fig. 38B). These data confirmed the anti-hypertrophic effect of GDF11 in pathological conditions, and, for the first time in a side by side comparison, that this effect is shared with MSTN, although at different doses.

Interestingly, statistical significance of GDF11-LD and -MD were maintained even after body weight normalization, suggesting that, in pathological conditions, GDF11 is capable of inducing a mass-reducing-effects on cardiac tissue independently from body weight loss. We also evaluated if the morphometrical changes in cardiac mass translated at the cellular level by measuring cardiomyocyte cross-sectional area and our data confirm our previous finding (Fig. 39). Together, all these data support the hypothesis that GDF11 and MSTN have similar anti-hypertrophic effect on cardiomyocytes, however displaying a different potency. Furthermore, MSTN does not induce cachexia at the doses investigated. Further investigations are ongoing to explain the different mechanism. We next sought to investigate whether reduction of pathological cardiac hypertrophy was associated with an improvement of cardiac function. Animals were subjected to echocardiographic examination and invasive hemodynamic assessment prior sacrifice. As shown in fig. 40A, both GDF11-LD and MSTN-HD reduced cardiac mass when compared to PBS (133.18±26.89 and 142.78±22.59 mg vs. 182.62±31.55 mg, respectively).

As expected, TAC was associated to deterioration of diastolic parameters when PBS is compared to sham surgery (dP/dt_{min}: -7522±2819 vs. -8629±1289 mmHg and Tau: 8.01±2.67 vs. 5.15±1.19 msec) (Fig. 40B). Surprisingly, both GDF11 and MSTN failed to improve parameters of diastolic function. We speculate that the persistence of the gradient because the mechanical obstruction is not removed upon treatment in the TAC model may in part explain these negative results requiring additional models of pathological cardiac hypertrophy.

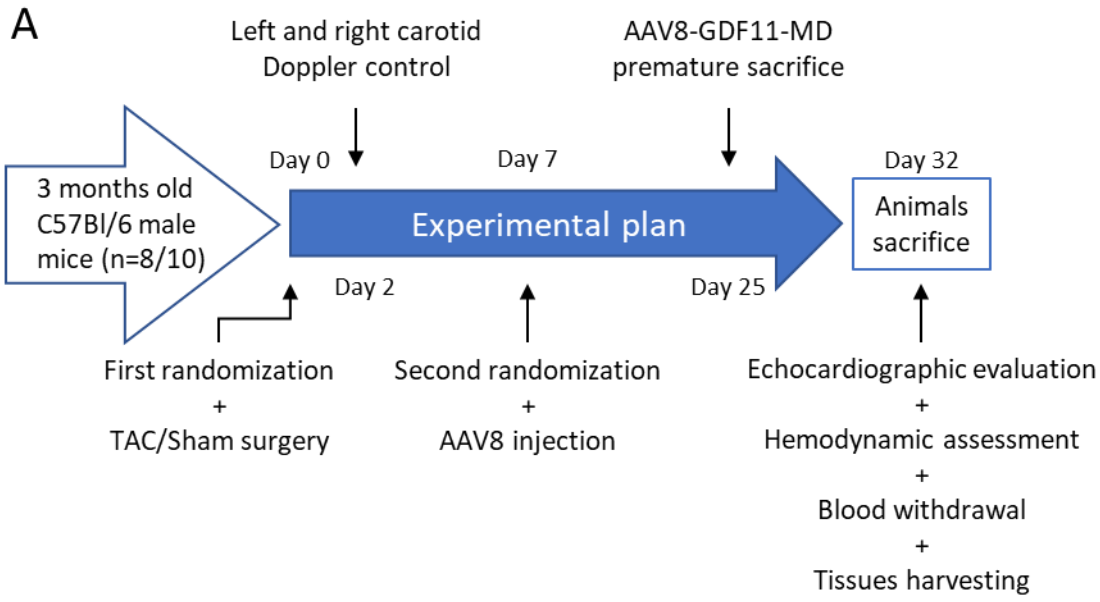

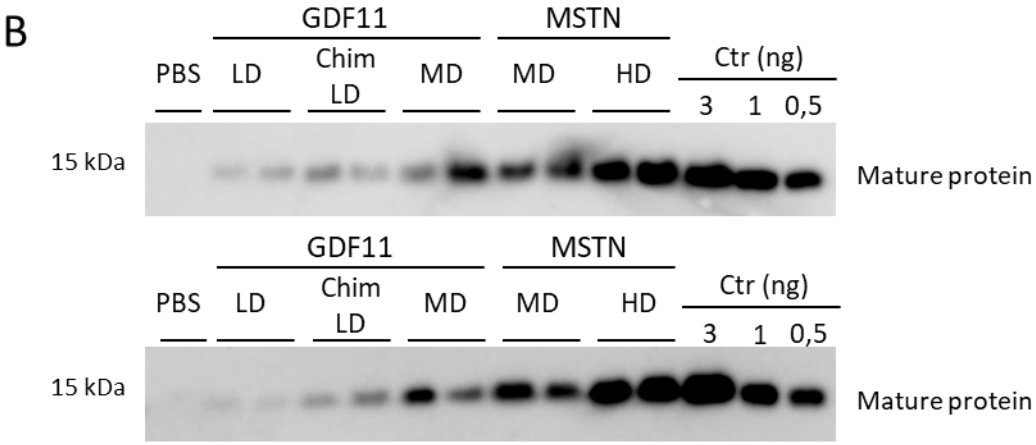

C

	(ng/µL)	
	GDF11	MSTN
Sham	0.22 ± 0,26	0.42 ± 0,35
PBS	0.23 ± 0,04	0.90 ± 0,62
GDF11-LD	2.55 ± 1,05	0.47 ± 0,21
GDF11-Chim-LD	3.89 ± 1,82	0.54 ± 0,37
GDF11-MD	5.43 ± 2,15	0.42 ± 0,26
MSTN-MD	0.39 ± 0,09	6.63 ± 2,34
MSTN-HD	0.13 ± 0,02	12.44 ± 1,77

Figure 37: Circulating levels of GDF11 and MSTN after AAV8 treatment in a model of pathological cardiac hypertrophy.

(A) Schematic of the experiment. 3 months male mice were randomized to receive TAC or sham operation. TAC was confirmed by Doppler analysis on common carotid arteries. One week later mice were furtherly randomized to receive systemic AAV8 vectors or PBS. Mice were sacrificed at day 18 or 25 post injection.

(B) Western blot quantification using the same volume of serum (1 µL, terminal blood withdrawal) was performed in each treatment group (n=4). Exact quantification of these bands is challenging because of low signal intensity and system does not discriminate GDF11 and MSTN proteins.

(C) Quantification using LC-MS/MS assay. Data shown as mean ± SD.

For each treatment group n=3/5 biological replicates were analyzed, to date, the remaining animals are still under analysis. GDF11 recombinant protein (0.5, 1, or 3 ng) was used as control (Ctr).

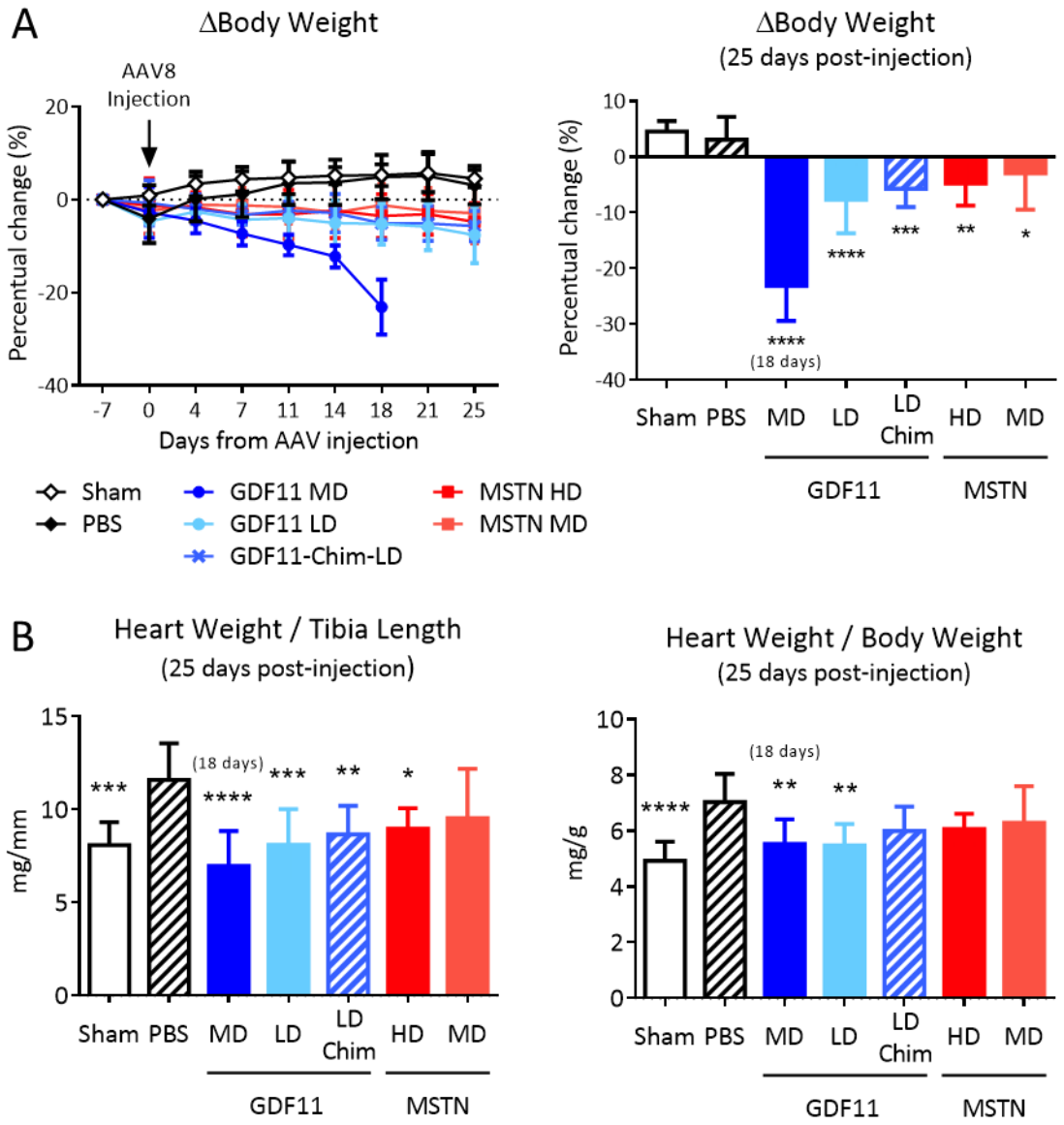

Figure 38: GDF11 and MSTN prevent pathological cardiac hypertrophy after TAC.

(A) Randomized, vehicle controlled, dose-dependent study of GDF11 and MSTN therapy in mice subjected to pressure overload shows a significant reduction in cardiac mass after GDF11 and with high doses of MSTN.

(B) Graphs representing HW/TL and HW/BW. As expected, both GDF11 and MSTN induce a dose dependent weight loss that was more severe with high GDF11. Because of poor body conditions mice that received GDF11-MD were sacrificed earlier (day 18 post injection).

Data are representative of a single experiment with n=8/10 biological replicates per group. Data shown as mean ± SD.

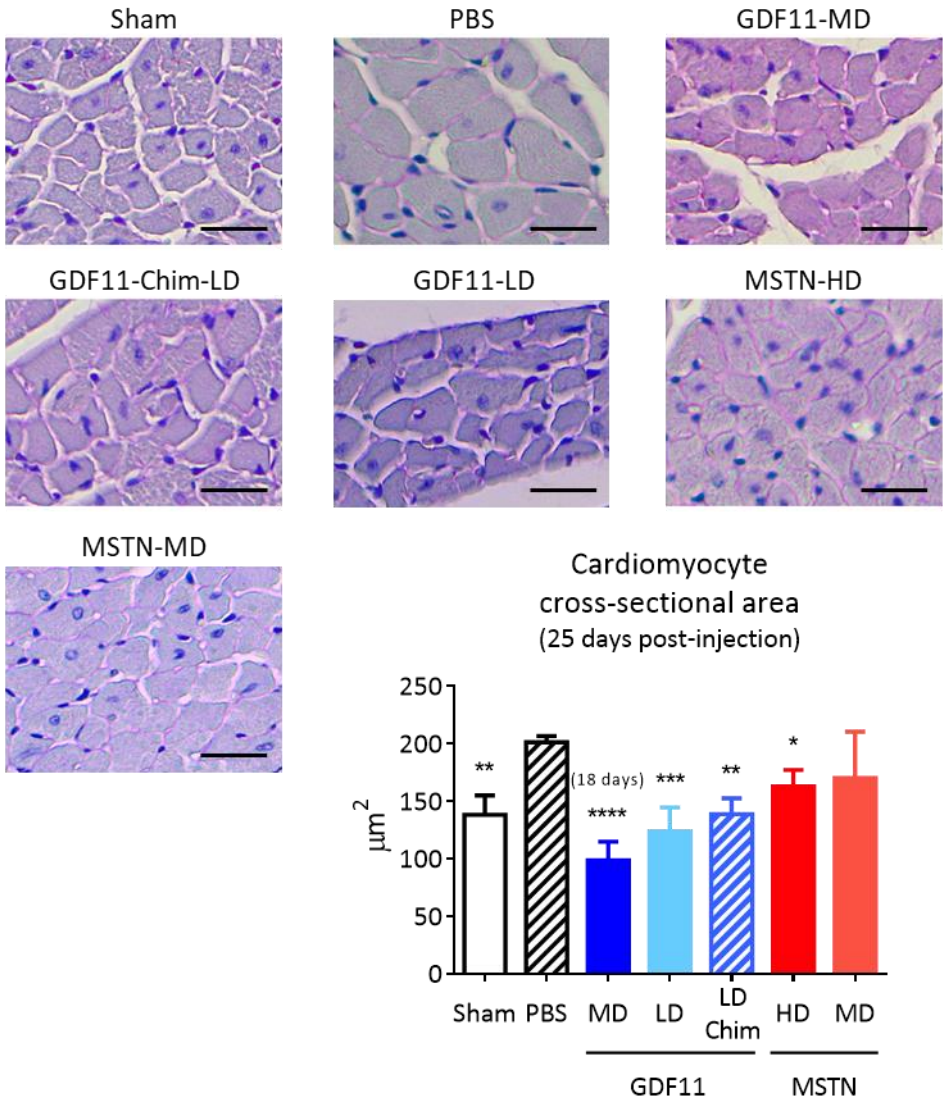

Figure 39: GDF11 and MSTN therapy after TAC reduces cardiomyocyte cross-sectional area.
(A) PAS staining of left ventricles after TAC surgery. Cardiomyocytes of TAC mice exposed to supraphysiologic levels of GDF11 and MSTN are smaller compared to PBS injected controls. (B) Graph representing cardiomyocyte cross-sectional area measured after PAS staining in mice subjected to TAC.
Data are representative of a single experiment with n=5/6 biological replicates per group. The scale bar represents 25 µm. Data shown as mean ± SD.

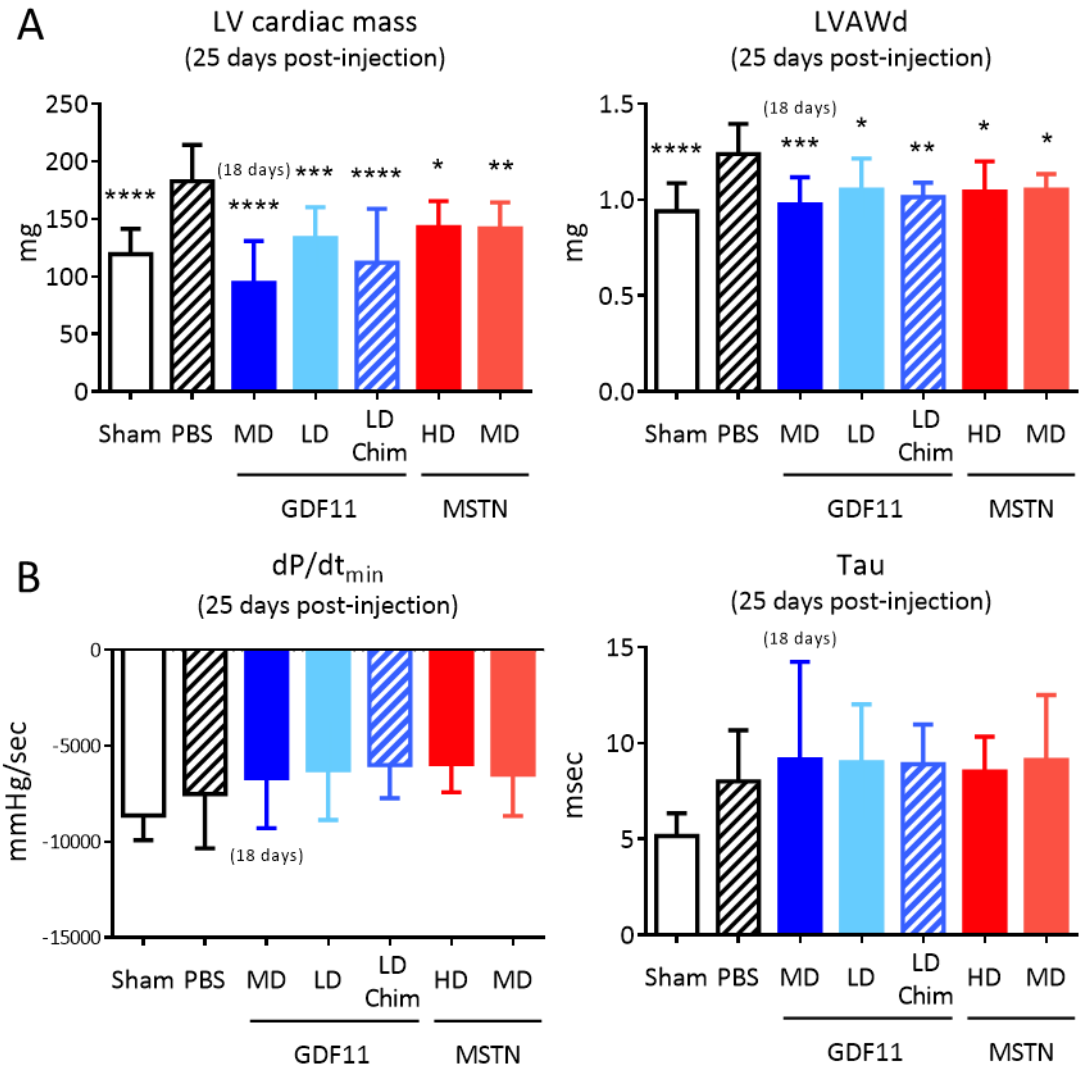

Figure 40: GDF11 and MSTN reduce cardiac mass but do not improve diastolic function after TAC.
(A)Echocardiographic evaluation confirmed a significant reduction in LV anterior wall thickness and LV cardiac mass upon treatment with GDF11 and MSTN.
(B) Graphs showing the maximal rate of pressure decay in the left ventricle (dP/dT_{min}) and the exponential decay of the ventricular pressure during isovolumic relaxation or isovolumic relaxation constant (Tau), measured by invasive hemodynamic assessment. An increase in diastolic function or an increase in relaxation causes increased dP/dt_{min} during isovolumic relaxation and decreased Tau. GDF11 and MSTN fail to improve both parameters of diastolic function after TAC.
Data are representative of a single experiment with n=8/10 biological replicates per group. Data shown as mean ± SD.

4.5.1. GDF11 and MSTN treatments were associated to skeletal muscles atrophy

We also evaluated the effect on skeletal mass of treatments with GDF11 and MSTN. We evaluated changes in weight of three different hindlimb skeletal muscles (tibialis anterior, quadriceps femoris and gastrocnemius). As expected, both GDF11 and MSTN significantly reduced skeletal muscle mass when compared to PBS treated animals (Fig. 41).

These observations confirmed again our previous findings where GDF11/MSTN-induced muscular atrophy is associate to a systemic body weight loss.

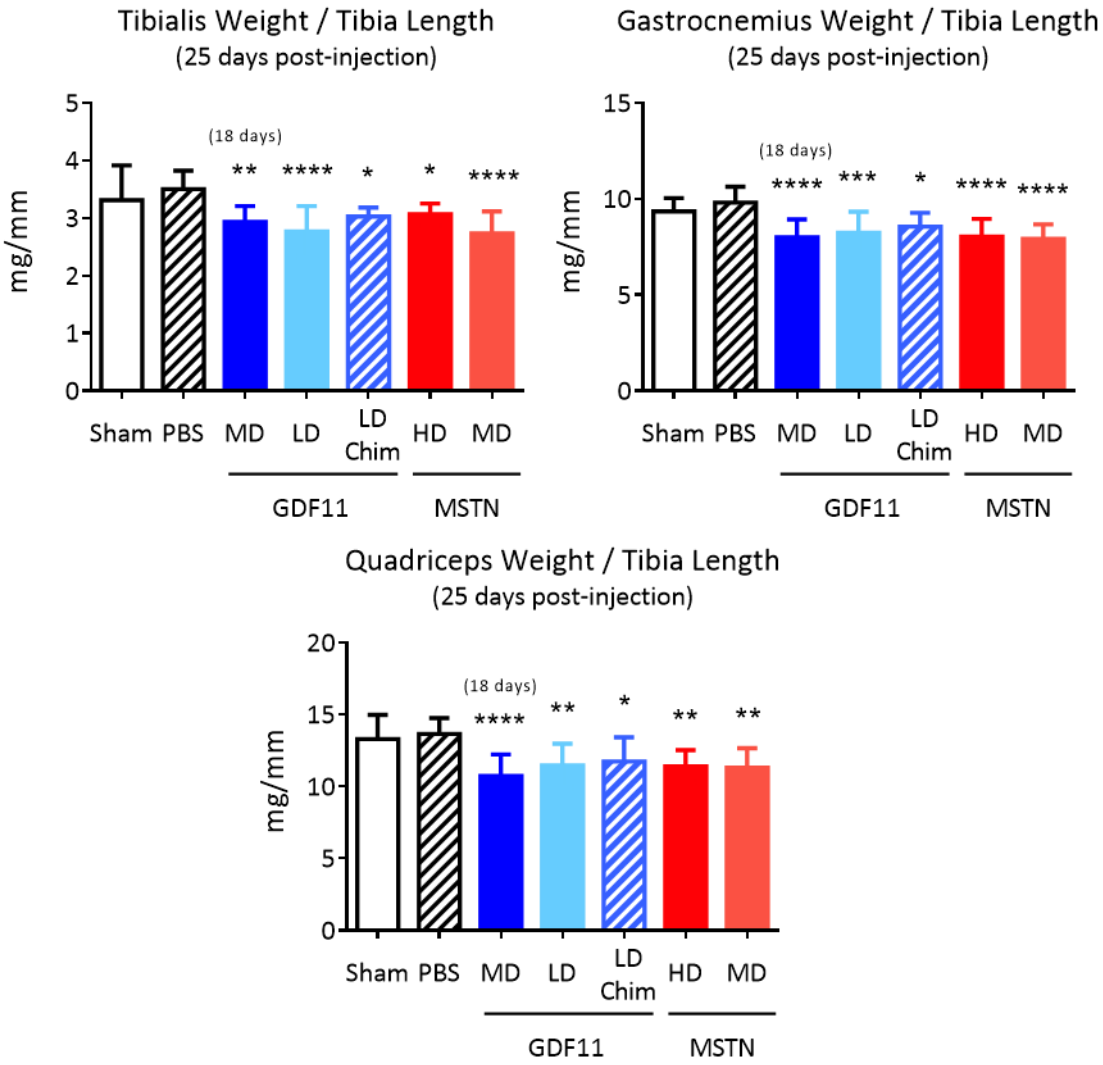

Figure 41: GDF11 and MSTN are associated to skeletal muscles atrophy after TAC.
Graphs showing tibialis anterior, quadriceps femoris and gastrocnemius weights normalized to tibia length.
Data are representative of a single experiment with n=8/10 biological replicates per group. Data shown as mean ± SD.

4.6. Circulating GDF11 and MSTN decline with aging in mice

As previously shown, circulating levels of GDF11 and MSTN can affect cardiac mass in a dose dependent manner. However, the high sequence homology between GDF11 and MSTN mature proteins has contributed to generate conflicting data on circulating levels and their effects on cardiac tissue. Most of these studies were relying on nonspecific detection methods that were not effectively able to discriminate GDF11 and MSTN. (Egerman et al., 2015; Loffredo et al., 2013; Poggioli et al., 2016).

In order to provide an accurate GDF11 and MSTN quantification, we collaborated with Dr. Olga Shevchuk (Leibniz, Institut für Analytische Wissenschaften, ISAS Campus, Dormund) to develop a LC-MS/MS-based assay to quantify GDF11 and MSTN in serum. This method was previously used to assess GDF11 and MSTN circulating levels in humans (Schafer et al., 2016). These studies have shown that GDF11 levels were not significantly altered by aging in humans while MSTN levels decrease throughout life in men (Schafer et al., 2016). Changes in circulating levels in mice has not been assessed yet by using a specific assay. We applied our newly developed assay to measure serum levels of GDF11 and MSTN in young (2 months old, n=6) and old (30 months old, n=6) C57Bl/6 female mice.

As shown in Fig 42, both GDF11 (0.0673 ± 0.0138 vs. 0.0446 ± 0.0171 ng/mL) and MSTN (26.489 ± 5.621 vs 13.190 ± 5.860 ng/mL) significantly decrease with aging in mice. To our knowledge, no other study has evaluated yet circulating GDF11 and MSTN in mice using a specific quantitative nanoLC-high resolution mass spectrometry approach. Interestingly, in WT mice, GDF11 circulating levels are around 2 order of magnitude lower than circulating MSTN and ten times lower than values measured in humans (Schafer et al., 2016; Semba et al., 2019). Further investigations are required to understand the biological relevance of these finding. The results of this study have been submitted for publication to the journal "Proteomics" (Wiley-VCH).

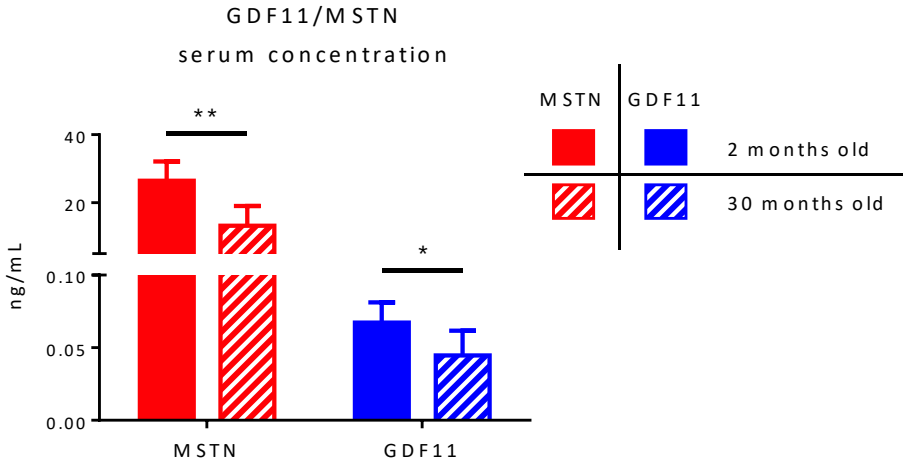

Figure 42: GDF11 and MSTN circulating levels decrease with aging in mice.
Data derived from LC-MS/MS assay show a significant reduction in circulating levels of GDF11 and MSTN in female WT C57Bl/6 30 months old mice when compared to young 2 months old mice. Data are representative of a single experiment with n=6 biological replicates per group. Data shown as mean ± SD.

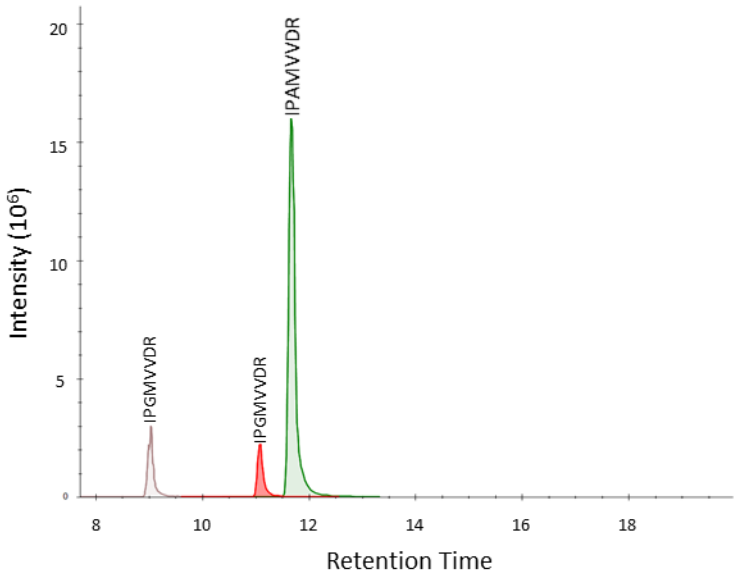

Peptide sequence	Isotope type	Precursor Mz	Product Mz	Fragment Ion
		MSTN		
IPAMVVDR	Heavy	450,7522	787,4131	y7
IPAMVVDR	Heavy	450,7522	690,3603	y6
IPAMVVDR	Heavy	450,7522	619,3232	y5
IPAMVVDR	Heavy	450,7522	488,2827	y4
IPAMVVDR	Heavy	450,7522	175,119	y1
IPAMVVDR	Light	455,7563	797,4214	y7
IPAMVVDR	Light	455,7563	700,3686	y6
IPAMVVDR	Light	455,7563	629,3315	y5
IPAMVVDR	Light	455,7563	498,291	y4
IPAMVVDR	Light	455,7563	185,1272	y1
		GDF11		
IPGMVVDR	Heavy	443,7444	773,3974	y7
IPGMVVDR	Heavy	443,7444	676,3447	y6
IPGMVVDR	Heavy	443,7444	619,3232	Y5
IPGMVVDR	Heavy	443,7444	389,2143	y3
IPGMVVDR	Light	448,7485	783,4057	y7
IPGMVVDR	Light	448,7485	686,3529	y6
IPGMVVDR	Light	448,7485	629,3315	y5
IPGMVVDR	Light	448,7485	498,291	y4
IPAMVVDR	Light	448,7485	399,2226	y3

Figure 43: MSTN and GDF11 peptides can be properly resolved using LC-MS/MS method. *Comparison of the two peptides used to discriminate and quantify MSTN and GDF11 in serum samples. Peptides are differing of 1 single amino acid as showed in the lower table. IPAMVVDR (MSTN) and IPGMVVDR (GDF11) were efficiently resolved thanks to different retention time, unique precursor m/z and fragmentation ions pattern. Figure was adapted from Camparini et al. (in revision).*

5. DISCUSSION

5.1. Recombinant proteins production as a tool to study GDF11 and MSTN biological differences

Until recently GDF11 has been mainly known for its role in embryonic development while its function during adult life has been poorly characterized. In 2013 GDF11 emerged as a circulating factor that declines with aging that reverse cardiac hypertrophy of aged animals (Loffredo et al., 2013; Walker et al., 2016).

This finding has attracted a lot of attention from the scientific community, raising controversies and contradictory results. Part of this conflicting data resides indeed in the homology (>90%) with MSTN. Due to their high similarities, GDF11 and MSTN have been pictured as two ligands with overlapping and distinct functions. This thesis aimed to clarify at least part of these controversies, and to increase the understanding of GDF11 and MSTN role in SMAD3/4 signaling and in regulating cardiac mass *in vivo*.

Our initial data were obtained using conditioned media enriched with GDF11 or MSTN secreted protein. These initials experimentation allowed us to understand the importance of the inactive latent complex in regulating GDF11/MSTN bioactivity and to discover that GDF11 and MSTN prodomains were associated to different mature protein yields. These new findings were directly applied towards the optimization of recombinant protein production and purification. The proteins purified during this step were crucial to perform *in vitro* studies regarding GDF11 and MSTN prodomains or mature forms.

Recombinant GDF11 and MSTN prodomains purification was successfully achieved and their biological activity was tested against respective and opposite ligand. Results were in line with previously published work (Jin et al., 2019; Thies et al., 2001) where both MSTN prodomain and GDF11 were able to inhibit both ligands respectively. However, our data were obtained from a side by side comparison of GDF11 and MSTN prodomains, showing a more potent inhibitory activity of GDF11 prodomain. The biological relevance of this finding is not clear; however, this finding may be important for a better understanding of GDF11 and MSTN differential kinetic and translated in possible therapeutic approaches that require a potent inhibition of both GDF11 and MSTN like in cachexia.

Production and purification of recombinant GDF11/MSTN inactive latent complexes and mature proteins was also proved to be feasible and furtherly confirmed the higher potency

of GDF11 when compared to MSTN. However, unfortunately, because of technical issues, yield was not sufficient to reach the order of milligrams necessary for *in vivo* experimentation. An intense work of protein purification process optimization could have been performed, but in order to overcome these technical limitations and to focus our efforts on *in vivo* studies, investigations were continued using AAV transducing full length GDF11 and MSTN.

This approach had also some advantages compared to daily recombinant protein injections, because GDF11/MSTN mature proteins are immediately active and their activity is not regulated by inactive latent complex formation. Conversely, transduction of full-length proteins lead to secretion of inactive latent complex that reduces GDF11/MSTN ligand activity. Considering the possible deleterious effects of exaggerated GDF11 signaling, in this case, a lower treatment potency could be desired especially because they are easier to modulate. Furthermore, administration of purified mature proteins could lead to different treatment tropism and/or different ligand antagonism from other GDF11/MSTN inhibitors in serum compared to administration of inactive latent complexes.

5.2. Type I TGF-β receptor comparison between cardiac and skeletal muscle tissue showed marked difference in ALK4 and ALK7 receptors

We also performed a series of experiments aiming at understanding signaling in heart and skeletal muscle that could explain differences in the effect of GDF11 and MSTN. An interesting result shows that cardiac tissue is enriched of all ALK4/5/7 receptors when compared to skeletal muscle tissue. This may explain why cardiomyocytes are more sensitive than skeletal myocytes to the effect of GDF11. Our data indicate that ALK7 plays a more relevant role in GDF11 signaling than MSTN in atrial cardiomyocytes, suggesting that part of GDF11 cardiac activity may be secondary to the use of this receptor. We acknowledge that this data was obtained in HL-1 cells, that may not recapitulate perfectly the cardiomyocytes receptors expression ratio. sgRNAs are not able to induce a complete KO of targeted proteins and, given the promiscuity of the pathway, SMAD3/4 signaling could be modulated by secondary pathways differentially active between HL-1 cells and cardiomyocytes.

In order to overcome these limitations, we are performing experiments in 3D cardiac

organoids by selectively silencing ALK4/5/7 receptors. These results will guide our future *in vivo* studies using transgenic mice to induce a cardiac specific KO of these receptors.

5.3. Intramyocardial injection of AAV9 does not induce changes in cardiac mass

An interesting observation came from the attempt to induce a sustained cardiac specific expression of GDF11 and MSTN. Limiting GDF11 activity to cardiac tissue could be beneficial, indeed several studies demonstrated how systemic elevated GDF11 circulating levels are associated to skeletal muscle atrophy and severe body weight loss (Hammers et al., 2017; Harper et al., 2018). Our negative data may be explained by the poor post-translational processing of GDF11 in cardiomyocytes, probably because of insufficient furin activity. Our data limit the possibility of using GDF11 as a cardiac paracrine therapy.

5.4. Systemic supraphysiological GDF11 circulating levels can reduce cardiac mass in healthy mice, but they are associated to dose-dependent reduction of body weight

Our data confirm the results of previous studies indicating that elevated systemic levels of GDF11 induce reduction in heart mass but are associated to significant body weight loss and skeletal muscle atrophy. We also show that by modulating GDF11 levels a reduction in cardiac mass can be achieved with negligible systemic side effects. These data suggest that a more precise knowledge of GDF11 pharmacokinetic is crucial to perform *in vivo* studies and possibly develop a therapeutic approach. Interestingly, no safety concerns emerged from MSTN dose ranging studies revealing a trend in cardiac mass reduction associated to a better therapeutic index.

5.5. GDF11 and MSTN can reduce cardiac mass in TAC mice, but they do not improve diastolic function

Our dose-response studies were crucial in identifying the correct AAV8 titers for GDF11 and MSTN delivery *in vivo* and were propaedeutic to studies using animal models of pathological cardiac hypertrophy, allowing to gain a view on their possible anti-

hypertrophic therapeutic potential. Indeed, in order to treat cardiac hypertrophy, novel treatments are required. Current pharmacological interventions are more focused on symptoms management than act directly on cardiac hypertrophy progression (Marian and Braunwald, 2017). However, cardiac hypertrophy is a heterogenous condition in which augmentation of cardiomyocytes area is only a part of the big picture. Indeed, cardiomyocyte hypertrophy is often accompanied by increased fibrosis and oxidative stress that may lead to ventricular stiffness and impairment of diastolic function. Assessing if GDF11 and MSTN treatments were able to reduce cardiac mass and improve cardiac function were two primary endpoints in order to evaluate their role as a novel therapeutic approach. Our *in vivo* results showed that both GDF11 and MSTN are able to reduce cardiac mass in a dose dependent manner, highlighting an overlap of functions on cardiac tissue that has not been shown before in a side to side study. GDF11 showed higher potency compared to MSTN in reducing cardiac mass, as shown in previous *in vitro* experiments based on SMAD3/4 activation. This observation could suggest that GDF11 and MSTN can exert their effect on cardiac mass through TGF-β signaling modulation, a hypothesis already described in skeletal muscle tissue (Sartori et al., 2009). In order to prove that these findings can be extended to cardiac tissue further experiments are required and are now ongoing. GDF11/MSTN signaling pathways will be investigated in order to identify possible pathway responsible for the anti-hypertrophic effect observed. Subsequently, results will be evaluated *in vitro* using 3D cardiac culture systems, where receptor agonist and chemical inhibitors will be used to furtherly test our hypothesis.

Unfortunately, GDF11/MSTN-dependent cardiac mass reduction in mice subjected to pressure overload was not accompanied by diastolic function improvement. The timing of the experiment limited to 4 weeks, the TAC model where the mechanical obstruction is not removed upon treatment and the lack of long term-survival data are major limitations that require further studies to elucidate the functional effect of GDF11 and MSTN.

A second important limitation for future therapeutic applications is that the dose of GDF11 and MSTN to reduce cardiac mass is still associated to body weight loss and skeletal muscle atrophy, a major concern for elderly people, the population that may benefit more from the anti-hypertrophic effect. This limitation could be overtaken by a better understanding of the pathways that are involved in both cardiomyocyte reversal of hypertrophy and

unwanted systemic side effects. A finer pharmacokinetic regulation by personalizing dose may also limit adverse effects.

5.6. Concluding remarks

In summary, our data indicate that the effect of supraphysiologic levels of GDF11 and MSTN on cardiomyocytes phenotype is similar suggesting that differences that have been observed may be secondary to differential potency of the two proteins. Our *in vitro* data confirm that GDF11 is more potent than MSTN in activating SMAD3/4 in cardiomyocytes and part of this difference can be attributed to differential use of type I TGF-β receptors, in particular Alk7. Our *in vivo* results suggest also that cardiac tissue is more sensitive than skeletal muscle to the effect of both proteins and we speculate that the enrichment of type I TGF-β receptors in the heart may be responsible for this effect. Additional studies aiming at understanding the precise molecular mechanisms of these differences are required and are currently ongoing using engineered heart tissues. Our data also confirmed that both GDF11 and MSTN can reduce body weight in mice in a dose-dependent manner while only GDF11 can induce a cachectic state. Interestingly, both GDF11 and MSTN can prevent pathological cardiac hypertrophy in mice and our data indicate that MSTN presents a safer profile when compared to GDF11. However, both GDF11 and MSTN failed in improving diastolic function in our model of pathological cardiac hypertrophy. Diastolic dysfunction after pressure overload is a multifactorial process and the prevention of cardiac hypertrophy may not be sufficient to restore cardiac function. We acknowledge that further *in vivo* studies using different models and different timing are required to clarify this aspect. Part of the controversies involving GDF11 are also related to the lack of specific assays that can distinguish it from MSTN. Aiming at understanding the role of changes in circulating levels of GDF11 and MSTN during physiologic and pathologic conditions in humans, we have also contributed to develop a novel assay based on mass spectrometry that can measure reliably both proteins. Interestingly, our preliminary data confirm the initial finding indicating an age-dependent decline of GDF11 in mice. In conclusion, GDF11 and MSTN have more overlapping effects on cardiac tissue than anticipated indicating that both proteins must be considered when modulation of their activity, both inhibitory and stimulatory, may be suggested for therapeutic uses.

Bibliography

Administration of Aging (2015). A Profile of Older Americans: 2015. Available online: https://aoaaclgov/Aging_Statistics/Profile/2015/docs/2015-Profilepdf.
Allen, D.L., Cleary, A.S., Speaker, K.J., Lindsay, S.F., Uyenishi, J., Reed, J.M., Madden, M.C., and Mehan, R.S. (2008). Myostatin, activin receptor IIb, and follistatin-like-3 gene expression are altered in adipose tissue and skeletal muscle of obese mice. American journal of physiology Endocrinology and metabolism *294*, E918-927.
Amirouche, A., Durieux, A.C., Banzet, S., Koulmann, N., Bonnefoy, R., Mouret, C., Bigard, X., Peinnequin, A., and Freyssenet, D. (2009). Down-regulation of Akt/mammalian target of rapamycin signaling pathway in response to myostatin overexpression in skeletal muscle. Endocrinology *150*, 286-294.
Amthor, H., Huang, R., McKinnell, I., Christ, B., Kambadur, R., Sharma, M., and Patel, K. (2002). The regulation and action of myostatin as a negative regulator of muscle development during avian embryogenesis. Developmental biology *251*, 241-257.
Amthor, H., Nicholas, G., McKinnell, I., Kemp, C.F., Sharma, M., Kambadur, R., and Patel, K. (2004). Follistatin complexes Myostatin and antagonises Myostatin-mediated inhibition of myogenesis. Developmental biology *270*, 19-30.
Andersson, O., Reissmann, E., and Ibanez, C.F. (2006). Growth differentiation factor 11 signals through the transforming growth factor-beta receptor ALK5 to regionalize the anterior-posterior axis. EMBO reports *7*, 831-837.
Annes, J.P., Munger, J.S., and Rifkin, D.B. (2003). Making sense of latent TGFbeta activation. Journal of cell science *116*, 217-224.
Aurigemma, G.P., Silver, K.H., Priest, M.A., and Gaasch, W.H. (1995). Geometric changes allow normal ejection fraction despite depressed myocardial shortening in hypertensive left ventricular hypertrophy. Journal of the American College of Cardiology *26*, 195-202.
Backs, J., Backs, T., Neef, S., Kreusser, M.M., Lehmann, L.H., Patrick, D.M., Grueter, C.E., Qi, X., Richardson, J.A., Hill, J.A.*, et al.* (2009). The delta isoform of CaM kinase II is required for pathological cardiac hypertrophy and remodeling after pressure overload. Proceedings of the National Academy of Sciences of the United States of America *106*, 2342-2347.
Banerjee, I., Fuseler, J.W., Price, R.L., Borg, T.K., and Baudino, T.A. (2007). Determination of cell types and numbers during cardiac development in the neonatal and adult rat and mouse. American journal of physiology Heart and circulatory physiology *293*, H1883-1891.
Baum, J., and Duffy, H.S. (2011). Fibroblasts and myofibroblasts: what are we talking about? Journal of cardiovascular pharmacology *57*, 376-379.
Becker, C., Lord, S.R., Studenski, S.A., Warden, S.J., Fielding, R.A., Recknor, C.P., Hochberg, M.C., Ferrari, S.L., Blain, H., Binder, E.F.*, et al.* (2015). Myostatin antibody (LY2495655) in older weak fallers: a proof-of-concept, randomised, phase 2 trial. The lancet Diabetes & endocrinology *3*, 948-957.
Bergmann, O., Bhardwaj, R.D., Bernard, S., Zdunek, S., Barnabe-Heider, F., Walsh, S., Zupicich, J., Alkass, K., Buchholz, B.A., Druid, H.*, et al.* (2009). Evidence for cardiomyocyte renewal in humans. Science *324*, 98-102.
Berk, B.C., Fujiwara, K., and Lehoux, S. (2007). ECM remodeling in hypertensive heart disease. The Journal of clinical investigation *117*, 568-575.
Bernardo, B.C., Weeks, K.L., Pretorius, L., and McMullen, J.R. (2010). Molecular distinction between physiological and pathological cardiac hypertrophy: experimental findings and therapeutic strategies. Pharmacology & therapeutics *128*, 191-227.
Beyer, H.M., Gonschorek, P., Samodelov, S.L., Meier, M., Weber, W., and Zurbriggen, M.D. (2015). AQUA Cloning: A Versatile and Simple Enzyme-Free Cloning Approach. PloS one *10*, e0137652.

Biesemann, N., Mendler, L., Kostin, S., Wietelmann, A., Borchardt, T., and Braun, T. (2015). Myostatin induces interstitial fibrosis in the heart via TAK1 and p38. Cell and tissue research *361*, 779-787.
Biesemann, N., Mendler, L., Wietelmann, A., Hermann, S., Schafers, M., Kruger, M., Boettger, T., Borchardt, T., and Braun, T. (2014). Myostatin regulates energy homeostasis in the heart and prevents heart failure. Circulation research *115*, 296-310.
Billet, S., Aguilar, F., Baudry, C., and Clauser, E. (2008). Role of angiotensin II AT1 receptor activation in cardiovascular diseases. Kidney international *74*, 1379-1384.
Billet, S., Bardin, S., Verp, S., Baudrie, V., Michaud, A., Conchon, S., Muffat-Joly, M., Escoubet, B., Souil, E., Hamard, G.*, et al.* (2007). Gain-of-function mutant of angiotensin II receptor, type 1A, causes hypertension and cardiovascular fibrosis in mice. The Journal of clinical investigation *117*, 1914-1925.
Bonnema, D.D., Webb, C.S., Pennington, W.R., Stroud, R.E., Leonardi, A.E., Clark, L.L., McClure, C.D., Finklea, L., Spinale, F.G., and Zile, M.R. (2007). Effects of age on plasma matrix metalloproteinases (MMPs) and tissue inhibitor of metalloproteinases (TIMPs). Journal of cardiac failure *13*, 530-540.
Boonman-de Winter, L.J., Rutten, F.H., Cramer, M.J., Landman, M.J., Liem, A.H., Rutten, G.E., and Hoes, A.W. (2012). High prevalence of previously unknown heart failure and left ventricular dysfunction in patients with type 2 diabetes. Diabetologia *55*, 2154-2162.
Borlaug, B.A., and Paulus, W.J. (2011). Heart failure with preserved ejection fraction: pathophysiology, diagnosis, and treatment. European heart journal *32*, 670-679.
Bortolussi, G., Zentillin, L., Vanikova, J., Bockor, L., Bellarosa, C., Mancarella, A., Vianello, E., Tiribelli, C., Giacca, M., Vitek, L.*, et al.* (2014). Life-long correction of hyperbilirubinemia with a neonatal liver-specific AAV-mediated gene transfer in a lethal mouse model of Crigler-Najjar Syndrome. Human gene therapy *25*, 844-855.
Braz, J.C., Bueno, O.F., Liang, Q., Wilkins, B.J., Dai, Y.S., Parsons, S., Braunwart, J., Glascock, B.J., Klevitsky, R., Kimball, T.F.*, et al.* (2003). Targeted inhibition of p38 MAPK promotes hypertrophic cardiomyopathy through upregulation of calcineurin-NFAT signaling. The Journal of clinical investigation *111*, 1475-1486.
Brown, R.D., Ambler, S.K., Mitchell, M.D., and Long, C.S. (2005). The cardiac fibroblast: therapeutic target in myocardial remodeling and failure. Annual review of pharmacology and toxicology *45*, 657-687.
Bujak, M., Ren, G., Kweon, H.J., Dobaczewski, M., Reddy, A., Taffet, G., Wang, X.F., and Frangogiannis, N.G. (2007). Essential role of Smad3 in infarct healing and in the pathogenesis of cardiac remodeling. Circulation *116*, 2127-2138.
Cain, B.S., Meldrum, D.R., Joo, K.S., Wang, J.F., Meng, X., Cleveland, J.C., Jr., Banerjee, A., and Harken, A.H. (1998). Human SERCA2a levels correlate inversely with age in senescent human myocardium. Journal of the American College of Cardiology *32*, 458-467.
Campbell, C., McMillan, H.J., Mah, J.K., Tarnopolsky, M., Selby, K., McClure, T., Wilson, D.M., Sherman, M.L., Escolar, D., and Attie, K.M. (2017). Myostatin inhibitor ACE-031 treatment of ambulatory boys with Duchenne muscular dystrophy: Results of a randomized, placebo-controlled clinical trial. Muscle & nerve *55*, 458-464.
Carroll, K.J., Makarewich, C.A., McAnally, J., Anderson, D.M., Zentilin, L., Liu, N., Giacca, M., Bassel-Duby, R., and Olson, E.N. (2016). A mouse model for adult cardiac-specific gene deletion with CRISPR/Cas9. Proceedings of the National Academy of Sciences of the United States of America *113*, 338-343.
Cash, J.N., Rejon, C.A., McPherron, A.C., Bernard, D.J., and Thompson, T.B. (2009). The structure of myostatin:follistatin 288: insights into receptor utilization and heparin binding. The EMBO journal *28*, 2662-2676.
Chen, W., and Frangogiannis, N.G. (2010). The role of inflammatory and fibrogenic pathways in heart failure associated with aging. Heart failure reviews *15*, 415-422.

Chen, Y., Guo, Q., Zhang, M., Song, S., Quan, T., Zhao, T., Li, H., Guo, L., Jiang, T., and Wang, G. (2016). Relationship of serum GDF11 levels with bone mineral density and bone turnover markers in postmenopausal Chinese women. Bone research *4*, 16012.
Chung, H.K., Ryu, D., Kim, K.S., Chang, J.Y., Kim, Y.K., Yi, H.S., Kang, S.G., Choi, M.J., Lee, S.E., Jung, S.B.*, et al.* (2017). Growth differentiation factor 15 is a myomitokine governing systemic energy homeostasis. The Journal of cell biology *216*, 149-165.
Cohn, R.D., Liang, H.Y., Shetty, R., Abraham, T., and Wagner, K.R. (2007). Myostatin does not regulate cardiac hypertrophy or fibrosis. Neuromuscular disorders : NMD *17*, 290-296.
Conboy, I.M., Conboy, M.J., Wagers, A.J., Girma, E.R., Weissman, I.L., and Rando, T.A. (2005). Rejuvenation of aged progenitor cells by exposure to a young systemic environment. Nature *433*, 760-764.
Corral-Debrinski, M., Shoffner, J.M., Lott, M.T., and Wallace, D.C. (1992). Association of mitochondrial DNA damage with aging and coronary atherosclerotic heart disease. Mutation research *275*, 169-180.
Cotton, T.R., Fischer, G., Wang, X., McCoy, J.C., Czepnik, M., Thompson, T.B., and Hyvonen, M. (2018). Structure of the human myostatin precursor and determinants of growth factor latency. The EMBO journal *37*, 367-383.
Crabos, M., Roth, M., Hahn, A.W., and Erne, P. (1994). Characterization of angiotensin II receptors in cultured adult rat cardiac fibroblasts. Coupling to signaling systems and gene expression. The Journal of clinical investigation *93*, 2372-2378.
Cucoranu, I., Clempus, R., Dikalova, A., Phelan, P.J., Ariyan, S., Dikalov, S., and Sorescu, D. (2005). NAD(P)H oxidase 4 mediates transforming growth factor-beta1-induced differentiation of cardiac fibroblasts into myofibroblasts. Circulation research *97*, 900-907.
Dai, D.F., Chen, T., Johnson, S.C., Szeto, H., and Rabinovitch, P.S. (2012). Cardiac aging: from molecular mechanisms to significance in human health and disease. Antioxidants & redox signaling *16*, 1492-1526.
Dai, D.F., and Rabinovitch, P.S. (2009). Cardiac aging in mice and humans: the role of mitochondrial oxidative stress. Trends in cardiovascular medicine *19*, 213-220.
Dai, D.F., Santana, L.F., Vermulst, M., Tomazela, D.M., Emond, M.J., MacCoss, M.J., Gollahon, K., Martin, G.M., Loeb, L.A., Ladiges, W.C.*, et al.* (2009). Overexpression of catalase targeted to mitochondria attenuates murine cardiac aging. Circulation *119*, 2789-2797.
deAlmeida, A.C., van Oort, R.J., and Wehrens, X.H. (2010). Transverse aortic constriction in mice. Journal of visualized experiments : JoVE.
DeBosch, B., Sambandam, N., Weinheimer, C., Courtois, M., and Muslin, A.J. (2006a). Akt2 regulates cardiac metabolism and cardiomyocyte survival. The Journal of biological chemistry *281*, 32841-32851.
DeBosch, B., Treskov, I., Lupu, T.S., Weinheimer, C., Kovacs, A., Courtois, M., and Muslin, A.J. (2006b). Akt1 is required for physiological cardiac growth. Circulation *113*, 2097-2104.
Delaughter, M.C., Taffet, G.E., Fiorotto, M.L., Entman, M.L., and Schwartz, R.J. (1999). Local insulin-like growth factor I expression induces physiologic, then pathologic, cardiac hypertrophy in transgenic mice. FASEB journal : official publication of the Federation of American Societies for Experimental Biology *13*, 1923-1929.
Demontis, F., Patel, V.K., Swindell, W.R., and Perrimon, N. (2014). Intertissue control of the nucleolus via a myokine-dependent longevity pathway. Cell reports *7*, 1481-1494.
Dennler, S., Itoh, S., Vivien, D., ten Dijke, P., Huet, S., and Gauthier, J.M. (1998). Direct binding of Smad3 and Smad4 to critical TGF beta-inducible elements in the promoter of human plasminogen activator inhibitor-type 1 gene. The EMBO journal *17*, 3091-3100.
Desmouliere, A., Geinoz, A., Gabbiani, F., and Gabbiani, G. (1993). Transforming growth factor-beta 1 induces alpha-smooth muscle actin expression in granulation tissue myofibroblasts and in quiescent and growing cultured fibroblasts. The Journal of cell biology *122*, 103-111.

Dichmann, D.S., Yassin, H., and Serup, P. (2006). Analysis of pancreatic endocrine development in GDF11-deficient mice. Developmental dynamics : an official publication of the American Association of Anatomists *235*, 3016-3025.
Dirkx, E., da Costa Martins, P.A., and De Windt, L.J. (2013). Regulation of fetal gene expression in heart failure. Biochimica et biophysica acta *1832*, 2414-2424.
Dong, J., Dong, Y., Dong, Y., Chen, F., Mitch, W.E., and Zhang, L. (2016). Inhibition of myostatin in mice improves insulin sensitivity via irisin-mediated cross talk between muscle and adipose tissues. International journal of obesity *40*, 434-442.
Du, X.J., Autelitano, D.J., Dilley, R.J., Wang, B., Dart, A.M., and Woodcock, E.A. (2000). beta(2)-adrenergic receptor overexpression exacerbates development of heart failure after aortic stenosis. Circulation *101*, 71-77.
Duran, J., Troncoso, M.F., Lagos, D., Ramos, S., Marin, G., and Estrada, M. (2018). GDF11 Modulates Ca(2+)-Dependent Smad2/3 Signaling to Prevent Cardiomyocyte Hypertrophy. International journal of molecular sciences *19*.
Dussiot, M., Maciel, T.T., Fricot, A., Chartier, C., Negre, O., Veiga, J., Grapton, D., Paubelle, E., Payen, E., Beuzard, Y.*, et al.* (2014). An activin receptor IIA ligand trap corrects ineffective erythropoiesis in beta-thalassemia. Nature medicine *20*, 398-407.
Egerman, M.A., Cadena, S.M., Gilbert, J.A., Meyer, A., Nelson, H.N., Swalley, S.E., Mallozzi, C., Jacobi, C., Jennings, L.L., Clay, I.*, et al.* (2015). GDF11 Increases with Age and Inhibits Skeletal Muscle Regeneration. Cell metabolism *22*, 164-174.
Eghbali, M., Blumenfeld, O.O., Seifter, S., Buttrick, P.M., Leinwand, L.A., Robinson, T.F., Zern, M.A., and Giambrone, M.A. (1989). Localization of types I, III and IV collagen mRNAs in rat heart cells by in situ hybridization. Journal of molecular and cellular cardiology *21*, 103-113.
Eghbali, M., Wang, Y., Toro, L., and Stefani, E. (2006). Heart hypertrophy during pregnancy: a better functioning heart? Trends in cardiovascular medicine *16*, 285-291.
Engelhardt, S., Hein, L., Wiesmann, F., and Lohse, M.J. (1999). Progressive hypertrophy and heart failure in beta1-adrenergic receptor transgenic mice. Proceedings of the National Academy of Sciences of the United States of America *96*, 7059-7064.
Esquela, A.F., and Lee, S.J. (2003). Regulation of metanephric kidney development by growth/differentiation factor 11. Developmental biology *257*, 356-370.
European Commission (2015). The 2015 Ageing Report: Economic and budgetary projections for the 28 EU Member States (2013-2060). Available online: https://eceuropaeu/eip/ageing/library/2015-ageing-report-economic-and-budgetary-projections-28-eu-member-states-2013-2060_en.
Favier, B., and Dolle, P. (1997). Developmental functions of mammalian Hox genes. Molecular human reproduction *3*, 115-131.
Frey, N., and Olson, E.N. (2003). Cardiac hypertrophy: the good, the bad, and the ugly. Annual review of physiology *65*, 45-79.
Fu, M., Zhou, J., Sun, A., Zhang, S., Zhang, C., Zou, Y., Fu, M., and Ge, J. (2012). Efficacy of ACE inhibitors in chronic heart failure with preserved ejection fraction--a meta analysis of 7 prospective clinical studies. International journal of cardiology *155*, 33-38.
Galiuto, L., Lotrionte, M., Crea, F., Anselmi, A., Biondi-Zoccai, G.G., De Giorgio, F., Baldi, A., Baldi, F., Possati, G., Gaudino, M.*, et al.* (2006). Impaired coronary and myocardial flow in severe aortic stenosis is associated with increased apoptosis: a transthoracic Doppler and myocardial contrast echocardiography study. Heart *92*, 208-212.
Gamer, L.W., Wolfman, N.M., Celeste, A.J., Hattersley, G., Hewick, R., and Rosen, V. (1999). A novel BMP expressed in developing mouse limb, spinal cord, and tail bud is a potent mesoderm inducer in Xenopus embryos. Developmental biology *208*, 222-232.
Gazoti Debessa, C.R., Mesiano Maifrino, L.B., and Rodrigues de Souza, R. (2001). Age related changes of the collagen network of the human heart. Mechanisms of ageing and development *122*, 1049-1058.

Ge, G., Hopkins, D.R., Ho, W.B., and Greenspan, D.S. (2005). GDF11 forms a bone morphogenetic protein 1-activated latent complex that can modulate nerve growth factor-induced differentiation of PC12 cells. Molecular and cellular biology *25*, 5846-5858.
Gentry, L.E., Lioubin, M.N., Purchio, A.F., and Marquardt, H. (1988). Molecular events in the processing of recombinant type 1 pre-pro-transforming growth factor beta to the mature polypeptide. Molecular and cellular biology *8*, 4162-4168.
Gersch, C., Dewald, O., Zoerlein, M., Michael, L.H., Entman, M.L., and Frangogiannis, N.G. (2002). Mast cells and macrophages in normal C57/BL/6 mice. Histochemistry and cell biology *118*, 41-49.
Gerstenblith, G., Frederiksen, J., Yin, F.C., Fortuin, N.J., Lakatta, E.G., and Weisfeldt, M.L. (1977). Echocardiographic assessment of a normal adult aging population. Circulation *56*, 273-278.
Glasser, C.E., Gartner, M.R., Wilson, D., Miller, B., Sherman, M.L., and Attie, K.M. (2018). Locally acting ACE-083 increases muscle volume in healthy volunteers. Muscle & nerve *57*, 921-926.
Gleizes, P.E., Munger, J.S., Nunes, I., Harpel, J.G., Mazzieri, R., Noguera, I., and Rifkin, D.B. (1997). TGF-beta latency: biological significance and mechanisms of activation. Stem cells *15*, 190-197.
Goffart, S., von Kleist-Retzow, J.C., and Wiesner, R.J. (2004). Regulation of mitochondrial proliferation in the heart: power-plant failure contributes to cardiac failure in hypertrophy. Cardiovascular research *64*, 198-207.
Golan, T., Geva, R., Richards, D., Madhusudan, S., Lin, B.K., Wang, H.T., Walgren, R.A., and Stemmer, S.M. (2018). LY2495655, an antimyostatin antibody, in pancreatic cancer: a randomized, phase 2 trial. Journal of cachexia, sarcopenia and muscle *9*, 871-879.
Golde, W.T., Gollobin, P., and Rodriguez, L.L. (2005). A rapid, simple, and humane method for submandibular bleeding of mice using a lancet. Lab animal *34*, 39-43.
Gottdiener, J.S., Bartz, T., DeFilippi, C., Kop, W., and Lloyd-Jones, D. (2012). Clinical and demographic characteristics of heart failure with preserved ejection fraction in comparison to hypertension without heart failure, elderly with risk factors, and healthy aging in population dwelling individuals <= 65 years of age. Journal of the American College of Cardiology *59*.
Gray, A.M., and Mason, A.J. (1990). Requirement for activin A and transforming growth factor--beta 1 pro-regions in homodimer assembly. Science *247*, 1328-1330.
Gu, H., Cao, Y., Qiu, B., Zhou, Z., Deng, R., Chen, Z., Li, R., Li, X., Wei, Q., Xia, X.*, et al.* (2016). Establishment and phenotypic analysis of an Mstn knockout rat. Biochemical and biophysical research communications *477*, 115-122.
Guerra, A., Oikonomidou, P.R., Sinha, S., Zhang, J., Lo Presti, V., Hamilton, C.R., Breda, L., Casu, C., La, P., Martins, A.C.*, et al.* (2019). Lack of Gdf11 does not improve anemia or prevent the activity of RAP-536 in a mouse model of beta-thalassemia. Blood *134*, 568-572.
Guo, T., Bond, N.D., Jou, W., Gavrilova, O., Portas, J., and McPherron, A.C. (2012). Myostatin inhibition prevents diabetes and hyperphagia in a mouse model of lipodystrophy. Diabetes *61*, 2414-2423.
Guo, T., Jou, W., Chanturiya, T., Portas, J., Gavrilova, O., and McPherron, A.C. (2009). Myostatin inhibition in muscle, but not adipose tissue, decreases fat mass and improves insulin sensitivity. PloS one *4*, e4937.
Hammers, D.W., Merscham-Banda, M., Hsiao, J.Y., Engst, S., Hartman, J.J., and Sweeney, H.L. (2017). Supraphysiological levels of GDF11 induce striated muscle atrophy. EMBO molecular medicine *9*, 531-544.
Hanna, M.G., Badrising, U.A., Benveniste, O., Lloyd, T.E., Needham, M., Chinoy, H., Aoki, M., Machado, P.M., Liang, C., Reardon, K.A.*, et al.* (2019). Safety and efficacy of intravenous bimagrumab in inclusion body myositis (RESILIENT): a randomised, double-blind, placebo-controlled phase 2b trial. The Lancet Neurology *18*, 834-844.
Hansson, J., Lind, L., Hulthe, J., and Sundstrom, J. (2009). Relations of serum MMP-9 and TIMP-1 levels to left ventricular measures and cardiovascular risk factors: a population-based study. European journal of cardiovascular prevention and rehabilitation : official journal of the European Society of Cardiology, Working Groups on Epidemiology & Prevention and Cardiac Rehabilitation and Exercise Physiology *16*, 297-303.

Harman, D. (1991). The aging process: major risk factor for disease and death. Proceedings of the National Academy of Sciences of the United States of America *88*, 5360-5363.
Harmon, E.B., Apelqvist, A.A., Smart, N.G., Gu, X., Osborne, D.H., and Kim, S.K. (2004). GDF11 modulates NGN3+ islet progenitor cell number and promotes beta-cell differentiation in pancreas development. Development *131*, 6163-6174.
Harper, S. (2014). Economic and social implications of aging societies. Science *346*, 587-591.
Harper, S.C., Brack, A., MacDonnell, S., Franti, M., Olwin, B.B., Bailey, B.A., Rudnicki, M.A., and Houser, S.R. (2016). Is Growth Differentiation Factor 11 a Realistic Therapeutic for Aging-Dependent Muscle Defects? Circulation research *118*, 1143-1150; discussion 1150.
Harper, S.C., Johnson, J., Borghetti, G., Zhao, H., Wang, T., Wallner, M., Kubo, H., Feldsott, E.A., Yang, Y., Joo, Y.*, et al.* (2018). GDF11 Decreases Pressure Overload-Induced Hypertrophy, but Can Cause Severe Cachexia and Premature Death. Circulation research *123*, 1220-1231.
Harrison, C.A., Al-Musawi, S.L., and Walton, K.L. (2011). Prodomains regulate the synthesis, extracellular localisation and activity of TGF-beta superfamily ligands. Growth factors *29*, 174-186.
Hartley, C.J., Reddy, A.K., Madala, S., Michael, L.H., Entman, M.L., and Taffet, G.E. (2008). Doppler estimation of reduced coronary flow reserve in mice with pressure overload cardiac hypertrophy. Ultrasound in medicine & biology *34*, 892-901.
Hebert, L.E., Weuve, J., Scherr, P.A., and Evans, D.A. (2013). Alzheimer disease in the United States (2010-2050) estimated using the 2010 census. Neurology *80*, 1778-1783.
Hees, P.S., Fleg, J.L., Lakatta, E.G., and Shapiro, E.P. (2002). Left ventricular remodeling with age in normal men versus women: novel insights using three-dimensional magnetic resonance imaging. The American journal of cardiology *90*, 1231-1236.
Heidenreich, P.A., Trogdon, J.G., Khavjou, O.A., Butler, J., Dracup, K., Ezekowitz, M.D., Finkelstein, E.A., Hong, Y., Johnston, S.C., Khera, A.*, et al.* (2011). Forecasting the future of cardiovascular disease in the United States: a policy statement from the American Heart Association. Circulation *123*, 933-944.
Heineke, J., Auger-Messier, M., Xu, J., Sargent, M., York, A., Welle, S., and Molkentin, J.D. (2010). Genetic deletion of myostatin from the heart prevents skeletal muscle atrophy in heart failure. Circulation *121*, 419-425.
Heineke, J., and Molkentin, J.D. (2006). Regulation of cardiac hypertrophy by intracellular signalling pathways. Nature reviews Molecular cell biology *7*, 589-600.
Helmes, M., Trombitas, K., Centner, T., Kellermayer, M., Labeit, S., Linke, W.A., and Granzier, H. (1999). Mechanically driven contour-length adjustment in rat cardiac titin's unique N2B sequence: titin is an adjustable spring. Circulation research *84*, 1339-1352.
Hennebry, A., Berry, C., Siriett, V., O'Callaghan, P., Chau, L., Watson, T., Sharma, M., and Kambadur, R. (2009). Myostatin regulates fiber-type composition of skeletal muscle by regulating MEF2 and MyoD gene expression. American journal of physiology Cell physiology *296*, C525-534.
Henry, B.A., and Clarke, I.J. (2008). Adipose tissue hormones and the regulation of food intake. Journal of neuroendocrinology *20*, 842-849.
Hill, J.J., Davies, M.V., Pearson, A.A., Wang, J.H., Hewick, R.M., Wolfman, N.M., and Qiu, Y. (2002). The myostatin propeptide and the follistatin-related gene are inhibitory binding proteins of myostatin in normal serum. The Journal of biological chemistry *277*, 40735-40741.
Hill, J.J., Qiu, Y., Hewick, R.M., and Wolfman, N.M. (2003). Regulation of myostatin in vivo by growth and differentiation factor-associated serum protein-1: a novel protein with protease inhibitor and follistatin domains. Molecular endocrinology *17*, 1144-1154.
Hittel, D.S., Berggren, J.R., Shearer, J., Boyle, K., and Houmard, J.A. (2009). Increased secretion and expression of myostatin in skeletal muscle from extremely obese women. Diabetes *58*, 30-38.
Huang, Z., Chen, D., Zhang, K., Yu, B., Chen, X., and Meng, J. (2007). Regulation of myostatin signaling by c-Jun N-terminal kinase in C2C12 cells. Cellular signalling *19*, 2286-2295.
Ichikawa, K.I., Hidai, C., Okuda, C., Kimata, S.I., Matsuoka, R., Hosoda, S., Quertermous, T., and Kawana, M. (1996). Endogenous endothelin-1 mediates cardiac hypertrophy and switching of

myosin heavy chain gene expression in rat ventricular myocardium. Journal of the American College of Cardiology *27*, 1286-1291.
Ignotz, R.A., and Massague, J. (1986). Transforming growth factor-beta stimulates the expression of fibronectin and collagen and their incorporation into the extracellular matrix. The Journal of biological chemistry *261*, 4337-4345.
Iozzo, R.V. (1999). The biology of the small leucine-rich proteoglycans. Functional network of interactive proteins. The Journal of biological chemistry *274*, 18843-18846.
Isenberg, G., Borschke, B., and Rueckschloss, U. (2003). Ca2+ transients of cardiomyocytes from senescent mice peak late and decay slowly. Cell calcium *34*, 271-280.
Janczewski, A.M., and Lakatta, E.G. (2010). Modulation of sarcoplasmic reticulum Ca(2+) cycling in systolic and diastolic heart failure associated with aging. Heart failure reviews *15*, 431-445.
Jiang, M.S., Liang, L.F., Wang, S., Ratovitski, T., Holmstrom, J., Barker, C., and Stotish, R. (2004). Characterization and identification of the inhibitory domain of GDF-8 propeptide. Biochemical and biophysical research communications *315*, 525-531.
Jiang, M.T., Moffat, M.P., and Narayanan, N. (1993). Age-related alterations in the phosphorylation of sarcoplasmic reticulum and myofibrillar proteins and diminished contractile response to isoproterenol in intact rat ventricle. Circulation research *72*, 102-111.
Jin, Q., Qiao, C., Li, J., Xiao, B., Li, J., and Xiao, X. (2019). A GDF11/myostatin inhibitor, GDF11 propeptide-Fc, increases skeletal muscle mass and improves muscle strength in dystrophic mdx mice. Skeletal muscle *9*, 16.
Jones, J.E., Cadena, S.M., Gong, C., Wang, X., Chen, Z., Wang, S.X., Vickers, C., Chen, H., Lach-Trifilieff, E., Hadcock, J.R.*, et al.* (2018). Supraphysiologic Administration of GDF11 Induces Cachexia in Part by Upregulating GDF15. Cell reports *22*, 3375.
Jordan, M., Schallhorn, A., and Wurm, F.M. (1996). Transfecting mammalian cells: optimization of critical parameters affecting calcium-phosphate precipitate formation. Nucleic acids research *24*, 596-601.
Judge, S., Jang, Y.M., Smith, A., Hagen, T., and Leeuwenburgh, C. (2005). Age-associated increases in oxidative stress and antioxidant enzyme activities in cardiac interfibrillar mitochondria: implications for the mitochondrial theory of aging. FASEB journal : official publication of the Federation of American Societies for Experimental Biology *19*, 419-421.
Katsimpardi, L., Litterman, N.K., Schein, P.A., Miller, C.M., Loffredo, F.S., Wojtkiewicz, G.R., Chen, J.W., Lee, R.T., Wagers, A.J., and Rubin, L.L. (2014). Vascular and neurogenic rejuvenation of the aging mouse brain by young systemic factors. Science *344*, 630-634.
Kehat, I., Davis, J., Tiburcy, M., Accornero, F., Saba-El-Leil, M.K., Maillet, M., York, A.J., Lorenz, J.N., Zimmermann, W.H., Meloche, S.*, et al.* (2011). Extracellular signal-regulated kinases 1 and 2 regulate the balance between eccentric and concentric cardiac growth. Circulation research *108*, 176-183.
Kempf, T., Eden, M., Strelau, J., Naguib, M., Willenbockel, C., Tongers, J., Heineke, J., Kotlarz, D., Xu, J., Molkentin, J.D.*, et al.* (2006). The transforming growth factor-beta superfamily member growth-differentiation factor-15 protects the heart from ischemia/reperfusion injury. Circulation research *98*, 351-360.
Kim, J., Wende, A.R., Sena, S., Theobald, H.A., Soto, J., Sloan, C., Wayment, B.E., Litwin, S.E., Holzenberger, M., LeRoith, D.*, et al.* (2008). Insulin-like growth factor I receptor signaling is required for exercise-induced cardiac hypertrophy. Molecular endocrinology *22*, 2531-2543.
Kim, J., Wu, H.H., Lander, A.D., Lyons, K.M., Matzuk, M.M., and Calof, A.L. (2005). GDF11 controls the timing of progenitor cell competence in developing retina. Science *308*, 1927-1930.
Kimple, M.E., Brill, A.L., and Pasker, R.L. (2013). Overview of affinity tags for protein purification. Current protocols in protein science *73*, Unit 9 9.
Kimura, T.E., Jin, J., Zi, M., Prehar, S., Liu, W., Oceandy, D., Abe, J., Neyses, L., Weston, A.H., Cartwright, E.J.*, et al.* (2010). Targeted deletion of the extracellular signal-regulated protein kinase 5 attenuates hypertrophic response and promotes pressure overload-induced apoptosis in the heart. Circulation research *106*, 961-970.

Kiriazis, H., Wang, K., Xu, Q., Gao, X.M., Ming, Z., Su, Y., Moore, X.L., Lambert, G., Gibbs, M.E., Dart, A.M.*, et al.* (2008). Knockout of beta(1)- and beta(2)-adrenoceptors attenuates pressure overload-induced cardiac hypertrophy and fibrosis. British journal of pharmacology *153*, 684-692.
Komrokji, R., Garcia-Manero, G., Ades, L., Prebet, T., Steensma, D.P., Jurcic, J.G., Sekeres, M.A., Berdeja, J., Savona, M.R., Beyne-Rauzy, O.*, et al.* (2018). Sotatercept with long-term extension for the treatment of anaemia in patients with lower-risk myelodysplastic syndromes: a phase 2, dose-ranging trial. The Lancet Haematology *5*, e63-e72.
Kondas, K., Szlama, G., Trexler, M., and Patthy, L. (2008). Both WFIKKN1 and WFIKKN2 have high affinity for growth and differentiation factors 8 and 11. The Journal of biological chemistry *283*, 23677-23684.
Kong, P., Christia, P., and Frangogiannis, N.G. (2014). The pathogenesis of cardiac fibrosis. Cellular and molecular life sciences : CMLS *71*, 549-574.
Kowal, S.L., Dall, T.M., Chakrabarti, R., Storm, M.V., and Jain, A. (2013). The current and projected economic burden of Parkinson's disease in the United States. Movement disorders : official journal of the Movement Disorder Society *28*, 311-318.
Kramer, M.G., Barajas, M., Razquin, N., Berraondo, P., Rodrigo, M., Wu, C., Qian, C., Fortes, P., and Prieto, J. (2003). In vitro and in vivo comparative study of chimeric liver-specific promoters. Molecular therapy : the journal of the American Society of Gene Therapy *7*, 375-385.
Lakatta, E.G., and Levy, D. (2003). Arterial and cardiac aging: major shareholders in cardiovascular disease enterprises: Part II: the aging heart in health: links to heart disease. Circulation *107*, 346-354.
Lam, C.S., Roger, V.L., Rodeheffer, R.J., Bursi, F., Borlaug, B.A., Ommen, S.R., Kass, D.A., and Redfield, M.M. (2007). Cardiac structure and ventricular-vascular function in persons with heart failure and preserved ejection fraction from Olmsted County, Minnesota. Circulation *115*, 1982-1990.
Latres, E., Pangilinan, J., Miloscio, L., Bauerlein, R., Na, E., Potocky, T.B., Huang, Y., Eckersdorff, M., Rafique, A., Mastaitis, J.*, et al.* (2015). Myostatin blockade with a fully human monoclonal antibody induces muscle hypertrophy and reverses muscle atrophy in young and aged mice. Skeletal muscle *5*, 34.
Le, V.Q., Iacob, R.E., Tian, Y., McConaughy, W., Jackson, J., Su, Y., Zhao, B., Engen, J.R., Pirruccello-Straub, M., and Springer, T.A. (2018). Tolloid cleavage activates latent GDF8 by priming the pro-complex for dissociation. The EMBO journal *37*, 384-397.
Leask, A. (2015). Getting to the heart of the matter: new insights into cardiac fibrosis. Circulation research *116*, 1269-1276.
Lee, S.J. (2010). Extracellular Regulation of Myostatin: A Molecular Rheostat for Muscle Mass. Immunology, endocrine & metabolic agents in medicinal chemistry *10*, 183-194.
Lee, S.J., and McPherron, A.C. (2001). Regulation of myostatin activity and muscle growth. Proceedings of the National Academy of Sciences of the United States of America *98*, 9306-9311.
Lee, Y.S., and Lee, S.J. (2013). Regulation of GDF-11 and myostatin activity by GASP-1 and GASP-2. Proceedings of the National Academy of Sciences of the United States of America *110*, E3713-3722.
Lerch, T.F., Shimasaki, S., Woodruff, T.K., and Jardetzky, T.S. (2007). Structural and biophysical coupling of heparin and activin binding to follistatin isoform functions. The Journal of biological chemistry *282*, 15930-15939.
Lessard, S.J., MacDonald, T.L., Pathak, P., Han, M.S., Coffey, V.G., Edge, J., Rivas, D.A., Hirshman, M.F., Davis, R.J., and Goodyear, L.J. (2018). JNK regulates muscle remodeling via myostatin/SMAD inhibition. Nature communications *9*, 3030.
Levy, D., Kenchaiah, S., Larson, M.G., Benjamin, E.J., Kupka, M.J., Ho, K.K., Murabito, J.M., and Vasan, R.S. (2002). Long-term trends in the incidence of and survival with heart failure. The New England journal of medicine *347*, 1397-1402.
LeWinter, M.M., and Granzier, H. (2010). Cardiac titin: a multifunctional giant. Circulation *121*, 2137-2145.

LeWinter, M.M., Wu, Y., Labeit, S., and Granzier, H. (2007). Cardiac titin: structure, functions and role in disease. Clinica chimica acta; international journal of clinical chemistry *375*, 1-9.
Li, L., Chen, Y., Li, J., Yin, H., Guo, X., Doan, J., Molkentin, J.D., and Liu, Q. (2015). TAK1 Regulates Myocardial Response to Pathological Stress via NFAT, NFkappaB, and Bnip3 Pathways. Scientific reports *5*, 16626.
Liang, Q., Bueno, O.F., Wilkins, B.J., Kuan, C.Y., Xia, Y., and Molkentin, J.D. (2003). c-Jun N-terminal kinases (JNK) antagonize cardiac growth through cross-talk with calcineurin-NFAT signaling. The EMBO journal *22*, 5079-5089.
Liao, P., Georgakopoulos, D., Kovacs, A., Zheng, M., Lerner, D., Pu, H., Saffitz, J., Chien, K., Xiao, R.P., Kass, D.A*., et al.* (2001). The in vivo role of p38 MAP kinases in cardiac remodeling and restrictive cardiomyopathy. Proceedings of the National Academy of Sciences of the United States of America *98*, 12283-12288.
Lim, C.C., Liao, R., Varma, N., and Apstein, C.S. (1999). Impaired lusitropy-frequency in the aging mouse: role of Ca(2+)-handling proteins and effects of isoproterenol. The American journal of physiology *277*, H2083-2090.
Liu, J.P. (2006). The function of growth/differentiation factor 11 (Gdf11) in rostrocaudal patterning of the developing spinal cord. Development *133*, 2865-2874.
Liu, Z., Chen, O., Wall, J.B.J., Zheng, M., Zhou, Y., Wang, L., Ruth Vaseghi, H., Qian, L., and Liu, J. (2017). Systematic comparison of 2A peptides for cloning multi-genes in a polycistronic vector. Scientific reports *7*, 2193.
Loffredo, F.S., Nikolova, A.P., Pancoast, J.R., and Lee, R.T. (2014). Heart failure with preserved ejection fraction: molecular pathways of the aging myocardium. Circulation research *115*, 97-107.
Loffredo, F.S., Steinhauser, M.L., Jay, S.M., Gannon, J., Pancoast, J.R., Yalamanchi, P., Sinha, M., Dall'Osso, C., Khong, D., Shadrach, J.L*., et al.* (2013). Growth differentiation factor 11 is a circulating factor that reverses age-related cardiac hypertrophy. Cell *153*, 828-839.
Lu, P., Takai, K., Weaver, V.M., and Werb, Z. (2011). Extracellular matrix degradation and remodeling in development and disease. Cold Spring Harbor perspectives in biology *3*.
Ludwig, F.C., and Elashoff, R.M. (1972). Mortality in syngeneic rat parabionts of different chronological age. Transactions of the New York Academy of Sciences *34*, 582-587.
Lunsford, W.R., Mc, C.C., Lupien, P.J., Pope, F.E., and Sperling, G. (1963). Parabiosis as a method for studying factors which affect aging in rats. Gerontologia *7*, 1-8.
MacLennan, D.H., and Kranias, E.G. (2003). Phospholamban: a crucial regulator of cardiac contractility. Nature reviews Molecular cell biology *4*, 566-577.
Makanji, Y., Harrison, C.A., Stanton, P.G., Krishna, R., and Robertson, D.M. (2007). Inhibin A and B in vitro bioactivities are modified by their degree of glycosylation and their affinities to betaglycan. Endocrinology *148*, 2309-2316.
Makanji, Y., Walton, K.L., Wilce, M.C., Chan, K.L., Robertson, D.M., and Harrison, C.A. (2008). Suppression of inhibin A biological activity by alterations in the binding site for betaglycan. The Journal of biological chemistry *283*, 16743-16751.
Mallat, Z., Fornes, P., Costagliola, R., Esposito, B., Belmin, J., Lecomte, D., and Tedgui, A. (2001). Age and gender effects on cardiomyocyte apoptosis in the normal human heart. The journals of gerontology Series A, Biological sciences and medical sciences *56*, M719-723.
Marian, A.J., and Braunwald, E. (2017). Hypertrophic Cardiomyopathy: Genetics, Pathogenesis, Clinical Manifestations, Diagnosis, and Therapy. Circulation research *121*, 749-770.
Maron, B.J., and Pelliccia, A. (2006). The heart of trained athletes: cardiac remodeling and the risks of sports, including sudden death. Circulation *114*, 1633-1644.
Massague, J. (2012). TGFbeta signalling in context. Nature reviews Molecular cell biology *13*, 616-630.
Matsuda, T., Zhai, P., Maejima, Y., Hong, C., Gao, S., Tian, B., Goto, K., Takagi, H., Tamamori-Adachi, M., Kitajima, S*., et al.* (2008). Distinct roles of GSK-3alpha and GSK-3beta phosphorylation in the heart under pressure overload. Proceedings of the National Academy of Sciences of the United States of America *105*, 20900-20905.

Mayer, U., Nischt, R., Poschl, E., Mann, K., Fukuda, K., Gerl, M., Yamada, Y., and Timpl, R. (1993). A single EGF-like motif of laminin is responsible for high affinity nidogen binding. The EMBO journal *12*, 1879-1885.
McCay, C.M., Pope, F., Lunsford, W., Sperling, G., and Sambhavaphol, P. (1957). Parabiosis between old and young rats. Gerontologia *1*, 7-17.
McDonagh, T.A., Morrison, C.E., Lawrence, A., Ford, I., Tunstall-Pedoe, H., McMurray, J.J., and Dargie, H.J. (1997). Symptomatic and asymptomatic left-ventricular systolic dysfunction in an urban population. Lancet *350*, 829-833.
McFarlane, C., Langley, B., Thomas, M., Hennebry, A., Plummer, E., Nicholas, G., McMahon, C., Sharma, M., and Kambadur, R. (2005). Proteolytic processing of myostatin is auto-regulated during myogenesis. Developmental biology *283*, 58-69.
McGivney, B.A., Browne, J.A., Fonseca, R.G., Katz, L.M., Machugh, D.E., Whiston, R., and Hill, E.W. (2012). MSTN genotypes in Thoroughbred horses influence skeletal muscle gene expression and racetrack performance. Animal genetics *43*, 810-812.
McMullen, J.R., Shioi, T., Huang, W.Y., Zhang, L., Tarnavski, O., Bisping, E., Schinke, M., Kong, S., Sherwood, M.C., Brown, J.*, et al.* (2004). The insulin-like growth factor 1 receptor induces physiological heart growth via the phosphoinositide 3-kinase(p110alpha) pathway. The Journal of biological chemistry *279*, 4782-4793.
McMullen, J.R., Shioi, T., Zhang, L., Tarnavski, O., Sherwood, M.C., Kang, P.M., and Izumo, S. (2003). Phosphoinositide 3-kinase(p110alpha) plays a critical role for the induction of physiological, but not pathological, cardiac hypertrophy. Proceedings of the National Academy of Sciences of the United States of America *100*, 12355-12360.
McMurray, J.J.V., Solomon, S.D., Inzucchi, S.E., Kober, L., Kosiborod, M.N., Martinez, F.A., Ponikowski, P., Sabatine, M.S., Anand, I.S., Belohlavek, J.*, et al.* (2019). Dapagliflozin in Patients with Heart Failure and Reduced Ejection Fraction. The New England journal of medicine.
McPherron, A.C. (2013). Through thick and thin: a circulating growth factor inhibits age-related cardiac hypertrophy. Circulation research *113*, 487-491.
McPherron, A.C., Huynh, T.V., and Lee, S.J. (2009). Redundancy of myostatin and growth/differentiation factor 11 function. BMC developmental biology *9*, 24.
McPherron, A.C., Lawler, A.M., and Lee, S.J. (1997). Regulation of skeletal muscle mass in mice by a new TGF-beta superfamily member. Nature *387*, 83-90.
McPherron, A.C., Lawler, A.M., and Lee, S.J. (1999). Regulation of anterior/posterior patterning of the axial skeleton by growth/differentiation factor 11. Nature genetics *22*, 260-264.
McPherron, A.C., and Lee, S.J. (1997). Double muscling in cattle due to mutations in the myostatin gene. Proceedings of the National Academy of Sciences of the United States of America *94*, 12457-12461.
McPherron, A.C., and Lee, S.J. (2002). Suppression of body fat accumulation in myostatin-deficient mice. The Journal of clinical investigation *109*, 595-601.
Mehta, P.A., Dubrey, S.W., McIntyre, H.F., Walker, D.M., Hardman, S.M., Sutton, G.C., McDonagh, T.A., and Cowie, M.R. (2009). Improving survival in the 6 months after diagnosis of heart failure in the past decade: population-based data from the UK. Heart *95*, 1851-1856.
Mei, W., Xiang, G., Li, Y., Li, H., Xiang, L., Lu, J., Xiang, L., Dong, J., and Liu, M. (2016). GDF11 Protects against Endothelial Injury and Reduces Atherosclerotic Lesion Formation in Apolipoprotein E-Null Mice. Molecular therapy : the journal of the American Society of Gene Therapy *24*, 1926-1938.
Melenovsky, V., Borlaug, B.A., Rosen, B., Hay, I., Ferruci, L., Morell, C.H., Lakatta, E.G., Najjar, S.S., and Kass, D.A. (2007). Cardiovascular features of heart failure with preserved ejection fraction versus nonfailing hypertensive left ventricular hypertrophy in the urban Baltimore community: the role of atrial remodeling/dysfunction. Journal of the American College of Cardiology *49*, 198-207.
Mitnitski, A.B., Mogilner, A.J., and Rockwood, K. (2001). Accumulation of deficits as a proxy measure of aging. TheScientificWorldJournal *1*, 323-336.

Miura, T., Kishioka, Y., Wakamatsu, J., Hattori, A., Hennebry, A., Berry, C.J., Sharma, M., Kambadur, R., and Nishimura, T. (2006). Decorin binds myostatin and modulates its activity to muscle cells. Biochemical and biophysical research communications *340*, 675-680.
Molkentin, J.D., Lu, J.R., Antos, C.L., Markham, B., Richardson, J., Robbins, J., Grant, S.R., and Olson, E.N. (1998). A calcineurin-dependent transcriptional pathway for cardiac hypertrophy. Cell *93*, 215-228.
Mosher, D.S., Quignon, P., Bustamante, C.D., Sutter, N.B., Mellersh, C.S., Parker, H.G., and Ostrander, E.A. (2007). A mutation in the myostatin gene increases muscle mass and enhances racing performance in heterozygote dogs. PLoS genetics *3*, e79.
Nag, A.C. (1980). Study of non-muscle cells of the adult mammalian heart: a fine structural analysis and distribution. Cytobios *28*, 41-61.
National Heart Lung and Blood Institute (2012). 2012 NHLBI Morbidity and Mortality Chart Book. Available online: https://wwwnhlbinihgov/research/reports/2012-mortality-chart-book.
Nicol, R.L., Frey, N., Pearson, G., Cobb, M., Richardson, J., and Olson, E.N. (2001). Activated MEK5 induces serial assembly of sarcomeres and eccentric cardiac hypertrophy. The EMBO journal *20*, 2757-2767.
Noh, J., Wende, A.R., Olsen, C.D., Kim, B., Bevins, J., Zhu, Y., Zhang, Q.J., Riehle, C., and Abel, E.D. (2015). Phosphoinositide dependent protein kinase 1 is required for exercise-induced cardiac hypertrophy but not the associated mitochondrial adaptations. Journal of molecular and cellular cardiology *89*, 297-305.
Nonnenmacher, M., and Weber, T. (2012). Intracellular transport of recombinant adeno-associated virus vectors. Gene therapy *19*, 649-658.
North, B.J., and Sinclair, D.A. (2012). The intersection between aging and cardiovascular disease. Circulation research *110*, 1097-1108.
O'Connell, K.E., Guo, W., Serra, C., Beck, M., Wachtman, L., Hoggatt, A., Xia, D., Pearson, C., Knight, H., O'Connell, M.*, et al.* (2015). The effects of an ActRIIb receptor Fc fusion protein ligand trap in juvenile simian immunodeficiency virus-infected rhesus macaques. FASEB journal : official publication of the Federation of American Societies for Experimental Biology *29*, 1165-1175.
Oh, J., Lee, Y.D., and Wagers, A.J. (2014). Stem cell aging: mechanisms, regulators and therapeutic opportunities. Nature medicine *20*, 870-880.
Okura, H., Takada, Y., Yamabe, A., Kubo, T., Asawa, K., Ozaki, T., Yamagishi, H., Toda, I., Yoshiyama, M., Yoshikawa, J.*, et al.* (2009). Age- and gender-specific changes in the left ventricular relaxation: a Doppler echocardiographic study in healthy individuals. Circulation Cardiovascular imaging *2*, 41-46.
Olivetti, G., Giordano, G., Corradi, D., Melissari, M., Lagrasta, C., Gambert, S.R., and Anversa, P. (1995). Gender differences and aging: effects on the human heart. Journal of the American College of Cardiology *26*, 1068-1079.
Olson, K.A., Beatty, A.L., Heidecker, B., Regan, M.C., Brody, E.N., Foreman, T., Kato, S., Mehler, R.E., Singer, B.S., Hveem, K.*, et al.* (2015). Association of growth differentiation factor 11/8, putative anti-ageing factor, with cardiovascular outcomes and overall mortality in humans: analysis of the Heart and Soul and HUNT3 cohorts. European heart journal *36*, 3426-3434.
Oudit, G.Y., and Kassiri, Z. (2007). Role of PI3 kinase gamma in excitation-contraction coupling and heart disease. Cardiovascular & hematological disorders drug targets *7*, 295-304.
Pacher, P., Nagayama, T., Mukhopadhyay, P., Batkai, S., and Kass, D.A. (2008). Measurement of cardiac function using pressure-volume conductance catheter technique in mice and rats. Nature protocols *3*, 1422-1434.
Palermo, D.P., DeGraaf, M.E., Marotti, K.R., Rehberg, E., and Post, L.E. (1991). Production of analytical quantities of recombinant proteins in Chinese hamster ovary cells using sodium butyrate to elevate gene expression. Journal of biotechnology *19*, 35-47.
Parasuraman, S., Raveendran, R., and Kesavan, R. (2010). Blood sample collection in small laboratory animals. Journal of pharmacology & pharmacotherapeutics *1*, 87-93.

Pathak, A., del Monte, F., Zhao, W., Schultz, J.E., Lorenz, J.N., Bodi, I., Weiser, D., Hahn, H., Carr, A.N., Syed, F.*, et al.* (2005). Enhancement of cardiac function and suppression of heart failure progression by inhibition of protein phosphatase 1. Circulation research *96*, 756-766.
Pedersen, B.K., and Febbraio, M.A. (2012). Muscles, exercise and obesity: skeletal muscle as a secretory organ. Nature reviews Endocrinology *8*, 457-465.
Perrino, C., Naga Prasad, S.V., Mao, L., Noma, T., Yan, Z., Kim, H.S., Smithies, O., and Rockman, H.A. (2006). Intermittent pressure overload triggers hypertrophy-independent cardiac dysfunction and vascular rarefaction. The Journal of clinical investigation *116*, 1547-1560.
Piacentino, V., 3rd, Weber, C.R., Chen, X., Weisser-Thomas, J., Margulies, K.B., Bers, D.M., and Houser, S.R. (2003). Cellular basis of abnormal calcium transients of failing human ventricular myocytes. Circulation research *92*, 651-658.
Piga, A., Perrotta, S., Gamberini, M.R., Voskaridou, E., Melpignano, A., Filosa, A., Caruso, V., Pietrangelo, A., Longo, F., Tartaglione, I.*, et al.* (2019). Luspatercept improves hemoglobin levels and blood transfusion requirements in a study of patients with beta-thalassemia. Blood *133*, 1279-1289.
Pirruccello-Straub, M., Jackson, J., Wawersik, S., Webster, M.T., Salta, L., Long, K., McConaughy, W., Capili, A., Boston, C., Carven, G.J.*, et al.* (2018). Blocking extracellular activation of myostatin as a strategy for treating muscle wasting. Scientific reports *8*, 2292.
Poggioli, T., Vujic, A., Yang, P., Macias-Trevino, C., Uygur, A., Loffredo, F.S., Pancoast, J.R., Cho, M., Goldstein, J., Tandias, R.M.*, et al.* (2016). Circulating Growth Differentiation Factor 11/8 Levels Decline With Age. Circulation research *118*, 29-37.
Popescu, L.M., Gherghiceanu, M., Hinescu, M.E., Cretoiu, D., Ceafalan, L., Regalia, T., Popescu, A.C., Ardeleanu, C., and Mandache, E. (2006). Insights into the interstitium of ventricular myocardium: interstitial Cajal-like cells (ICLC). Journal of cellular and molecular medicine *10*, 429-458.
Predonzani, A., Arnoldi, F., Lopez-Requena, A., and Burrone, O.R. (2008). In vivo site-specific biotinylation of proteins within the secretory pathway using a single vector system. BMC biotechnology *8*, 41.
Purcell, N.H., Wilkins, B.J., York, A., Saba-El-Leil, M.K., Meloche, S., Robbins, J., and Molkentin, J.D. (2007). Genetic inhibition of cardiac ERK1/2 promotes stress-induced apoptosis and heart failure but has no effect on hypertrophy in vivo. Proceedings of the National Academy of Sciences of the United States of America *104*, 14074-14079.
Qin, F., Siwik, D.A., Lancel, S., Zhang, J., Kuster, G.M., Luptak, I., Wang, L., Tong, X., Kang, Y.J., Cohen, R.A.*, et al.* (2013). Hydrogen peroxide-mediated SERCA cysteine 674 oxidation contributes to impaired cardiac myocyte relaxation in senescent mouse heart. Journal of the American Heart Association *2*, e000184.
Rae, M.J., Butler, R.N., Campisi, J., de Grey, A.D., Finch, C.E., Gough, M., Martin, G.M., Vijg, J., Perrott, K.M., and Logan, B.J. (2010). The demographic and biomedical case for late-life interventions in aging. Science translational medicine *2*, 40cm21.
Rebbapragada, A., Benchabane, H., Wrana, J.L., Celeste, A.J., and Attisano, L. (2003). Myostatin signals through a transforming growth factor beta-like signaling pathway to block adipogenesis. Molecular and cellular biology *23*, 7230-7242.
Redfield, M.M., Jacobsen, S.J., Burnett, J.C., Jr., Mahoney, D.W., Bailey, K.R., and Rodeheffer, R.J. (2003). Burden of systolic and diastolic ventricular dysfunction in the community: appreciating the scope of the heart failure epidemic. Jama *289*, 194-202.
Regan, C.P., Anderson, P.G., Bishop, S.P., and Berecek, K.H. (1997). Pressure-independent effects of AT1-receptor antagonism on cardiovascular remodeling in aortic-banded rats. The American journal of physiology *272*, H2131-2138.
Rifkin, D.B., Mazzieri, R., Munger, J.S., Noguera, I., and Sung, J. (1999). Proteolytic control of growth factor availability. APMIS : acta pathologica, microbiologica, et immunologica Scandinavica *107*, 80-85.

Rockman, H.A., Koch, W.J., and Lefkowitz, R.J. (2002). Seven-transmembrane-spanning receptors and heart function. Nature *415*, 206-212.
Rockman, H.A., Ross, R.S., Harris, A.N., Knowlton, K.U., Steinhelper, M.E., Field, L.J., Ross, J., Jr., and Chien, K.R. (1991). Segregation of atrial-specific and inducible expression of an atrial natriuretic factor transgene in an in vivo murine model of cardiac hypertrophy. Proceedings of the National Academy of Sciences of the United States of America *88*, 8277-8281.
Rose, B.A., Force, T., and Wang, Y. (2010). Mitogen-activated protein kinase signaling in the heart: angels versus demons in a heart-breaking tale. Physiological reviews *90*, 1507-1546.
Rothermel, B.A., McKinsey, T.A., Vega, R.B., Nicol, R.L., Mammen, P., Yang, J., Antos, C.L., Shelton, J.M., Bassel-Duby, R., Olson, E.N*., et al.* (2001). Myocyte-enriched calcineurin-interacting protein, MCIP1, inhibits cardiac hypertrophy in vivo. Proceedings of the National Academy of Sciences of the United States of America *98*, 3328-3333.
Rubinsztein, D.C., Marino, G., and Kroemer, G. (2011). Autophagy and aging. Cell *146*, 682-695.
Sadoshima, J., and Izumo, S. (1993). Molecular characterization of angiotensin II--induced hypertrophy of cardiac myocytes and hyperplasia of cardiac fibroblasts. Critical role of the AT1 receptor subtype. Circulation research *73*, 413-423.
Sambrook, J., and Russell, D.W. (2006). Preparation and Transformation of Competent E. coli Using Calcium Chloride. CSH protocols *2006*.
Santra, M., Reed, C.C., and Iozzo, R.V. (2002). Decorin binds to a narrow region of the epidermal growth factor (EGF) receptor, partially overlapping but distinct from the EGF-binding epitope. The Journal of biological chemistry *277*, 35671-35681.
Sartori, R., Milan, G., Patron, M., Mammucari, C., Blaauw, B., Abraham, R., and Sandri, M. (2009). Smad2 and 3 transcription factors control muscle mass in adulthood. American journal of physiology Cell physiology *296*, C1248-1257.
Satoh, M., Matter, C.M., Ogita, H., Takeshita, K., Wang, C.Y., Dorn, G.W., 2nd, and Liao, J.K. (2007). Inhibition of apoptosis-regulated signaling kinase-1 and prevention of congestive heart failure by estrogen. Circulation *115*, 3197-3204.
Schafer, M.J., Atkinson, E.J., Vanderboom, P.M., Kotajarvi, B., White, T.A., Moore, M.M., Bruce, C.J., Greason, K.L., Suri, R.M., Khosla, S*., et al.* (2016). Quantification of GDF11 and Myostatin in Human Aging and Cardiovascular Disease. Cell metabolism *23*, 1207-1215.
Schmidt, U., del Monte, F., Miyamoto, M.I., Matsui, T., Gwathmey, J.K., Rosenzweig, A., and Hajjar, R.J. (2000). Restoration of diastolic function in senescent rat hearts through adenoviral gene transfer of sarcoplasmic reticulum Ca(2+)-ATPase. Circulation *101*, 790-796.
Schneyer, A.L., Wang, Q., Sidis, Y., and Sluss, P.M. (2004). Differential distribution of follistatin isoforms: application of a new FS315-specific immunoassay. The Journal of clinical endocrinology and metabolism *89*, 5067-5075.
Schonherr, E., Broszat, M., Brandan, E., Bruckner, P., and Kresse, H. (1998). Decorin core protein fragment Leu155-Val260 interacts with TGF-beta but does not compete for decorin binding to type I collagen. Archives of biochemistry and biophysics *355*, 241-248.
Schriner, S.E., Linford, N.J., Martin, G.M., Treuting, P., Ogburn, C.E., Emond, M., Coskun, P.E., Ladiges, W., Wolf, N., Van Remmen, H*., et al.* (2005). Extension of murine life span by overexpression of catalase targeted to mitochondria. Science *308*, 1909-1911.
Schuelke, M., Wagner, K.R., Stolz, L.E., Hubner, C., Riebel, T., Komen, W., Braun, T., Tobin, J.F., and Lee, S.J. (2004). Myostatin mutation associated with gross muscle hypertrophy in a child. The New England journal of medicine *350*, 2682-2688.
Schulman, S.P., Lakatta, E.G., Fleg, J.L., Lakatta, L., Becker, L.C., and Gerstenblith, G. (1992). Age-related decline in left ventricular filling at rest and exercise. The American journal of physiology *263*, H1932-1938.
Scudellari, M. (2015). Ageing research: Blood to blood. Nature *517*, 426-429.
Seals, D.R., and Melov, S. (2014). Translational geroscience: emphasizing function to achieve optimal longevity. Aging *6*, 718-730.

Semba, R.D., Zhang, P., Zhu, M., Fabbri, E., Gonzalez-Freire, M., Carlson, O.D., Moaddel, R., Tanaka, T., Egan, J.M., and Ferrucci, L. (2019). Relationship of Circulating Growth and Differentiation Factors 8 and 11 and Their Antagonists as Measured Using Liquid Chromatography-Tandem Mass Spectrometry With Age and Skeletal Muscle Strength in Healthy Adults. The journals of gerontology Series A, Biological sciences and medical sciences *74*, 129-136.
Shah, M., Foreman, D.M., and Ferguson, M.W. (1994). Neutralising antibody to TGF-beta 1,2 reduces cutaneous scarring in adult rodents. Journal of cell science *107 (Pt 5)*, 1137-1157.
Shimasaki, S., Koga, M., Esch, F., Cooksey, K., Mercado, M., Koba, A., Ueno, N., Ying, S.Y., Ling, N., and Guillemin, R. (1988). Primary structure of the human follistatin precursor and its genomic organization. Proceedings of the National Academy of Sciences of the United States of America *85*, 4218-4222.
Shioi, T., and Inuzuka, Y. (2012). Aging as a substrate of heart failure. Journal of cardiology *60*, 423-428.
Shioi, T., Kang, P.M., Douglas, P.S., Hampe, J., Yballe, C.M., Lawitts, J., Cantley, L.C., and Izumo, S. (2000). The conserved phosphoinositide 3-kinase pathway determines heart size in mice. The EMBO journal *19*, 2537-2548.
Sidis, Y., Mukherjee, A., Keutmann, H., Delbaere, A., Sadatsuki, M., and Schneyer, A. (2006). Biological activity of follistatin isoforms and follistatin-like-3 is dependent on differential cell surface binding and specificity for activin, myostatin, and bone morphogenetic proteins. Endocrinology *147*, 3586-3597.
Sidis, Y., Schneyer, A.L., and Keutmann, H.T. (2005). Heparin and activin-binding determinants in follistatin and FSTL3. Endocrinology *146*, 130-136.
Sinha, M., Jang, Y.C., Oh, J., Khong, D., Wu, E.Y., Manohar, R., Miller, C., Regalado, S.G., Loffredo, F.S., Pancoast, J.R.*, et al.* (2014). Restoring systemic GDF11 levels reverses age-related dysfunction in mouse skeletal muscle. Science *344*, 649-652.
Siwik, D.A., Pagano, P.J., and Colucci, W.S. (2001). Oxidative stress regulates collagen synthesis and matrix metalloproteinase activity in cardiac fibroblasts. American journal of physiology Cell physiology *280*, C53-60.
Smith, R.C., and Lin, B.K. (2013). Myostatin inhibitors as therapies for muscle wasting associated with cancer and other disorders. Current opinion in supportive and palliative care *7*, 352-360.
Smith, S.C., Zhang, X., Zhang, X., Gross, P., Starosta, T., Mohsin, S., Franti, M., Gupta, P., Hayes, D., Myzithras, M.*, et al.* (2015). GDF11 does not rescue aging-related pathological hypertrophy. Circulation research *117*, 926-932.
Soonpaa, M.H., Kim, K.K., Pajak, L., Franklin, M., and Field, L.J. (1996). Cardiomyocyte DNA synthesis and binucleation during murine development. The American journal of physiology *271*, H2183-2189.
Springer, J., Adams, V., and Anker, S.D. (2010). Myostatin: Regulator of muscle wasting in heart failure and treatment target for cardiac cachexia. Circulation *121*, 354-356.
Stewart, S., MacIntyre, K., Hole, D.J., Capewell, S., and McMurray, J.J. (2001). More 'malignant' than cancer? Five-year survival following a first admission for heart failure. European journal of heart failure *3*, 315-322.
Swinne, C.J., Shapiro, E.P., Lima, S.D., and Fleg, J.L. (1992). Age-associated changes in left ventricular diastolic performance during isometric exercise in normal subjects. The American journal of cardiology *69*, 823-826.
Tachibana, H., Perrino, C., Takaoka, H., Davis, R.J., Naga Prasad, S.V., and Rockman, H.A. (2006). JNK1 is required to preserve cardiac function in the early response to pressure overload. Biochemical and biophysical research communications *343*, 1060-1066.
Takahashi, S., Nakagawa, T., Banno, T., Watanabe, T., Murakami, K., and Nakayama, K. (1995). Localization of furin to the trans-Golgi network and recycling from the cell surface involves Ser and Tyr residues within the cytoplasmic domain. The Journal of biological chemistry *270*, 28397-28401.

Terman, A., Kurz, T., Navratil, M., Arriaga, E.A., and Brunk, U.T. (2010). Mitochondrial turnover and aging of long-lived postmitotic cells: the mitochondrial-lysosomal axis theory of aging. Antioxidants & redox signaling *12*, 503-535.
The Human Protein Atlas (2019). Protein and RNA expression of Furin. Available online at https://www.proteinatlas.org/ENSG00000140564-FURIN/tissue.
Thies, R.S., Chen, T., Davies, M.V., Tomkinson, K.N., Pearson, A.A., Shakey, Q.A., and Wolfman, N.M. (2001). GDF-8 propeptide binds to GDF-8 and antagonizes biological activity by inhibiting GDF-8 receptor binding. Growth factors *18*, 251-259.
Thompson, T.B., Lerch, T.F., Cook, R.W., Woodruff, T.K., and Jardetzky, T.S. (2005). The structure of the follistatin:activin complex reveals antagonism of both type I and type II receptor binding. Developmental cell *9*, 535-543.
Thompson, W.W., Weintraub, E., Dhankhar, P., Cheng, P.Y., Brammer, L., Meltzer, M.I., Bresee, J.S., and Shay, D.K. (2009). Estimates of US influenza-associated deaths made using four different methods. Influenza and other respiratory viruses *3*, 37-49.
Trendelenburg, A.U., Meyer, A., Rohner, D., Boyle, J., Hatakeyama, S., and Glass, D.J. (2009). Myostatin reduces Akt/TORC1/p70S6K signaling, inhibiting myoblast differentiation and myotube size. American journal of physiology Cell physiology *296*, C1258-1270.
Trexler, M., Banyai, L., and Patthy, L. (2002). Distinct expression pattern of two related human proteins containing multiple types of protease-inhibitory modules. Biological chemistry *383*, 223-228.
Trifunovic, A., Wredenberg, A., Falkenberg, M., Spelbrink, J.N., Rovio, A.T., Bruder, C.E., Bohlooly, Y.M., Gidlof, S., Oldfors, A., Wibom, R.*, et al.* (2004). Premature ageing in mice expressing defective mitochondrial DNA polymerase. Nature *429*, 417-423.
UaH, I. (2012). Ageing in the Twenty-First Century A Celebration and A Challenge: UNFPA and HelpAge International. Available online: http://wwwunfpaorg/publications/ageing-twenty-first-century.
Ulm, S., Liu, W., Zi, M., Tsui, H., Chowdhury, S.K., Endo, S., Satoh, Y., Prehar, S., Wang, R., Cartwright, E.J.*, et al.* (2014). Targeted deletion of ERK2 in cardiomyocytes attenuates hypertrophic response but provokes pathological stress induced cardiac dysfunction. Journal of molecular and cellular cardiology *72*, 104-116.
Ungvari, Z., Orosz, Z., Labinskyy, N., Rivera, A., Xiangmin, Z., Smith, K., and Csiszar, A. (2007). Increased mitochondrial H2O2 production promotes endothelial NF-kappaB activation in aged rat arteries. American journal of physiology Heart and circulatory physiology *293*, H37-47.
United Nations, D.o.E.a.S.A., Population Division (2015). World Population Ageing 2015. Available online:
http://wwwunorg/en/development/desa/population/publications/pdf/ageing/WPA2015_Reportpdf.
van Esch, J.H., Gembardt, F., Sterner-Kock, A., Heringer-Walther, S., Le, T.H., Lassner, D., Stijnen, T., Coffman, T.M., Schultheiss, H.P., Danser, A.H.*, et al.* (2010). Cardiac phenotype and angiotensin II levels in AT1a, AT1b, and AT2 receptor single, double, and triple knockouts. Cardiovascular research *86*, 401-409.
Vega, R.B., Rothermel, B.A., Weinheimer, C.J., Kovacs, A., Naseem, R.H., Bassel-Duby, R., Williams, R.S., and Olson, E.N. (2003). Dual roles of modulatory calcineurin-interacting protein 1 in cardiac hypertrophy. Proceedings of the National Academy of Sciences of the United States of America *100*, 669-674.
Vermij, S.H., Abriel, H., and van Veen, T.A. (2017). Refining the molecular organization of the cardiac intercalated disc. Cardiovascular research *113*, 259-275.
Vermulst, M., Wanagat, J., Kujoth, G.C., Bielas, J.H., Rabinovitch, P.S., Prolla, T.A., and Loeb, L.A. (2008). DNA deletions and clonal mutations drive premature aging in mitochondrial mutator mice. Nature genetics *40*, 392-394.

Walker, R.G., Czepnik, M., Goebel, E.J., McCoy, J.C., Vujic, A., Cho, M., Oh, J., Aykul, S., Walton, K.L., Schang, G.*, et al.* (2017). Structural basis for potency differences between GDF8 and GDF11. BMC biology *15*, 19.
Walker, R.G., McCoy, J.C., Czepnik, M., Mills, M.J., Hagg, A., Walton, K.L., Cotton, T.R., Hyvonen, M., Lee, R.T., Gregorevic, P.*, et al.* (2018). Molecular characterization of latent GDF8 reveals mechanisms of activation. Proceedings of the National Academy of Sciences of the United States of America *115*, E866-E875.
Walker, R.G., Poggioli, T., Katsimpardi, L., Buchanan, S.M., Oh, J., Wattrus, S., Heidecker, B., Fong, Y.W., Rubin, L.L., Ganz, P.*, et al.* (2016). Biochemistry and Biology of GDF11 and Myostatin: Similarities, Differences, and Questions for Future Investigation. Circulation research *118*, 1125-1141; discussion 1142.
Walton, R.D., Jones, S.A., Rostron, K.A., Kayani, A.C., Close, G.L., McArdle, A., and Lancaster, M.K. (2016). Interactions of Short-Term and Chronic Treadmill Training With Aging of the Left Ventricle of the Heart. The journals of gerontology Series A, Biological sciences and medical sciences *71*, 1005-1013.
Weber, K.T. (1989). Cardiac interstitium in health and disease: the fibrillar collagen network. Journal of the American College of Cardiology *13*, 1637-1652.
Weiss, A., and Attisano, L. (2013). The TGFbeta superfamily signaling pathway. Wiley interdisciplinary reviews Developmental biology *2*, 47-63.
Wilkins, B.J., Dai, Y.S., Bueno, O.F., Parsons, S.A., Xu, J., Plank, D.M., Jones, F., Kimball, T.R., and Molkentin, J.D. (2004). Calcineurin/NFAT coupling participates in pathological, but not physiological, cardiac hypertrophy. Circulation research *94*, 110-118.
World Health Organization (2014). Global Health Estimates: Deaths by Cause, Age, Sex and Country, 2000-2012. Geneva, WHO.
Wu, H.H., Ivkovic, S., Murray, R.C., Jaramillo, S., Lyons, K.M., Johnson, J.E., and Calof, A.L. (2003). Autoregulation of neurogenesis by GDF11. Neuron *37*, 197-207.
Xu, A., and Narayanan, N. (1998). Effects of aging on sarcoplasmic reticulum Ca2+-cycling proteins and their phosphorylation in rat myocardium. The American journal of physiology *275*, H2087-2094.
Xu, J., Kimball, T.R., Lorenz, J.N., Brown, D.A., Bauskin, A.R., Klevitsky, R., Hewett, T.E., Breit, S.N., and Molkentin, J.D. (2006). GDF15/MIC-1 functions as a protective and antihypertrophic factor released from the myocardium in association with SMAD protein activation. Circulation research *98*, 342-350.
Yadin, D., Knaus, P., and Mueller, T.D. (2016). Structural insights into BMP receptors: Specificity, activation and inhibition. Cytokine & growth factor reviews *27*, 13-34.
Yancy, C.W., Jessup, M., Bozkurt, B., Butler, J., Casey, D.E., Jr., Drazner, M.H., Fonarow, G.C., Geraci, S.A., Horwich, T., Januzzi, J.L.*, et al.* (2013). 2013 ACCF/AHA guideline for the management of heart failure: executive summary: a report of the American College of Cardiology Foundation/American Heart Association Task Force on practice guidelines. Circulation *128*, 1810-1852.
Yang, J., Ratovitski, T., Brady, J.P., Solomon, M.B., Wells, K.D., and Wall, R.J. (2001). Expression of myostatin pro domain results in muscular transgenic mice. Molecular reproduction and development *60*, 351-361.
Yang, W., Chen, Y., Zhang, Y., Wang, X., Yang, N., and Zhu, D. (2006). Extracellular signal-regulated kinase 1/2 mitogen-activated protein kinase pathway is involved in myostatin-regulated differentiation repression. Cancer research *66*, 1320-1326.
Yang, Y., Cui, J., Xue, F., Zhang, C., Mei, Z., Wang, Y., Bi, M., Shan, D., Meredith, A., Li, H.*, et al.* (2015). Pokemon (FBI-1) interacts with Smad4 to repress TGF-beta-induced transcriptional responses. Biochimica et biophysica acta *1849*, 270-281.
Zacchigna, S., Zentilin, L., and Giacca, M. (2014). Adeno-associated virus vectors as therapeutic and investigational tools in the cardiovascular system. Circulation research *114*, 1827-1846.

Zhang, D., Gaussin, V., Taffet, G.E., Belaguli, N.S., Yamada, M., Schwartz, R.J., Michael, L.H., Overbeek, P.A., and Schneider, M.D. (2000). TAK1 is activated in the myocardium after pressure overload and is sufficient to provoke heart failure in transgenic mice. Nature medicine *6*, 556-563.
Zhang, T., Johnson, E.N., Gu, Y., Morissette, M.R., Sah, V.P., Gigena, M.S., Belke, D.D., Dillmann, W.H., Rogers, T.B., Schulman, H.*, et al.* (2002). The cardiac-specific nuclear delta(B) isoform of Ca2+/calmodulin-dependent protein kinase II induces hypertrophy and dilated cardiomyopathy associated with increased protein phosphatase 2A activity. The Journal of biological chemistry *277*, 1261-1267.
Zhang, T., Maier, L.S., Dalton, N.D., Miyamoto, S., Ross, J., Jr., Bers, D.M., and Brown, J.H. (2003). The deltaC isoform of CaMKII is activated in cardiac hypertrophy and induces dilated cardiomyopathy and heart failure. Circulation research *92*, 912-919.
Zhang, Y.H., Cheng, F., Du, X.T., Gao, J.L., Xiao, X.L., Li, N., Li, S.L., and Dong de, L. (2016). GDF11/BMP11 activates both smad1/5/8 and smad2/3 signals but shows no significant effect on proliferation and migration of human umbilical vein endothelial cells. Oncotarget *7*, 12063-12074.
Zhao, Q.D., Viswanadhapalli, S., Williams, P., Shi, Q., Tan, C., Yi, X., Bhandari, B., and Abboud, H.E. (2015). NADPH oxidase 4 induces cardiac fibrosis and hypertrophy through activating Akt/mTOR and NFkappaB signaling pathways. Circulation *131*, 643-655.
Zhou, J., Wang, J., Shen, B., Chen, L., Su, Y., Yang, J., Zhang, W., Tian, X., and Huang, X. (2014). Dual sgRNAs facilitate CRISPR/Cas9-mediated mouse genome targeting. The FEBS journal *281*, 1717-1725.
Zhu, X., Topouzis, S., Liang, L.F., and Stotish, R.L. (2004). Myostatin signaling through Smad2, Smad3 and Smad4 is regulated by the inhibitory Smad7 by a negative feedback mechanism. Cytokine *26*, 262-272.
Zile, M.R., Baicu, C.F., Ikonomidis, J.S., Stroud, R.E., Nietert, P.J., Bradshaw, A.D., Slater, R., Palmer, B.M., Van Buren, P., Meyer, M.*, et al.* (2015). Myocardial stiffness in patients with heart failure and a preserved ejection fraction: contributions of collagen and titin. Circulation *131*, 1247-1259.
Zimmers, T.A., Jiang, Y., Wang, M., Liang, T.W., Rupert, J.E., Au, E.D., Marino, F.E., Couch, M.E., and Koniaris, L.G. (2017). Exogenous GDF11 induces cardiac and skeletal muscle dysfunction and wasting. Basic research in cardiology *112*, 48.